ETAA1 promotes genome stability through activation of ATR

By

Thomas Edwin Bass

Dissertation

Submitted to the Faculty of the

Graduate School of Vanderbilt University

in partial fulfillment of the requirement

for the degree of

DOCTOR OF PHILOSPHY

in

Biochemistry

December 15, 2018

Nashville, Tennessee

Approved:

David Cortez, Ph.D

John York, Ph.D

Walter Chazin, Ph.D

Scott Hiebert, Ph.D

Brandt Eichman, Ph.D

To my beautiful and loving wife, Lauren

and

To my family

ACKNOWLEDGEMENTS

Research for this dissertation was made possible by funding from the Biochemical and Chemical Training for Cancer Research training grant (T32CA009582-28).

I would like to thank my mentor, Dr. David Cortez for the guidance he has provided over the last five years. He has given encouragement, support, and wisdom throughout my graduate career while also challenging me to become a better scientist. I truly appreciate all the time he has invested in my training and believe the quality and quantity of research conducted in the Cortez lab reflect his unquenchable thirst for data and discovery.

I would also like to thank my committee members for their continued support during my time at Vanderbilt. Thank you, Dr. Walter Chazin for being my committee chair, collaborating with us on the ETAA1 project, and organizing biweekly basketball games. Dr. John York, I have appreciated all your support, encouragement, and admire your unique perspective on all things except which North Carolina school is superior. Dr. Scott Hiebert, thank you for your helpful contributions, insights, and teaching me the inner workings of the cell cycle. Lastly, thanks Dr. Brandt Eichman for all your help and guidance.

I owe many thanks to all the members of the Cortez lab, both past and present. First, I would like to thank the Cortez lab alumni: doctors Jessica Luzwick, Akosua Badu-Nkasnsah, Kami Bhat, Lisa Poole, Gina Kavanaugh, Huzefa Dungrawala, and Clint Carroll. Thank you all for helping show me the ropes and being great friends. I would also like to thank Gloria Glick and Nancy Zhao for all of your help and assistance with my projects. A special thanks goes out to Gina, Jessica, Clint, Gloria, and Nancy for directly helping me with experiments that contributed greatly to my paper. To the current Cortez lab members, Dr. Kareem Mohni, Dr. Sarah Wessel, Dr. Maroof Zafar, Dr. Madison Adolph, Dr. Wenpeng Liu, Dr. Kavi Mehta, Vaughn Thada, Petria Thompson, Archana Krishnamoorthy, Taha Mohamed, and Jorge Rua

Fernandez thanks for your continued assistance and support. I hope all of you will do well in the future.

I would also like to thank my family for all their continued love, encouragement, and support throughout graduate school. Thank you all so much for always being there when needed. Lastly, I would like to thank my wife Lauren for the unbelievable blessing she has been during the past five years. Thank you for always making me feel better and encouraging me when life gets crazy and stressful. I look forward to all our future adventures together.

TABLE OF CONTENTS

Page

DEDICATION ii

ACKNOWLEDGEMENTS iii

LIST OF TABLES viii

LIST OF FIGURES ix

LIST OF ABBREVIATIONS xi

Chapter

I. INTRODUCTION 1

The DNA Damage Response 3
Regulation of the DDR by PIKKs 5
DNA-PK and non-homologous end joining 7
ATR/ATM kinases 9
ATM and homologous recombination 9
ATR and the replication stress response 11
Regulation of ATR 13
Recruitment of ATR by RPA-ssDNA 13
Mec1^{ATR} activation 14
ATR activation by TOPBP1 15
ATR activation by ETAA1 18
Requirements for ATR/Mec1 activation 19
ATR regulation of cell cycle checkpoints 20
ATR regulation of the intra-S-phase checkpoint 20
Regulation of origin firing 22
Stabilization of stalled forks 23
Cell cycle arrest 25
ATR regulation of the S/G_2 checkpoint 26
ATR regulation of the G_2/M checkpoint 26
ATR regulation of the mitotic checkpoint 27
Spindle assembly checkpoint 27
ATR and CHK1 function during mitosis 29
Targeting the DDR response in cancer 30

II. MATERIALS AND METHODS 33

Antibodies 33
Cell lines 36
Cell growth assays 37
Cell profiler 37
Clonogenic survival assay 37
COMET assay 38
Neutral COMET assays 38
Alkaline COMET assays 38
CRISPR knockout cell generation 39
gRNA design 39
gRNA plasmid construction 40
Primer design and optimization of amplifying genomic DNA 41
gRNA optimization 42
Genomic DNA purification and PCR 42
CRISPR knock-in cell generation (auxin-inducible cell lines) 43
Fiber labeling 43
Flow cytometry 44
BrdU/PI incorporation 44
Mitotic index by pH3 S10 45
Gel filtration 45
Gene ontology analysis 46
Kinase assays 46
Immunofluorescence 47
Immunoprecipitation 47
iPOND 48
NMR analysis 50
NP40 lysis 50
Nuclear extract preparation 50
Packaging lentiviral particles 51
Phosphatase treatment of cell lysates 52
Phosphoproteomics 53
Preparation of samples 53
TiO_2 enrichment of phosphopeptides 54
LC-MS/MS analysis of enriched phosphorylated peptides 55
Phosphoproteomics analysis 56
Protein purification 57
Induction of protein 57
Purification of protein 57
Proximity ligation assay 58
Sister chromatid exchange assay 59
Viability assay using alamar blue 60

III. ETAA1 ACTS AT STALLED REPLICATION FORKS TO MAINTAIN GENOME INTEGRITY 61

Introduction 61
Results 62
ETAA1 is an RPA-interacting protein that localizes to stalled forks 62
ETAA1 binds two RPA domains to recruit it to damaged forks 66
ETAA1 is a replication stress response protein 69
ETAA1 interacts with multiple DDR proteins including ATR and BLM 74

ETAA1 activates ATR 77
ETAA1 requires its RPA-interaction and ATR-activation domains to maintain genome stability 80
ETAA1-deficient cells exhibit elevated levels of SCEs 83
ETAA1 and TOPBP1 function in distinct pathways 87
Discussion 91
Conclusions 93

IV. QUANTITATIVE PHOSPHOPROTOMICS REVEALS MITOTIC FUNCTION OF THE ATR-ACTIVATOR ETAA1 94

Introduction 94
Results 95
Generation of cell lines deficient for ATR activators 95
Quantitative phosphoproteomics identifies ETAA1 and TOPBP1-dependent phosphosites 100
Gene ontology analysis of ETAA1 and TOPBP1-dependent phosphorylation 102
ETAA1 regulates and interacts with mitotic proteins 106
ETAA1 regulates Aurora B kinase activity through an ATR pathway 108
Loss of mitotic ETAA1-ATR signaling results in chromosome alignment defects 108
Discussion 114
Conclusion 117

V. DISCUSSION AND FUTURE DIRECTIONS

Summary 144
Discussion 145
Defining ATR/Mec1 activators 145
Characterizing how ATR/Mec1 activators work 146
Benefits of having multiple ATR/Mec1 activators 147
Temporal regulation of ATR signaling 147
Separation of ATR signaling pathways 149
ATR activators may respond to unique DNA lesions 150
Regulation of ETAA1 155
ETAA1 is phosphorylated during replication stress 155
ETAA1 demonstrates delayed localization to sites of replication stress 159
Future Directions 161
Defining mechanism of ETAA1 regulation 161
Comparing ETAA1 and TOPBP1 substrate specificity 163
Conclusions 164

REFERENCES 166

LIST OF TABLES

Table Page

2.1 Antibodies 33

2.2 Cell Lines 36

2.3 Cell profiler pipelines 37

2.4 gRNA sequences 39

4.1 ETAA1-dependent phosphosites 118

4.2 TOPBP1-dependent phosphosites 123

4.3 ETAA1 and TOPBP1-dependent phosphosites 135

4.4 ETAA1-dependent GO terms 137

4.5 TOPBP1-dependent GO terms 139

LIST OF FIGURES

Figure		Page
1.1	Overview of the DNA damage response	4
1.2	Domain layout and structural similarities of ATR, ATM, and DNA-PK	6
1.3	DNA-PK and non-homologous end joining	8
1.4	ATM and homologous recombination	10
1.5	Sources of replication stress	12
1.6	ATR and replication stress response	17
1.7	ATR and cell cycle checkpoints	21
1.8	ATR stabilizes stalled forks through regulation of SMARCAL1	24
1.9	Spindle assembly checkpoint	28
3.1	ETAA1 is enriched at stalled replication forks and interacts with RPA	63
3.2	ETAA1 colocalizes with RPA at sites of replication stress	65
3.3	RPA recruits ETAA1 to damaged replication forks	67
3.4	ETAA1 interacts with RPA through the RPA32C and RPA70N domains	68
3.5	Loss of EAA1 results in increased DNA damage and sensitivity to DNA damaging agents	70
3.6	ETAA1 knockdown causes hypersensitivity to replication stress	71
3.7	ETAA1 knockdown does not cause sensitivity to all DNA damaging agents	72
3.8	ETAA1 is needed to recover from replication stress	73
3.9	ETAA1 promotes fork stability	75
3.10	ETAA1 interacts with multiple DNA damage response proteins	76
3.11	ETAA1 is required for RPA phosphorylation in multiple cell types	78
3.12	ETAA1 activates ATR	79
3.13	ETAA1 overexpression causes DNA damage signaling	81
3.14	An interaction with RPA is needed for ETAA1 to maintain genome integrity	84
3.15	The ETAA1 ATR activation domain is needed to maintain fork stability	85
3.16	The ETAA1 ATR activation domain is needed for ATR signaling	86
3.17	ETAA1 deficient cells have elevated sister chromatid exchanges and genetic instability	88

3.18 ETAA1 and TOPBP1 act in separate pathways to regulate ATR and maintain genome stability 89
4.1 Production of ETAA1 and TOPBP1-deficient cell lines 96
4.2 Characterization of ETAA1 and TOPBP1-deficient cell lines 98
4.3 Quantitative phosphoproteomics identified ETAA1 and TOPBP1-dependent phosphosites 101
4.4 TOPBP1-dependent phosphorylation gene ontology analysis 103
4.5 ETAA1-dependent gene ontology analysis 105
4.6 ETAA1 regulates phosphoproteins at kinetochores and spindles 107
4.7 Analysis of ETAA1 and TOPBP1-dependent phosphoproteins 109
4.8 ETAA1-dependent activation regulates Aurora B kinase activity 110
4.9 ETAA1 activation of ATR is required for proper chromosome alignment and a fully functional SAC 112
4.10 Length of mitosis is unchanged by loss of ETAA1, TOPBP1, or ATR activity .. 113
4.11 Models for ATR activation 116
5.1 Potential benefits of utilizing multiple ATR activators 148
5.2 Generation of 5'ss/dsDNA junctions for TOPBP1 activation of ATR 151
5.3 DNA structures that may require ETAA1 activation of ATR 153
5.4 ETAA1 is phosphorylated during replication stress 156
5.5 Kinetics of ETAA1 modification and ATR signaling 158
5.6 Kinetics of recruitment of ETAA1, TOPBP1, and RPA 160
5.7 Model of ETAA1 regulation and ATR signaling after treatment with camptothecin 162

LIST OF ABBREVIATIONS

53BP1	p53 binding protein 1
AAD	ATR Activation Domain
ACA	Anti-Centromere-Antibodies
ACN	Acetonitrile
AID	Auxin Inducible Degron
APC/C	Anaphase Promoting Complex
ATR	ATM and Rad3-related
ATRi	ATR inhibitor
ATRIP	ATR-Interacting Protein
ATM	Ataxia Telangiectasia Mutated
AURKB	Aurora B Kinase
BLM	Bloom Syndrome Protein
BrdU	Bromodeoxyuridine/5-bromo-2'-deoxyuridine
BTR	BLM/TopoIIIα/RMI1/RMI2 complex
BUB1	Budding uninhibited by benzimidazoles 1
BUB3	Budding uninhibited by benzimidazoles 3
BUBR1	BUB1-Related 1
bp	Base pairs
BRCA1	Breast cancer type 1 susceptibility protein
BRCA2	Breast cancer type 2 susceptibility protein
BSA	Bovine Serum Albumin
Cas9	CRISPR Associated 9
CDC20	Cell division cycle 20
CDC25	Cell division cycle 25

CDC45	Cell division cycle 45
CDK1	Cyclin Dependent Kinase 1
CDK2	Cyclin Dependent Kinase 2
cDNA	Complementary DNA
CHK1	Checkpoint kinase 1
CHK1i	CHK1 inhibitor
CHK2	Checkpoint kinase 2
CINP	CDK2-interacting protein
CISP	Cisplatin
CldU	5-Chloro-2′-deoxyuridine
CMG	CDC45-MCM-GINS
CP	Chromatin Pellet
CPT	Camptothecin
CRISPR	Clustered Regularly Interspaced Short Palindromic Repeats
CtIP	CTBP-Interacting Protein
DAPI	4′,6-diamidino-2-phenylindole
Ddc1	DNA Damage Checkpoint 1
DDR	DNA Damage Response
dHJ	Double Holliday junction
DMEM	Dulbecco's Modified Eagle's Medium
DNA	Deoxyribonucleic acid
DNA2	DNA synthesis defective 2
DNA-PK	DNA Dependent Protein Kinase
dNTPs	deoxyribonucleotide triphosphate
Dpb11	DNA replication regulator DPB11
DSB	Double-Stranded breaks

dsDNA	Double-stranded DNA
DTT	Dithiothreitol
EDTA	Ethylenediaminetetraacetic acid
EdU	5-Ethynyl-2´-deoxyuridine
ETAA1	Ewing Tumor Associated Antigen 1
EXO1	Exonuclease 1
EV	Empty Vector
FAT	FRAP-ATM-TRRAP
FATC	FAT C-terminus
FDR	False Discovery Rate
FL	Full Length
FOXM1	Forkhead Box M1
GFP	Green Fluorescent Protein
GST	Glutathione S-transferase
GWAS	Genome Wide Association Studies
H2B	Histone 2B
H3	Histone 3
HBSS	Hank's Balanced Salt Solution
HEAT	Huntingtin, Elongation factor 3, A subunit of protein phosphatase 2A and TOR1
HEK	Human Embryonic Kidney
HEMCES	5-Hydroxymethylcytosine Binding, ES Cell Specific
HEPES	2-[4-(2-hydroxyethyl)piperazin-1-yl]ethanesulfonic acid
HLTF	Helicase Like Transcription Factor
HR	Homologous Recombination
HU	Hydroxy Urea

IAA	Indole-3-acetic acid
IdU	Iododeoxyuridine
IP	Immunoprecipitation
IPTG	Isopropyl β-D-1-thiogalactopyranoside
IR	Ionizing Radiation
iPOND	isolation of Proteins On Nascent DNA
kDa	kilo-Dalton
LB	Luria Broth
LC	Liquid Chromatography
LIG4	DNA Ligase 4
MAD	Mec1 Activation Domain
MAD2	Mitotic Arrest Deficient 2
MCC	Mitotic Checkpoint Complex
MCM	Minichromosome maintenance
Mec1	Mitosis Entry Checkpoint 1
MMS	Methyl methanesulfonate
MRN	Mre11-Rad50-Nbs1
MS/MS	Tandem mass spectrometry
MUS81	Crossover junction endonuclease MUS81
MYT1	Myelin transcription factor 1
NE	Nuclear Extract
NEB	Nuclear Envelope Breakdown
NHEJ	Non-Homologous End Joining
NMR	Nuclear Magnetic Resonance
NT	Non-Targeting
OB fold	Oligonucleotide/oligosaccharide-binding folds

PARP	Poly ADP Ribose Polymerase
PBS	Phosphate Buffered Saline
PCNA	Proliferating Cell Nuclear Antigen
pcv	Packed Cell Volume
PEI	polyethylenimine
PI	Propidium Iodide
PIKK	Phosphoinositide 3-kinase related protein kinase
PMSF	Phenylmethane sulfonyl fluoride
PNK	Polynucleotide 5'-hydroxyl-kinase
pnv	Packed Nuclear Volume
POL α	DNA polymerase α
POLII	RNA polymerase II
PP2A	Serine/threonine-protein phosphatase 2A
PP4	Serine/threonine-protein phosphatase 4
PP6	Serine/threonine-protein phosphatase 6
PRD	PIKK Regulatory Domain
PTM	Post-Translational Modification
Q	Glutamine
RFC	Replication Factor C
R-loops	RNA-DNA loops
Rad 17	Radiation sensitive 17
Rad 24	Radiation sensitive 24
RADX	RPA-related, RAD51-antagonist on X-chromosome
RHINO	Rad9, Hus1, Rad1 interacting nuclear orphan
RMI1	RecQ-mediated genome instability protein 1
RMI2	RecQ-mediated genome instability protein 2

RNR	Ribonucleotide reductase
rpm	Rotations Per Minute
ROS	Reactive Oxygen Species
RPA	Replication Protein A
RS	Replication Stress
RSR	Replication Stress Response
S	Serine
SAC	Spindle Assembly Checkpoint
SCE	Sister Chromatid Exchange
SD	Standard Deviation
SDS	Sodium Dodecyl Sulfate
SDS-PAGE	Sodium dodecyl sulfate-polyacrylamide gel electrophoresis
SILAC	stable isotope labeling of amino acids in cell culture
SIOD	Schimke immunoosseous dysplasia
SLX1	Structure-specific endonuclease subunit SLX1
SLX4	Structure-specific endonuclease subunit SLX4
ssDNA	single-stranded DNA
SMARCAL1	SWI/SNF, matrix associated, actin dependent regulator of chromatin A-like 1
T	Threonine
TFE	trifluoroethanol
TOP III α	DNA topoisomerase III-α
TOPBP1	Topoisomerase 2 Binding protein 1
Unt	Untreated
UV	Ultraviolet
WEE1	WEE1 G2 Checkpoint Kinase

Wip1	Wild-type p53-induced phosphatase 1
WRN	Werner syndrome ATP-dependent helicase
WT	Wild Type
XLF	XRCC4-like factor
XPF	DNA repair endonuclease XPF
XRCC4	X-ray repair cross-complementing protein 4
YFP	Yellow Fluorescent Protein
ZRANB3	Zinc Finger RANBP2-Type Containing 3

CHAPTER I

INTRODUCTION

As each cell cycles, it must faithfully replicate its DNA and ensure equal separation of the duplicated genetic information into the dividing daughter cells. In human cells, DNA replication requires accurately duplicating more than 6 billion base pairs of DNA in just a matter of hours. This already daunting task is even more challenging considering cells must overcome several obstacles to replication such as DNA lesions, common fragile sites, repetitive sequences, DNA secondary structure, and collisions with transcription machinery (Zeman and Cimprich, 2014). All of these impediments block DNA replication and can cause slowing or stopping of the replication fork, which is globally termed replication stress (RS). In addition to unavoidable endogenous threats, our DNA is under constant barrage from exogenous genotoxic sources such as ultraviolet radiation (UV light), ionizing radiation (IR), and chemical agents resulting in tens of thousands of DNA lesions per cell per day (Ciccia and Elledge, 2010). A failure to accurately complete DNA replication or repair damaged DNA results in loss of genetic information, which can lead to cell death or disease.

Luckily, our genomes are under constant surveillance for DNA damage and our cells have an arsenal of repair proteins to maintain genome integrity. However, cellular responses to DNA damage and replication stress must be coordinated with cell cycle progression ensuring cells have enough time to complete DNA replication or repair before progressing to the next phase of the cell cycle. To prevent passage of compromised genetic information, cells activate a signal transduction pathway called the DNA damage response (DDR), which is regulated by three apical kinases: ATM (Ataxia Telangiectasia Mutated), ATR (ATM and Rad3-related) and DNA-PK (DNA Dependent Protein Kinase) (Ciccia and Elledge, 2010). After sensing genotoxic

stress, these kinases rapidly initiate the DDR through phosphorylation of substrates, recruiting repair proteins to sites of damage while arresting cell cycle progression through activation of cell cycle checkpoints.

Hundreds of proteins participate in the DDR with diverse enzymatic activities and biological functions. One of the ongoing goals of the Cortez lab is to identify and characterize new DDR proteins. One methodology developed by the Cortez lab that has proved especially powerful for identifying new replication and repair proteins is isolation of proteins on nascent DNA (iPOND) (Sirbu et al., 2011, 2013). By combining iPOND with stable isotope labeling of amino acids in cell culture (SILAC) and liquid chromatography-tandem mass spectrometry (LC-MS/MS), Dr. Huzefa Dungrawala and other Cortez lab members were able to identify proteins located at a normal replication fork and stalled replication fork (Dungrawala et al., 2015). Utilizing this SILAC-iPOND-MS approach combined with other genetic and proteomic screens, our lab has identified and characterized five new DNA repair and RS proteins in the last nine years: CDK2-interacting protein (CINP) SWI/SNF, matrix associated, actin dependent regulator of chromatin A-like 1 (SMARCAL1), RPA-related, RAD51-antagonist on X-chromosome (RADX), 5-Hydroxymethylcytosine Binding, ES Cell Specific (HEMCES), and Ewing Tumor Associated Antigen 1 (ETAA1) (Lovejoy et al., 2009; Bansbach et al., 2009; Bass et al., 2016; Dungrawala et al., 2017, Mohni et al., 2019).

The work outlined in this dissertation focuses on a previously uncharacterized protein, ETAA1, that we identified as a potential RS protein by iPOND and another proteomic screen. In Chapter III, I will describe how we identified ETAA1 as a RS protein and subsequently characterized it as a novel activator of ATR. In Chapter IV, I will describe how I utilized quantitative phosphoproteomics to determine how the two ATR activators, ETAA1 and TOPBP1 (Topoisomerase-IIβ binding protein 1) differentially regulate ATR signaling. Additionally, I will discuss the function of ETAA1 to activate ATR during mitosis at centromeric regions. Finally, in

Chapter V I will discuss the impact of these results and outline some future directions of study for ETAA1 and ATR activation. In this chapter, I will introduce the key concepts of the DDR, replication stress, and the functions of ATR throughout the cell cycle.

The DNA damage response

Our DNA is under constant barrage by environmental genotoxic agents such as UV light and reactive chemicals that result in tens of thousands of DNA lesions a day per cell (Hoeijmakers, 2009). Additionally, genomic instability can arise from unavoidable endogenous sources such as reactive byproducts of metabolism, and replication stress (RS) (Ciccia and Elledge, 2010). A failure to recognize and respond to DNA damage and RS can result in loss of genetic information causing disease and cancer.

Genome maintenance requires constant surveillance for damaged DNA and after recognition of genotoxic stress, cells must recruit repair proteins with the appropriate enzymatic activity to the DNA lesion. Simultaneously, cell cycle checkpoints must preclude cell cycle progression until completion of DNA repair. To coordinate these responses to DNA damage, cells have developed an elaborate signal transduction pathway called the DNA damage response (DDR) (Fig 1.1) (Ciccia and Elledge, 2010). Initialization of DDR signaling begins with recognition of aberrant DNA structures like double-stranded breaks (DSBs) or single-stranded DNA (ssDNA) by sensor proteins such as the Ku70/Ku80 complex, Mre11-Rad50-Nbs1 (MRN) complex, or Replication protein A (RPA). Sensor proteins bind DNA lesions and recruit apical kinases that relay this signal to mediator proteins. Mediators are kinases which further propagate the signal to downstream effector proteins, promoting DNA repair. The DDR effector proteins are an enzymatically diverse group consisting of helicases, polymerases, nucleases, topoisomerases, and other DNA modifying enzymes. DDR effector proteins also consist of transcription factors

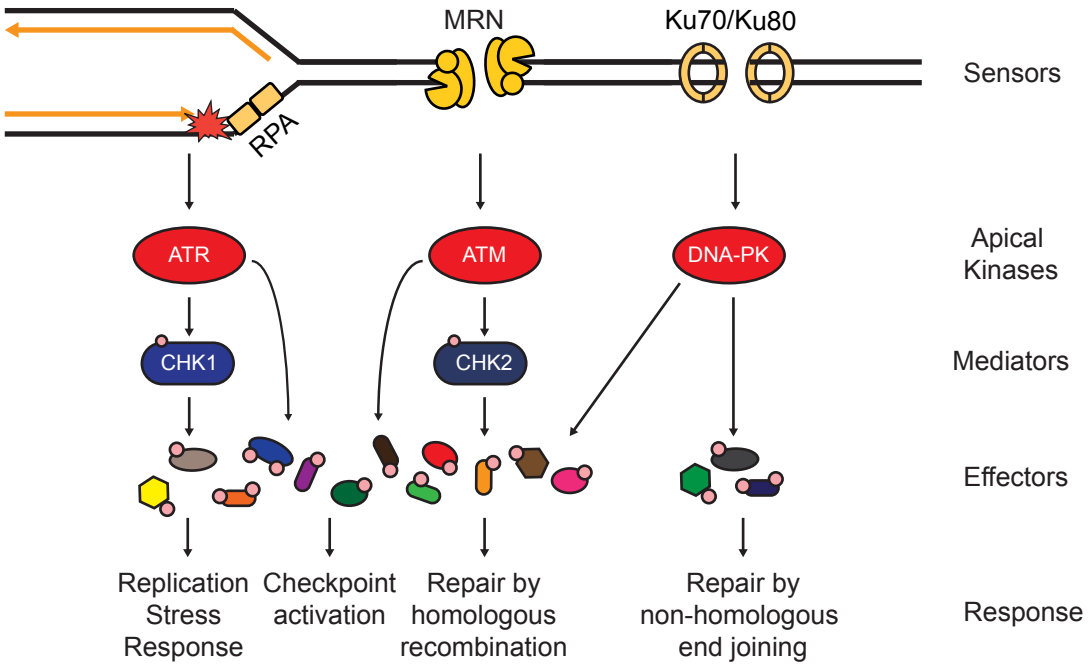

Figure 1.1 Overview of the DNA Damage response (DDR). The DDR is initiated by recognition of aberrant DNA structures like single-stranded DNA or double strand breaks by sensor proteins such as RPA, MRN, or Ku70/Ku80. Sensor proteins recruit the apical kinases ATR, ATM, and DNA-PK which relay the signal to mediators such as CHK1 and CHK2. Mediators propagate the signal to downstream effector proteins and help the apical kinases coordinate DNA repair and checkpoint activation.

and other cell cycle regulators that arrest cell cycle progression, or if the extent of damage is too severe, they may induce apoptosis rather than pass on the compromised genetic material.

Regulation of the DDR by PIKKs

The apical regulators of the DDR pathway that transduce the signal from the DNA damage sensors to the DDR effectors are the phosphoinositide 3-kinase related protein kinases (PIKKs), ATR, ATM, and DNA-PK (DNA Dependent protein kinase) (Blackford and Jackson, 2017). ATR, ATM, and DNA-PK share similar domain organization, structural features, and substrate specificity; each kinase preferentially phosphorylates a serine or threonine followed by glutamine (S/TQ) (Kim et al., 1999; Bennetzen et al., 2010). Highlighting their importance as master regulators of the DDR, mutations in all three kinases are associated with cancer and disease; ATM deficiency is associated with Ataxia Telangiectasia, mutations in ATR cause Seckel syndrome, and loss of DNA-PK increases risk of multiple cancer types (O'Driscoll et al., 2003; Savitsky et al., 1995; Goodwin et al., 2015).

The C-terminus of all PIKKs is highly conserved, harboring a kinase domain surrounded by FRAP, ATM, TRRAP (FAT), FAT C-terminus (FATC) domains, and PIKK regulatory domains (PRD) (Fig. 1.2A). The FAT domain surrounds and stabilizes the kinase domain while the FATC domain is required for activation and the PRD domain regulates kinase activity through interactions with activators (Fig. 1.2 B-D) (Mordes et al., 2008a; Banin et al., 1998; Priestley et al., 1998; Baretić and Williams, 2014). The N-terminus of PIKKs are less well conserved but consist of large numbers of Huntingtin, Elongation factor 3, a subunit of protein phosphatase 2A and TOR1 (HEAT)-repeat domains that help mediate protein-protein interactions (Perry and Kleckner, 2003; Baretić and Williams, 2014). Additionally, all three kinases harbor S/TQ motifs,

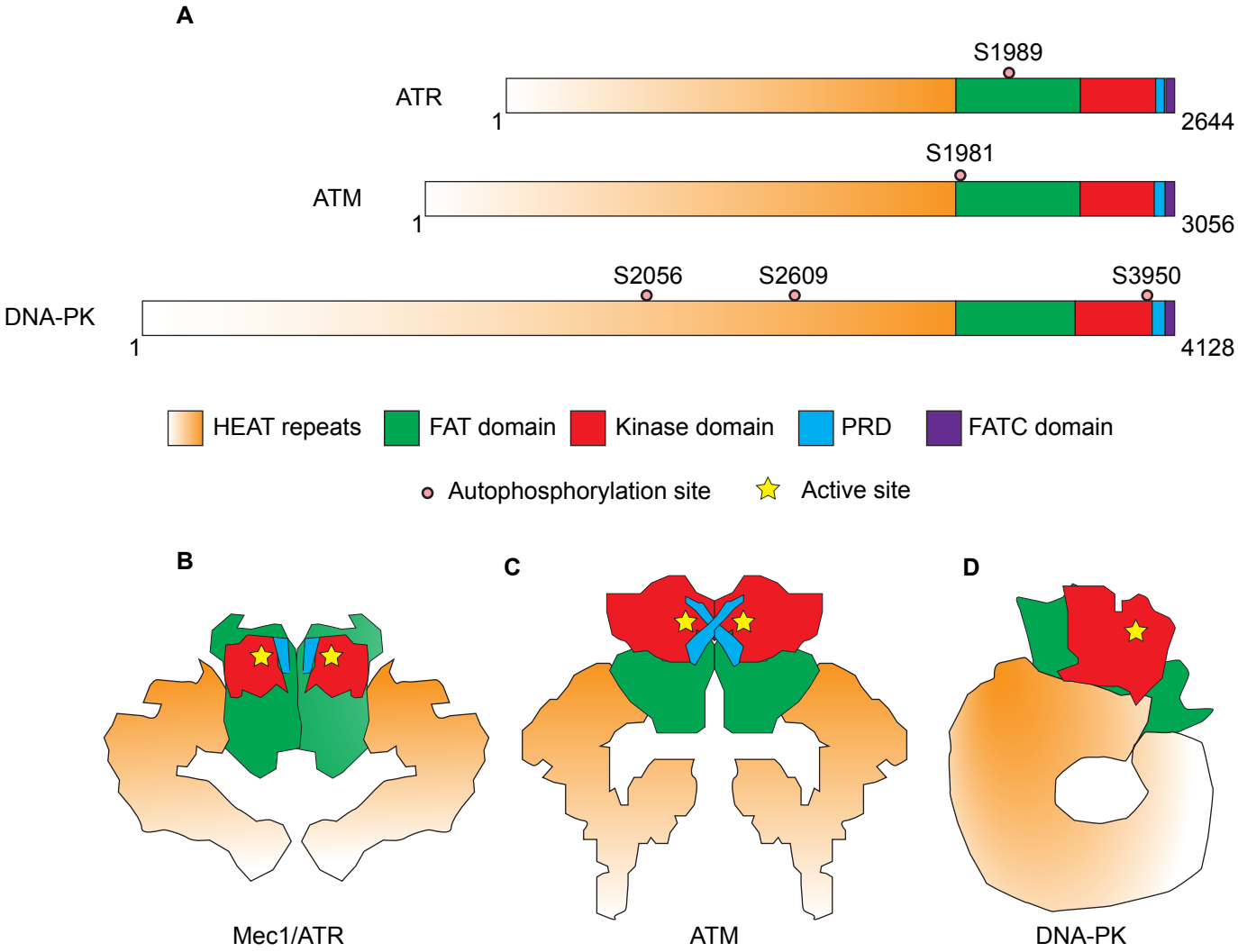

Figure 1.2 Domain layout and structure similiarities of ATR, ATM, and DNA-PK. **(A)** Diagram of ATR, ATM, and DNA-PK domain structures showing location of the FAT, kinase, PRD, and FATC domains. **(B-D)** Cartoons of the three demensional structures of ATR/Mec1, ATM, and DNA-PK. Cartoons were produced from structures detailed in (Imseng et al., 2018). The inactive dimeric form of Mec1/ATR is shown in **B** and the inactive dimeric form of ATM is shown in **C**. The monomeric form of DNA-PK is shown in **D**.

which they can autophosphorylate (Fig. 1.2A) (Blackford and Jackson, 2017). These autophosphorylation marks are important indicators of kinase activation and may regulatekinase activity (Nam et al., 2011b; Bakkenist and Kastan, 2003; Chan et al., 2002). In addition to sequence similarities, all three kinases share three dimensional structural similarities, a C-terminal head unit composed of the FAT-kinase-FATC domains and a N-terminal cradle/solenoid unit composed of the heat repeats. (Fig. 1.2 B-D) (Wang et al., 2017, 2016; Sibanda et al., 2017; Sawicka et al., 2016; Imseng and Aylett, 2018).

Ensuring proper activation of the DDR, all three kinases share common regulatory themes (Lovejoy and Cortez, 2009). DDR kinase activity is dependent on recruitment to specific DNA lesions by a DDR sensor protein. Additionally, the DDR kinases require an activating protein to simulate kinase activity. In mammalian cells, Ku70/Ku80 both recruits and activates DNA-PK at DNA ends (Gottlieb and Jackson, 1993). Similarly, the MRN complex serves dual functions to recruit and activate ATM (Lee and Paull, 2005). RPA bound to ssDNA recruits ATR via its obligate interaction partner ATRIP (Cortez et al., 2001; Zou and Elledge, 2003), while the ATR-activating proteins TOPBP1 and ETAA1 stimulate its kinase activity (Kumagai et al., 2006; Haahr et al., 2016; Bass et al., 2016).

DNA-PK and non-homologous end joining

DSBs are one of the most threatening DNA lesions to a cell and are caused by exogenous sources such as ionizing radiation and endogenous sources such as reactive oxygen species derived as metabolic byproducts (Mehta and Haber, 2014). DNA-PK primarily regulates a small group of proteins in response to DSBs to promote repair through a pathway called non-homologous end joining (NHEJ) (Fig 1.3). NHEJ is the preferred DSB repair

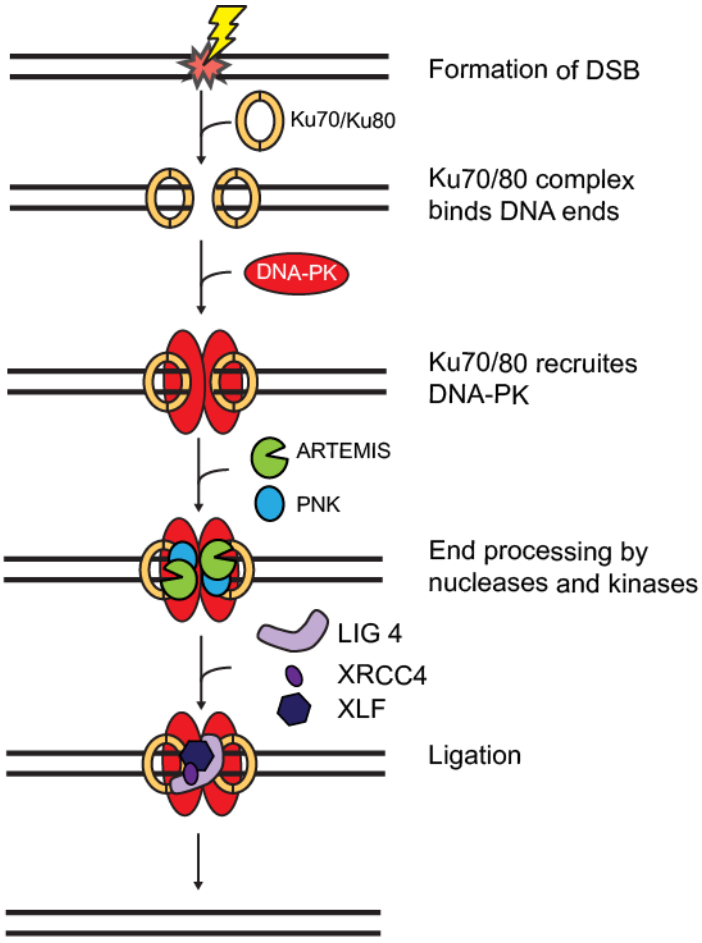

Figure 1.3 DNA-PK and DSB repair by non-homologous end joining. DNA ends are rapidly bound by the Ku70/Ku80 heterodimer which recruits DNA-PK. Nucleases such as ARTEMIS and kinases such as PNK process incompatible DNA ends prior to ligation by XRCC4/XLF/Lig4.

pathway in mammalian cells and is utilized throughout the cell cycle. Within seconds of DSB formation, DNA ends are bound by the Ku70/Ku80 heterodimer which recruits DNA-PK stabilizing the break and preventing extensive end resection (Mahaney et al., 2009). Nucleases such as ARTEMIS and kinases such as PNK (polynucleotide 5'-hydroxyl-kinase) process incompatible DNA ends prior to ligation by XRCC4 (X-ray repair cross-complementing protein 4)/XLF (XRCC4-like factor) /LIG4 (DNA Ligase 4) (Mahaney et al., 2009; Chiruvella et al., 2013).

ATR/ATM kinases

ATR and ATM are large (>300 kDa), evolutionarily conserved kinases that can phosphorylate hundreds of proteins in response to DNA damage or replication stress (Matsuoka et al., 2007). There is extensive overlap of the proteins phosphorylated by ATM and ATR and both signal through downstream checkpoint kinases, CHK1 (Checkpoint kinase 1) and CHK2 (Checkpoint Kinase 2) although ATR preferentially phosphorylates CHK1 while ATM phosphorylates CHK2.

Despites their similarities both kinases have distinctive cellular functions and mechanisms of regulation. ATM forms dimers in the absence of stress but takes on an active monomeric form following DNA damage (Bakkenist and Kastan, 2003). ATR forms a heterodimer with its obligate binding partner, ATRIP (ATR-Interacting Protein) (Cortez et al., 2001). Furthermore, ATR and ATM respond to different types of DNA damage. DSBs activate ATM while a wide range of lesions including stalled replication forks, RNA-DNA loops (R-loops), and unprotected telomere ends activate ATR.

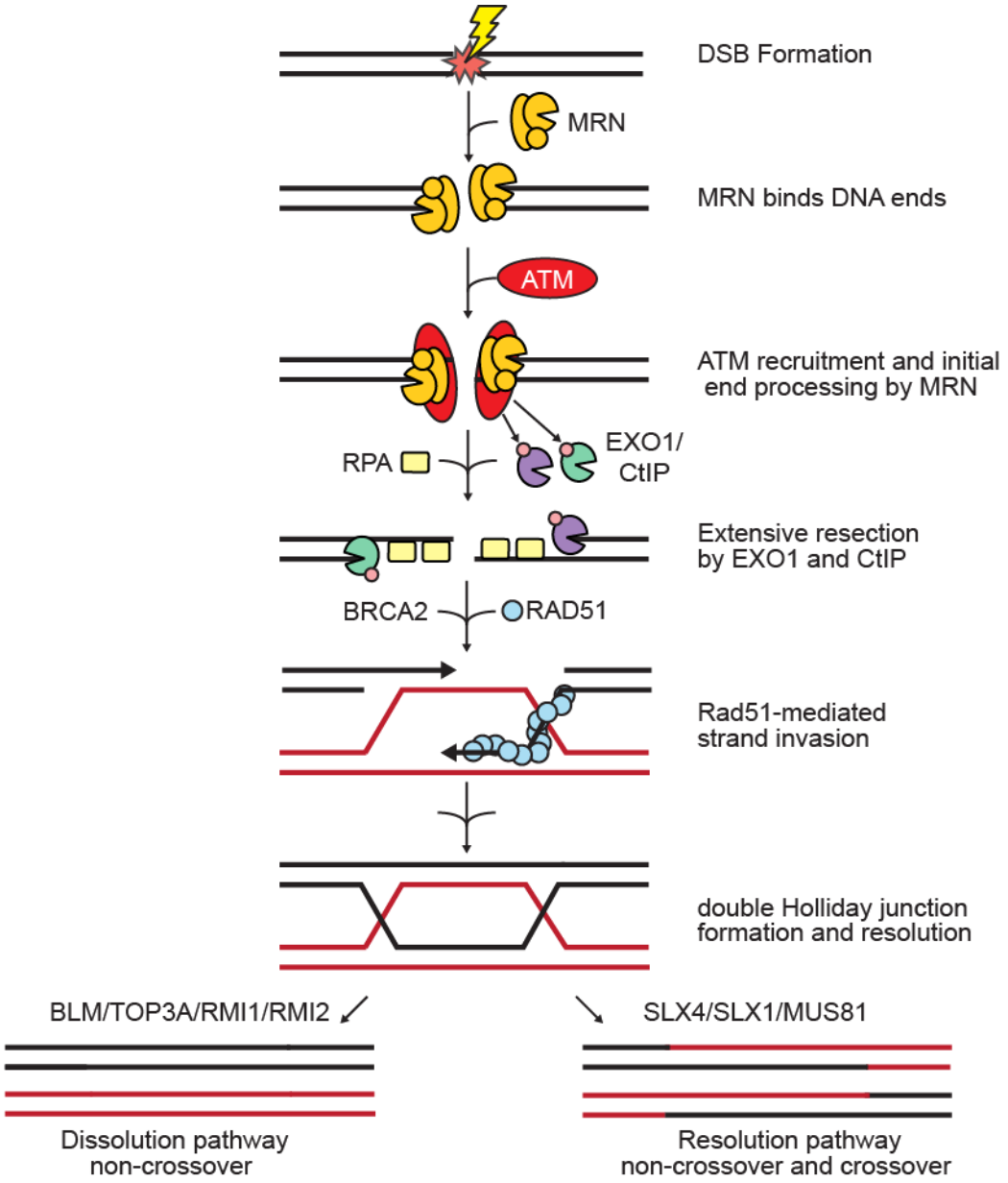

Figure 1.4 ATM and DSB repair by homologous recombination. Following formation of a DSB, DNA ends are bound by the MRN complex which completes the initial steps of DNA resection and recruits and activates ATM. ATM phosphorylation of CtIP and EXO1 stimulates DNA resection generating ssDNA bound by RPA. BRCA2 mediates displacement of RPA on ssDNA and promotes assembly of RAD51 filaments leading to strand invasion of homologous DNA. Polymerases extend the invading strand using the homologous DNA as a template. Once replicated past the break, capture of the second end of the invading strand forms a double Holliday junction (dHJ). Removal of the dHJ occurs through dissolution by the BTR complex or resolution by structure specific nucleases generating non-crossover and crossover recombination products respectively.

ATM and homologous recombination

ATM promotes the repair of DSBs through homologous recombination (HR), a pathway that utilizes a homologous DNA sequence as a repair template promoting error-free repair (Fig 1.4). The requirement for a homologous DNA template limits HR to S and G_2 phases of the cell cycle when a sister chromatid is available. Following DSB formation, DNA ends are bound by the MRN complex which completes the initial steps of DNA resection and recruits and activates ATM (Williams et al., 2007; Lee and Paull, 2005). ATM regulation of DNA end resection is a determinate of DSB repair choice, promoting HR over NHEJ. ATM phosphorylation of CtIP (CTBP-Interacting Protein) and EXO1 (Exonuclease 1) stimulates DNA end resection generating ssDNA bound by RPA (Bolderson et al., 2010; You and Bailis, 2010). BRCA2 with DSS1 mediates displacement of RPA on ssDNA and promotes assembly of RAD51 filaments leading to strand invasion of homologous DNA. Polymerases extend the invading strand using the homologous DNA as a template. Once replicated past the break, capture of the second end of the invading strand forms a double Holliday junction (dHJ). Removal of dHJs occurs through dissolution by BLM (Bloom syndrome protein)/TOPOIII-α (DNA topoisomerase III-α) or resolution by structure specific nucleases, generating non-crossover or crossover recombination products respectively (Raynard et al., 2006; Wu et al., 2006; Bussen et al., 2007).

ATR and the replication stress response

In human cells, the process of DNA replication requires accurately replicating more than 6 billion base pairs of DNA in just a matter of hours. This already daunting task is even more challenging considering cells must overcome several obstacles to replication such as DNA lesions, common fragile sites, repetitive sequences, DNA secondary structure, and collisions with transcription machinery (Fig. 1.5 A-F) (Zeman and Cimprich, 2014). All these impediments

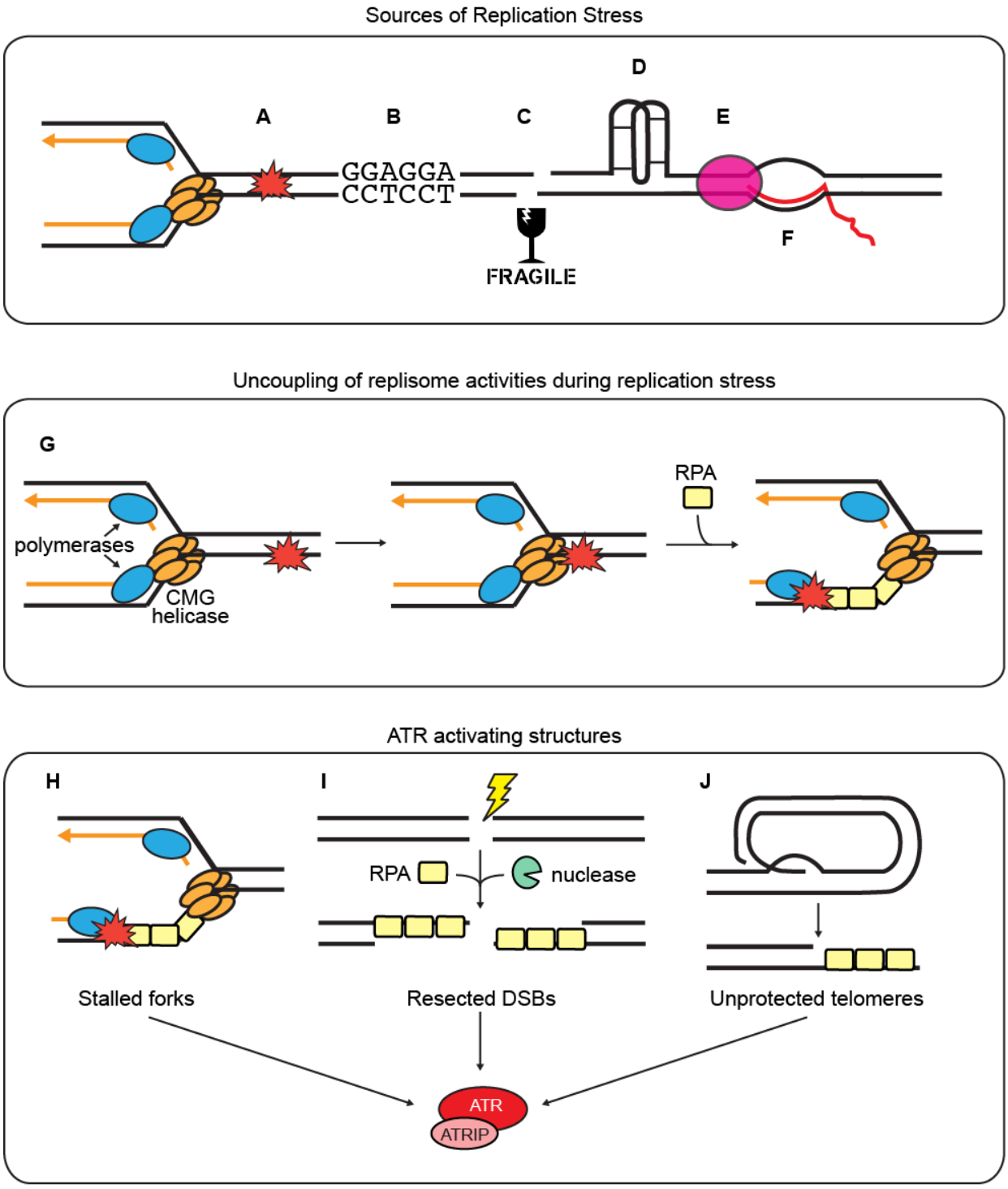

Figure 1.5 Sources of replication stress and ATR activating structures. Replication stress can arise from a variety of sources such as DNA lesions **(A)**, repetitive sequences **(B)**, common fragile sites **(C)**, DNA secondary structures **(D)**, collisions with transcription machinery **(E)**, and R-loops **(F)**. **(G)** When the replisome encounters a DNA lesion it can be bypassed by the CMG replicative helicase but may block progression of the polymerase. Uncoupling of helicase and polymerase activities at a stalled fork generates ssDNA which is bound by RPA. ATR is recruited to RPA coated ssDNA and can therefore respond to a wide range of genomic threats such as stalled replication forks **(H)**, resected double strand breaks **(I)**, and unprotected telomeres **(J)**.

block DNA replication and can cause slowing or stopping of the replication fork termed replication stress (RS). A failure to manage RS can occlude completion of DNA replication resulting in genome instability.

To counteract RS, cells utilize ATR to activate a component of the DDR called the replication stress response (RSR). RS can arise from many sources but results in one common aberrant DNA structure, ssDNA. Replication stressors stall polymerase activity, resulting in uncoupling of helicase and polymerase activities at the replication fork generating ssDNA (Fig. 1.5 G). RPA binds ssDNA that accumulates at sites of RS and recruits the master regulator of the RSR, ATR. Following stimulation of kinase activity by an activating protein, ATR phosphorylates downstream effector proteins, such as CHK1 promoting replication fork stabilization, cell cycle arrest, and inhibition of new origin firing (Cimprich and Cortez, 2008). ATR activation and cellular responses to ATR signaling is closely examined in subsequent chapters.

In conclusion, three PIKKs, DNA-PK, ATM, and ATR regulate the DDR, coordinating responses to genotoxic stress. DNA-PK and ATM primarily direct cellular responses to DSBs while ATR responds to various DNA lesions and replication stress. Of the three master DDR regulators, only ATR is required for life in human cells. This final difference emphasizes the essential nature of ATR to maintain genome integrity. The widespread functions of ATR to manage replication stress and regulate checkpoints throughout the cell cycle is detailed below.

Regulation of ATR activity

Recruitment of ATR by RPA-ssDNA

A wide range of genomic stressors recruit and activate ATR such as stalled replication forks, dsDNA breaks, and unprotected telomeres (Fig. 1.5 H-J). While diverse in their

composition and origin, these stressors have one common DNA structure that recruits ATR, single stranded DNA (ssDNA) coated by RPA.

RPA is a heterotrimeric complex composed of RPA1 (70 kDa subunit), RPA2 (32 kDa subunit), and RPA3 (14 kDA subunit) (Zou et al., 2006). RPA is an indispensable component of all DNA metabolic pathways such as DNA replication, DNA repair, and cell cycle checkpoints. RPA binds ssDNA using four OB (oligonucleotide/oligosaccharide-binding) fold domains, three of which reside in RPA1 while the remaining OB fold is located in RPA2. RPA also contains two primary protein-protein interaction domains, the RPA70N domain of RPA1 and the RPA32C domain of RPA2, that facilitate recruitment of DNA replication and repair proteins. Additionally, post-translational modifications (PTMs) of RPA, such as phosphorylation by ATR, ATM, and DNA-PK, minimalize ssDNA generation and stimulates DNA repair (Vassin et al., 2009; Anantha et al., 2007).

During RS, RPA binds and protects ssDNA, functioning as a platform to recruit additional DNA repair proteins. Indeed, RPA coated ssDNA is the underlying signal that initiates the RSR by recruiting ATR/ATRIP (Zou and Elledge, 2003). RPA recruitment of ATR/ATRIP is mediated by a direct interaction between the basic cleft of the RPA70N domain of RPA1 and a conserved acidic domain in ATRIP (Ball et al., 2007). However, recruitment of ATR to sites of replication stress is not sufficient for its activation, an activating protein must also interact with ATR to stimulate its kinases activity. The requirement for two independently recruited proteins to localize to sites of RS is a regulatory mechanism that ensures appropriate activation of ATR only during RS. In yeast, three activators regulate the ATR-orthologue, $Mec1^{ATR}$ (Mitosis entry checkpoint 1), while vertebrates have two known activators of ATR, TOPBP1 and ETAA1.

Mec1^{ATR} activation

The RSR is highly conserved throughout eukaryotes. As in mammalian cells, initiation of the RSR in *Saccharomyces cerevisiae* begins with recruitment of Mec1^{ATR} to RPA coated ssDNA through an interaction with Ddc2^{ATRIP}. Activation of Mec1^{ATR} relies on three activating proteins, Dpb11^{TOPBP1} (DNA replication regulator DPB11), Ddc1^{Rad9} (DNA Damage Checkpoint 1) and Dna2 (DNA synthesis defective 2) (Mordes et al., 2008b; Navadgi-Patil and Burgers, 2009, 2008a; Kumar and Burgers, 2013). Dpb11^{TOPBP1} is an essential protein required for DNA initiation and is the yeast orthologue of TOPBP1. Recruitment of Dpb11^{TOPBP1} to sites of replication stress is dependent on the interaction with Ddc1^{Rad9}, a member of the heterotrimeric 17-3-1 checkpoint clamp composed of Rad17^{Rad1}, Mec3^{Hus1}, and Ddc1^{Rad9}. RPA directs loading of the 17-3-1 checkpoint clamp to 5' ssDNA-dsDNA junctions through interactions with the Rad24-RFC (Replication factor C) clamp loading complex (Majka et al., 2006). After localization of both Mec1^{ATR} and Dpb11^{TOPBP1} to sites of RS, Dpb11^{TOPBP1} interacts with Mec1^{ATR} stimulating its kinase activity.

Ddc1^{Rad9} has dual functions in Mec1^{ATR} activation. In addition to recruiting Dpb11^{TOPBP1}, Ddc1^{Rad9} can also directly activate Mec1^{ATR}.(Navadgi-Patil and Burgers, 2009) This ability appears to be unique to *Saccharomyces cerevisiae* as Ddc1^{Rad9} orthologues in *Schizosaccharomyces pombe* and higher eukaryotes do not share this activity.

Similarly, Dna2 is a multifunctional enzyme moonlighting as a Mec1^{ATR} activator (Kumar and Burgers, 2013). Dna2 is a dual nuclease/helicase required for Okazaki fragment maturation. Mec1^{ATR} activation does not require either enzymatic activity but instead utilizes the unstructured N-terminal tail of Dna2. Although human DNA2 is also a nuclease/helicase that processes Okazaki fragments, it has not been shown to activate ATR.

The three Mec1^{ATR} activators function to regulate timing of Mec1 activation and direct what substrates get phosphorylated. The cell-cycle-specific utilization of each MEC1 activator allows for temporal regulation of Mec1 throughout the process of cell division (Navadgi-Patil and Burgers, 2011). Ddc1^{Rad9} activates Mec1^{ATR} during G_1, while both Ddc1^{Rad9} and Dpb11^{TOPBP1} activate Mec1^{ATR} during G_2 (Navadgi-Patil et al., 2011; Navadgi-Patil and Burgers, 2009). During S-phase, all three Mec1^{ATR} activators contribute to Mec1^{ATR} activation with partial redundancy. Only after mutation of all three activators is Mec1^{ATR} activity abolished. Additionally, Mec1^{ATR} activators direct Mec1^{ATR} to phosphorylate substrates proximal to the activator allowing their localization to dictate Mec1^{ATR} signaling (Lanz et al., 2018).

ATR activation by TOPBP1

As previously mentioned, the RSR begins with ATR/ATRIP recruitment to RPA-coated ssDNA. However, localization of ATR to sites of RS is not sufficient to trigger ATR signaling, an activating protein is also required to stimulate ATR kinase activity. In vertebrates, two activating proteins, TOPBP1 and ETAA1 can subsequently trigger ATR activity. My graduate studies focused on identifying ETAA1 as a novel ATR activating protein and examining how ETAA1 or TOPBP1 activation of ATR influences ATR signaling.

Originally identified in a yeast two-hybrid screen as a Topoisomerase II β-interacting protein (Yamane et al., 1997), TOPBP1 was the first identified ATR activator (Kumagai et al., 2006). TOPBP1 is a large (173 kDa), conserved protein containing nine BRCA1 carboxyl-terminal (BRCT) motifs. TOPBP1 orthologues in budding and fission yeast, Dpb11 and Cut5, have functions in both DNA replication and checkpoint activation (Saka and Yanagida, 1993; Araki et al., 1995). Likewise, TOPBP1 serves dual functions and is required for initiation of DNA replication (Garcia et al., 2005). TOPBP1 is required for cell viability and even a single point mutation in the TOPBP1-ATR activation domain (AAD) results in embryonic lethality in mice (Zhou et al., 2013).

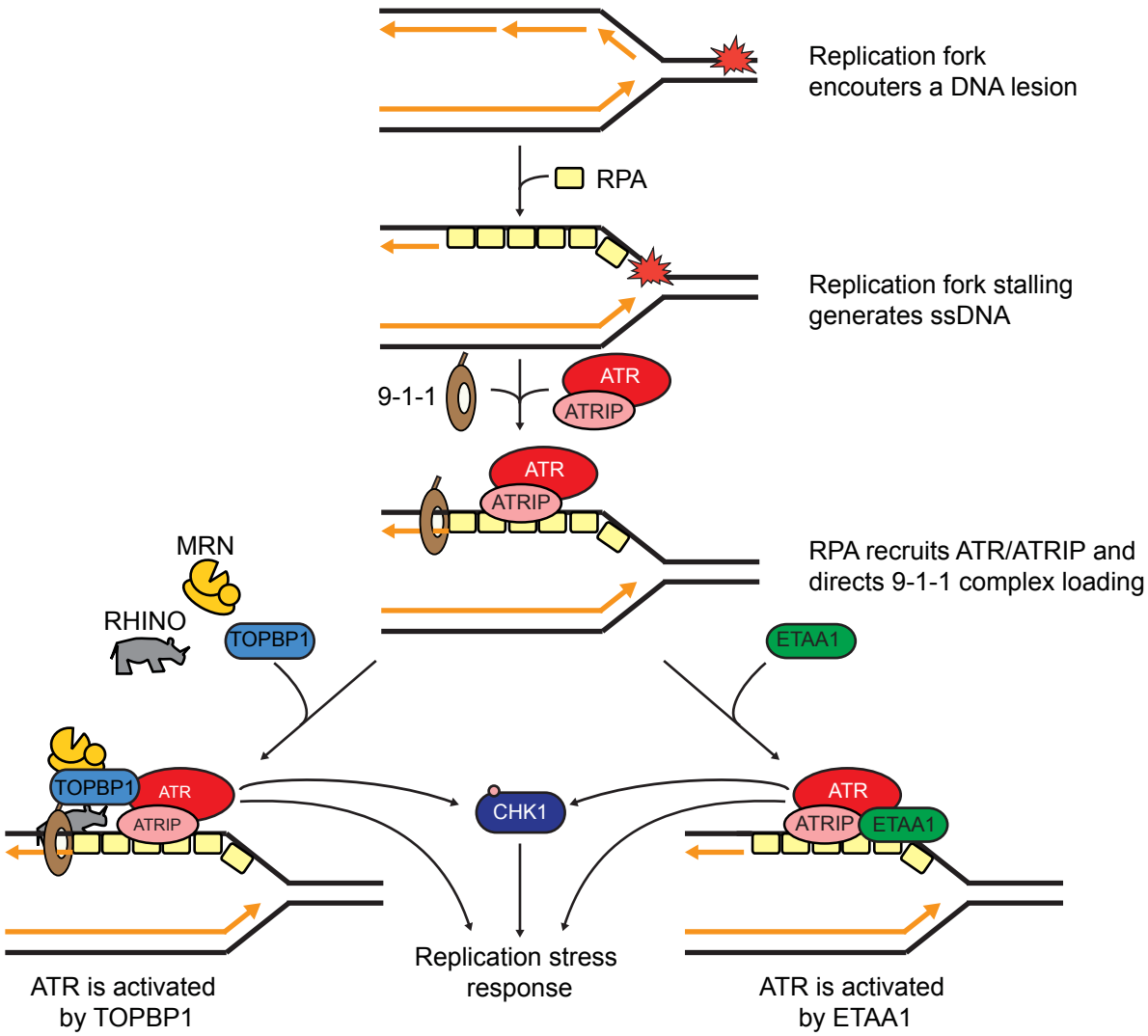

Figure 1.6 ATR and the replication stress response. DNA lesions stall polymerase activity resulting in uncoupling of helicase and polymerase activities generating ssDNA. RPA binds ssDNA, then recruits the ATR/ATRIP complex and directs loading of the 9-1-1 complex by RAD17-RFC. TOPBP1 is recruited to sites of replication stress and stimulates ATR through interactions with Rad9 of the 9-1-1 complex, MRN, and RHINO. ETAA1 is recruited to sites of replication stress by RPA and can activate ATR independent of TOPBP1/Rad9. Once activated, ATR can phosphorylate downstream effectors such as CHK1 which further propagates the signal promoting replication stress response.

TOPBP1 activation of ATR is well conserved throughout eukaryotes and homologous to Dpb11 activation of Mec1. Recruitment of TOPBP1 to sites of RS occurs through contributions by multiple interaction partners (Fig 1.6). Rad9, a component of the heterotrimeric 9-1-1 checkpoint clamp consisting of Rad9-Rad1-Hus1, recruits TOPBP1 to sites of replication stress through a direct interaction with its phosphorylated C-terminal tail and the first two BRCT domains of TOPBP1 (Delacroix et al., 2007a; Lee et al., 2007a). RPA stimulates the clamp loading activity of the Rad17-RFC clamp loading complex and directs loading of the 9-1-1 checkpoint clamp to 5' ssDNA-dsDNA junctions (Ellison and Stillman, 2003). RHINO (Rad9, Hus1, Rad1 interacting nuclear orphan) associates with the 9-1-1 complex and TOPBP1 through independent domains and is required for full ATR activation, although it does not promote or stabilize the TOPBP1-911 interaction (Cotta-Ramusino et al., 2011; Lindsey-Boltz et al., 2015). In *Xenopus* egg extracts, the MRN complex can recruit TOPB1 to ss/dsDNA junctions independent of the 9-1-1 complex, however 9-1-1 is still required for TOPBP1-dependent ATR activation (Duursma et al., 2013). After recruitment, TOPBP1 interacts with ATR stimulating its kinase activity and activating the RSR.

ATR activation by ETAA1

ETAA1 was originally identified as a cell surface antigen in Ewing's tumors and therein derived its name, Ewing tumor associated antigen 1(Borowski et al., 2006). Subsequent studies, including my own work, have identified ETAA1 as a nuclear protein that can activate ATR (Bass et al., 2016; Haahr et al., 2016; Lee et al., 2016). ETAA1 is a large (103 kDA) protein conserved throughout vertebrates. In addition to interacting with ATR, ETAA1 interacts with the BLM/TOP IIIα/RMI1/RMI2 complex to promote genome stability (Bass et al., 2016). Unlike TOPBP1, cells deficient for ETAA1 are viable in human and mice, albeit ETAA1 knockout mice are born at less than Mendelian frequencies indicating a partial embryonic lethality (Bass et al.,

2016; Haahr et al., 2016; Miosge et al., 2017). Genome-wide association studies (GWAS) found that single-nucleotide polymorphisms at the ETAA1 locus increase pancreatic cancer risk suggesting ETAA1 is a cancer gene (Childs et al., 2015b; Klein et al., 2018; Wu et al., 2012). Additionally, defective ETAA1 in Ewing's tumors may explain why these tumor types have high replicative stress (Nieto-Soler et al., 2016).

Localization of ETAA1 to sites of RS occurs through the same mechanism as ATR/ATRIP, RPA coated ssDNA (Fig. 1.6). ETAA1 directly binds the RPA70N domain of RPA1 and RPA32C domain of RPA2 through two RPA-interaction motifs (Bass et al., 2016; Haahr et al., 2016; Lee et al., 2016; Feng et al., 2016). Both RPA-interaction motifs are sufficient for its localization to sites of RS, however the RPA32C interacting domain of ETAA1 appears to be the primarily localization determinant (Bass et al., 2016). Once localized, ETAA1 can trigger ATR signaling using an AAD with microhomology to the TOPBP1-AAD.

Requirements for ATR/Mec1 activation

Identifying the attributes that constitute an ATR or Mec1 activating protein has been an important focus for examining RSR regulation and identifying novel ATR/Mec1 activating proteins. Although ATR and Mec1 activators share minimal homology there are many common structural themes of ATR/Mec1 activators. First, all ATR/Mec1 activators require a domain that promotes recruitment to sites of RS independent of ATR/Mec1. The interaction between ATR/Mec1 and their activators is inherently weak, preventing non-specific activation away from sites of RS. Therefore, checkpoint activation only occurs if the sustained local concentration of both kinase and activator is sufficiently high. Independent recruitment of ATR/Mec1 and their activators requires at least two different protein complexes to recognize the presence of RS or DNA damage, ensuring activation of ATR/Mec1 only when and where appropriate. Although the means of recruitment to sites of RS is different, loss or mutation of RS localization domains in

ATR/Mec1 activating proteins results in compromised checkpoint signaling (Bass et al., 2016; Haahr et al., 2016; Lee et al., 2007a). Conversely, overexpression of AAD/MADs (Mec1 activation domain) results in aberrant RSR signaling bypassing the requirement for RS or DNA damage (Bass et al., 2016; Kumagai et al., 2006; Haahr et al., 2016; Lanz et al., 2018).

In addition to containing a localization domain, all activators must contain an ATR/Mec1 activation domain (AAD/MAD). While AADs and MADs have limited primary sequence homology all have two aromatic residues located inside an intrinsically disordered domain (Wanrooij et al., 2015). Mutation of just one of these aromatic residues can result in a complete loss of function to activate ATR/Mec1. For example, mutation of tryptophan (W) 107 located in the ETAA1-AAD prevents ETAA1 from activating ATR and phenocopies ETAA1 null cells (Bass et al., 2016). Likewise, mutation of W1147 ablates TOPBP1 ability to activate ATR and results in embryonic lethality in mice (Kumagai et al., 2006; Zhou et al., 2013). While the two aromatic residues are essential for ATR/Mec1 activation, surrounding sequences contribute by stabilizing the interaction between activator and kinase (Wanrooij et al., 2015). Additionally, ongoing work by Cortez lab member Vaughn Thada suggest that a predicted coiled-coil domain is also an essential component of the AADs in ETAA1 and TOPBP1.

ATR regulation of cell cycle checkpoints

ATR activation ensures completion of DNA replication and repair prior to progression to the next stage of the cell cycle. In this section I will outline the functions of ATR to regulate the intra-S-phase checkpoint, S/G_2 checkpoint, G_2/M checkpoint, and mitotic checkpoint and the biological responses of ATR signaling during each checkpoint (Fig. 1.7)

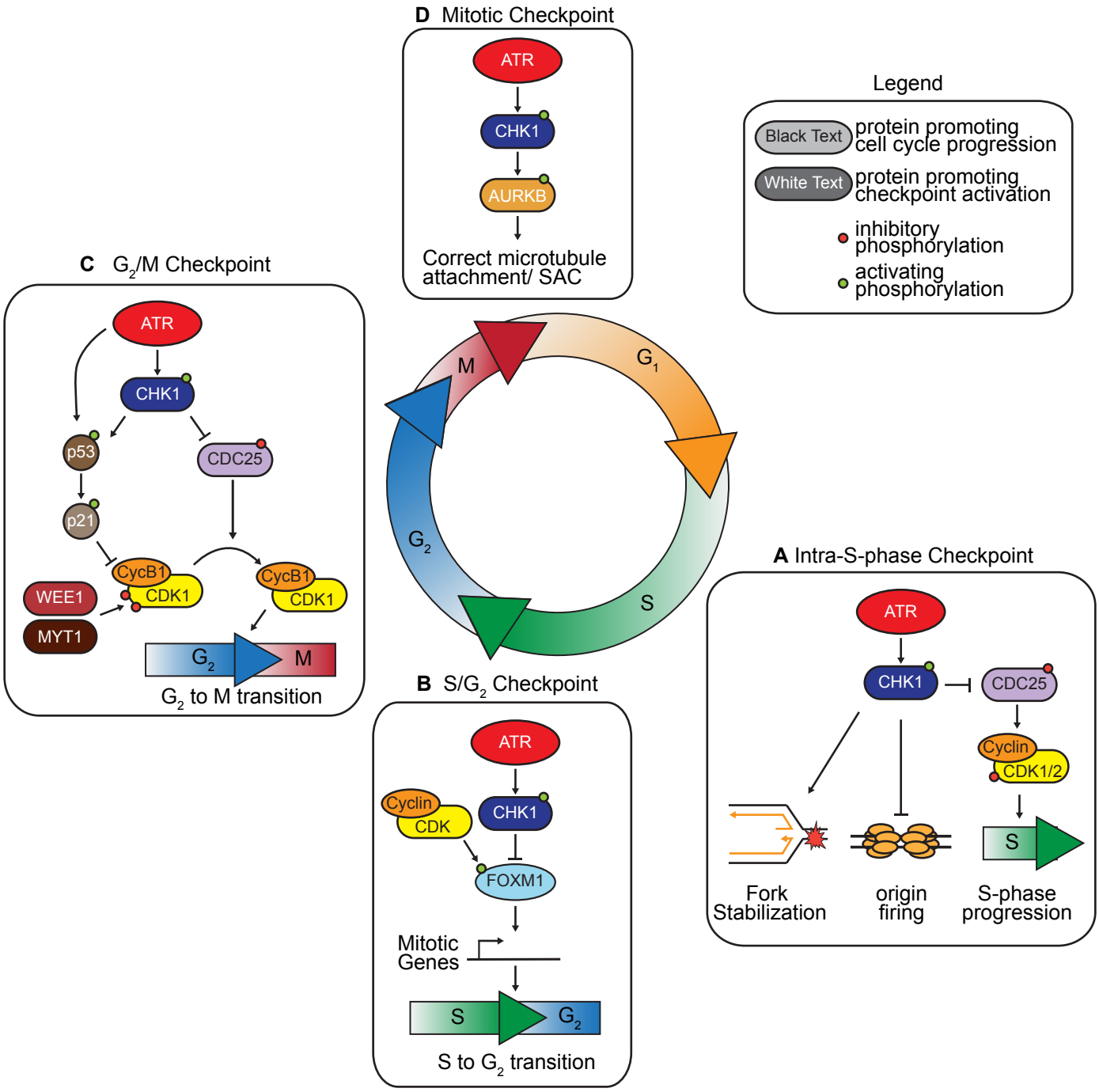

Figure 1.7 ATR regulates checkpoints throughout the cell cycle. **(A)** ATR regulates the intra-S-phase checkpoint promoting fork stabilization, inhibition of origin firing, and blocks S-phase progression. ATR arrests cell cycle progression through CHK1-dependent inactivation of CDC25. CDC25 is a phosphatase that removes inhibitory phosphorylations on the CDK1/2 kinases that drive S-phase progression. **(B)** ATR-CHK1 controls the S/G_2 transition by suppressing phosphorylation of the transcription factor, FOXM1 until completion of DNA replication. Phosphorylation of FOXM1 by CDKs promotes transcription of a mitotic gene network required for the transition to G_2 phase. **(C)** The CDK1/cyclinB complex drives entry into mitosis but is blocked by inhibitory phosphorylations from WEE1 and MYT1. Dephosphorylation of CDK1 by CDC25 promotes entry into mitosis. In the presence of DNA damage, ATR activates CHK1 which inhibits CDC25 activity via phosphorylation. Protracted G_2 arrest is maintained through transcription factors p53 and p21 which regulate expression of CHK1-inhibiting proteins. **(D)** ATR and CHK1 regulate the mitotic checkpoint through phosphorylation of the mitotic kinase Aurora B. Aurora B promotes kinetochore-microtubule attachment and regulates the spindle assembly checkpoint.

ATR regulation of the intra-S-phase checkpoint

Replication stress occurs every S-phase as cells deal with unavoidable obstacles that impede DNA replication such as DNA damage, difficult to replicate sequences, and shortages of deoxynucleotide triphosphate (dNTP) pools. To ensure faithful duplication of the genome, ATR enforces the intra-S-phase checkpoint, activating the RSR and coordinating cell cycle progression with completion of DNA replication. While ATR primarily regulates proteins localized to chromatin and near sites of RS, downstream effector kinases such as CHK1 propagate signaling away from sites of RS and throughout the nucleus. Together this signaling cascade promotes a widespread response affecting almost every nuclear biological process including DNA metabolism, cell cycle regulation, protein metabolism, and gene expression (Matsuoka et al., 2007). Below, I highlight three specific functions of ATR during S-phase to promote genome stability: regulation of origin firing, stabilization of stalled replication forks, and induction of cell cycle arrest.

Regulation of origin firing

Eukaryotic cells prepare for DNA replication during G_1 by loading the minichromosome maintenance complex 2-7(MCM2-7) at origins of replication through a processed called origin licensing (Cook, 2009). During S-phase, origins are activated after the MCM complex interacts with Cdc45 (cell division Cycle 45) and the GINS complex forming the CMG (Cdc45-MCM-GINS) replicative helicase. Although several thousand origins are licensed, only about 10% fire during an unperturbed S-phase, the remainder lying dormant (McIntosh and Blow, 2012). Dormant origins are capable of initiating, but are not required for completion of DNA replication, and are therefore passively replicated by forks originating from neighboring origins.

DNA replication is a temporally organized process with regulated staggering of origin firing ensuring specific chromosomal regions are replicated in early, mid, or late S-phase.

During an unperturbed S-phase, ATR and CHK1 negatively regulate origin firing, preventing premature initiation of late-replicating origins (Cook, 2009). Furthermore, treatment with drugs that induce replication stress cause premature stalling of forks, activating the intra-S-phase checkpoint. ATR activation in response to RS suppresses global firing from late-replicating origins by regulating Cdc45 recruitment to chromatin (Costanzo et al., 2003). Preventing late-firing origins from initiating replication limits widespread polymerase stalling and excessive formation of ssDNA which can result in RPA exhaustion (Couch and Bansbach, 2013; Toledo et al., 2013). While suppressing global origin firing, ATR promotes firing of dormant origins near sites of RS, ensuring completion of replication by neighboring replication forks (Ge and Blow, 2010).

Stabilization of stalled forks

DNA lesions can impede replisome progression resulting in a stalled replication fork. ATR is essential for stabilizing stalled forks, ensuring the stalled polymerase can restart replication following repair or bypass of the lesion. Failure to rescue stalled forks can result in accumulation of ssDNA and depletion of pools of RPA, formation of DSBs by structure-specific nucleases, and replisome dissociation termed fork collapse (Carr et al., 2011; Muñoz et al., 2009; Toledo et al., 2013). Inhibition of ATR during RS suggests that ATR does not regulate replisome stability but protects forks from collapsing by preventing RPA exhaustion through inhibition of origin firing and regulating the activity of fork remodeling enzymes (Fig. 1.8A) (Dungrawala et al., 2015; Couch and Bansbach, 2013).

One replication fork stabilization mechanism regulated by ATR and mediated by helicases such as SMARCAL1 (SWI/SNF, matrix associated, actin dependent regulator of chromatin A-like 1), HLTF (Helicase Like Transcription Factor), and ZRANB3 (Zinc Finger RANBP2-Type Containing 3) is fork reversal (Bansbach et al., 2009; Ciccia et al., 2009, 2012; Yusufzai and Kadonaga, 2010; Kile et al., 2015). During fork reversal, fork remodeling enzymes

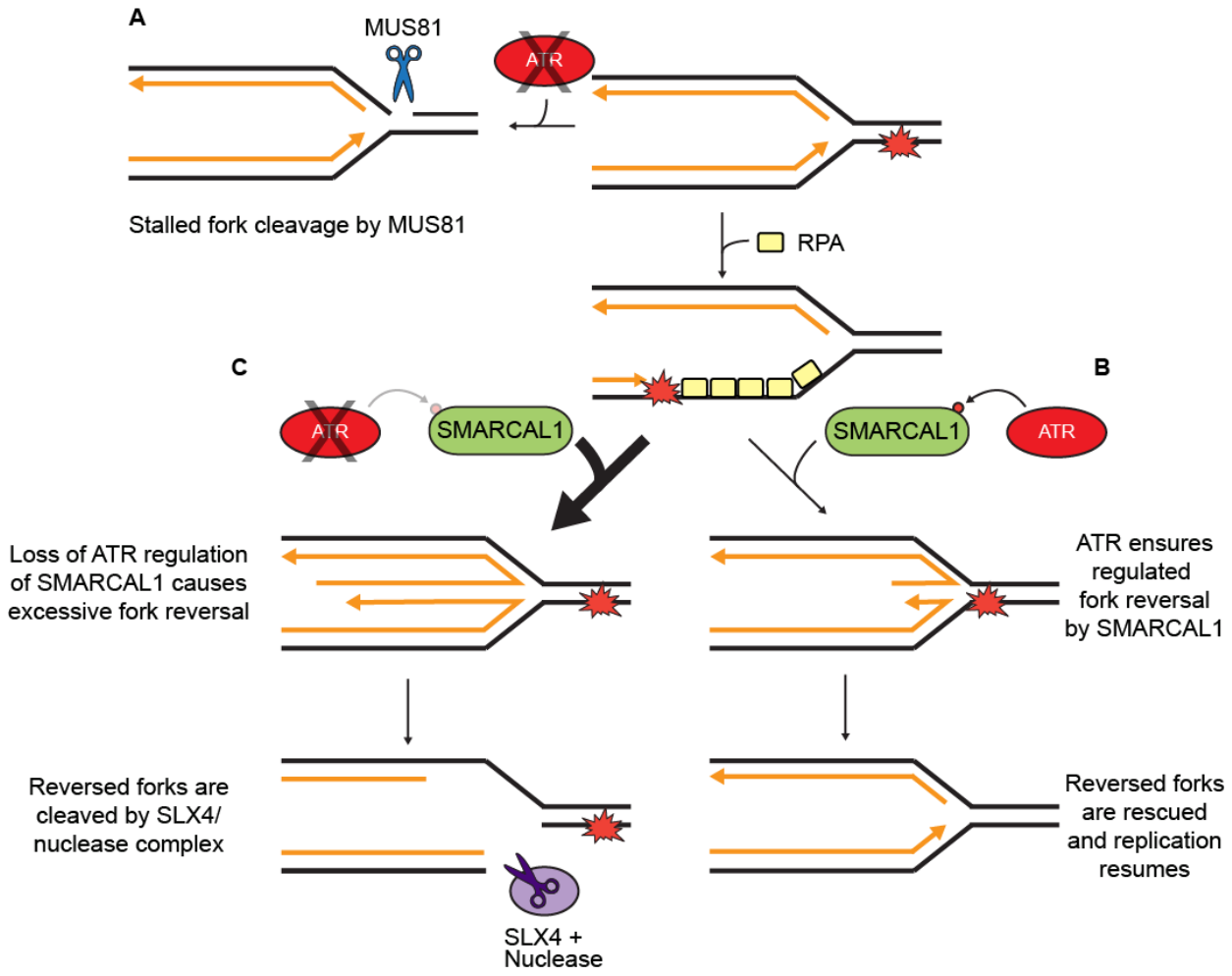

Figure 1.8 ATR stabilizes stalled forks through regulation of SMARCAL1. (A) Loss of ATR activity results in increased double strand breaks during replication stress due to fork cleavage by the nuclease MUS81. To protect forks, ATR regulates a process called fork reversal. During fork reversal, fork remodeling enzymes regress the replication fork, annealing and extruding the newly synthesized strands resulting in a four-way junction resembling a chicken foot. **(B)** ATR phosphorylates the fork remodeling enzyme SMARCAL1 on S652 limiting its activity and ensuring proper fork reversal. Once the lesion is repaired, reversed forks are restored and replication can resume. **(C)** Loss of ATR regulation of SMARCAL1 results in excessive fork reversal and generate a substrate that is cleaved by SLX4 complexed nucleases.

regress the replication fork, annealing and extruding the newly synthesized strands resulting in a four-way junction resembling a chicken foot (Fig. 1.8B). Once conditions are favorable, the reversed fork is rescued by conversion of the four-way chicken foot structure to a standard three-way replication fork and polymerization can resume.

Fork reversal frequently occurs during RS and protects stalled forks by allowing bypass of DNA lesions, halting replication during periods of unsuitable conditions, and preventing ssDNA accumulation that could result in DSBs (Neelsen and Lopes, 2015). Highlighting the importance of fork reversal as an instrument of genome maintenance, many diseases are associated with deficiencies in fork remodeling enzymes. Loss or mutation of the fork remodeling enzymes SMARCAL1, BLM, and WRN (Werner syndrome ATP-dependent helicase), are associated with Schimke immunoosseous dysplasia (SIOD), Bloom's syndrome, and Werner's syndrome respectively (Boerkoel et al., 2002; Carroll et al., 2013; Ellis et al., 1995; Yu et al., 1996). However, fork reversal is a double edged-sword, with excessive fork reversal generating substrates for site-specific nucleases such as MUS81, SLX1/SLX4, and XPF (Couch and Bansbach, 2013).

ATR directly regulates fork reversal through phosphorylation of fork remodeling enzymes such as SMARCAL1 and WRN (Werner syndrome ATP-dependent helicase) (Couch and Bansbach, 2013; Ammazzalorso et al., 2010; Mutreja et al., 2018). ATR prevents excessive fork reversal through phosphorylation of S652 of SMARCAL1, inhibiting its fork remodeling activities (Couch and Bansbach, 2013). Loss of ATR-dependent regulation of SMARCAL1 increases DSB formation due to SLX4-dependent cleavage of reversed forks (Fig. 1.8C). Therefore, ATR regulation of fork reversal stabilizes stalled forks and helps maintain genome integrity.

Cell cycle arrest

Another crucial function of ATR during the intra-S-phase checkpoint is to promote cell cycle arrest during RS. Cyclin dependent kinases (CDKs) form active protein complexes with cyclins to drive cell cycle progression via regulatory phosphorylation networks. The CDC25 phosphatases CDC25A, CDC25B, and CDC26C remove inhibitory phosphates from CDK1 and CDK2 sustaining high CDK activity required for S-phase progression (Saldivar et al., 2017). ATR signaling induces cell cycle arrest by CHK1-dependent phosphorylation and inactivation of the CDC25 phosphatases (Karlsson-Rosenthal and Millar, 2006) (Fig. 1.7A). The mechanism of inhibition for each CDC25 family member varies. Phosphorylation of CDC25A results in its degradation by the proteasome while CDC25C is sequestered in the cytoplasm (Mailand et al., 2000; Peng et al., 1997).

ATR regulation of the S/G_2 checkpoint

In a collaboration with the Cimprich lab, I identified ATR as a regulator of the newly defined S/G_2 checkpoint, ensuring completion of DNA replication before cells enter G_2 (Saldivar et al., 2018). CDK phosphorylation of the transcription factor Forkhead Box M1 (FOXM1) on T600 is required for expression of a G_2/M gene network promoting the transition from S-phase to G_2. During S-phase, ATR and CHK1 repress early onset of G_2 by suppressing phosphorylation of FOXM1 (Fig 1.7B). As S-phase ends, ATR activity declines allowing phosphorylation of FOXM1 and transition to G_2. This ATR function is dependent on ETAA1-acitvation and not a TOPBP1-activation of ATR.

ATR regulation of the G_2/M checkpoint

The G_2/M checkpoint prevents entry into mitosis in the presence of DNA damage. ATR and ATM can both induce the G_2/M checkpoint although the ATR-CHK1 pathway may be the primary regulator (Lin and Dutta, 2007). The CyclinB1/CDK1 complex drives entry into mitosis but phosphorylation on Tyrosine 14 and 15 by MYT1 (myelin transcription factor 1) and WEE1 (WEE1 G_2 Checkpoint Kinase) inactivates the complex (Nigg, 2001). Dephosphorylation of CDK1 by the CDC25 phosphatases activates the CyclinB1/CDK1 complex promoting entry into mitosis. In response to DNA damage, ATR/ATM promote stabilization of WEE1 and inhibition of CDC25 via phosphorylation by CHK1/2 resulting in a G_2 arrest (Fig 1.7C). Additionally, ATR/ATM can promote protracted G_2 arrest through a pathway dependent on the transcription factors p53 and p21 which regulate expression of CDK1-inhibiting proteins (Lukas et al., 2004). Counteracting the checkpoint signal, Wip1, PP2A, PP4, and PP6 remove inhibitory or stimulating phosphate groups on WEE1, CDC25, and p53. ATR/ATM signaling diminishes as DNA repair progresses, further reducing the checkpoint signal and coordinating release from G_2 arrest with completion of DNA repair (Deckbar et al., 2011).

ATR regulation of the mitotic checkpoint

Spindle Assembly Checkpoint (SAC)

ATR and CHK1 are also active during mitosis and function to promote Aurora B kinase signaling, chromosome stability and alignment, and robust activation of the mitotic checkpoint also referred to as the spindle assembly checkpoint (SAC). The SAC maintains genome integrity by delaying anaphase onset until accurate bipolar attachment of all chromosomes to the mitotic spindle ensuring equal separation of genetic material into the dividing daughter cells (Fig. 1.9) (Lara-Gonzalez et al., 2012).

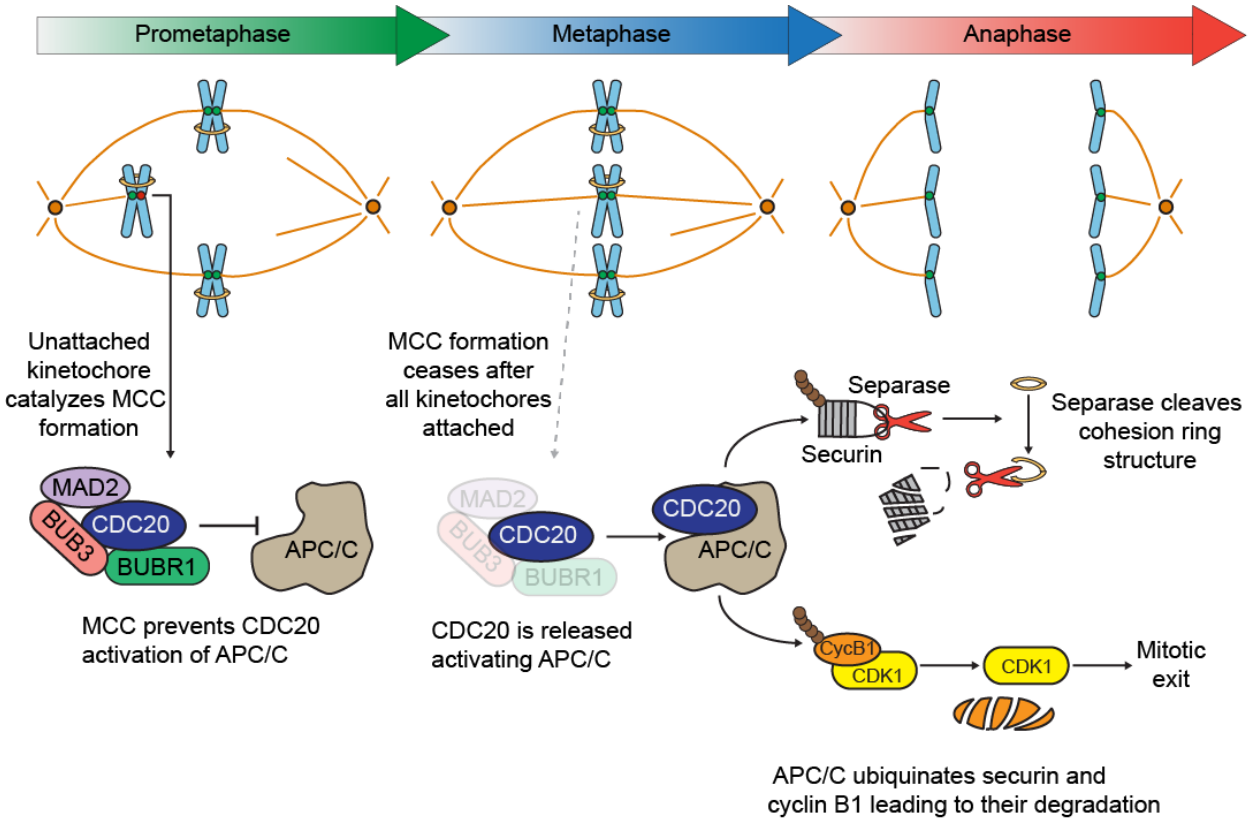

Figure 1.9 Spindle Assembly Checkpoint. During prometaphase, unattached kinetochores catalyze the formation of the mitotic checkpoint complex (MCC) composed of MAD2, BUB3, BUBR1, and CDC20. Once all kinetochores are attached to the mitotic spindle, MCC formation ceases releasing CDC20 to activate the E3 ubiquitin ligase APC/C. APC/C ubiquinates securin and cyclin B1 leading to their degradation. Degradation of securin releases separase which cleaves a subunit of the cohesion ring structure allowing the sister chromatids to separate, beginning anaphase. Degradation of cyclin B1 inactivates CDK1 promoting mitotic exit.

Following completion of DNA replication, cohesion proteins hold duplicated chromosomes together maintaining their identity as sister chromatids until separation at anaphase. The SAC ensures accurate chromosome segregation by preventing cohesion ring opening until correct alignment of all chromosomes on the mitotic spindle. This is achieved by formation of the mitotic checkpoint complex (MCC) composed of BUBR1, BUB3, MAD2 and CDC20 at unattached kinetochores. Kinetochores are complex structures composed of at least 80 different proteins assembled at the centromere of each sister chromatid and serve as an attachment site for spindle microtubules. The kinase BUB1 mediates recruitment of the MCC components to unattached kinetochores catalyzing formation of the MCC (Meraldi and Sorger, 2005). BUBR1 and MAD2 inhibit anaphase onset by directly binding CDC20 preventing it from activating the anaphase promoting complex (APC/C) (Lara-Gonzalez et al., 2012).

The APC/C is an E3 ubiquitin ligase complex that targets proteins for degradation, such as mitotic cyclins and securin (Pines, 2011). Once all kinetochores are properly attached, the MCC complex releases CDC20 allowing activation of APC/C and promoting entry into anaphase. Anaphase onset is promoted by degradation of CyclinB1 inactivating CDK1 and degradation of securin, an inhibitor of the protease separase. Once released, separase cleaves a subunit of the cohesion ring structure allowing ring opening and separation of the sister chromatids.

ATR and CHK1 function during mitosis

CHK1 was first tied to the mitotic checkpoint in yeast and flies after loss of CHK1 delayed the onset of anaphase in mitotic cells following induction of DNA damage (Collura et al., 2005; Royou et al., 2005). Subsequent studies found that both CHK1 and ATR regulate the mitotic checkpoint through CHK1-dependent phosphorylation of the mitotic kinase Aurora B (Fig. 1.7D) (Zachos et al., 2007; Peddibhotla et al., 2009; Petsalaki et al., 2011; Kabeche et al., 2017). Aurora B kinase contributes to a number of mitotic processes such as kinetochore

stabilization, kinetochore-microtubule attachment, and regulation of the SAC (Krenn and Musacchio, 2015). During mitosis, ATR can localize to centromeres through an Aurora A-regulated interaction with CENPF, allowing it to bind RPA-coated R-loops. Once activated, ATR promotes CHK1 phosphorylation of Aurora B preventing formation of lagging chromosomes. Additionally, loss of mitotic CHK1-Aurora B activity causes chromosome missegregation and reduced recruitment of SAC proteins such as BubR1 to kinetochores (Zachos et al., 2007; Petsalaki et al., 2011). Due to deficiencies in the SAC, cells treated with small molecular inhibitors of ATR and CHK1 are unable to sustain mitotic arrest in the presence of taxol (Zachos et al., 2007).

My work described in Chapter IV expands the functions of ATR during mitosis and demonstrates that the ATR-activator ETAA1 is required for mitotic ATR activation at centromeric regions. Loss of ETAA1 results in reduced phosphorylation of SAC proteins such as BUB1 and BUBR1 and decreased histone 3 phosphorylation. Additionally, loss of ETAA1-dependent ATR signaling results in decreased Aurora B kinase activity, chromosomal misalignment, and decreased SAC activity. While TOPBP1 was not required for ATR activation at kinetochores, previous studies indicate that TOPBP1 does function during mitosis at sites of under-replication but that it is independent of ATR signaling (Pedersen et al., 2015). Additionally, TOPBP1 localizes to ultra-fine anaphase bridges and promotes their resolution through direct recruitment of topoisomerase IIα. (Germann et al., 2014; Broderick et al., 2015). Therefore, while TOPBP1 is active during mitosis, its functions do not appear tied to ATR activation.

In conclusion, ATR is an essential protein required for proper cell cycle progression and genome maintenance. ATR phosphorylates hundreds of proteins regulating DNA metabolic processes throughout the cell cycle. As a result, defects in ATR signaling pathways make proliferating cells susceptible to genome instability. Therefore, small molecule inhibitors to ATR and other DDR proteins are currently being evaluated as potential cancer therapies.

Targeting ATR in cancer

Cancer is a tremendous threat to human health, with an estimated 18 million people predicted to develop cancer this year (Bray et al., 2018). Mutations in oncogenes or tumor suppressors drive cancer development, causing unrestrained growth of abnormal cells. In cancer, the normally highly ordered process of cell division is deregulated, allowing cells to bypass cell cycle checkpoints without having met the criteria required to proceed to the next stage of the cell cycle. Although this gives cancer cells limitless replicative potential, they are ill prepared for the challenging task of DNA replication. Therefore, a hallmark of all cancers is increased replication stress (Macheret and Halazonetis, 2015). Replication stress in cancer cells can be traced to a number of sources such as deregulated origin licensing, shortages of doxynucleotides, and increased transcription during S-phase, causing increased collisions between replication and transcription machinery (Macheret and Halazonetis, 2015). Additionally, most cancers have deficiencies in one or more pathways of the DDR due to selective pressures occurring during tumor development (Jackson and Bartek, 2009).

To exploit these disadvantages, the most prevalent non-invasive cancer treatments are radiotherapy and chemotherapies that generate DNA damage. Ionizing radiation therapy induces free radicals and reactive oxygen species which damage DNA forming single-stranded and double-stranded breaks. Common chemotherapeutic agents also induce DNA damage or RS, such as platinum salts which cause interstrand DNA crosslinks, topotecan which traps topoisomerase I on DNA, and gemcitabine which inhibits ribonucleotide reductase (RNR) depleting levels of deoxyribonucleotide triphosphates (dNTPs). DNA-damaging therapeutic agents are advantageous due to their higher toxicity in cancer cells than most normal cell types. Genotoxic agents are most lethal during S-phase, when cells are particularly vulnerable to DNA-

damage. Therefore, rapidly proliferating cells, such as cancer cells, are more likely to be targeted by these agents than normal tissues, which are mostly composed of quiescent cells.

The efficacy of DNA-damaging agents can be further improved by inhibition of DDR signaling pathways. Currently, therapies targeting important DDR proteins such as ATR, ATM, and CHK1 are being developed as potential cancer treatments (O'Connor, 2015). Many of these inhibitors are currently in clinical trials in combination with other DNA-damaging therapeutic agents. For example, the ATR inhibitors (ATRi) VX970 and AZD6738 are being currently used with replication stress inducing agents such as gemcitabine, cisplatin, and topotecan (O'Connor, 2015). DDR inhibitors may also prove useful as monotherapies through induction of synthetic lethality. Two genes are synthetically lethal if mutation or inhibition of a gene/protein alone has no effect on cellular viability but defects in both genes/proteins results in cell death (Kaelin, 2005). ATR inhibition is synthetically lethal with loss of ERCC1, XRCC1, CDC25A, and ARID1A (Mohni et al., 2014; Sultana et al., 2013; Ruiz et al., 2016; Williamson et al., 2016). As the ability to sequence tumor DNA and identify specific mutations in cancer becomes a standardized practice of care, synthetic lethal relationships will be more easily exploited.

CHAPTER II

MATERIALS AND METHODS

Antibodies

Table 2.1 Antibodies. Provided are the antibodies used for western blotting (WB), immunofluorescence (IF) and flow cytometry (FC). Antibody concentrations, host, vendor, catalog number, molecular weight and location in the Cortez lab are provided.

Table 2.1 Antibodies

Antibody	Dilution	Species	Company	Catalog Number	Location (Cortez Lab)	Molecular Weight (kDA)	Use
Anti-centromere antibodies (ACA)	1:200	Human	Antibodies Inc.	15-234-0001	Box12-A2		IF
ATM	1:2,500	Rabbit	Abcam	Ab206-1000	Box1-A1	350	WB
ATM pS1981	1:600	Rabbit	Affinity Bio Reagents	PA1-21770	Box5-A3	350	WB
ATR (N-19)	1:1,000	Goat	Santa Cruz	SC-1887	Box1-A3	301	WB
ATR pS1989	1:1,000	Rabbit	Epitomics	VAN 7P	Box7-F5	301	WB
ATRIP 403	1:1,000	Rabbit	Cortez		Box2-A3	86	WB
ATRIP C	1:1,000	Rabbit	Cortez		Box2-A1	86	WB
ATRIP N	1:1,000	Rabbit	Cortez		Box2-A2	86	WB
Aurora B	1:200	Rabbit	Bethyl	A300-431A	Box10-F9	39	IF
Aurora B pT232	1:200	Rabbit	Roche	600-401-677	Box12-B1	39	IF
BLM (C-18)	WB=1:1,000 IF=1:200	Goat	Santa Cruz	sc-7790	EFBox1-G8	159	WB, IF
BLM (H-300)	1:1,000	Rabbit	Santa Cruz	sc-14018	EFBox1-G9	159	WB
BRCA1	1:1,000	Mouse	Calbiochem	OP-92	Box1-B1	220	WB
BRCA2	1:1,000	Mouse	Calbiochem	OP-95	Box9-H8	384	WB
BrdU	1:1,000	Mouse	BD	555627	Box10-A4		IF
BrdU (CldU)	1:100	Rat	Abcam	ab6326	4°		IF
BrdU (IdU)	1:100	Mouse	BD	347580	4°		IF

Bub1	WB=1:1,000 IF=1:200	Rabbit	Bethyl	A300-373A-M	Box10-E7	122	WB, IF
CENPF	WB=1:1,000 IF=1:200	Rabbit	Abcam	ab5	Box12-A4	330	WB, IF
Chk1 (G-4)	1:1,000	Mouse	Santa Cruz	sc-8408	Box3-D3	55	WB
Chk1 pS317	WB=1:1,000 IF=1:200	Rabbit	Cell Signaling	2344S	Box4-A1	55	WB, IF
Chk1 pS345	WB=1:1,000 IF=1:200	Rabbit	Cell Signaling	2341S	Box4-A3	55	WB, IF
Chk2	1:,2000	Rabbit	Cortez		Box2-H5	61	WB
Chk2 pT68	1:1,000	Rabbit	Cell Signaling	2661S	Box 4-A5	61	WB
Cyclin A	1:1,000	A300-373A-M	Santa Cruz	sc-751	Box1-C7	60	IF
ETAA1	1:1,000*	Rabbit	Cortez (Covance)		Box 7-H7	103	WB, IP
ETAA1 (VU446)	1:1,000*	Rabbit	Cortez (Covance)		Box 10-D9	103	WB, IP
FANCD2 (Fi17)	1:1,000	Mouse	Santa Cruz	sc-20022	Box3-D5	166	WB
Flag	WB=1:1,000 IF=1:200	Rabbit	Sigma	F7425	Box3-F8		WB, IF
Flag (M2)	WB=1:1,000 IF=1:200	mouse	Sigma	F-3165	Aliquots in box -20		WB, IF, IP
GAPDH	1:50,000	Mouse	Millipore	MAB374	Box1-F4	36	WB
GFP	WB=1:1,000 IF=1:200	Rabbit	Abcam	ab290	Box12-A1		WB, IF
H2A	1:1,000	Rabbit	Abcam	ab18255	Box4-G8	14	WB
H2A pT120	WB=1:1,000 IF=1:200	Rabbit	Active Motif	61195	Box12-B2	14	WB, IF
H2AX (not phospho)	1:5,000	Rabbit	Bethyl	A300-082A	Box3-H8	17	WB
H2B	1:5,000	Rabbit	Abcam	ab1790	Box5-E7	15	WB
H3	1:5,000	Rabbit	Abcam	ab46765	Box5-A7	15	WB
HA	1:1,000	Rabbit	Abcam	ab9110	Box4-H4		WB
HA	WB=1:1,000 IF=1:200	Rat	Roche	11 867 423 001	Box7-D9		WB, IF
HLTF	1:1,000	Rabbit	Cimprich		Box13-B1	114	WB
Ku70	1:1,000	Mouse	Abcam	ab3114	Box9-C1	70	WB
Ku80	1:500	Rabbit	Abcam	ab33242	Box9-C2	80	WB
MCM2	1:10,000	Mouse	BD	39289		100	WB
MCM2 pS108	1:10,000	Mouse	Bethyl	IHC-00014	Box1-H9	100	WB
MDC1	1:500	Rabbit	Bethyl	BL578	Box3-A6	220	WB
MRE11	1:1,000	Mouse	Gene Tex	GTX30294	Box1-C3	81	WB
MUS81	1:1,000	Mouse	Novus	NBP1-00609N	Box 6-D5	66	WB

ORC2	1:5,000	Rabbit	BD	551178	Box4-G7	66	WB
p53 (DO-1)	1:1,000	Mouse	Santa Cruz	SC-126	Box2 D6	44	WB
p53 pS15	1:1,000	Rabbit	Cell Signaling	9284	Box4-A7	44	WB
PCNA	1:1,000	Rabbit	Santa Cruz	SC-7907	Box2-F4	29	WB
pH3 S10	WB=1:1,000 IF=1:200 FC=1:400	Rabbit	Cell Signaling	3377	Box9-G6	15	WB, IF, FC
pH3 S28	1:200	Rabbit	Upstate	07-145	Box4-F2	15	IF
RAD17	1:2,500	Goat	Bethyl	A300-151A	Box6-G3	77	WB
RAD17 S645	1:1,000	Rabbit	Bethyl		Box3-B7	77	WB
RAD51 (H-92)	1:200	Rabbit	Santa Cruz	sc-8349	Box7-A1	37	IF
RAD9	1:2,000	Rabbit	Bethyl	A300-890A	Box6-G2	50	WB
RAD9 pS387	1:500	Rabbit	ABGENT	AP3230a	Box6-C4	50	WB
RMI1	1:1,000	Rabbit	Bethyl	A300-631A-M	Box 10-B1	27	WB
RMI2	1:1,000	Rabbit	Abcam	ab122685	Box 10-C2	16	WB
RPA32	WB=1:1,000 IF=1:200	Mouse	Abcam	2175	Box1 B9	32	WB, IF, IP
RPA32 pS33	WB=1:1,000 IF=1:200	Rabbit	Novus	NB100-54	Box10 D4	32	WB, IF
RPA32 pS33	WB=1:1,000 IF=1:200	Rabbit	Bethyl	A300-246A	Box10 E9	32	WB, IF
RPA32 pS4/8	WB=1:1,000 IF=1:200	Rabbit	Bethyl	A300-245A	EFBox1-B8	32	WB, IF
RPA70	WB=1:1,000 IF=1:200	Rabbit	Cell Signaling	2267	Box4-G5	70	WB, IP, IF
SGO2	1:200	Rabbit	Bethyl	A301-262A-M	Box10-E8	28	IF
SLX4	1:1,000	Rabbit	Bethyl	A302-269A-1	Box7-D3	200	WB
SMARCAL1	1:5,000	Rabbit	Bethyl	A301-616A	Box2-I2	110	WB
SMARCAL1 (909)	1:1,000	Rabbit	Cortez		Box6-A7	110	WB
SMARCAL1 pS652	1:1,000	Rabbit	Cortez		Box6-C1	110	WB
SMC1	1:1,000	Rabbit	Novus	NB100-204	EFBox F7	150	WB
SMC1 pS957	1:1,000	Rabbit	Novus	NB100-205	EFBox F8	150	WB
TOP3A (N-	1:1,000	Goat	Santa Cruz	sc-11257	Box7-I1	109	WB

20)							
TOPBP1	1:1,000	Rabbit	Bethyl	A300-111A-1	Box3-E3	185	WB, IF
tubulin (B-7)	1:200	Rabbit	Santa Cruz	sc-5286	EF-Box2-c5	50	IF
ZRANB3	1:1,000	Rabbit	J. Chen		Box7-C8	123	WB
γH2AX	1:1,000	Rabbit	Cell Signaling	2577	Box4-F4	17	IF
γH2AX (JBW301)	WB=1:1,000 IF= 1:500	Mouse	Millipore	05-636	Box6-I7	17	WB, IF

All antibodies were blocked in 5% milk in TBS/t and diluted in 1% milk in TBS/t for western blotting unless denoted with an asterisk. Antibodies with asterisk were diluted and blocked in Odyssey blocking buffer. For IF experiments cells were blocked with 5% BSA in PBS and diluted in 1% PBS in PBS.

Cell culture

Table 2.2 Cell lines. Cell lines are given with optimal media and transfection reagents.

Table 2.2 Cell lines			
Cell Line	**Media**	**Plasmid transfection reagent**	**siRNA transfection reagent**
U2OS	DMEM+7.5% FBS	PEI/Fugene	Dharmafect1
HCT116	McCoy's 5A +10%FBS	PEI/Fugene	RNAiMax
HEK293T	DMEM+7.5% FBS	PEI	RNAiMax
HeLa	DMEM+7.5% FBS	Lipofectamie 2000	RNAiMax
A549	RPMI+10% FBS	PEI	Dharmafect1
BT549	RPMI+10% FBS	PEI	Dharmafect1
H157	RPMI+10% FBS	PEI	Dharmafect1

Cell growth assays

Plated $5x10^4$ HCT116 cells in a 35 mm dish and left untreated or treated with 500 μM IAA. Cells were counted every 24 hours for four days. Cell number and percent viable cells was measured after trypan blue staining using a Countess II automated cell counter.

Cell profiler

Table 2.3 Cell profiler pipelines. Pipelines used for image analysis are provided with a description of their use. Pipelines are available for download on the Cortez lab server in the Cell Profiler folder.

Table 2.3 Cell profiler pipelines	
Pipeline Name	**Description**
H2AX intensity.cppipe	Measure intensity of a channel (i.e. γH2AX) using a DAPI mask
RPA_foci.cpproj	Count and measure intensity of foci in one channel using a DAPI mask
ETAA1_RPA.cppipe	Count and measure intensity of foci in two channels using a DAPI mask
ETAA1_RPA_TOPBP1.cppipe	Count and measure intensity of foci in three channels using a DAPI mask
Mitotic PLA assay.cppipe	Count and measure intensity of foci in one channel using DAPI and as a mask. Nuclei are hand selected allowing only a subset of cells to be analyzed (i.e. mitotic cells)
Kinetochores.cppipe	Count and measure intensity of foci in two channels using\ DAPI and another channel (kinetochores) as masks. Nuclei are hand selected allowing only a subset of cells to be analyzed (i.e. mitotic cells)

Clonogenic survival assay

U2OS cells were seeded onto 60-mm cell culture plates at 200–5,000 cells per plate in triplicate. The following day, cells were treated with drug, washed, and released into fresh growth medium for 14 days prior to staining with methylene blue.

COMET Assay

Neutral COMET assays

Three days after transfection, cells were left untreated or treated with 100 nM CPT for 3 hrs. Cells were harvested by trypsinization and washed once with cold PBS. Cells were resuspended in 1 mL of cold PBS to get $2x10^5$ cells/mL. During this time, low melting

temperature agarose (Trevigen) was melted and held in a 42 °C water bath. To prepare slides, 10 µL of cell suspension was mixed with 100 µL of agarose and spread into one well of a COMET slide (Trevigen). (Best to keep agarose at 42 °C when adding cells and spread immediately) Two wells were prepared per treatment condition. Place samples to be compared on same slide. Slides were allowed to gel for 15 minutes at 4°C. Slides were then immersed in pre-chilled Lysis Buffer (Trevigen) for 1 hour at 4°C. Slides were rinsed once with pre-chilled TAE (40 mM Tris Base, 20 mM Acetic acid, 1 mM EDTA, pH 8.45), then washed for 30 minutes immersed in TAE at 4°C. Slides were then electrophoresed for 1 hour at 21V immersed to a depth of at least 0.5 cm in TAE. After electrophoresis, slides were immersed in DNA Precipitation Solution (1M NH_4Ac, 87% ethanol) for 30 minutes at room temperature. Next, slides were immersed in 70% ethanol for 30 minutes at room temperature then dried for 15 minutes at 45°C and stored overnight at room temperature. Slides were stained with 50 mL of 1X SYBR Green I (Trevigen) for 30 minutes at room temperature. SYBR Green solution was decanted and slides allowed to dry at least 30 minutes before visualizing slides on the 20x objective. At least 20 images were taken per well and scored for tail moment using CometScore software (http://www.autocomet.com). At least 100 comets were scored for each condition.

Alkaline COMET assays

Three days after transfection, cells were left untreated or treated with 100 nM CPT for 3 hrs. Cells were harvested by trypsinization and washed once with cold PBS. Cells were resuspended in 1 mL of cold PBS to get $2x10^5$ cells/mL. During this time, low melting temperature agarose (Trevigen) was melted and held in a 42°C water bath. To prepare slides, 10 µL of cell suspension was mixed with 100 µL of agarose and spread into one well of a COMET slide (Trevigen). Two wells were prepared per treatment condition. Place samples to be compared on same slide. Slides were allowed to gel for 15 minutes at 4°C. Slides were then immersed in pre-chilled Lysis Buffer (Trevigen) for 1 hour at 4°C. Slides were Immersed in

Alkaline electrophoresis solution (pH>13, 200 mM NaOH, 1 mM EDTA) for 20 min at room temp in the dark. Slides were then electrophoresed for 1 hour at 21V immersed to a depth of at least 0.5 cm in alkaline electrophoresis solution. Immersed slides twice in water for 5 min each, then in 70% ethanol for 5 min. Slides were dried for 15 minutes at 37°C. Slides were stained with 100 µL of 1X SYBR Green I (Trevigen) for 30 minutes at room temperature. SYBR Green solution was decanted and slides allowed to dry at least 30 minutes before visualizing slides on the 20x objective.

CRISPR knockout cell generation

Table 2.4 gRNA sequences. The gRNA sequences and corresponding plasmid used for CRISPR genome editing are provided below. The PAM for each gRNA is shown in bold.

Target	Editing strategy	gRNA Sequence	Plasmid Name
ZRANB3	knock out	AGCTTTGCTCTTAGTCTGTC**AGG**	pTB08
ZRANB3	knock out	TTTTTTATGTTATGAACCCT**AGG**	pTB10
SMARCAL1	knock out	CATCCTCCGTGCGCTTCACC**TGG**	pTB14
SMARCAL1	knock out	CTTTGACCTTCTTAGCAAGT**TGG**	pTB16
ETAA1	knock out	ATTTGATAGATCAAAACTG**TGG**	pTB54
ETAA1	knock out	GAAGAAGAACTTATGAAAC**TGG**	pTB56
ETAA1	Tag C-terminus	TTCTTTAATGAAATATTAGT**TGG**	pTB75
ETAA1	Remove exon 2	GTTCTCCTAATGATCCAGA **TGG**	pTB58
ETAA1	Remove exon 2	CTAGTCAGATAATAGCATC**GGG**	pTB60
TOPBP1	Tag C-terminus	GGACTGGATTATCACAAAAG**AGG**	pTB111

gRNA design

Identify high scoring gRNAs targeting gene of interest using CRISPR design tool. For knockout generation I recommend ordering at least 2-3 gRNAs per gene that are 50-150 bp apart and target the N terminal of the gene. CRISPR design tool can be found at http://crispr.mit.edu/.

Design forward and reverse overhangs flanking gRNAs according to the following page. Use the pX330 overhangs: http://www.genome-engineering.org/crispr/wp-content/uploads/2014/05/CRISPR-Reagent-Description-Rev20140509.pdf

gRNA plasmid construction

Insert gRNAs into pSPCas9(BB)-2A-GFP or pSPCas9(BB)-2A-Puro using the following protocol:

1. Phosphorylate and anneal each pair of oligos: (forward and reverse gRNAs for gene of interest)
   1 ul oligo 1 (100μM)
   1 ul oligo 2 (100μM)
   1 ul 10X T4 Ligation Buffer (NEB)
   6.5 ul ddH2O
   0.5 ul T4 PNK (NEB)
   10 ul total

Anneal in a thermocycler using the following parameters:
   37°C 30 min
   95°C 5 min and then ramp down to 25°C at 5°C/min

Dilute the annealed oligo 1:250 (250-fold).

2. Set up digestion-ligation reaction:
   X μL pSpCas9-GFP or pSpCas9-PURO (100ng)
   2 μL phosphorylated and annealed oligo duplex from step 1 (1:250 dilution)
   2 μL 10X Tango buffer (or FastDigest Buffer)
   1 μL DTT (10mM to a final concentration of 1mM)
   1 μL ATP (10mM to a final concentration of 1mM)
   1 μL FastDigest BbsI (Thermo Fisher Fermentas)
   0.5 μL T7 DNA ligase
   Y μL ddH2O
   20 μL total

Incubate the ligation reaction in a thermocycler:
   37°C 5 min
   23°C 5 min
   Cycle the previous two steps for 6 cycles (total run time 1h)
   4 °C hold until ready to proceed

4. Transformation with 1-2 μL of the final product into competent cells
5. Pick colony and sequence verify the clones
   1. Miniprep
      Performed miniprep from 3mL overnight cultures using Sigma miniprep kit according to standard protocol.
   2. AgeI/BbsI Digest

Component	Amount (μL)
DNA (from miniprep)	3
FastDigest Buffer	2

Water	14.6
AgeI	0.2
BbsI	0.2

Run out samples on a 0.8% agarose gel. If linear then insert of gRNA was successful. If you have 7.5 and 1 kb fragments then gRNA insertion was unsuccessful. (Should work ~90% of the time. If all clones are incorrect then check for AgeI or BbsI restriction site in gRNA)

Primer design and optimization for amplifying genomic DNA

Primers that flank the targeted region are required for screening. I design 2-3 primer pairs that produce products 250-600 bp with the targeted region contained within the middle of the primer pairs.

Test primer combinations using the PCR conditions given below:

Component	Amount Added	Final Concentration	Cycling
H_2O	31 µL		98 °C 3 min
5x Phusion HF	10 µL	1x	98 °C 10 s
10 mM DNTPs	1 µL	200 µM	55 °C 15 s
10 µM Forward Primer	1 µL	0.5 µM	72 °C 15 s
10 µM Reverse Primer	1 µL	0.5 µM	72 °C 2 min
Template gDNA	5 µL	50 ng	Hold 4 °C
DMSO	1.5 µL	3%	
Phusion polymerase	0.5 µL	1 unit/ PCR reaction	Total 35 cycles

Run out samples on a 1.3 % agarose gel. Best primer combination can be improved by changing annealing temperature. If no primer pairs produced a product, ordering new primers may be faster and cheaper than several rounds of optimization

gRNA optimization

Determine best gRNA combination by transfecting 293T cells with pairs of puro-Cas9-gRNA plasmids. Begin selection 24 hours after transfection by adding 1-2 µg puromycin. Select cells for 48 hours then harvest cells for gDNA purification. Screen for genomic editing using

optimized PCR combination. Edited clones should have a PCR product that smaller is by the distance between the gRNAs used. The most effective gRNA pair will have the brightest intensity of the smaller band compared to untransfected cells.

Transfection and selection of 293T cells with gRNAs

Day 1
1. Plate 5 x 10^5 293T cells per well in each well of a 6-well dish

Day 2
2. Dilute 1 µg of each gRNA into 20 µL of OptiMEM
3. Add 4.8 µL of PEI at 1 mg/mL and mix by flicking gently
4. Incubate for 15 min at room temperature
5. Overlay cells with 2 mL media
6. Next day begin selection by adding 1-2 µg of puromycin.
7. Continue selection for 48 hrs until control plate is all dead

Plate surviving cells at a clonal density in either 10 cm plates or 96 well dish. Should take 2-3 weeks for cells to form colonies.

Genomic DNA purification and PCR

Pick colonies from 10-cm dish to 24-well dish and continue to expand. Once cells are confluent in a 24-well dish I passage 10% of the cells and pellet the remaining 90% for gDNA purification using the Wizard gDNA purification kit. Use kit according to manufacturer's instructions. Screen clones by PCR using your optimized primers. Genome editing will be evident by the presence of a smaller band. Validate knockout cells by western and DNA sequencing.

CRISPR knock-in cell generation (auxin-inducible cell lines)

I produced TOPBP1 and ETAA1 cells tagged with an auxin inducible degron (AID) using the protocol described in (Natsume et al., 2016). First, I produced vectors containing gRNAs located near the desired site of editing using the protocol described above. Knocking in tags or

mutations requires homology arms of at least 150 bp to the region surrounding the targeted editing site. Additionally, the PAM site of the gRNA must also be edited in the homology donor to prevent cleavage by Cas9. To produce a homology vector, I order a geneblock containing homology arms separated by a BamH1 restriction site and HindIII and Not1 sites on either end of the gene block. The geneblock was then cloned into pBSK using HindIII/Not1 digest. The AID degron with neomycin (Neo) and hygromycin (Hygro) selectable markers was removed from pMK289 (AID-mClover-NeoR, Addgene plasmid:72827) and pMK290 (AID-mClover-Hygro, Addgene plasmid:72828) by BamH1 digest and inserted between the homology arms in pBSK. Both neomycin and hygromycin –encoding template plasmids were cotransfected with pSpCas9(BB)-2A-Puro (Addgene plasmid #48139) containing a guide RNA proximal to the desired site of editing. Cells with homozygous editing were selected by 700 µg/ml G418, and 100 µg/ml HygroGold and confirmed by DNA sequencing and SDS-PAGE immunoblotting.

Fiber Labeling

Plated 1.5x 10^5 siRNA transfected U2OS cells in a 35 mm dish. Plated a few extra dishes that contained unlabled U2OS cells for dilution. Place 1x HBSS and DMEM in incubator to equilibrate overnight. Next day cells were treated with 20 µM IdU for 20 minutes. Cells were then washed twice with equilibrated HBSS and then treated with 100 µM CldU for 20 minutes or left untreated. For CPT treated cells, added 100 µM CldU and 2.5 µM CPT onto cells and let incubate for 45 min. Cells were then washed twice with HBSS, collected by trypsinization, and pelleted at 2,000 xg for 3 min. Cells were resuspended in about 200 µL ice cold PBS to get a concentration of 1x10^6 cells/mL. Labeled cells were diluted 1:2 with non-labeled cells before adding 2 µL of cell suspension near the white frosted end of a slide. Cells were lysed in spreading buffer (0.5% SDS, 200 mM Tris-HCl pH 7.4, 50 mM EDTA) for 6 min before spreading fibers by tilting slide 15°. Slides were air dried for 40 min before fixation in 3:1

methanol: acetic acid for 2 min. Air dry the slides for 20 min. Slides can be stored for up to 5 days at 4°C.

Denature the DNA with 2.5 M HCl for 30 min. Rinse slides three times in PBS. Block in 10% goat serum in PBS with 0.1% Triton X-100. Incubate 1 hour in rat monoclonal anti-BrdU (anti-CldU (Abcam, ab6326; 1:00 dilution) and mouse anti-BrdU (anti-IdU Becton Dickinson, 347580; 1:100 dilution) diluted in PBS containing 10% goat serum and 0.1% Triton X-100. Rinse three times in PBS following incubation with primary antibodies. Stain with secondary antibodies (Alexa-594 goat anti-rat IgG and Alexa-488 goat anti-mouse (Invitrogen); 1:350 dilutions) diluted in PBS containing 10% goat serum and 0.1% Triton X-100 for 30 min in dark. Slides were then mounted with 100 µL Prolong Gold. At least 100 fibers were imaged and measured per condition.

Flow Cytometry

BrdU/PI incorporation

Cells were labeled for 20-40 minutes with 10 µM BrdU prior to drug treatment, harvested, washed once in phosphate buffered saline (PBS), resuspended in 70% ethanol and incubated at -20°C. Following a wash with 0.5% BSA in PBS, cells were permeabilized and DNA denatured by resuspending in 2N HCl in PBS with 0.5% Triton X-100 for 30 minutes. The Triton/HCl solution was removed and the cells resuspended for two minutes in 0.1 M sodium borate prior to washing once with 0.5% BSA/PBS and incubation in 0.5% BSA/PBS containing 0.5% Tween-20 and Alexa-488 conjugated mouse mAb to BrdU (Invitrogen, MObu1 antibody 1:50 in 200ul for 1million cells -- best to count them before harvesting so all samples have same numbers) for 30 minutes. Cells were washed once with 0.5% BSA/PBS then resuspended in PBS containing 5 mg/mL propidium iodide and 10mg/ml RNase A. Cells were incubated for 2

hours at 37 °C or overnight at room temperature before collecting flow cytometry data on a BD FACScalibur. Data was analyzed and graphs produced with FlowJo.

Mitotic index by pH3 S10

Harvest cells collecting both floating and adherent cells. Resuspend cells in 300 µL of cold PBS. Add 700 µL of cold 100% ethanol and mix immediately to fix cells. Fix cells for 60 min or overnight at –20 °C. Following fixation, wash cells twice with cold PBS. Cells were then permeabilized in 1.0 mL of ice cold 0.25% tritionX-100 in PBS for 15 min on ice. Centrifuge cells at 2 min then rinse cells (without pipetting) in PBS/1%BSA. Centrifuge again and resuspend cells in 100 µL of room temp PBS/1%BSA with pH3 S10 antibody at 1:400 dilution. Incubate for 1 hr at room temperature resuspending cells every 15 minutes by flicking tube. Following incubation with antibodies wash twice with PBS/1%BSA. Next, resuspend cells in 100 µL of PBS/1%BSA + anti-rabbit FITC antibody at 1:50 dilution and incubate 30 min at room temperature in the dark. Secondary antibodies were removed, and cells washed once with PBS/1%BSA and once with PBS. Cells were stained with 25 µg/mL propidium iodide+0.1mg/mL RNase in 750 µL of PBS for 30 min at room temperature. Cells were filtered and measured on flow cytometer.

Gel filtration

HEK293T nuclear extract was loaded onto a Superdex 200 column equilibrated with gel filtration buffer (150 mM NaCl, 25 mM HEPES pH 7.5, 10% glycerol, 1 mM DTT) and eluted at 0.20 mL/ min with collection of 0.5 mL fractions. Equal volumes of each fraction were immunoblotted directly or immunoprecipitated with anti-ETAA1 antibodies prior to the ETAA1 immunoblot.

Gene ontology analysis

ETAA1 and TOPBP1 proteins were analyzed using the ClueGO plugin for Cytoscape (Bindea et al., 2009; Shannon et al., 2003). For grouping of GO terms the kappa score was set to 0.4 and the number of overlapping genes to combine groups was set to 50%.

Kinase assays

Kinase assays were performed by Jessica Luzwick as described in (Mordes et al., 2008a). Assays measuring the basal ATR activity were performed by immunoprecipitating Flag-ATR protein using anti-Flag M2 agarose beads (Sigma) from TGN buffer (50 mM Tris, 150 mM NaCl, 10% glycerol, 1% Tween 20, 5 µg/mL aprotinin, 5 µg/mL leupeptin, 1 mM NaF, 50 mM β-glycerol phosphate, 1 mM sodium vanadate, 1 mM dithiothreitol, 1 mM phenylmethylsulfonyl fluoride) cell lysates. Immunoprecipitates were washed three times in TGN buffer, once in TGN + 500 mM LiCl, and twice in kinase buffer (10 mM HEPES at pH 7.5, 50 mM NaCl, 50 mM β-glycerol phosphate, 10 mM MgCl2, 1 mM diothiothreitol) prior to performing kinase reactions. Assays measuring ETAA1 or TopBP1 stimulation of ATR activity were performed by immunoprecipitating Flag-ATR/HA-ATRIP complexes using anti-HA agarose beads (Sigma). Immunoprecipitates were washed three times in TGN buffer, once in TGN + 500 mM LiCl, and twice in kinase buffer prior to performing kinase reactions. GST-TopBP1 AAD or GST-ETAA1 AAD was added to the reactions prior to adding ATP and substrate. All reactions were stopped within the linear range of the assay and analyzed by SDS-PAGE and autoradiography.

Immunofluorescence

U2OS, HCT116, HeLa, H157, or BT549 cells were washed once with PBS and then fixed in 3% paraformaldehyde for 10 min at room temperature. For examining proteins localized

on chromatin, cells were pre-extracted using 0.5% triton X extraction buffer (0.5% triton X, 20 mM HEPES, pH 7.4, 50 mM NaCl, 3 mM $MgCl_2$, 300 mM sucrose) at 4 °C for 5 min before fixation. After fixation, slides were washed three times with PBS and treated with 0.5% Triton X in PBS for 5 min at room temperature. Slides were washed three times with PBS then blocked with 5% BSA in PBS for 15 min to 1 hour. After blocking, cells were incubated with antibody diluted in 1% BSA in PBS for 1 hr to overnight. Slides were removed from primary, washed three times with PBS, and then incubated with secondary Alexa fluor antibodies. Secondary antibodies were removed, cells washed three times in PBS, and slides mounted on glass coverslips using Prolong Gold mounting media with DAPI. Immunofluorescent images were obtained with a Zeiss Axioplan or Nikon microscope with fixed camera exposure times.

Immunoprecipitation

Most immunoprecipitations (IPs) were completed using nuclear extracts although I have also used cells lysates after NP40 lysis. I use 1.5-8 mg of nuclear extract/cell lysate per immunoprecipitation. Extract was mixed with 3 μg of antibody and rotated at 4 °C for 1-4 hrs. The antibody-extract mixture was combined with 50-80 μL protein A or protein G dynabeads after beads were washed three times with dialysis buffer or lysis buffer and rotated at 4 °C for 1 hr. Beads were magnetically separated from IP mixture using a magnetic rack and flow through removed. Beads were washed three times with dialysis buffer or lysis buffer. After last wash bound proteins were eluted by addition of 30 μL 2X SDS sample buffer and boiling for 5 min. For FLAG IPs proteins were eluted by adding 35 μL of Flag peptide (0.25 mg/mL) and incubating on ice for 1.5 hours, flicking tube every 15 min. After elution, beads were magnetically separated, and eluate removed and combined with 2X SDS buffer.

iPOND (isolation of Proteins on Nascent DNA)

iPOND protocol is adapted from (Dungrawala and Cortez, 2015). Plated 9 plates of both heavy and light cells at 25 x 10^6 the day before the experiment. Add 23 µl of the 10 mM EdU stock into 23 ml of cell culture medium in each dish to achieve a final EdU concentration of 10 µM. Pulsed cells for 7.5 minutes. After 7.5 minutes of EdU added 100 µM CPT (15, 30 and 60 min) and left for indicated time points. After designated CPT treatment time, immediately fix the cells on a dish by adding 10 mL of 1% (wt/vol) formaldehyde in PBS and incubating for 10 min at room temperature. Quench cross-linking by adding 1 mL of 1.25 M glycine. Collect the sample by scraping with a cell lifter and transfer it to a 50-mL conical tube. Note the volume. Centrifuge for 5 min at 900xg, 4 °C. Decant the supernatant. Wash pellets three times with PBS and centrifuge for 5 min at 900xg, 4 °C. Vortex to resuspend pellets in PBS. Resuspend the cells in permeabilization buffer at a concentration of 1 × 10^7 cells per mL. Incubate the cells at RT for 30 min. Spin down for 5 min at 900xg, 4 °C. Wash the cells once with cold 0.5% (wt/vol) BSA in PBS, then in PBS. Centrifuge the cells for 5 min at 900xg, 4 °C to pellet after washes. Combine the click reaction cocktail reagents on ice to contain a final concentration of 10 mM sodium ascorbate, 2 mM CuSO4, 10 µM biotin-azide, in PBS. Resuspend the cell pellets from in the click reaction cocktail by vortexing. Combine the heavy and light samples with each other at this step. Rotate the reactions at room temperature for 2 hr in the dark. Centrifuge the samples for 5 min at 900xg, 4 °C, and decant the supernatants. Wash the cells once with cold 0.5% (wt/vol) BSA in PBS, using the same volume as used in click reaction for one sample. Pellet by centrifugation for 5 min at 900xg, 4°C, then wash with PBS. Prepare the lysis buffer (1% SDS in 50 mM Tris-HCl, pH 8.0) by adding aprotinin and leupeptin before use and place on ice. Resuspend the samples from at a concentration of 1.5 × 10^7 cells per 100 µL of lysis buffer and transfer them to 1.5-ml centrifuge tubes on ice. **–** resuspend very slowly with p1000 – NO VORTEXING- minimum bubbles.

Sonicate the cells by using a microtip sonicator and the following settings: pulse: 20 s constant pulse, 40 s pause; power: 13–16 Watts; repeat pulse 1× for every 200 µL of cell lysate; total pulse time: 4–5 min per sample. Centrifuge the samples for 10 min at 16,100xg, room temperature in a tabletop centrifuge. Filter the supernatant through a 90-µm nylon mesh into a new tube. Place the tube on ice. Note the lysate volume. Dilute the lysate 1:1 (vol/vol) with cold PBS containing 1 µg/mL of aprotinin and leupeptin. To capture biotin-tagged nascent DNA, each sample is incubated with streptavidin MyOne C1 beads using 100 µL for every 10 x 10^7 cells. First, gently vortex the vial of dynabeads for 30 sec. Pipette the required volume of beads. Note the volume. Resuspend the beads for all samples together in a total volume of 1 mL lysis buffer containing aprotinin and leupeptin. Wash the beads again with 1 mL of lysis buffer containing aprotinin and leupeptin. Wash the beads once with 1 mL of PBS containing aprotinin and leupeptin; carefully aspirate the supernatant. Resuspend the beads in volume of bead used with PBS containing protease inhibitors. Add an equal volume of beads to each sample. Rotate the biotin captures at room temperature for 1 hr (in the dark if photocleavable biotin azide is used). Separate the dynabeads with the captured DNA and associated proteins for 2 min using the magnetic stand. Split into 4 eppendorf tubes. Resuspend in 1 mL of lysis buffer to wash the beads. Rotate at room temperature for 5 min. Separate the beads using the magnetic stand and aspirate the supernatant. Repeat each wash with Low salt wash buffer, High salt wash buffer and LiCl salt wash buffer. Repeat lysis buffer washes 2 more times. Note: second time – use 1 ml to pool all samples. To elute proteins bound to nascent DNA, add 25 µL of 2X sample buffer and resuspend the beads. Incubate the capture sample for 30 min at 95 °C to reverse cross-links (At intervals of ten minutes, centrifuge the tube at 1000rpm for 1 min and place the tubes back in the heat block. Centrifuge the boiled samples for 1 min at 1,000 rpm, room temperature. Place the tubes on the magnetic stand. Collect the supernatant. The supernatant is the ‘eluted capture’ sample and is ready to use in immunoblotting and Mass spec procedures.

NMR analysis

Two-dimensional ^{15}N-^{1}H HSQC NMR spectra were used to monitor titrations of RPA32C and RPA70N with peptides corresponding to $ETAA1_{888-909}$ and $ETAA1_{594-609}$. Peptides were resuspended in 25 mM Tris, 75 mM NaCl, pH 7.0 and titrated in increments into a sample of 60 μM, ^{15}N-enriched RPA32C or 100 μM RPA70N in 25 mM Tris, 75 mM NaCl, pH 7.0. Data were collected on a 600 MHz Bruker Avance III spectrometer equipped with a 5 mm single-axis z gradient inverse cryoprobe. Ten titration points were collected at molar ratios of peptide to protein of approximately 1:6, 1:3, 1:1.5, 1:1, 3:1, 5:1, 11:1, 21:1, and 80:1.

NP40 lysis

For most western blotting experiments, I lysed cells using a NP40 lysis buffer (150 mM NaCl, 50 mM Tris-Cl, pH 7.5, 10% glycerol, 0.5% NP40). After trypsinization cells were washed once with PBS and pelleted at 1,000 xg for 3 min. Pelleted cells were resuspended in a volume of NP40 approximately four-times the pellet size and incubated on ice for 20-30 min. Lysates were then cleared by centrifugation at 16,000xg for 15 min at 4 °C. Lysate concentration was determined by Bradford assay. Lysates were prepared for SDS-PAGE by addition of SDS-PAGE buffer and incubation at 95 °C for 5 min.

Nuclear extract preparation

Wash cells 1x with cold PBS then add 2 mLs of cold PBS and scrape cells into a 50 mL conical. Spin cells at 2553 x g for 10 min at 4°C. Record the packed cell volume (pcv) and rapidly resuspend the cells in five times the packed cell volume of hypotonic buffer (10 mM HEPES pH 7.9, 1.5 mM $MgCl_2$,10 mM KCl, 0.2 mM PMSF, 0.5 mM DTT). Centrifuge cells for 5 min at 2,553 x g at 4°C. Resuspend the cells to a volume 3 times the pcv and allow to swell on

ice for 10 min. Transfer the cells to a glass Dounce homogenizer. Homogenize cells with 10 slow strokes. (keep dounce on ice and make sure it has a B type pestle). Transfer cells to Eppendorf tubes and centrifuged at 3,300 x g for 15 min at 4 °C. Measure the packed nuclear volume (pnv) and resuspend the nuclei in a volume of low-salt buffer (20 mM HEPES pH 7.9, 25% glycerol, 1.5 mM $MgCl_2$,20 mM KCl, 0.2 mM EDTA, 0.2 mM PMSF, 0.5 mM DTT) equal to ½ pnv. Add ½ pnv of high-salt buffer (same as low salt buffer but with 1.2 mM KCl) dropwise to cells under with gentle mixing (slow vortex or invert tube after every few drops). Allow the nuclei to extract for 30 min on rotator in cold room. Pellet the nuclei by centrifuging for 30 min at 16,000 xg at 4 °C. Remove supernatant as nuclear extract. Dialyze the extract in a 3,500 MW dialysis tubing for 1 hour against dialysis buffer (20 mM HEPES, pH 7.9, 10% glycerol, 100 mM KCl, 0.2 mM EDTA, 0.2 mM PMSF, 0.5 mM DTT). Remove the extract from the dialysis cassette and centrifuge for 20 min at 16,000 x g at 4 °C. After pelleting nuclear debris, collect supernatant. This is nuclear extract and can be used for downstream functions such as immunoprecipitation.

Packaging Lentiviral Particles

Protocol 1

Day 1: Plate 4-5 x 10^6 293T cells in a 100mm dish. Cells should be about 80% confluent on the day of transfection (Day 2).

Day 2: Transfect cells with 4 μg lentiviral vector, 3μg psPAX2, and 1μg pMD2.G in 100 μL DMEM and add 24μL of 1mg/mL PEI. Incubate for 10-15 minutes at room temperature and add to 10 mL of complete media on cells. Also transfected with empty viral vector for empty vector control.

Day 3: Aspirate media, wash cells once in PBS, and add 7 mL DMEM + 10% FBS + Pen/Strep.

Day 4: Collect media in a 15 mL tube and place at 4°C. Add another 7 mL media to the transfected cells.

Day 5: Collect media and pool with the media from the day before in the 15 mL tube. Spin the collected media at low speed to pellet any cellular debris. Move supernatant to a new 15 mL tube and aliquot. Freeze aliquots at -80°C. I suggest making 1mL aliquots.

Protocol 2

Day 1: Plate 3-4 x 10^6 GP2-293 cells in a 100 mm dish. Cells should be about 60% confluent on the day of transfection.

Day 2: Transfect cells with 4 µg pLPCX or appropriate lentiviral vector and 2 µg pVSV-G using PEI based transfection method. Dilute DNA in 100mL DMEM or Optimem and add 24mL of 1mg/mL PEI. Incubate for 10-15 minutes at room temperature and add to 10mL of complete media on cells.

Day 3: Aspirate media, wash cells once in PBS, and add 5-6mL complete media.

Day 6: Collect media and pass through 0.2 µM filter. Freeze aliquots at -80°C. Make 1mL aliquots.

Note: I have used both protocols above successfully although I believe I get better results with protocol 2.

Phosphatase treatment of cell lysates

Took 60 µg of lysate from CPT-treated and untreated cells and added 1.1 µL of 10x (Protein MetalloPhosphatases) PMP buffer, 1.1 µL of 10x MnCl, and 1 µL Lambda Protein phosphatase. Mixture was incubated for 10, 20, 30, or 60 minutes at 30 °C before reaction was stopped by addition of 11 µL 2x SDS Sample buffer and boiling for 5 min. Proteins were examined for gel mobility shifts or phospho-specific antibodies by SDS-PAGE.

Phosphoproteomics

Preparation of samples

For each condition 4.5 x10^7 HCT116-WT and HCT116-ETAA1ΔAAD or TOPBP1-AID cells were grown in heavy (^{13}C) and light (^{12}C) SILAC DMEM with 10% dialyzed FBS. The following day, cells were treated with 100 nM CPT following a two-hour pretreatment with 500 μM IAA. Approximately 7 x 10^7 cells were harvested for each labeling condition, counted, and combined in a 1:1 ratio. Cells were resuspended in hypotonic buffer (10 mM HEPES pH 7.9, 1.5 mM $MgCl_2$,10 mM KCl, 0.2 mM PMSF, 0.5 mM DTT) for 10 min at 4°C and lysed via dounce homogenization. Nuclei were pelleted at 3,300xg for 15 min at 4°C and then resuspended in low salt buffer (20 mM HEPES pH 7.9, 25% glycerol, 1.5 mM $MgCl_2$,20 mM KCl, 0.2 mM EDTA, 0.2 mM PMSF, 0.5 mM DTT) followed by mixing with an equal amount of high salt buffer (same as low salt buffer but with 1.6 mM KCl). Following a 30 min incubation at 4 °C nuclear extracts were centrifuged for 20 min at 16,000xg.

The supernatant contained nuclear soluble proteins which were dialyzed (20 mM HEPES, pH 7.9, 10% glycerol, 100 mM KCl, 0.2 mM EDTA, 0.2 mM PMSF, 0.5 mM DTT) for 1 hour at 4°C. Following dialysis, DTT was added to 20 mM and nuclear extract was incubated for 30 min at room temperature. Denatured proteins were alkylated by addition of 50 mM chloroacetamide and incubated for 40 min at room temperature. Phosphoproteins were subsequently proteolyzed by treatment with trypsin. The chromatin pellet was resuspended in denaturation buffer (8 M Urea, 100 mM Tris pH 8.0, 20 mM DTT) and incubated for 30 min at room temperature. Denatured proteins were alkylated by addition of 50 mM chloroacetamide and incubated for 40 min at room temperature. Proteins were then proteolyzed by LysC (1:100 (mg:mg)) and incubated overnight at 30°C. Phosphopeptides were then diluted 1:4 with ammonium bicarbonate and then trypsinized.

SILAC-labeled samples were combined such that equal protein per light or heavy SILAC state were combined for each experimental replicate. To the combined SILAC protein lysates, 128 uL of trifluoroethanol (TFE) was added to make each sample contain 50% TFE. Proteins were reduced by addition of 2uL of 0.5M TCEP for 1h at room temperature, and carbamidomethylation was completed by treatment with 4uL of 500mM iodoacetamide for 30 min in the dark at room temperature. Samples were diluted 10-fold with 100mM Tris HCl, pH 8.0 to reduce the solution to 5% TFE, and proteins were digested overnight at 37 °C with proteomics-grade trypsin (Sigma Chemical Co., St. Louis, MO) at a ratio of 1:25 enzyme to protein. The resulting peptides were then desalted by solid-phase extraction (Sep-pak Light C18 cartridges, WAT023501 Waters corporation, Milford, MA). Digested samples were first acidified with TFA, diluted 2-fold with 0.1% TFA, and loaded via syringe onto the Sep-pak SPE material. After sample loading, the cartridges were washed with 0.1% TFA, and peptides were eluted with 60% acetonitrile, 0.1% TFA and 80% acetonitrile. Three sequential 0.5mL elutions were performed, and eluates were reduced to dryness via vacuum centrifugation.

TiO_2 enrichment of phosphopeptides

Phosphopeptides were enriched as previously described (Chaturvedi et al., 2014). Purified tryptic peptides were resuspended in 0.05% heptafluorbutyric acid/ 2% ACN containing 300 mg/ml lactic acid. Thirty mg of Titanosphere TiO_2 5 μm beads (GL Sciences, Japan) were used per 1 mg of digested protein. The beads were first washed with 0.05% HFBA/ 80% ACN, and then added to the resuspended tryptic peptides. The mixtures were rotated at room temperature for 30 min at room temperature, centrifuged for 30 sec at 5,000xg, and the supernatant was discarded. The phosphopeptide-bound beads were washed with 500 µL of 0.05% HFBA/ 80% ACN containing 300 mg/mL lactic acid and then twice with 500 µL of 0.05% HFBA/ 80% ACN. Phosphopeptides were eluted from the TiO_2 beads using 500 µL of 0.5M ammonia and then twice with 500 µl of 5M ammonia prior to drying by vacuum centrifugation. Each eluate was reconstituted in 0.1% formic acid.

LC-MS/MS analysis of enriched phosphorylated peptides

Peptides were loaded onto a self-packed biphasic C18/SCX MudPIT column using a Helium-pressurized cell (pressure bomb). The MudPIT column consisted of 360 x 150 μm i.d. fused silica, which was fitted with a filter-end fitting (IDEX Health & Science) and packed with 6cm of Luna SCX material (5μm, 100Å) followed by 4cm of Jupiter C18 material (5μm, 300Å, Phenomenex). Once the sample was loaded, the MudPIT column was connected using an M-520 microfilter union (IDEX Health & Science) to an analytical column (360 μm x 100 μm i.d.), equipped with a laser-pulled emitter tip and packed with 20cm of C18 reverse phase material (Jupiter, 3μm beads, 300Å, Phenomenex). Using a Dionex Ultimate 3000 nanoLC and Autosampler, MudPIT analysis was performed with an 11-step salt pulse gradient (25, 50, 75, 100, 150, 200, 250, 300, 500, 750, and 1M ammonium acetate). Following each salt pulse, peptides were gradient-eluted from the reverse analytical column at a flow rate of 350nL/min, and the mobile phase solvents consisted of 0.1% formic acid, 99.9% water (solvent A) and 0.1% formic acid, 99.9% acetonitrile (solvent B). For the peptides from the first 10 SCX fractions, the reverse phase gradient consisted of the following: 1-6min, 2 %B (salt loading from autosampler); 6-83 min, 2-50 %B; 83-84 min, 50 %B, 84-84.5 min, 50-2 %B; 84.5-95min, 2 %B (column equilibration). For the last SCX-eluted peptide fraction, the peptides were eluted from the reverse phase analytical column using a gradient of 1-6min, 2 %B (salt loading from autosampler); 6-83 min, 2-98 %B; 83-84 min, 98 %B, 84-84.5 min, 98-2 %B; 84.5-95min, 2 %B (column requilibration). Peptides were introduced via nano-electrospray into a Q Exactive Plus or Q Exactive HF spectrometer (Thermo Scientific). For each sample analyzed, the Q Exactive instrument was operated in data-dependent mode acquiring HCD MS/MS scans after each MS1 scan on the 15 most abundant ions using an MS1 ion target of 3 × 106 ions and an MS2 target of 1 × 105 ions. The HCD-normalized collision energy was set to 27, dynamic exclusion was set to 30 s, and peptide match and isotope exclusion were enabled.

For peptide and protein identification, data were analyzed using the Maxquant software package, version 1.3.0.5 (Cox and Mann, 2008; Cox et al., 2011). MS/MS spectra were searched again the human subset of the UniprotKB protein database. Precursor mass tolerance was set to 20ppm for the first search, and for the main search, a 6ppm precursor mass tolerance was used. The maximum precursor charge state was set to 6. Modifications included oxidation of methionine, carbamidomethylation of cysteine, N-terminal acetylation, and phosphorylation of serine, threonine, and tyrosine. Enzyme specificity was set to trypsin, and a maximum of 2 missed cleavages were allowed. The false discovery rate (FDR) for peptide and protein identifications was set to 1%. SILAC peptide ratios were obtained from the MaxQuant Evidence table.

Phosphoproteomics Analysis

Prior to analysis, the outputs from MaxQuant were filtered to remove reverse sequences and known contaminants. The SILAC ratios for each experiment were $\log_2$ transformed using Perseus. The median value for each phosphosite was calculated for the nuclear extract (NE) and chromatin pellet (CP) fractions. Phosphosites that were observed at least twice with a median change in abundance in activator-deficient cells of at least 1.5 fold in either the nuclear soluble or chromatin fractions are reported as dependent on that activator. ATR and CHK1 phosphorylation motifs were analyzed using Icelogo (Colaert et al., 2009). Comparison of ETAA1 and TOPBP1 phosphorylation sites at kinetochores was performed using Phosphopath, a Cytoscape application (Raaijmakers et al., 2015; Shannon et al., 2003).

Protein purification

Induction of protein

Transformed Artic express cells with GST expression vector. Following day pick colonies from Artic Express Cell transformation plate to test for induction. Inoculated 1mL LB + 20 µg/ml

gentamycin + kanamycin using a single colony and incubated overnight at 37°C. Removed 60 μL overnight culture and inoculated 3 mLs LB (NO ANTIBOTICS) for each sample. Incubated cultures for 3 hrs at 30°C at 250 rpm. Removed 100 μL from each culture to save as uninduced sample. Transferred cultures to 13°C at 250 rpm for 10 minutes. Added 1mM IPTG to each culture and incubated at 13°C at 250 rpm for 24 hours. Removed 100 μL from each culture for induced sample. Ran samples on a 10% SDS-PAGE gel to check for induction.

Took two of the 1 mL overnight cultures and inoculated 200 mL of LB without antibiotics at 37 °C, periodically checking OD600. Once OD600 reaches ~0.6 (about 2 hours), induce bacteria with 200μl of 1M IPTG to give a final concentration of 1mM IPTG. Note: make 1M IPTG fresh each time. Incubate cultures at 12 °C for 24 hrs. After induction, pellet bacteria at 5,000xg for 15 min at 4°C. Remove supernatant and store pellet at -20°C until ready to purify protein.

Purification of protein

Resuspend bacterial pellet in 15 mL (7.5mL/100mL bacterial culture) pre-chilled NET buffer (25mM Tris pH 8.0, 50mM NaCl, 0.1mM EDTA, 5% Glycerol, 1mM DTT, 0.1mM PMSF, Aprotinin, Leupeptin). Transfer to round bottom 40mL tube and sonicate suspension 3 times in cold room. (Setting 4, Duty cycle 90, 15 seconds). After 3 sonications removed half of culture and sonicated 3 more times. Incubate suspension on ice for 1 minute between sonications. After sonication, add 780 μL of 20% Triton X-100 to 15 mLs of bacteria to get a 1% final concentration. Incubate on ice for 30 minutes and then centrifuge at 5,000 x g for 10 min at 4°C. Meanwhile, aliquot 200 μL glutathione sepharose bead slurry in microcentrifuge tube. Wash beads twice with 1 mL of NET buffer. For washes, centrifuge beads at 500 x g for 1 minute. Transfer supernatant (cleared lysate) to new tube. Save 20 μL sample of cleared lysate and 20μL sample of pellet to run on gel. Pellet can be stored at -20 C

Incubate cleared lysate with washed glutathione beads on rotator for 2.5 hrs. Wash beads three times with 10 mL NET buffer and 1% Triton-X.

Meanwhile, prepare Elution buffer (75mM Tris pH 8.0, 15 mM Glutathione, 0.1 µg/µL Leupeptin) Note: For 1mL of buffer: 75µL of 1M Tris pH 8.0, 4.61mg Glutathione, 1µL Leupeptin stock After washes, transfer beads to microfuge tube, spin down beads (30sec, 1,000xg) and remove supernatant. Add 200µL elution buffer to 200µL bead slurry (equal volumes). For each elution, incubate on rotator for 5 min at room temp, then centrifuge beads at 500xg for 30-60 s. Remove supernatant and store on ice. Repeat for a total of four elutions, keeping each elution separate. Take 20µL sample of each elution and 10µL sample of beads. Examine purification strategy by running the following samples on gel: Cleared lysate, pellet, beads before elution, each elution sample (4), beads after elution. Coomassie stain gel. Combine desired elutions and proceed with dialysis.

Proximity ligation assay

Cells were plated and fixed as described for other immunofluorescence experiments. After fixation, cells were blocked with Duolink Blocking solution in PBS for 1 hour at 37 °C. Cells were incubated in primary antibodies diluted 1:200 in Duolink antibody diluent for 1 hour at 37°C. Slides were removed from primary and washed twice for five minutes in 1x Wash Buffer A at room temperature. Slides were incubated with Secondary PLUS and MINUS antibodies diluted 1:5 in Duolink Antibody Diluent for 1 hour at 37 °C. Slides were removed from secondary antibodies and washed twice for five minutes in 1x Wash Buffer A. Diluted ligase 1:40 in 1x ligation buffer incubate for 30 min at 37 °C. Removed slides from ligation mixture and washed twice for five minutes in 1x Wash Buffer A. Diluted polymerase 1:80 in 1x amplification solution. Added polymerase to slides and incubate for 100 min at 37 °C. Removed amplification buffer and washed twice for 10 min in 1x Wash buffer B. Then washed slides in 0.01x Wash Buffer B for one minute. Slides were mounted with 12µL Duolink In Situ Mounting Medium containing DAPI and sealed with clear nail polish. Slides were imaged on a Nikon Eclipse scope.

Sister chromatid exchange assay

Protocol was adapted from (German and Alhadeff, 2001). The next morning after siRNA transfection, added BrdU to final concentration of 10 μM to cells. Covered plates with aluminum foil and left in incubator for 48 hours (2 cell cycles). After 48 hours added colcemid to a final concentration of 150 ng/mL (60 μL of 10 μg/mL stock for 4 mLs in 6 well dish). Enriched for mitotic cells for 2-4 hours. Transferred medium (floating cells) and trypsinized cells to new tube. Spin cells at 180 xg for 5 min. Aspirate supernatant leaving 0.2 mL media and resuspend cells gently tapping bottom of the tube. Add 6 mLs of prewarmed (37 °C) 75 mM KCL dropwise for first 1 mL while gently vortexing. Incubate for 16 min at 37 °C. Add four drops of fixative (3:1 solution of methanol: glacial acetic acid), gently invert and spin down cells at 180 x g for 5 min. Aspirate supernatant leaving 0.2 mL of 75 mM KCl solution. Resuspend pellet by gently tapping and add 5 mL of freshly prepared fixative dropwise for the first 1 mL while gently vortexing. Incubate for 20 min at 4 °C. Spin down cells at 180 xg for 5 min. Repeat washes in fixative three times. Resuspend the pellet in small volume of fixative (200 μL) until the cell suspension looks slightly cloudy. Slides should be prechilled in freezer before use. Draw cells into plastic transfer pipet (or cut off bottom of yellow pipet tip). Hold 6 in (15 cm) above the slide and place 2 drops onto the slide with enough room for the drops not to touch. Stand slides on a slant to dry (use tilted racks for fiber labeling) covering with foil. After a few hours move slides to dark drawer to let dry for 2-3 days. Stain slides with 0.1 mg/mL acridine orange in dH_2O for 5 min at room temperature. Wash slides extensively for 2 min under running dH_2O tap water. Put them in coplin jar and let water pour over them. Incubate slides for 1 min in Sorenson Buffer, pH 6.8 (0.1 M Na_2HPO_4, 0.1 M NaH_2PO_4) and then mount in Sorenson buffer. To mount place two 75 μL drops on slide and then place rectangular slide on top View immediately on scope at 100 x using YFP filter. Count the number of SCEs per spread.

Viability assay using alamar blue

Trypsinize U2OS cells and plate in 96-well plate at a density of 4,000 ($4x10^3$) cells per well in a volume of 100 µL. For a full 96 wells prepare 15 mL of DMEM + 7.5% FBS with $6x10^5$ cells to give $4x10^3$ cells/100 µL. Prepare drug dilutions at 10X higher than the desired concentration and add 10µL of drug per well. Drug ranges are given below:

Range of drug dilutions:	
Camptothecin	0.01 µM-1 µM
Olaparib (Parp inhibitor)	1 µM- 100 µM
BMN673	10 nM-1 µM
Etoposide	1-100 µM
Cisplatin	0.1 µM-10 µM
MMS	0.0005%-0.05%
Mitomycin C	2.5-250 ng/mL
Formaldehyde	0.1 µM-1 mM
Bleomycin	5-500 nM
HU	0.1-10 mM

After 24 hours of drug treatment, cells were washed once with DMEM then replace with fresh full media. Olaparib and BMN763 were not washed out. Three to four days after drug treatment, media was removed and replaced with DMEM+7.5% FBS supplemented with alamar Blue. The alamar blue stock is 10X, so dilute alamar blue 1:10 in media. Return cells to incubator for 4-5 hours. Read on plate reader.

CHAPTER III

ETAA1 ACTS AT STALLED REPLICATION FORKS TO MAINTAIN GENOME INTEGRITY

Introduction

DNA replication is challenged by difficult to replicate sequences, DNA damage, and collisions with transcriptional machinery. DNA damage response (DDR) pathways respond to replication stress to maintain genome stability, and DDR defects cause developmental disorders and cancer (Ciccia and Elledge, 2010) (Zeman and Cimprich, 2014).

Replication protein A (RPA) binds and protects single-stranded DNA (ssDNA) at stalled replication forks (Fanning et al., 2006). It also recruits DDR proteins such as ATRIP which is part of the ATR/ATRIP checkpoint kinase complex (Zou and Elledge, 2003; Ball et al., 2005; Cortez et al., 2001). ATR is then activated by a direct interaction with TOPBP1 (Kumagai et al., 2006), which requires RHINO, and the RAD9/RAD1/HUS1 (9-1-1) and MRE11/RAD50/NBS1 (MRN) complexes for its ATR-activating function (Lindsey-Boltz et al., 2015; Cotta-Ramusino et al., 2011; Duursma et al., 2013). In budding yeast, there are at least three $Mec1^{ATR}$-activating proteins including Dpb11 (a TOPBP1 orthologue), Ddc1, and Dna2 (Mordes et al., 2008b; Navadgi-Patil and Burgers, 2009, 2008a; Kumar and Burgers, 2013). As yet, TOPBP1 is the only known ATR activator in mammals.

A second RPA interacting protein at stalled forks is the BLM helicase (Brosh et al., 2000). Mutations in *BLM* cause Bloom syndrome (Ellis et al., 1995), and BLM-deficient cells suffer from chromosomal abnormalities such as an increase in sister chromatid exchanges (SCEs) (Chaganti et al., 1974; Croteau et al., 2014). BLM functions with Topoisomerase IIIα, RMI1, and RMI2 (BTR complex) to generate non-cross over products during recombination (Plank et al., 2006; Raynard et al., 2006; Singh et al., 2008; Wu and Hickson, 2003; Wu et al.,

2006; Xu et al., 2008a). TOPBP1 interacts with BLM and regulates its ability to prevent SCEs through a mechanism reported to be independent of its ATR activating function (Blackford et al., 2015; Wang et al., 2013).

ETAA1 is an uncharacterized protein that derives its name from a study of Ewing tumor antigens (Borowski et al., 2006). Additionally, ETAA1 was identified as an ATM/ATR substrate (Matsuoka et al., 2007), and genome wide association studies found single nucleotide polymorphisms at the *ETAA1* locus increase pancreatic cancer risk (Childs et al., 2015a; Wu et al., 2012). We find that ETAA1 is a replication stress response protein that localizes to stalled forks via a direct interaction with RPA. It also interacts with several other DDR proteins including ATR/ATRIP and the BTR complexes. ETAA1 maintains genome integrity by activating ATR using a motif that has sequence similarity to the TOPBP1 ATR-activation domain (AAD). Furthermore, ETAA1 acts in a distinct pathway from TOPBP1.

Results

ETAA1 is an RPA-interacting protein that localizes to stalled forks

We recently conducted a proteomic screen utilizing iPOND (isolation of Proteins On Nascent DNA) combined with quantitative mass spectrometry to identify proteins enriched at stalled replication forks (Dungrawala et al., 2015). Samples treated with hydroxyurea (HU) for 15 minutes or two hours were compared to untreated cells (Fig. 3.1A). 72 proteins are significantly enriched at the HU-stalled forks compared to elongating forks at these times (Dungrawala et al., 2015). These include known DDR proteins like ATR, RPA, BLM, SMARCAL1, BRCA1, FANCJ, MMS22L, and TONSL as well as ETAA1 (Fig. 3.1B).

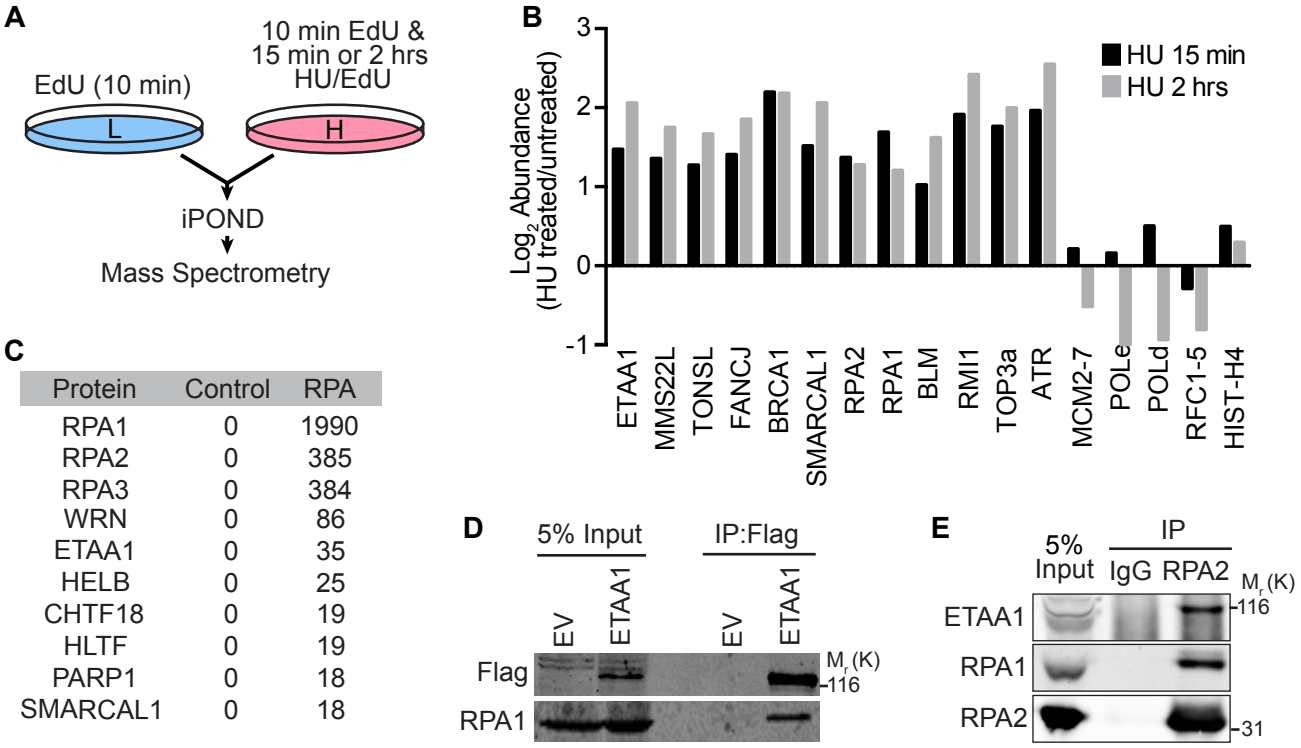

Figure 3.1 ETAA1 is enriched at stalled replication forks and interacts with RPA. (A) HEK293T cells grown in heavy isotope media and incubated with EdU and HU were compared to EdU-labeled cells grown in light isotope media. Replication fork proteins were isolated and detected by iPOND and mass spectrometry. (**B)** The $\log_2$ of the average abundance ratio for selected proteins or complexes is depicted. (**C)** Flag-RPA1 was immunopurified from HEK293T nuclear extracts and interacting proteins were identified by mass spectrometry. The table indicates the number of peptides identified for each protein. The control sample was an immunopurification from untransfected cells. **(D)** HEK293T cells were transfected with a Flag-ETAA1 or empty expression vector (EV), and nuclear extracts used for immunoprecipitation with Flag antibodies. Immunoprecipitates were immunoblotted with the indicated antibodies after separation by SDS-PAGE. Representative blots from one of five independent experiments are shown. **(E)** Nuclear extracts from HEK293T cells were used for immunoprecipitation with RPA2 or control IgG antibodies followed by immunoblotting. Representative blots from one of two independent experiments are shown.

A proteomic screen to identify RPA-interacting proteins also identified ETAA1 (Fig. 3.1C). We validated the interaction by co-immunoprecipitation of RPA with Flag-ETAA1 (Fig. 3.1D). Additionally, RPA2 co-immunoprecipitates with endogenous ETAA1 (Fig. 3.1E).

While a previous study identified ETAA1 on the cell surface or in the cytoplasm (Borowski et al., 2006), we found ETAA1 is localized exclusively in the nucleus. Overexpressed Flag-ETAA1 localizes to intranuclear foci in approximately 25% of cells and is diffusely pan-nuclear in others (Fig. 3.2A). When it is localized to foci, ETAA1 co-localizes with RPA (Fig. 3.2A). Overexpressed ETAA1 is also localized in foci when cells are treated with agents that cause replication stress including camptothecin (CPT), cisplatin (CISP), and hydroxyurea (HU) (Fig. 3.2B). These ETAA1 foci also co-localize with RPA and partially co-localize with γH2AX.

The untreated cells overexpressing ETAA1 with focal localization almost invariably contained elevated γH2AX levels, and many of the cells with pan-nuclear ETAA1 also contain elevated γH2AX suggesting that ETAA1 overexpression stimulates DNA damage signaling (Fig. 3.2C). To better assess how ETAA1 localizes without overexpression, we generated stable cell lines by lentiviral infection and used fluorescence activated cell sorting to select for the 10% of cells with the lowest GFP-ETAA1 levels. In over 95% of these cells, ETAA1 is localized diffusely throughout the nucleoplasm, but after treatment with CPT, it localizes to nuclear foci that also contain RPA and γH2AX (Fig. 3.2D, E). Most cells with ETAA1 foci also contained cyclin A indicating they are in S or G_2 phase (Fig. 3.2F). We conclude that ETAA1 overexpression induces DNA damage signaling and ETAA1 focal accumulation, but that when it is expressed at lower levels it is primarily recruited to replication foci in response to stress.

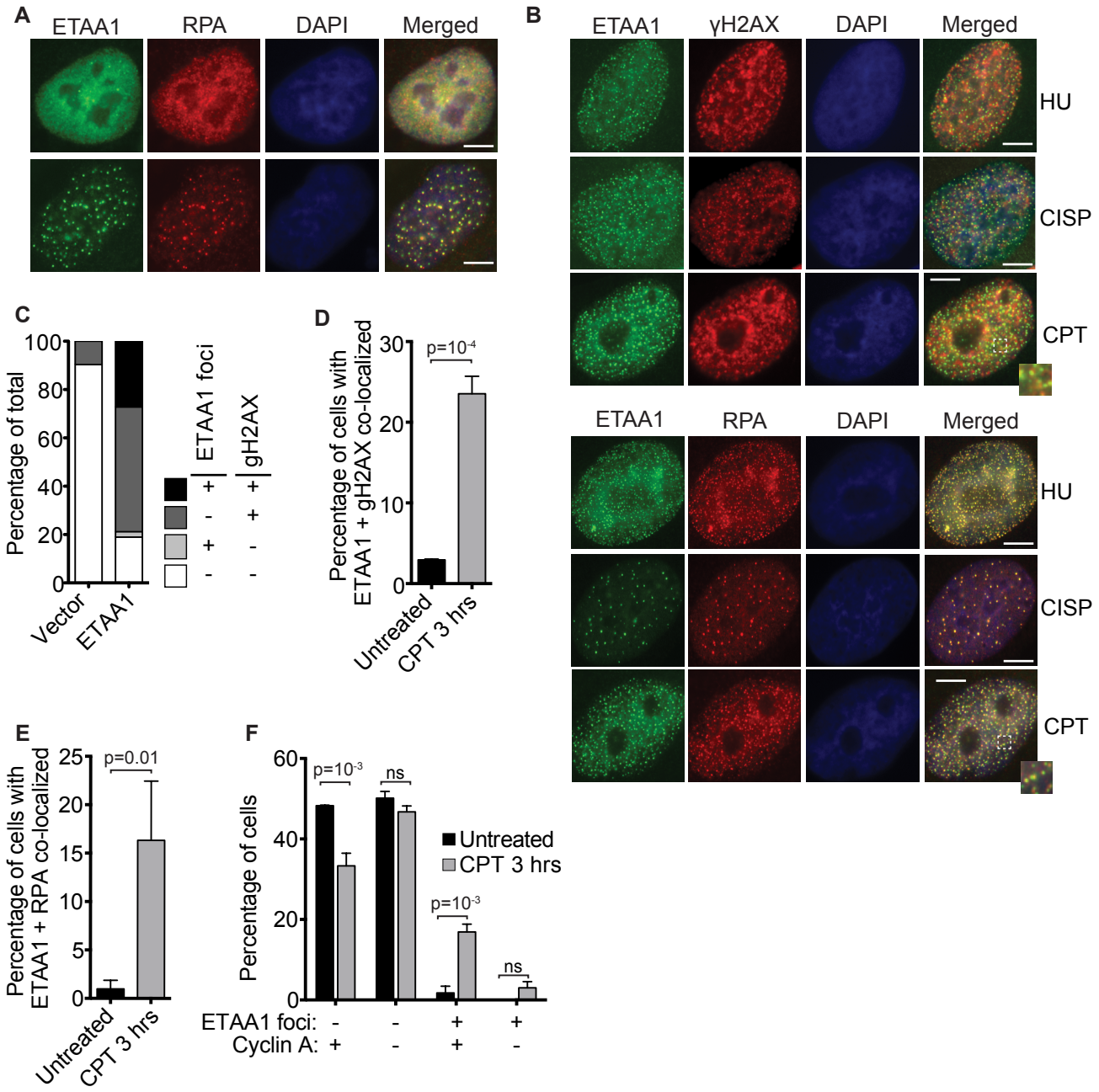

Figure 3.2 ETAA1 colocalizes with RPA at sites of replication stress. (A-C) U2OS cells were transiently transfected with a Flag-ETAA1 expression vector and stained and imaged for Flag-ETAA1, RPA, and γH2AX. Scale bars are 5 μm. In **(B)** cells were treated with HU, cisplatin, or camptothecin (CPT) for 3 hrs. **(D-F)** Stable cell lines expressing GFP-Flag-ETAA1 were sorted by flow cytometry to select the 10% of cells expressing the lowest levels, stained for Flag-ETAA1, RPA, γH2AX, and cyclin A as indicated, and scored for focal co-localization before and after treatment with 100 nM CPT. Error bars are SEM from n=3 experiments; student's, two-tailed, unpaired t-test.

ETAA1 binds two RPA domains to recruit it to damaged forks

To test whether the interaction with RPA recruits ETAA1 to stalled forks, we first examined a series of ETAA1 fragments for their ability to co-immunoprecipitate RPA. RPA binding is largely restricted to an ETAA1 fragment containing amino acids 571-926 (Fig. 3.3 A,B). Sequence alignments identified an evolutionarily conserved motif within this fragment consisting of amino acids 900-912 that closely resembles the RPA32C binding motif of other RPA32C-interacting proteins including SMARCAL1 and TIPIN (Bansbach et al., 2009; Mer et al., 2000) (Fig. 3.4A). An NMR chemical shift perturbation approach demonstrated that this ETAA1 motif binds directly to the same surface of RPA32C as previously observed for other RPA32C-interacting proteins (Mer et al., 2000; Feldkamp et al., 2014) (Fig. 3.4B,C)

Deletion of the ETAA1 RPA32C interaction motif (ETAA1Δ32) greatly reduced but did not eliminate its ability to associate with RPA and localize to foci (Fig. 3.3 E, and Fig. 3.4 D-F). Knockdown of RPA70 in cells expressing ETAA1Δ32 abrogated this residual localization suggesting an additional RPA-interaction surface (Fig. 3.3F). Indeed, fragments of ETAA1 containing either residues 600-678 or 574-724 co-immunoprecipitate RPA; whereas ETAA1 fragments containing residues 2-569, 623-885 or 623-724 do not (Fig. 3.3A,C, D), thereby narrowing the interacting motif to amino acids 600-623. This region has sequence homology to the RPA70N-interacting peptides of ATRIP, MRE11, RAD9, and p53(Xu et al., 2008b) (Fig. 3.4G). NMR chemical shift mapping with this ETAA1 peptide indicates that it directly binds the basic cleft in RPA70N (Fig. 3.4H). Deletion of this motif in ETAA1 (ETAA1Δ70) caused a slight reduction in RPA co-immunoprecipitation, and modest impairment in localization to RPA foci (Fig. 3.3 E, and Fig. 3.4 E,F). Deletion or mutation of both RPA binding motifs largely abolished RPA co-immunoprecipitation and eliminated focal accumulation (Fig. 3.3E,G, and Fig. 3.4E,F). Thus, ETAA1 interacts with both the 70N and 32C domains of RPA, and these interactions recruit ETAA1 to stalled replication forks.

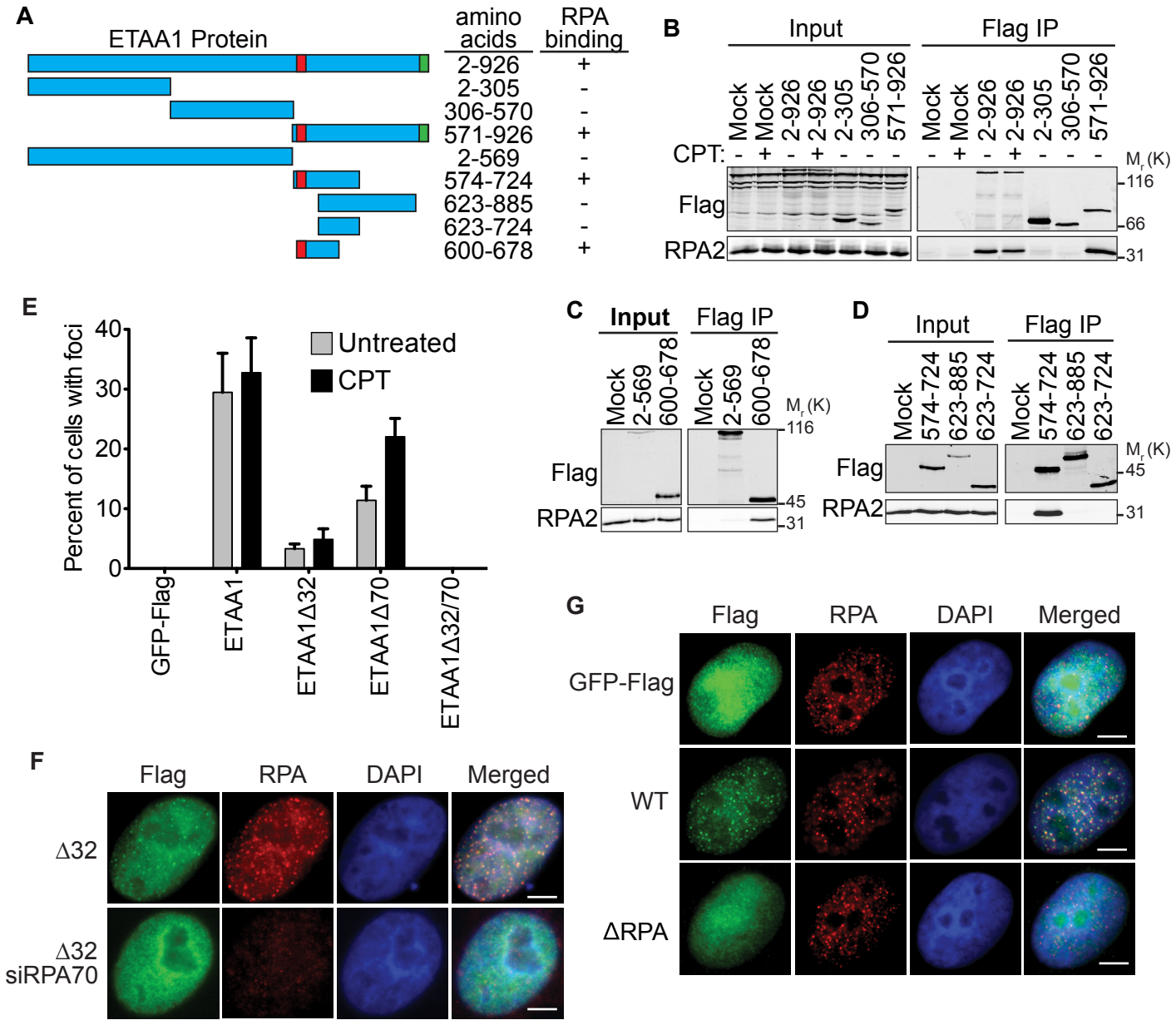

Figure 3.3 RPA recruits ETAA1 to damaged replication forks. (A) Schematic of ETAA1 fragments tested for their ability to bind RPA. **(B-D)** Nuclear extracts were prepared from HEK293T cells after transfection with the indicated GFP-Flag-NLS-ETAA1 expression vectors. Flag immunoprecipitates were separated by SDS-PAGE and examined by immunoblotting. Mock, mock-transfected. Cells were treated with 100 nM CPT for 3 hrs prior to lysis where indicated. The interaction between ETAA1 and RPA was not changed substantially in cells treated with CPT. Representative blots from one of two independent experiments are shown. **(E)** Quantitation of cells containing ETAA1 foci after transfection with the indicated ETAA1 expression vectors. Mean and SEM from n=3 experiments is shown. **(F)** U2OS cells were transfected with an ETAA1 expression vector missing the C-terminal RPA32 interaction motif (ETAA1Δ32) in combination with non-targeting or RPA siRNA and imaged for ETAA1 and RPA localization after a challenge with 100 mM CPT. **(G)** ETAA1Δ cells were transduced with lentivirus to express empty vector (GFP-Flag), GFP-Flag-ETAA1 (WT), or GFP-Flag-ETAA1 with point mutations (residues 606-611 mutated from DVDDDL to NAAIRS) in the RPA70N motif and deletion of the ETAA1-RPA32C (deletion of residues 885-926) interaction motif (ETAA1ΔRPA). Cells were treated with 100 nM CPT for 3 hrs. RPA, and Flag-GPF-ETAA1 were visualized by immunofluorescence. Representative images from one of two independent experiments in F and G are shown. Scale bars are 5 μm.

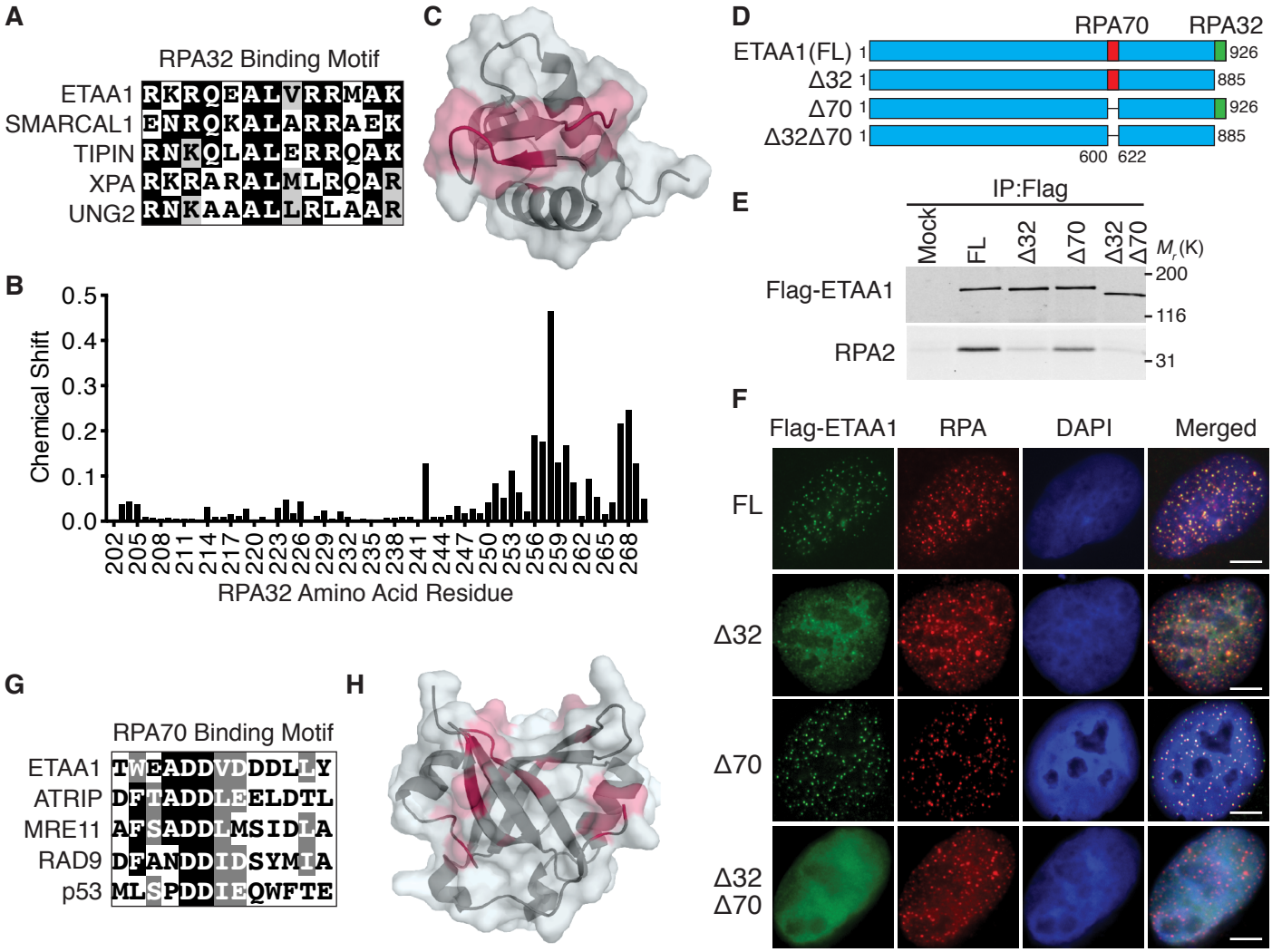

Figure 3.4 ETAA1 interacts with RPA through the RPA32C and RPA70N domains. (A) Sequence alignment of ETAA1 900-912 with the RPA32C binding motif of other RPA32C-interacting proteins. **(B)** Plot of RPA32C chemical shift perturbations induced by the binding of the ETAA1 peptide calculated from ^{15}N-^{1}H HSQC NMR spectra of ^{15}N-labeled RPA32C obtained in the absence and presence of peptide. **(C)** Map of RPA32C residues with chemical shift perturbations greater than one standard deviation (SD) above the mean (red) on the structure of RPA32C (PDBID 4OU0). **(D)** Schematic diagram of ETAA1 mutants examined in **E** and **F**. **(E)** Nuclear extract from HEK293T cells mock transfected or transfected with ETAA1 expression constructs were used for immunoprecipitation with Flag antibodies; FL, full length. Immunoprecipitates were immunoblotted with Flag or RPA2 antibodies. **(F)** U2OS cells were transfected with the indicated ETAA1 expression vectors and treated with 100 nM CPT for 3 hrs prior to examining ETAA1 and RPA localization. Scale bars are 5 μm. **(G)** Sequence alignment of ETAA1599-611 with the RPA70N-interaction motif of other RPA70N-interacting proteins. **(H)** Map of RPA70N residues with chemical shift perturbations greater than one SD above the mean (red) on the structure of RPA70N (PDBID 2B29) calculated from NMR ^{15}N-^{1}H HSQC spectra of ^{15}N-labeled RPA70N obtained in the absence and presence of ETAA1 peptide. All panels are representative of two experiments.

ETAA1 is a replication stress response protein

To determine if ETAA1 has an essential function in the replication stress response, we examined the consequences of *ETAA1* gene silencing. Even in untreated U2OS cells, ETAA1 knockdown caused an increase in the appearance of DNA damage markers including increased γH2AX and chromatin-associated RPA (Fig. 3.5A, B). These differences were more pronounced in cells challenged with either HU or CPT, and happened in multiple cancer cell lines including HeLa, H157, and BT549 (Fig. 3.6 A, B). The increase in chromatin-associated RPA suggested that there may be additional ssDNA in ETAA1-deficient cells. Indeed, staining with BrdU antibodies in non-denaturing conditions confirmed this ssDNA increase (Fig. 3.5C).

ETAA1 knockdown resulted in hypersensitivity to CPT as well as etoposide (Fig. 3.5D-G). This phenotype is not due to off-target effects since multiple siRNAs cause hypersensitivity (Fig. 3.6C). Furthermore, we generated *ETAA1Δ* cells using CRISPR-Cas9 and again found that two independent knockout cell lines were hypersensitive to CPT and contain elevated ssDNA levels (Fig. 3.5 C,D,H). Additionally, expression of a wild-type ETAA1 cDNA in *ETAA1Δ* cells was able to complement this defect (Fig. 3.5I). ETAA1-deficient cells are also hypersensitive to HU (Fig. 3.5J). Hypersensitivity is not limited to ETAA1-deficient U2OS cells as knockdown of ETAA1 in most other cell types also caused hypersensitivity to both CPT and HU (Fig. 3.6 D-K). However, we did not observe increased sensitivity to ionizing radiation, cisplatin, or the PARP inhibitors Olaparib or BMN673 in ETAA1-deficient cells (Fig. 3.7 A-D).

In the absence of added genotoxic stress, ETAA1-deficient cell populations exhibited slightly higher percentages of cells with greater than 2n DNA content compared to controls (Fig. 3.8A) consistent with some difficulty in DNA replication. After HU challenge, control cells rapidly resume DNA synthesis and complete the cell division cycle by 16 hrs. ETAA1 knockdown resulted in a slightly slower recovery with fewer cells able to complete the cell division cycle (Fig. 3.8B). The differences between control and ETAA1-deficient cells were even

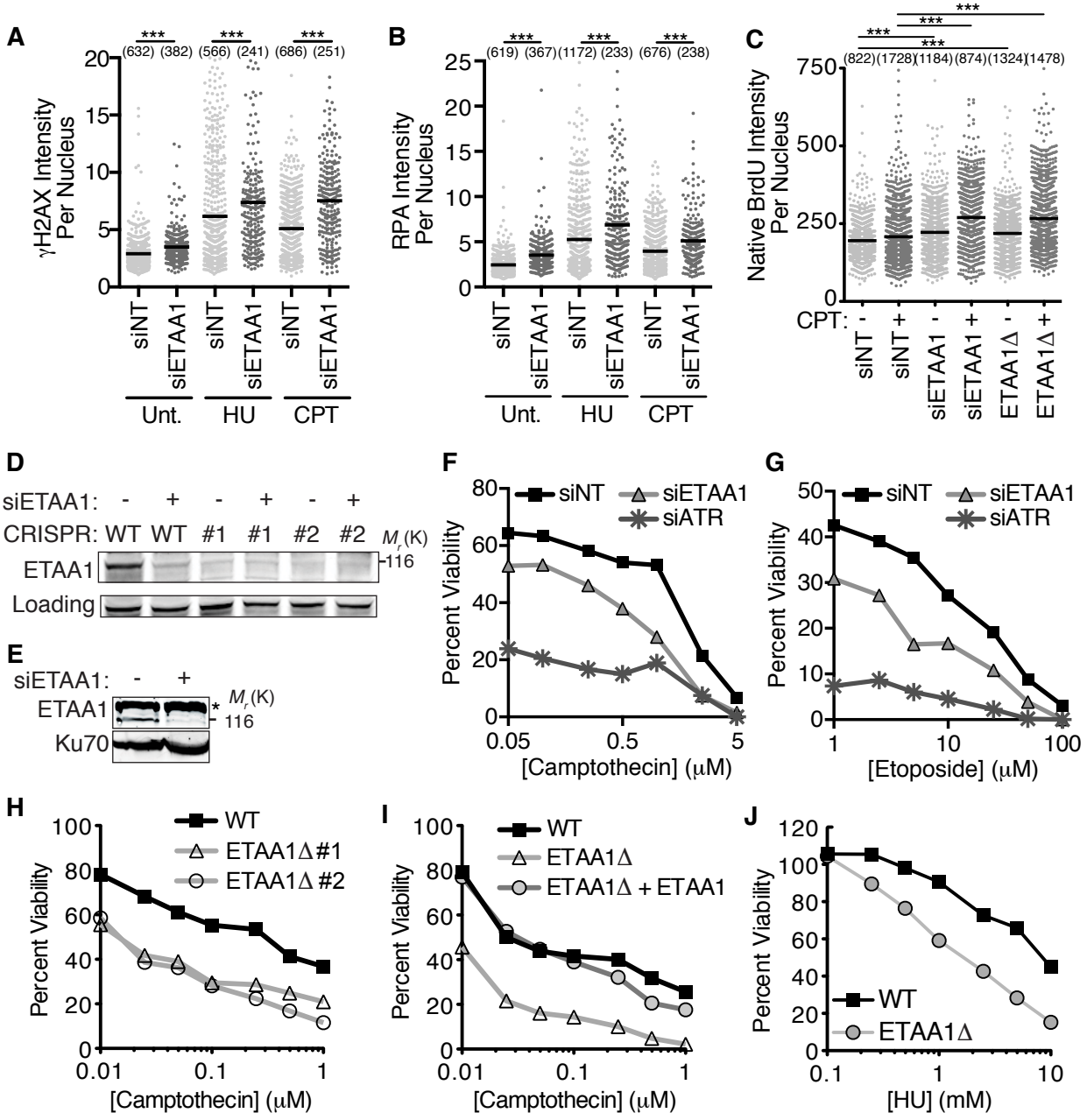

Figure 3.5. Loss of ETAA1 results in increased DNA damage and sensitivity to DNA damaging agents. (A,B) U2OS cells transfected with non-targeting (NT) or ETAA1 siRNAs were left untreated (Unt), or treated with 2 mM HU or 100 nM CPT for 3 hrs. Soluble proteins were extracted with detergent prior to fixation. γH2AX and RPA intensity were quantified by immunofluorescence imaging. **(C)** U2OS cells transfected with siRNA or ETAA1Δ U2OS cells were labeled with BrdU for 24 hrs and then treated with CPT for 3 hrs as indicated. Cells were fixed and stained with BrdU antibodies in non-denaturing conditions to measure ssDNA levels. In **A-C** the intensity of each nucleus and mean intensity from a representative experiment of at least two independent experiments is shown. Significance was determined by the Mann-Whitney test. ***p<0.001 The numbers avove each sample indicates the n value, which represents the number of nuclei imaged. **(D) I**mmunoblot to confirm ETAA1 siRNA knockdown and gene deletion. A cross-reacting protein that migrates at a similar position as ETAA1 is observed in some ETAA1 immunoblots. **(E)** Nuclear extracts were prepared from U2OS cells transfected with pooled ETAA1 siRNAs and ETAA1 was detected by immunoblotting after SDS-PAGE. Star denotes cross-reacting protein. **(F-G)** U2OS cells were transfected with NT, ETAA1, or ATR siRNAs and treated with CPT or etoposide for 24 hrs. Viability compared to untreated cells was measured 72 hrs after initial addition of drug. Untreated cell viability was set at 100%. **(H-J)** Wild-type or ETAA1Δ U2OS cells were treated with CPT or HU for 24 hrs and viability was measured as in **F** and **G**. In **I** ETAA1Δ cells stably expressing wild type ETAA1 were also examined. In all viability assays, the mean viability from three technical replicates of a representative experiment is graphed.

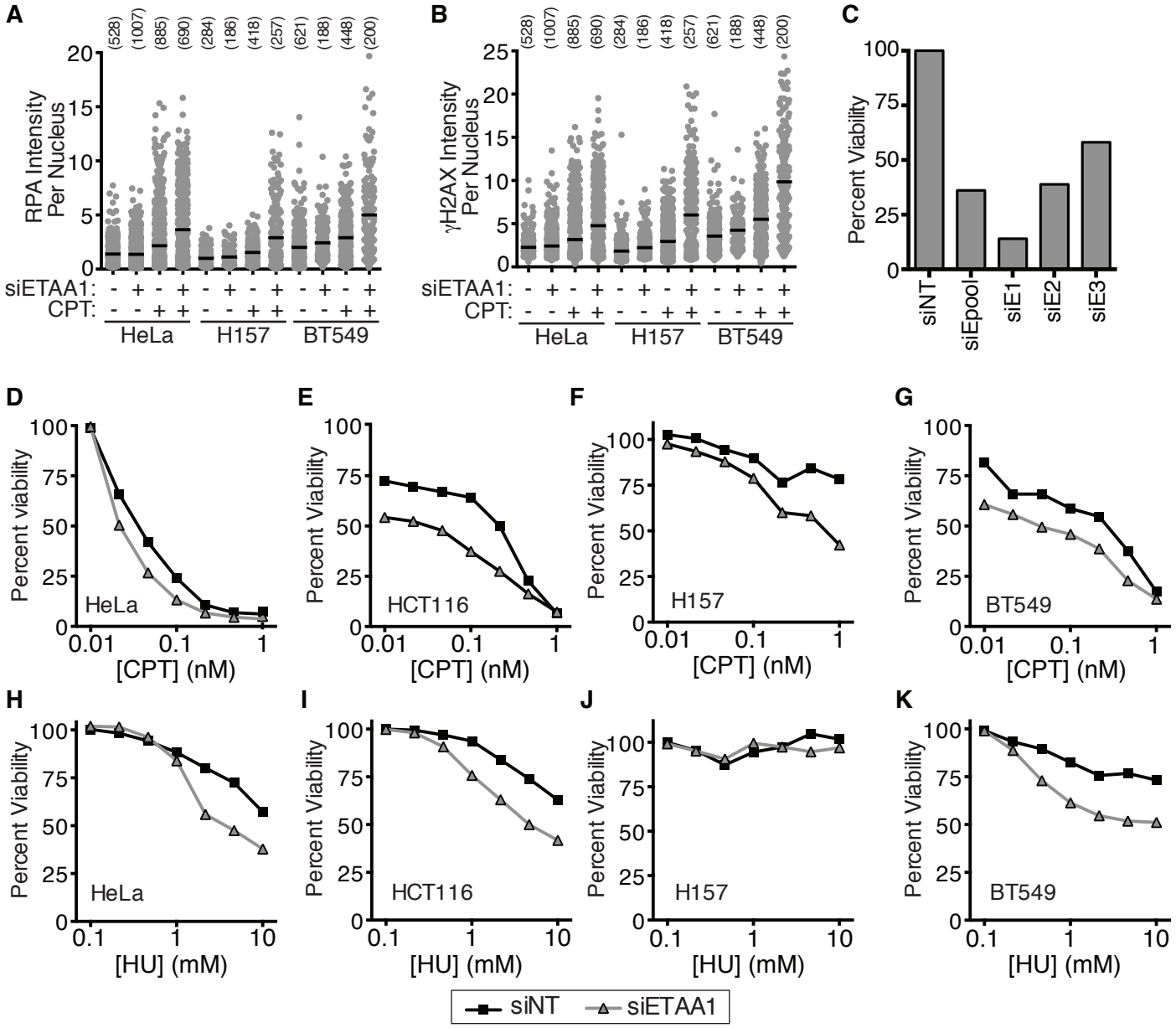

Figure 3.6. ETAA1 knockdown causes hypersensitivity to replication stress. (A,B) HeLa, H157, and BT549 cells transfected with non-targeting (NT) or ETAA1 siRNAs were left untreated or treated with 100 nM CPT for 3 hrs. Cells were fixed and RPA foci and γH2AX intensity were quantified by immunofluorescence imaging. The intensity of each nucleus, mean intensity, and number of nuclei imaged is depicted. **(C)** U2OS cells were transfected with non-targeting or ETAA1 siRNAs. All siRNAs target different regions of the ETAA1 coding sequence or 3' UTR. siE1, siE3, and siE3 are different from the four ETAA1 siRNAs in the pool. Viability was measured 48 hrs after challenging the cells with 0.5 μM CPT for 24 hrs. Data show the mean of three independent experiments for siNT and siETAA1 pool and two for the other siRNAs. **(D-K)** HeLa, HCT116, H157, and BT549 cells were transfected with non-targeting or ETAA1 siRNAs and viability was measured 72 hrs after challenge with CPT or HU. Data show the mean from three technical replicates.

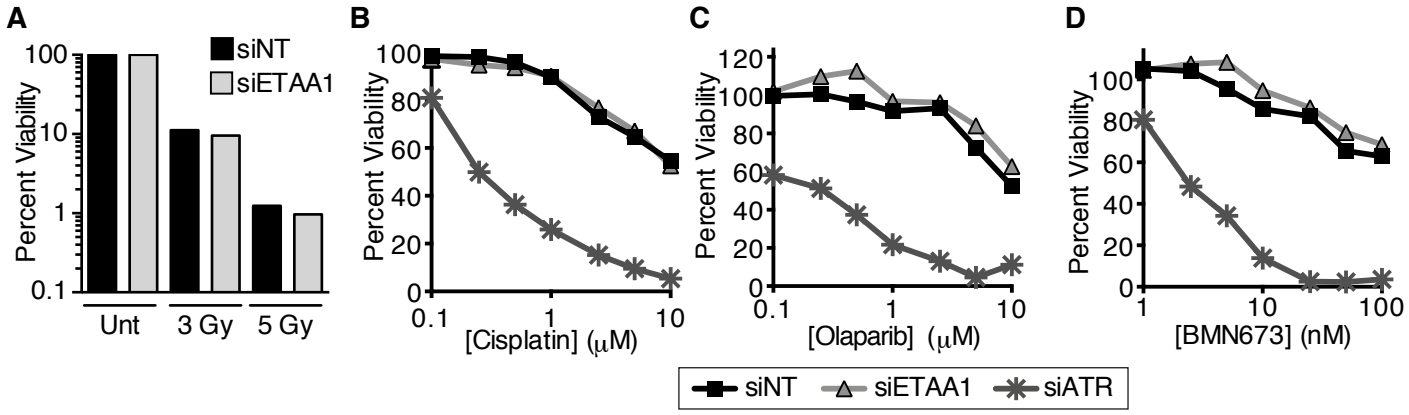

Figure 3.7 ETAA1 knockdown does not cause sensitivity to all DNA damaging agents (A) U2OS cells were transfected with non-targeting or ETAA1 siRNAs and exposed to 0, 3, or 5 Gy ionizing radiation. Cell viability was determined by clonogenic assay. **(B-D)** U2OS cells were transfected with non-targeting or ETAA1 siRNAs and viability was measured 72 hrs after challenge with cisplatin, olaparib, or BMN673. ATR siRNA was used as a positive control. In **A-D** the mean viability from from three replicates. One representative experiment is shown and the experiments were completed twice independently.

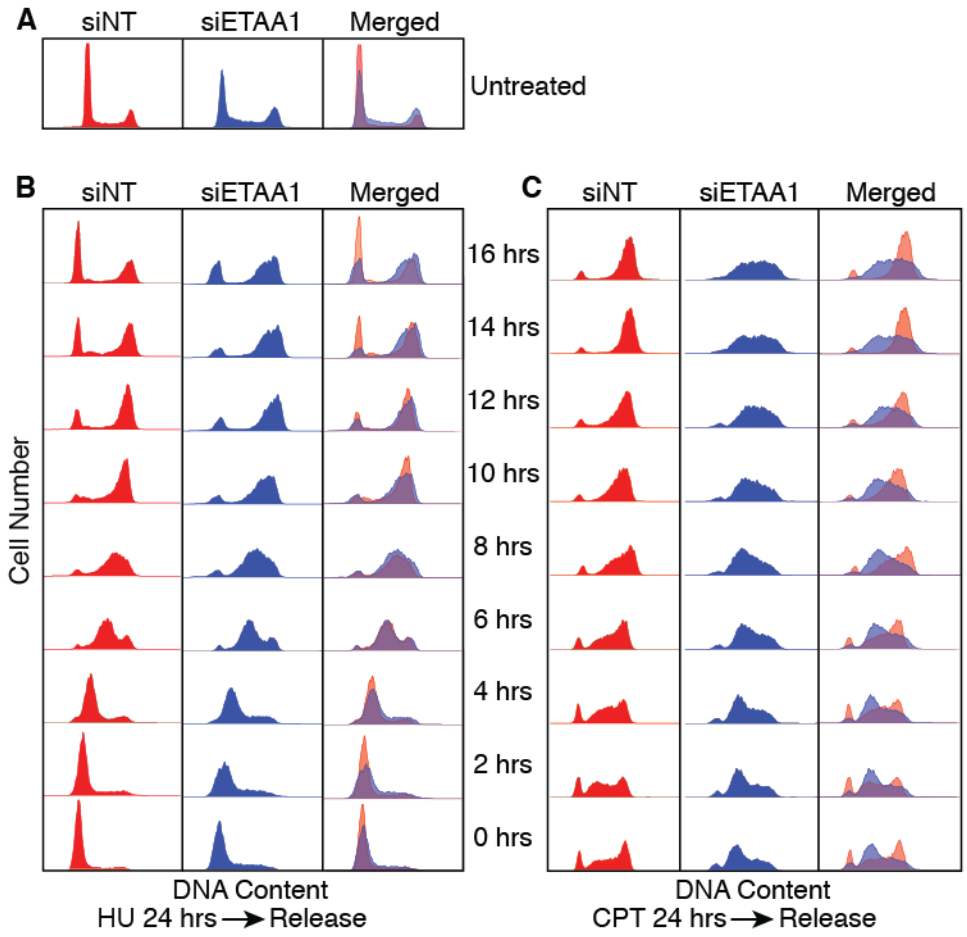

Figure 3.8. ETAA1 is needed to recover from replication stress. (A-C) U2OS cells were transfected with non-targeting or ETAA1 siRNAs and left untreated **(A)** or challenged with 2 mM HU **(B)** or 100 nM CPT **(C)** for 24 hrs. After 24 hrs, drug was removed and samples were collected every 2 hrs for 16 hrs. Collected cells were fixed, stained with propidium iodide, and DNA content was measured by flow cytometry. Data is representative of two experiments.

more pronounced upon treatment with CPT. These cells accumulated in early to mid S-phase and were largely unable to complete DNA synthesis after removing CPT (Fig. 3.8C).

To confirm that ETAA1-deficient cells have difficulty in DNA replication in response to replication stress, we performed DNA fiber labeling experiments. Elongation rates in unchallenged *ETAA1Δ* and control U2OS cells are similar (0.21±0.01 μm/min and 0.20±0.01 μm/min respectively). *ETAA1Δ* cells treated with CPT exhibit significant shortening of replication track lengths compared to controls consistent with increased fork collapse (Fig. 3.9A, B). We also observed an increase in origin firing in *ETAA1Δ* cells (Fig. 3.9C). Furthermore, neutral comet assays indicate that ETAA1-deficient cells contain elevated levels of double-strand breaks with and without added replication stress (Fig. 3.9D). Thus, we conclude that ETAA1 is needed to maintain replication fork stability.

ETAA1 interacts with multiple DDR proteins including ATR and BLM

ETAA1 lacks any predicted domain structure other than a potential coiled-coil motif. To determine if it exerts its genome maintenance functions through protein-protein interactions we immunopurified Flag-ETAA1 and identified ETAA1-interacting proteins by mass spectrometry. As expected, all three subunits of RPA were observed in the ETAA1 immunopurifications (Fig. 3.10A). In addition, ETAA1 complexes contain many proteins that act at damaged replication forks including all four subunits of the BTR complex, both subunits of the ATR/ATRIP checkpoint kinase complex, BRCA1, BRCA2, HLTF, FANCM and FANCJ.

We validated that overexpressed ETAA1 interacts with BLM, HLTF, BRCA1, BRCA2 and ATR/ATRIP in co-immunoprecipitation experiments (Fig. 3.10B, C). In contrast, we did not observe FANCD2 in the ETAA1 immunoprecipitates. ETAA1 co-fractionates with BLM, TOP3α, and RMI1 over a size exclusion column (Fig. 3.10D). Some ATR, RPA2 and HLTF also co-

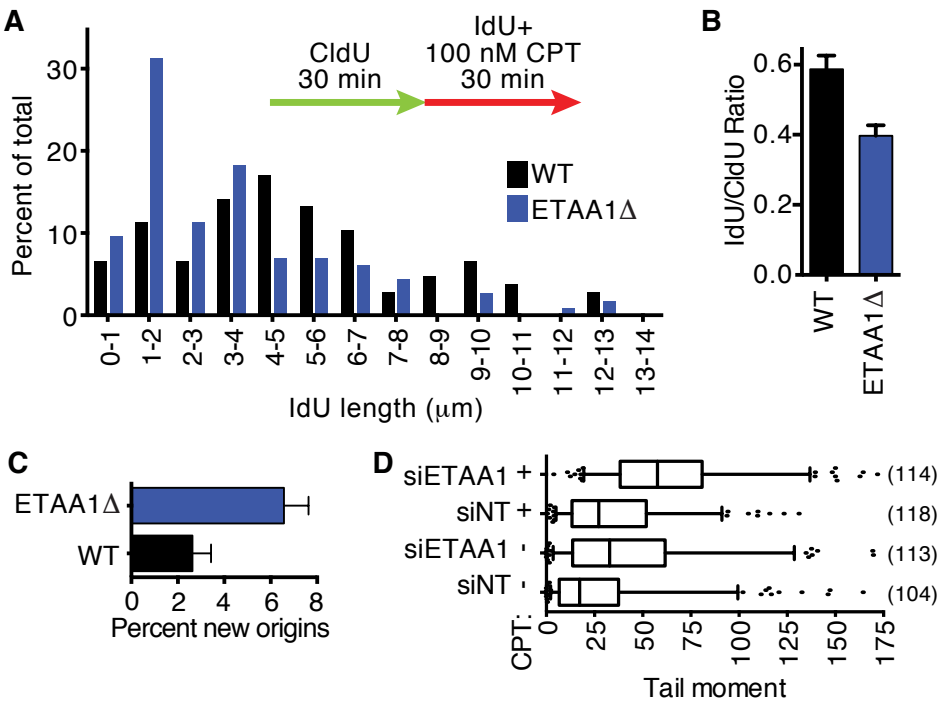

Figure 3.9 ETAA1 promotes fork stability. (A-B) Wild-type or ETAA1 knockout cells were labeled with CldU and IdU and treated with 100 nM CPT as indicated during the second labeling period. DNA fibers stretched on a microscope slide were stained with IdU and CldU antibodies, imaged, and the lengths of fiber tracks measured. n=107 and 116 fibers for WT and ETAA1Δ respectively. One of two biological replicates is shown. **(C)** The percent of new origins (red only fibers) were also quantitated. n=500 fibers for WT and 508 fibers for ETAA1Δ. **(D)** U2OS cells transfected with non-targeting or ETAA1 siRNAs and left untreated or treated with 1 μM CPT for 1 hr were subjected to a neutral comet assay to measure double-strand breaks. The box depicts 25-75%, whiskers are 5-95%, and the line is the median value. The numbers of comets measured (n values) from one of two independent experiments are indicated.

A

Protein	ETAA1 #1	ETAA1 #2	Ctrl #1	Ctrl #2
ETAA1	731	544	1	0
RPA1	86	57	11	9
RPA2	14	9	4	1
RPA3	7	16	2	4
BLM	12	21	0	9
RMI1	4	9	0	0
RMI2	0	2	0	0
TOP3A	3	7	0	0
ATR	20	7	1	0
ATRIP	3	2	0	0
HLTF	9	22	1	2
BRCA1	18	6	1	2
BRCA2	40	18	4	0
FANCM	7	2	0	0
FANCJ	4	1	0	0

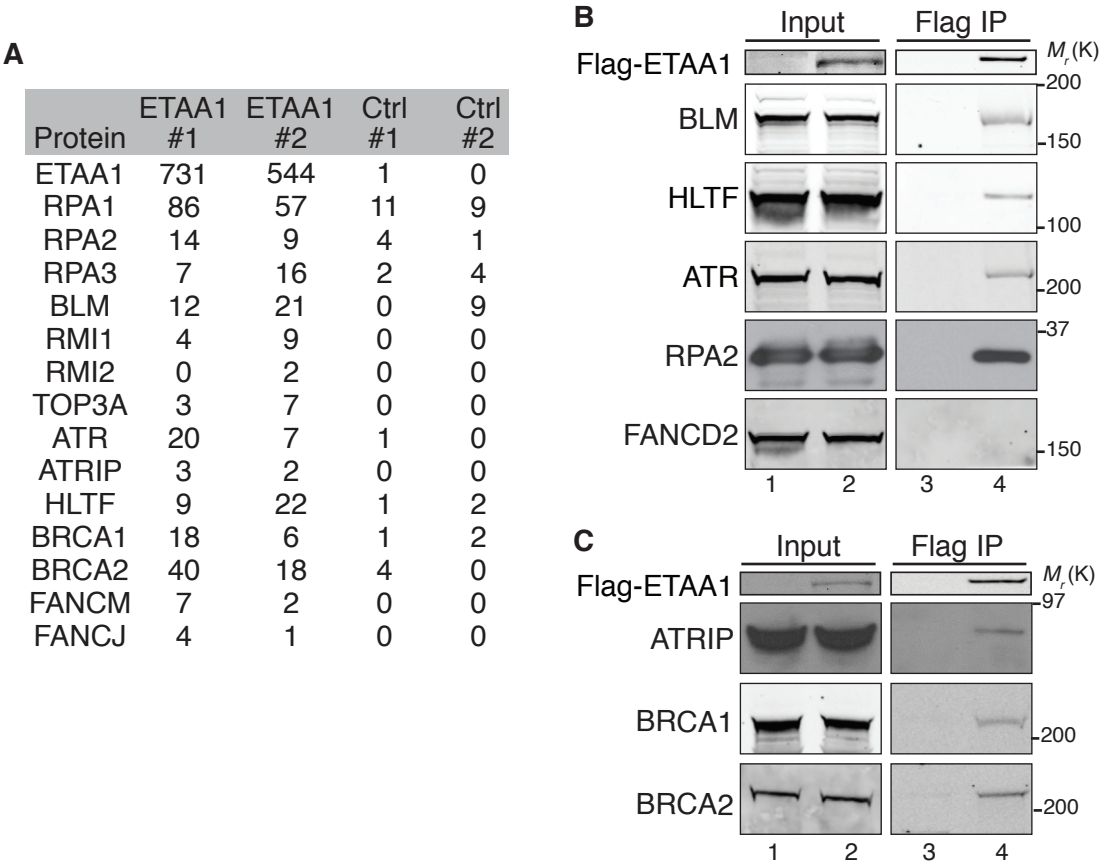

Figure 3.10 ETAA1 interacts with multiple DNA damage response proteins. (A) Flag-ETAA1 was immunoprecipitated from nuclear extracts of HEK293T cells, and immunoprecipitated proteins were identified by mass spectrometry. Extracts in the second replicate were treated with benzonase and RNAse prior to the immunopurification. Shown are peptide counts from two experiments including untransfected cell populations (Ctl). **(B,C)** HEK293T cells were mock transfected (lanes 1 and 3) or transfected with a Flag-GFP-ETAA1 expression vector (lanes 2 and 4) and ETAA1 was immunoprecipitated using Flag antibodies. Co-precipitating proteins were separated by SDS-PAGE and detected by immunoblotting. **(D)** HEK293T nuclear extracts were fractionated on a Superdex 200 column. Protein fractions were then separated using SDS-PAGE and immunoblotted with the indicated antibodies. To detect ETAA1, it was immunoprecipitated from the fractions prior to immunoblotting. The reason ETAA1 migrates as a doublet in some gel conditions is not known but may represent post-translational modifications.

fractionate in these high molecular weight complexes. Thus, ETAA1 likely participates in one or more large DDR protein complexes.

ETAA1 activates ATR

Since ETAA1 interacts with ATR and ATRIP we next asked whether it participates in the ATR signaling pathway by examining ATR substrate phosphorylation. We observe a modest decrease in RPA phosphorylation in U2OS cells transfected with ETAA1 siRNA (Fig. 3.11A). This difference cannot be explained by decreased RPA association with damaged replication forks in ETAA1-deficient cells since there is actually an increase in chromatin-associated RPA (Fig. 3.5B). Quantitation of multiple experiments confirmed the differences in RPA phosphorylation in two clones of *ETAA1Δ* HEK293T cells (Fig. 3.11B, C). Decreased RPA phosphorylation following ETAA1 knockdown was also observed in HeLa, HCT116, H157, BT549, and A549 cells (Fig. 3.11E). In contrast to RPA, ATR-dependent CHK1 phosphorylation was largely unaffected by ETAA1 inactivation (Fig. 3.11A,D,E). There is a change in ETAA1 protein migration and detection on immunoblots following treatment with CPT consistent with it being an ATM/ATR substrate (Fig. 3.11E) (Matsuoka et al., 2007).

To understand whether the defective RPA phosphorylation in ETAA1-deficient cells is due to a defect in ATR regulation, we mapped the ATR-binding motif in ETAA1 to an N-terminal region (Fig. 3.12A). Sequence analysis identified a highly evolutionarily conserved tryptophan (residue 107) accompanied by a short region of sequence similarity to the ATR-activation domain (AAD) of TOPBP1 within this region (Fig. 3.12B). In TOPBP1 this tryptophan is essential to bind and activate ATR (Kumagai et al., 2006). Mutation of ETAA1 W107 to alanine reduced the ability of ETAA1 to co-immunoprecipitate ATR (Fig. 3.12A).

Based on the similarity to TOPBP1 and the reduction in RPA phosphorylation in ETAA1-deficient cells, we considered the possibility that ETAA1 acts as a direct ATR activator. Indeed, like the TOPBP1 AAD, an ETAA1 fragment containing amino acids 75-250 purified from *E. coli*

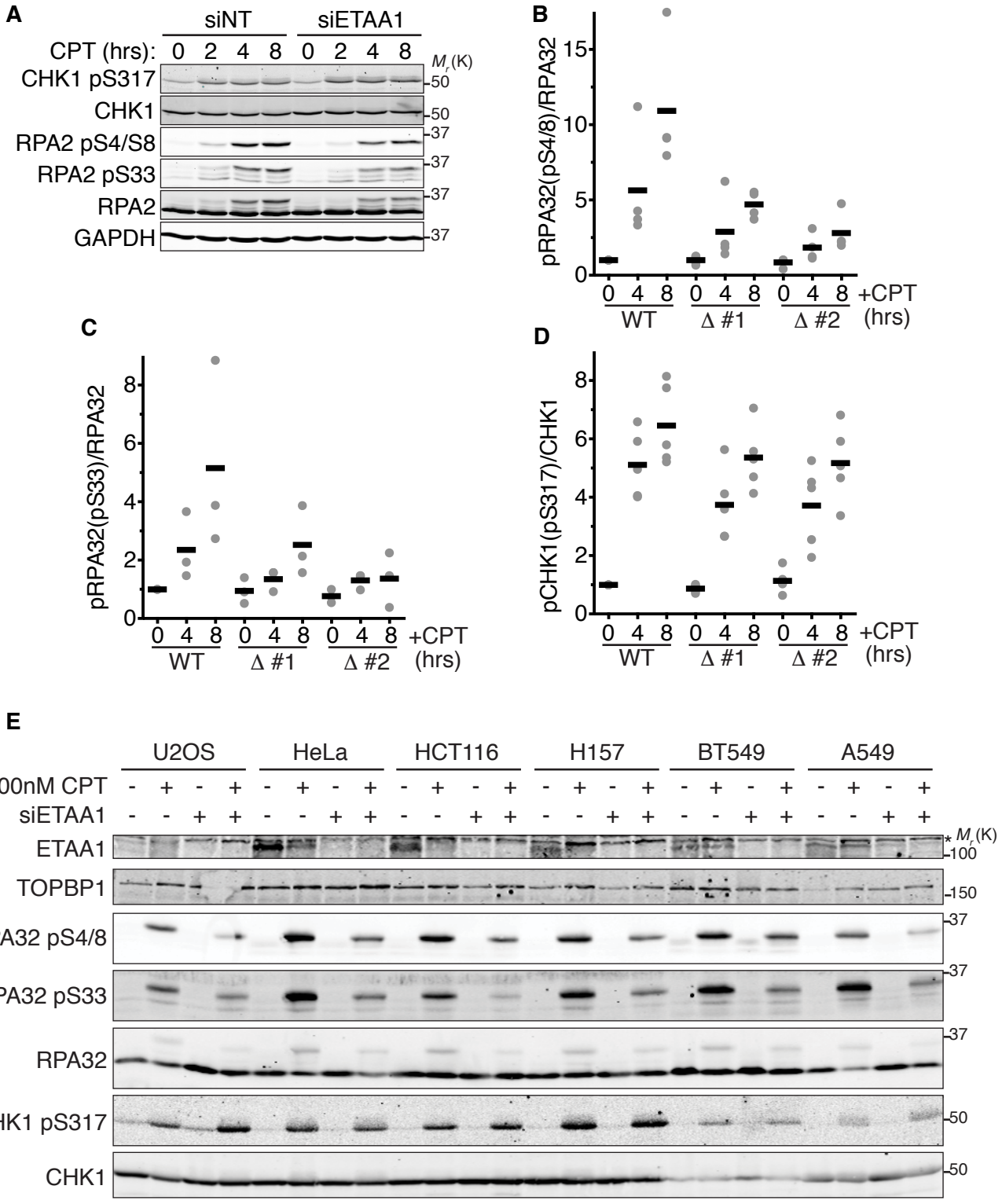

Figure 3.11. ETAA1 is required for RPA phosphorylation in multiple cell types. (A) U2OS cells transfected with non-targeting or ETAA1 siRNAs or **(B-D)** wild-type and two ETAA1Δ HEK293T cell clones were treated with 100 nM CPT for 2, 4, or 8 hrs. Cell lysates were separated by SDS-PAGE and immunoblotted with the indicated antibodies. The blots in a are representative of two experiments. **(B-D)** The amount of phosphorylated versus total RPA and CHK1 from n=4, 3, and 5 experiments in b, c, and d respectively is shown. Black bars are the mean. **(E)** U2OS, HeLa, HCT116, H157, BT549, and A549 cells transfected with non-targeting or ETAA1 siRNAs were left untreated or treated with 100 nM CPT for 8 hrs. Proteins were separated by SDS-PAGE and detected by immunoblotting.

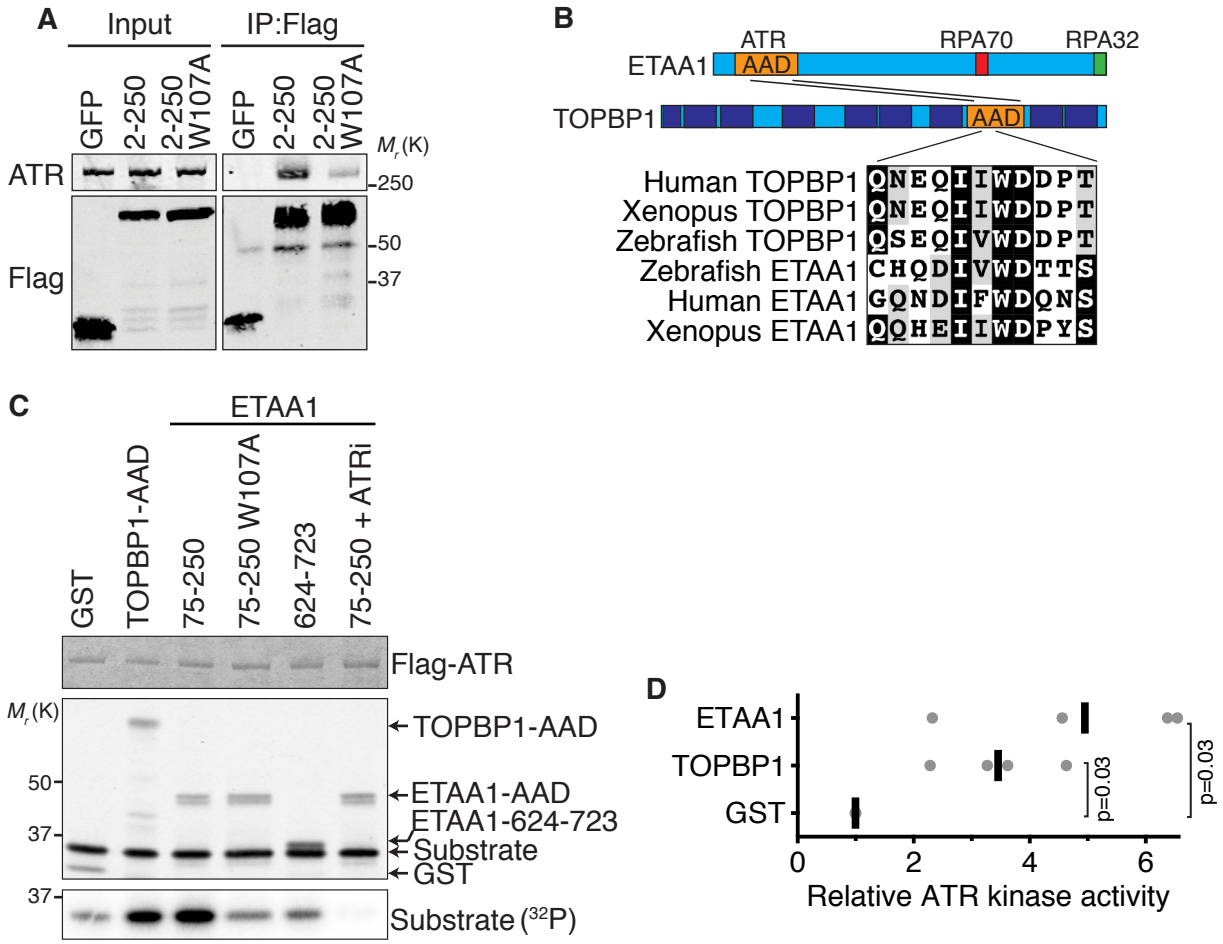

Figure 3.12 ETAA1 activates ATR. (A) Immunoprecipitates of GFP-Flag-NLS-tagged ETAA1 fragments expressed in HEK293T cells were immunoblotted for Flag and ATR. Representative blots from one of two independent experiments are shown. **(B)** Schematic diagram of the ETAA1 protein indicating the ATR-interacting domain and evolutionarily conserved sequence similarity with the TOPBP1-AAD. **(C)** Purified ATR/ATRIP complexes were incubated with GST-TOPBP1 or ETAA1 proteins purified from E. coli, substrate, and γ-32P-ATP. The kinase reactions were separated by SDS-PAGE prior to immunoblotting or quantitating substrate phosphorylation by phosphorimaging. ATRi, ATR inhibitor. **(D)** ATR kinase activity relative to the control reaction of n=4 independent experiments is graphed. Significance was calculated with the Mann-Whitney test.

activates ATR *in vitro* (Fig. 3.12 C,D). This activation requires W107, other fragments of ETAA1 do not stimulate ATR, and an ATR inhibitor eliminates the kinase activity indicating specificity. Thus, ETAA1 contains an AAD within amino acids 75-250, and ETAA1 is a direct ATR activator like TOPBP1.

We hypothesized that the increased DNA damage signaling that we observed in cells overexpressing ETAA1 (Fig. 3.1) could be due to ectopic activation of ATR like what happens upon TOPBP1-AAD overexpression (Kumagai et al., 2006; Toledo et al., 2008; Ball et al., 2007). It is also possible that ETAA1 overexpression could cause damage by interfering with RPA function yielding an RPA-exhaustion-like phenotype (Toledo et al., 2013). To test these ideas, we overexpressed various ETAA1 proteins and measured γH2AX. The high level of γH2AX induced by wild-type ETAA1 is reduced but not eliminated by mutation of the RPA-interacting motifs (Fig. 3.13A,C,E). These proteins are expressed at least 10-fold higher than the stable ETAA1 expressing cell lines that lack spontaneous ETAA1 foci (Fig. 3.13F). A fragment of ETAA1 missing the ETAA1 AAD (aa251-926) does not cause γH2AX despite its ability to localize to RPA-foci (Fig. 3.13B-D).

The ETAA1 AAD by itself is sufficient to induce γH2AX when highly overexpressed and the level of γH2AX induced is correlated with its expression level (Fig. 3.13B,C,E,G). In contrast, the ETAA1 AAD containing the W107A mutation largely does not induce damage signaling (Fig. 3.13B,C,H). Thus, we conclude that overexpression of ETAA1 promotes DNA damage signaling by binding both RPA and ATR, and high levels of expression of just the ETAA1 AAD is sufficient to activate ATR.

ETAA1 requires its RPA-interaction and ATR-activation domains to maintain genome stability

We next tested whether the ETAA1 replication stress response functions are dependent on its ability to bind RPA and activate ATR. First, we complemented the *ETAA1Δ* cells with wild-

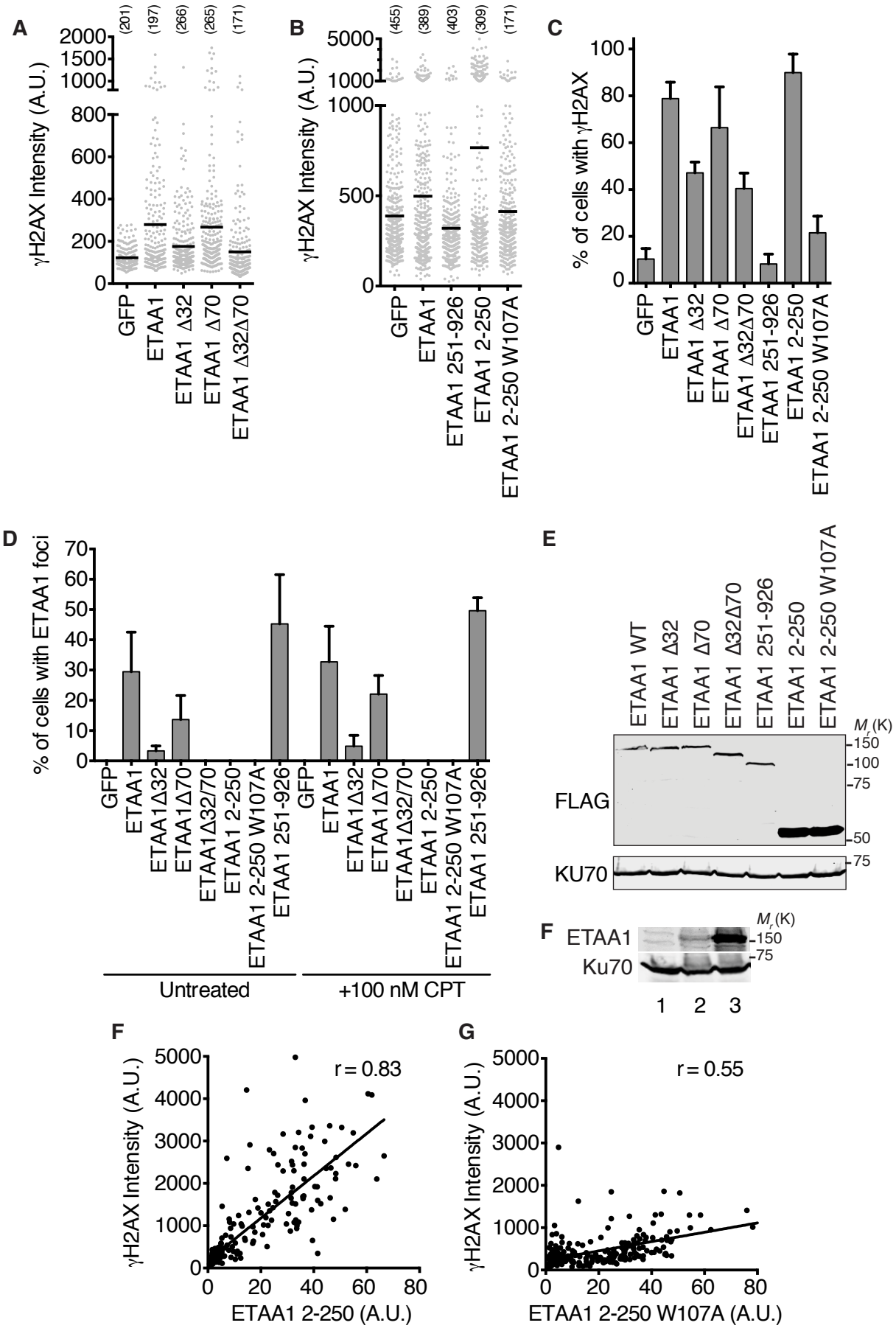

Figure 3.13. ETAA1 over-expression causes DNA damage signaling.

Figure 3.13. ETAA1 over-expression causes DNA damage signaling (continued). (A-H) U2OS cells were transfected with the indicated GFP-Flag-NLS-ETAA1 protein expression vectors, and GFP and γH2AX were visualized by immunofluorescence imaging. **(A,B)** Cell Profiler was used to quantitate γH2AX intensity in ETAA1 expressing cells. The intensity of each nucleus, mean intensity, and number of nuclei imaged is depicted. Data represent one out of three experiments in a and one out of two experiments in **B. (C,D)** The percentage of cells with γH2AX or ETAA1 foci were scored manually in blinded samples. Mean and SEM from n=4 experiments is graphed. **(E)** Immunoblot of proteins to examine expression levels. **(F) I**mmunoblot of untransfected (lane 1), transiently transfected (lane 3), and stable ETAA1 expressing cell lines after sorting (lane 2). **(G,H)** GFP-Flag-ETAA1-2-250 or 2-250-W107A intensity versus γH2AX intensity is plotted. Pearson correlation coefficient is shown. Data in **E-H** are representative of two experiments.

type or RPA binding mutant GFP-ETAA1 cDNA. Cells were sorted to select for the 10% of cells with the lowest expression of GFP-ETAA1 proteins (Fig. 3.14A, B). While wild-type ETAA1 fully complements the CPT hypersensitivity of *ETAA1Δ* cells, the ETAA1-ΔRPA expressing cells remain modestly hyper-sensitive (Fig. 3.14C). Furthermore, *ETAA1Δ* cells also exhibited significantly higher levels of genome instability as measured by micronuclei formation, which could be rescued by wild-type but not RPA-binding defective ETAA1 (Fig. 3.14D). Thus, we conclude that RPA binding is needed for ETAA1 to maintain genome stability.

To examine the cellular functions of the ETAA1 AAD and avoid problems caused by ETAA1 overexpression we devised a strategy to delete the AAD in the endogenous *ETAA1* gene locus. A portion of the AAD including W107 is encoded by *ETAA1* exon 2. Cas9-mediated deletion of exon 2 using two guide RNAs spanning the 5' intron-exon boundary results in the production of an ETAA1 mRNA in which exon 1 splices to exon 3. This mutation maintains the open reading frame and results in the expression of an ETAA1Δexon2 protein missing residues 76-118 that remains capable of binding RPA (Fig. 3.15A,B).

ETAA1Δexon2 cells show a very similar reduction in DNA replication track lengths as the *ETAA1Δ* cells in response to a CPT challenge (Fig. 3.15C,D). They also exhibit a reduction in RPA phosphorylation (Fig. 3.16A,B,C), although there is no obvious defect in CHK1 or MCM2 phosphorylation (Fig. 3.16A,D).

ETAA1-deficient cells exhibit elevated levels of SCEs

Many of the other proteins that ETAA1 associates with are involved in recombination-based repair mechanisms. However, we did not observe a significant hypersensitivity of ETAA1-deficient cells to ionizing radiation (Fig. 3.7A) or PARP inhibition (Fig. 3.7C,D). The interaction of ETAA1 with both HLTF and the BTR complex was of interest since the budding yeast orthologue of HLTF (RAD5) promotes template switching, while the BLM orthologue (SGS1)

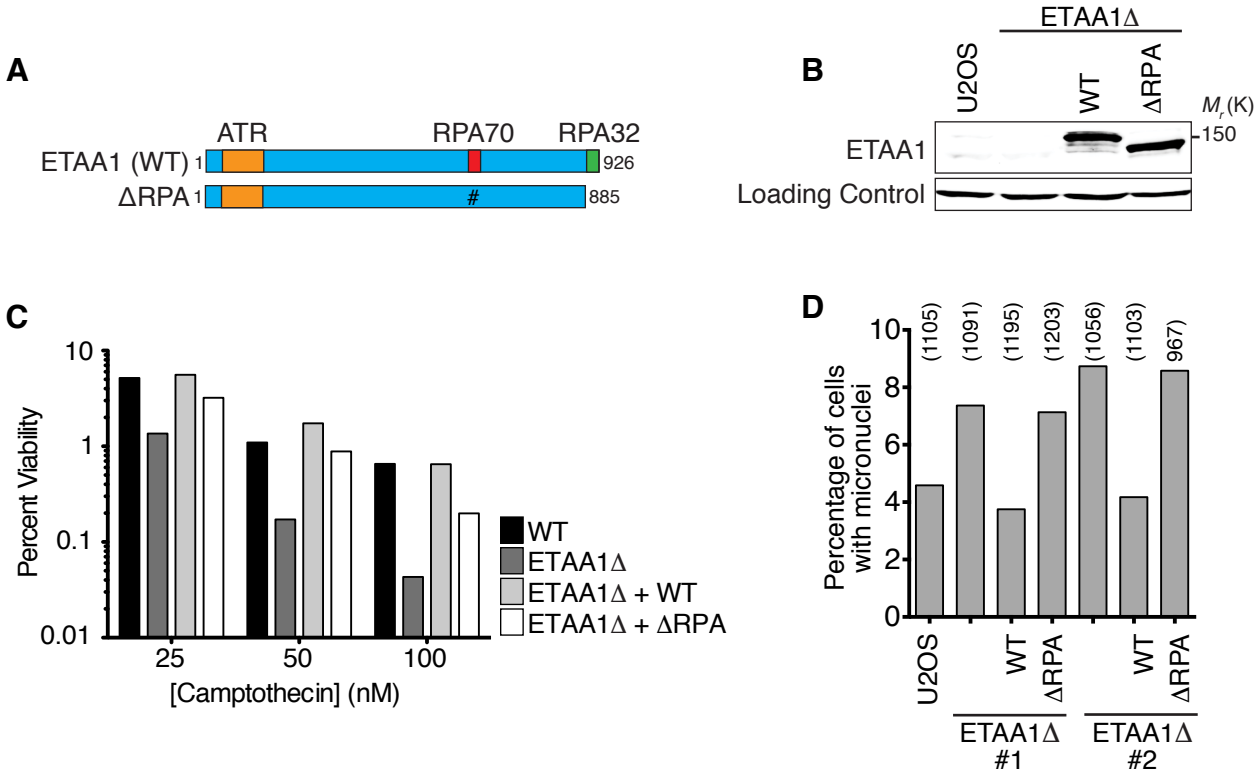

Figure 3.14. An interaction with RPA is needed for ETAA1 to maintain genome integrity. (A,B) ETAA1Δ cells were infected with wild-type or RPA binding-deficient ETAA1 lentiviruses. After antibiotic selection, the cell populations were sorted to select for the 10% of cells expressing the lowest amount of ETAA1 protein. (b) Immunoblot shows that the complemented cells overexpress approximately equal amounts of wild-type (WT) and ETAA1ΔRPA proteins. **(C)** Cell populations were challenged with the indicated concentrations of CPT and cell viability measured after 72 hrs. The mean viability from three technical replicates from one of two independent experiments is shown. **(D)** The percentage of cells with micronuclei was scored in the indicated cell populations. Data from two independent complemented ETAA1Δ clones are shown. The mean percentage of cells with micronuclei and total number of nuclei scored from five technical replicates of one of two biological replicates is shown.

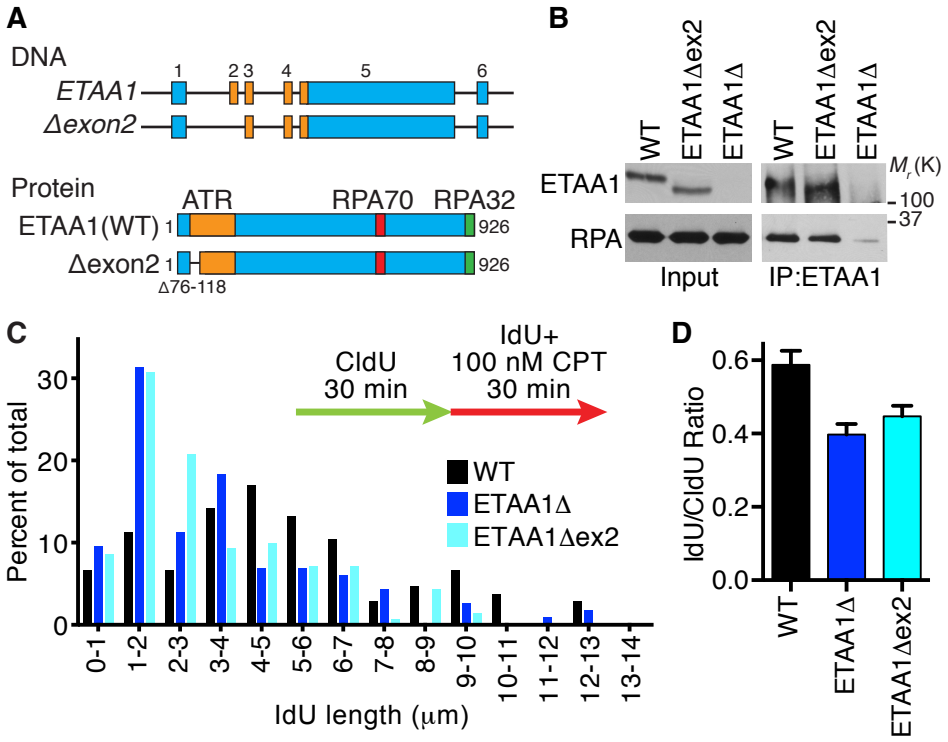

Figure 3.15 The ETAA1 ATR activation domain is needed to maintain fork stability **(A)** Schematic of the ETAA1Δexon2 gene and protein. **(B)** ETAA1 immunoprecipitates from wild-type, ETAA1Δ, and ETAA1 Δexon2 cells were immunoblotted for ETAA1 and RPA. Data are representative of two experiments. **(C, D)** Cells were labeled with CldU and IdU and treated with 100 nM CPT during the second labeling period. DNA fibers stretched on a microscope slide were stained with IdU and CldU antibodies, imaged, and the lengths of fiber tracks measured. n=107, 116, and 105 fibers for WT, ETAA1Δ, and ETAA1Δexon2 respectively. One of two biological replicates is shown.

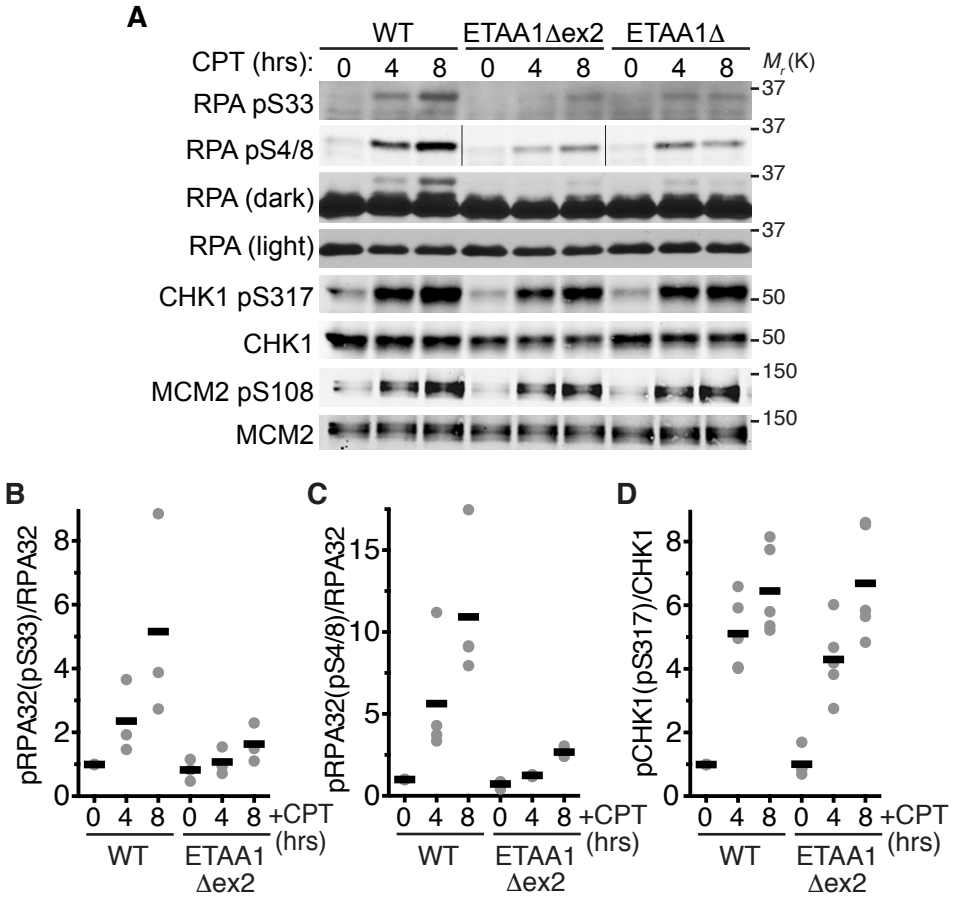

Figure 3.16 The ETAA1 ATR activation domain is needed for ATR signaling (A-D) Wild-type, ETAA1Δ, and ETAA1Δexon2 HEK293T cells were treated with 100 nM CPT for 0, 4, or 8 hrs. Cell lysates were immunoblotted for phosphorylated and total RPA and CHK1. Black bars are the mean from n=3, 4, and 5 experiments in **B**, **C**, and **D** respectively.

helps to dissolve these repair intermediates to prevent crossovers (Putnam et al., 2010). The human BTR complex also promotes non-crossover repair outcomes during replication fork repair (Wu et al., 2006; Bussen et al., 2007; Raynard et al., 2006). Thus, a defining characteristic of BLM-deficient cells is a striking increase in SCEs. Indeed, BLM silencing increases SCEs by approximately 10-fold while silencing ETAA1 resulted in a 2.5-fold increase (Fig. 3.17A,B). *ETAA1Δ* cells also exhibited an increased frequency of SCEs compared to controls (Fig. 3.17C). The frequency of SCEs in *ETAA1Δ* and wild-type cells transfected with BLM siRNA were not different suggesting an epistatic relationship (Fig. 3.17C). Both ETAA1 and BLM-deficiency also yield increased levels of micronuclei, and again ETAA1 and BLM are epistatic for this phenotype (Fig. 3.17D,E). *ETAA1Δexon2* cell lines also exhibit elevated levels of micronuclei and SCEs similar to the *ETAA1Δ* cells indicating that ETAA1 must be able to activate ATR to prevent genetic instability (Fig. 3.17F, G).

ETAA1 and TOPBP1 function in distinct pathways

ETAA1 is similar to TOPBP1 in that both activate ATR, complex with BLM, and prevent SCEs. Thus, we considered whether they function in the same or distinct pathways. Unlike ETAA1 deficiency, TOPBP1 knockdown has a strong affect on ATR-dependent CHK1 phosphorylation (Fig. 3.18A). However, we consistently observe that RPA phosphorylation is primarily dependent on ETAA1 and only modestly affected by TOPBP1 knockdown. We also did not observe TOPBP1 in our ETAA1 purifications suggesting they function in distinct pathways.

TOPBP1 binding and ATR activation requires ATR amino acids between the kinase and FATC domains called the PIKK regulatory domain (PRD) (Mordes et al., 2008a). Mutations in the PRD do not interfere with the basal activity of ATR, but they greatly reduce the ability of TOPBP1 to activate ATR (Mordes et al., 2008a). Like TOPBP1, ETAA1-dependent ATR activation is greatly diminished by ATR PRD mutations (Fig. 3.18B). This result and the

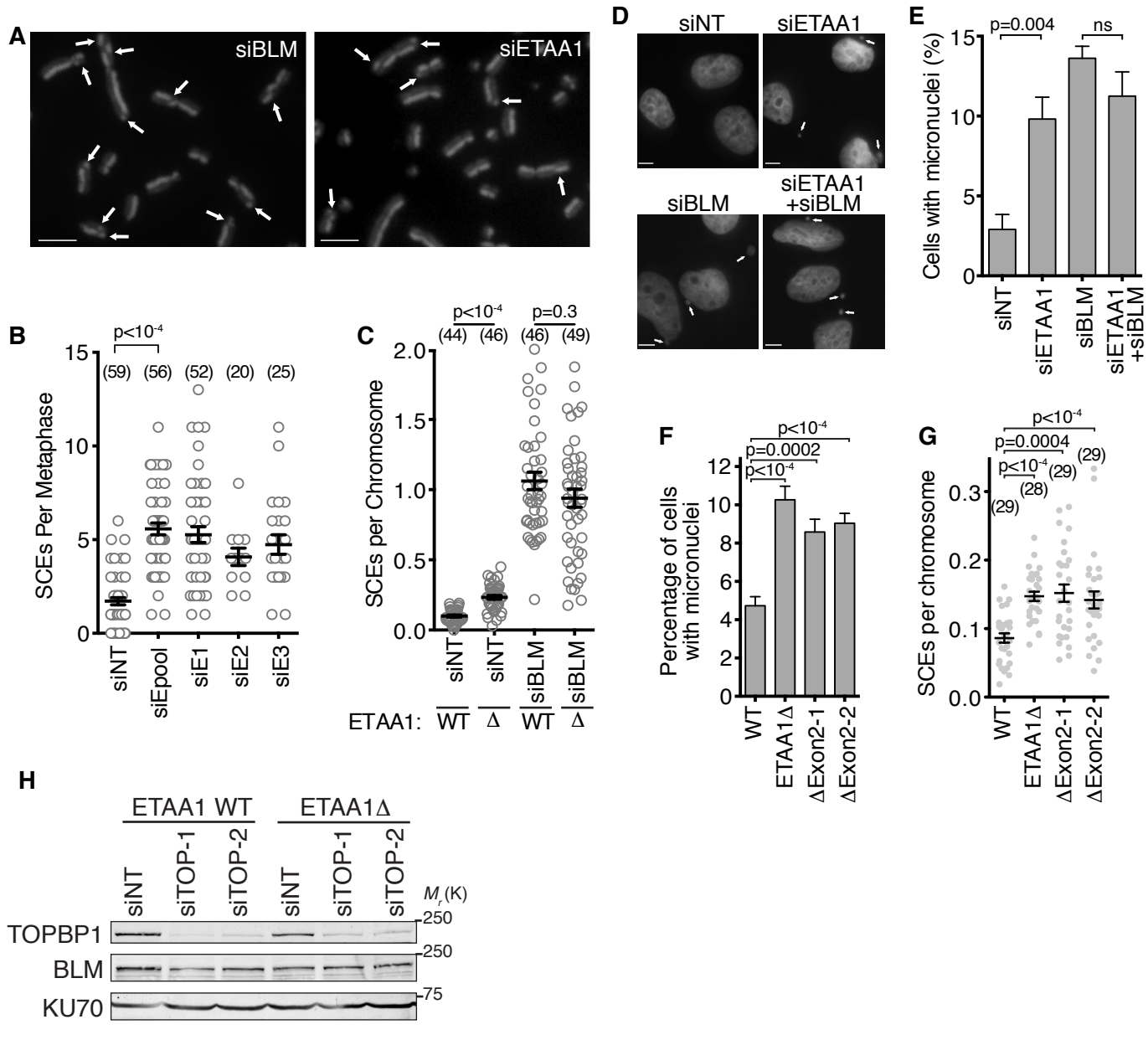

Figure 3.17 ETAA1 deficient cells have elevated sister chromatid exchanges and genetic instability. (A,B) SCEs were imaged and scored after ETAA1 knockdown. Scale bars are 5 μm. Four eperiments were performed for siNT and siEpool and one experiment was completed for the other siRNAs. Mean and SEM from a representative experiment is shown and significance calculated by ANOVA with a Dunnett multiple comparison post-test. The number of metaphases analyzed (n value) is indicated. **(C)** SCEs were scored in wild-type or ETAA1Δ U2OS cells transfected with non-targeting or BLM siRNAs. Data are representative from three independent experiments and significance was calculated with a Mann-Whitney test. The number of metaphases (n value) is indicated. **(D,E)** Micronuclei were imaged and scored in U2OS cells transfected with non-targeting, ETAA1, or BLM siRNAs as indicated. Data are mean and SD of n=3 independent experiments. Scale bar is 5 μm. **(F)** Micronuclei and **(G)** SCEs were scored in wild-type, ETAA1Δ, and two independent ETAA1Δexon2 U2OS cell clones. Mean, SEM, and number of metaphases analyzed (n value) is presented. Significance in e, f and g was determined by ANOVA with a Dunnett multiple comparison post-test. **(H)** WT and ETAA1Δ U2OS cells were transfected with non-targeting or two siRNAs targeting TOPBP1. Cell lysates were immunoblotted with the indicated antibodies.

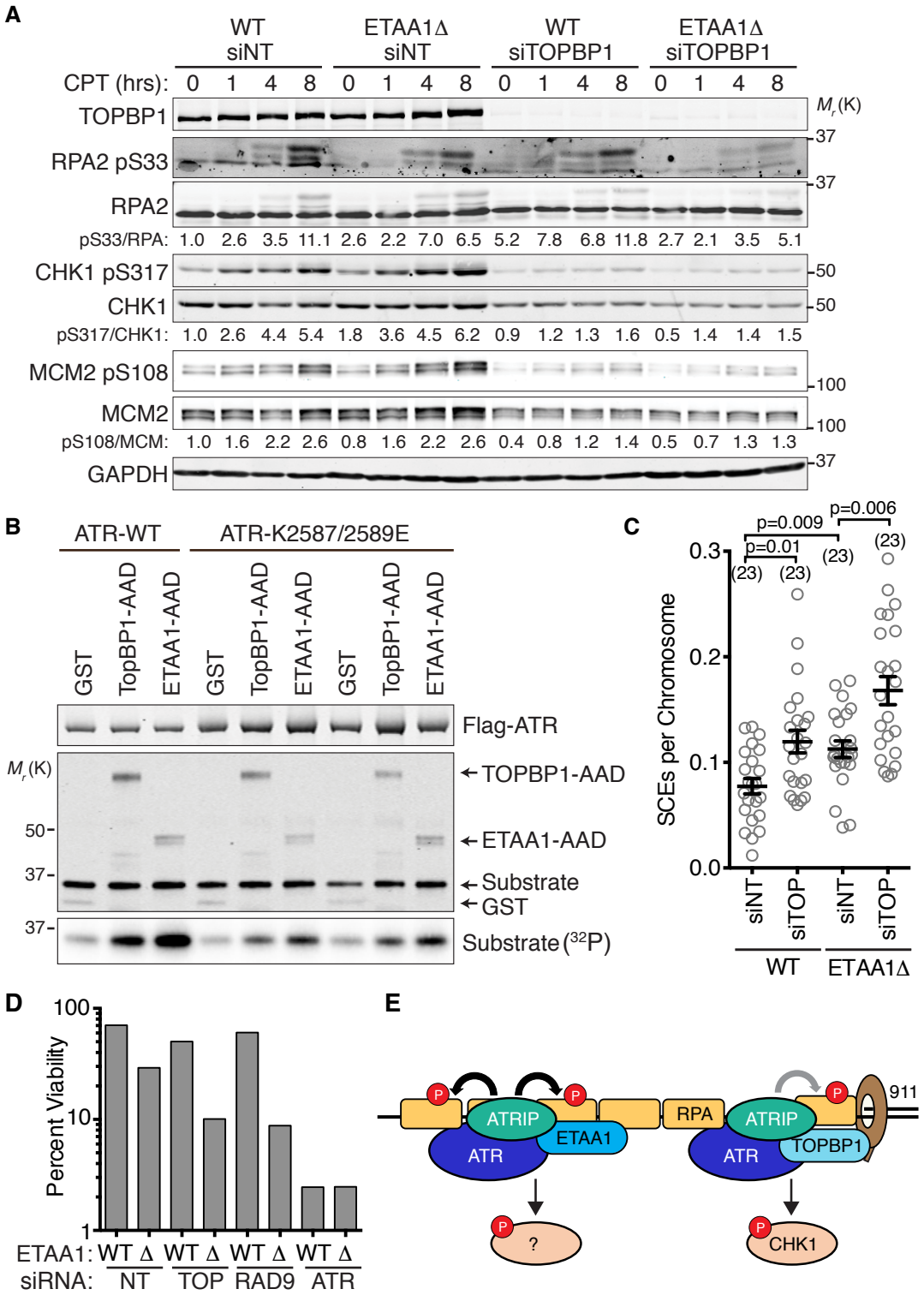

Figure 3.18 ETAA1 and TOPBP1 act in separate pathways to regulate ATR and maintain genome stability. (A) Wild-type or ETAA1Δ U2OS cells were transfected with non-targeting or TOPBP1 siRNAs, treated with 100 nM CPT for the indicated times, lysed, and immunoblotted with the indicated antibodies. Blots are representative of two experiments.

Figure 3.18 ETAA1 and TOPBP1 act in separate pathways to regulate ATR and maintain genome stability (continued). **(B)** Purified wild-type or mutant ATR/ATRIP complexes were incubated with GST or the AAD domains of TOPBP1 or ETAA1 in the presence of substrate and γ-32P-ATP. The kinase reactions were separated by SDS-PAGE prior to immunoblotting or quantitating substrate phosphorylation by phosphorimaging. Two independent replicates of the mutant ATR kinase reactions are shown. **(C)** SCEs in wild-type or ETAA1Δ U2OS cells transfected with non-targeting or TOPBP1 siRNAs were quantitated. Error bars are SEM and significance was calculated with a Mann-Whitney test. The number of metaphases scored (n value) is indicated. **(D)** Cells transfected with non-targeting, TOPBP1, RAD9, or ATR siRNAs were challenged with 10 nM CPT for 24 hrs and viability was determined by clonogenic assay. Untreated viability was set at 100%. Bars indicate the mean of three technical replicates from a representative experiment of two independent experiments **(E)** Simplified model of ATR activation by ETAA1 and TOPBP1. The 911 complex stabilizes TOPBP1 at stalled forks and assists in the TOPBP1-dependent activation pathway. ETAA1 is recruited directly by RPA and functions independently of 911 and TOPBP1 to activate ATR.

similarity of the AAD motifs suggest that ETAA1 and TOPBP1 utilize a similar mechanism to activate ATR.

ETAA1 requires its AAD to prevent SCEs (Fig. 3.17G), while TOPBP1 is reported to regulate SCEs independently of its AAD (Wang et al., 2013; Blackford et al., 2015). TOPBP1 knockdown yields a similar increase in SCEs as ETAA1-deficiency and TOPBP1 knockdown in *ETAA1Δ* cells further increases SCE frequency above that of either TOPBP1 or ETAA1-deficiency alone again consistent with operation in distinct pathways (Fig. 3.18C). Previous studies have made conflicting conclusions about whether TOPBP1 regulation of BLM is through changing its stability (Wang et al., 2013; Blackford et al., 2015). We did not observe large changes in BLM protein levels when we knocked down TOPBP1, and ETAA1 deficiency also does not alter BLM protein levels (Fig 3.17H).

Finally, if ETAA1 and TOPBP1 pathways are distinct we would expect loss of ETAA1 to be synthetically lethal with TOPBP1 or 911 deficiency. Indeed, knockdown of TOPBP1 or RAD9 resulted in decreased survival of *ETAA1Δ* cells following a challenge with CPT (Fig. 3.18D). Taken together, these data indicate that ETAA1 and TOPBP1 function in distinct pathways to activate ATR signaling and maintain genome stability.

Discussion

Previous studies identified three ATR (Mec1) activators in budding yeast (Dpb11, Ddc1, and Dna2) (Navadgi-Patil and Burgers, 2009, 2008a; Kumar and Burgers, 2013). We now report that human cells contain at least two ATR activators, TOPBP1 and ETAA1. This conclusion is consistent with that of the accompanying paper that independently identified ETAA1 as an ATR activator (Haahr et al., 2016). TOPBP1 is the Dpb11 functional orthologue; however, ETAA1

does not resemble any of the yeast ATR activating proteins outside of the key residues needed to activate ATR.

TOPBP1 and ETAA1 act in separate pathways to maintain genome integrity and regulate ATR. The ability of ETAA1 to bind directly to RPA distinguishes it from TOPBP1, which requires the MRN and 911 complexes for its recruitment and ATR activating function (Duursma et al., 2013; Delacroix et al., 2007a). 911 is only loaded on DNA gaps when a free 5' end is available at the ssDNA-dsDNA junction. Thus, extensive ssDNA generation may not generate more 911-TOPBP1-ATR signaling complexes. We propose that ETAA1 helps to propagate ATR activation along stretches of ssDNA since it can bind RPA and function independently of 911 (Fig. 3.18E).

RPA is particularly dependent on ETAA1 for phosphorylation; whereas other ATR substrates like CHK1 and MCM2 are more dependent on TOPBP1. CHK1 phosphorylation requires the replisome component CLASPIN (Kumagai and Dunphy, 2000), and MCM2 is part of the replicative helicase. Thus, it is possible that the proximity to the replisome where it may be more likely to have a 5' DNA junction to load 911/TOPBP1 could determine ETAA1 vs. TOPBP1 dependency. The ability of TOPBP1 and ETAA1 to interact with DDR proteins or their relative level of expression, which differs considerably across cell types, may be additional levels of substrate selection.

In conclusion, ETAA1 is a replication stress response protein needed to maintain genome stability. ETAA1 complexes with multiple DDR proteins and one mechanism of ETAA1 action in the replication stress response is as a direct ATR activator. The requirement for ETAA1 to maintain genome stability could be why polymorphisms in the *ETAA1* locus increase the risk of pancreatic cancer (Childs et al., 2015a; Wu et al., 2012).

Conclusions

The replication stress response is well conserved throughout eukaryotes; however, yeast have three proteins that can activate Mec1, while eukaryotes had only one known ATR activator, TOPBP1. Our data identified the previously uncharacterized protein ETAA1 as a potential replication stress response protein in two proteomic screens. We validated its function during replication stress and discovered that like TOPBP1, ETAA1 can stimulate ATR kinase activity, identifying it as a second activator of ATR. Furthermore, we found that ETAA1 contains two RPA-interacting motifs that are necessary for its localization to sites of RS. Loss of ETAA1 or deletion of its AAD sensitizes cells to replication stress and DNA damage. Lastly, found that ETAA1 and TOPBP1 regulate ATR through separate pathways.

CHAPTER IV

QUANTITATIVE PHOSPHOPROTOMICS REVEALS MITOTIC FUNCTION OF THE ATR-ACTIVATOR ETAA1

Introduction

ATR is an apical DNA damage response (DDR) kinase that promotes genome stability by regulating the cell division cycle and cellular stress responses (Saldivar et al., 2017). ATR signaling coordinates the DNA replication stress response, controls the S/G_2 and G_2/M transitions to ensure completion of DNA replication before mitosis, and ensures proper chromosome separation during mitosis (Cimprich and Cortez, 2008; Saldivar et al., 2018; Kabeche et al., 2017; Zachos et al., 2007).

In budding yeast there are at least three activators of the ATR-orthologue, Mec1 that regulate timing of Mec1 activation and direct what substrates are phosphorylated (Kumar and Burgers, 2013; Mordes et al., 2008b; Navadgi-Patil and Burgers, 2008b, 2009; Bastos de Oliveira et al., 2015). The cell-cycle-specific utilization of each Mec1 activator allows for temporal regulation of Mec1 throughout the process of cell division (Navadgi-Patil and Burgers, 2011). Additionally, Mec1 activators direct Mec1 to phosphorylate substrates proximal to the activator promoting localization-dependent Mec1 signaling (Lanz et al., 2018).

In mammalian cells, ATR kinase activity is regulated by at least two ATR-activating proteins ETAA1 and TOPBP1 (Bass et al., 2016; Haahr et al., 2016; Lee et al., 2016; Kumagai et al., 2006). Although ETAA1 and TOPBP1 share similar ATR activation domains and may interact with ATR similarly (Bass et al., 2016), they are recruited to DNA via different mechanisms. ETAA1 is recruited by a direct interaction with RPA bound to single stranded DNA (ssDNA) (Bass et al., 2016; Haahr et al., 2016; Feng et al., 2016; Lee et al., 2016); whereas

TOPBP1 is recruited to the 5' junction of single and double-stranded DNA by the RAD9/RAD1/HUS1 (9-1-1) complex with assistance from RHINO and the MRE11/RAD50/NBS1 (MRN) complex (Delacroix et al., 2007b; Lee et al., 2007b; Cotta-Ramusino et al., 2011; Lindsey-Boltz et al., 2015; Duursma et al., 2013).

Loss of ETAA1 or TOPBP1 differentially effect phosphorylation of ATR substrates such as CHK1 and RPA in cells exposed to replication stress (Bass et al., 2016). ETAA1 also appears especially important for the newly described function of ATR in controlling the S/G_2 transition in unstressed cells (Saldivar et al., 2018). To more globally determine how ETAA1 and TOPBP1 influence ATR signaling, we utilized quantitative phosphoproteomics to identify changes in protein phosphorylation in cells deficient for each ATR-activator. These data indicated that ETAA1 may be particularly important for the mitotic functions of ATR. Indeed, ETAA1-dependent activation of ATR during mitosis promotes Aurora B kinase signaling, prevents chromosomal misalignment during metaphase and maintains the spindle assembly checkpoint. Thus, ETAA1 may be the primary ATR activator to control cell division in unstressed cells while TOPBP1 has a dominant function in response to replication stress.

Results

Generation of cell lines deficient for ATR activators

To interrogate the unique functions of ETAA1 and TOPBP1, we utilized CRISPR/Cas9 genome editing to generate HCT116 cells deficient for each ATR activator. ETAA1 function was disrupted by targeting the 5' splice junction of exon 2, resulting in an in-frame deletion of *ETAA1* that removes part of the ATR activation domain (AAD) containing a tryptophan residue required to activate ATR (Fig. 4.1A, B). These ETAA1ΔAAD cells express a mutant ETAA1 protein

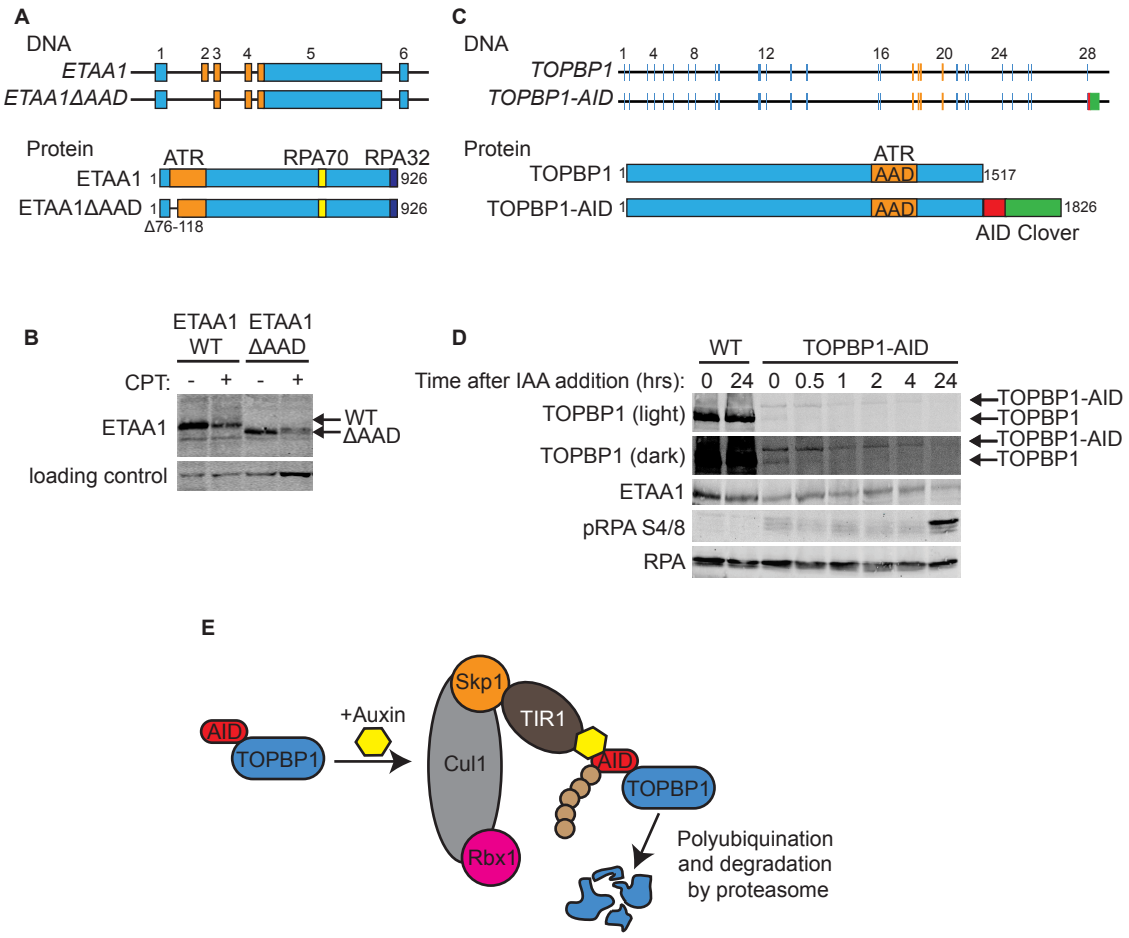

Figure 4.1 Production of ETAA1 and TOPBP1-deficient cell lines. (A) Schematic of the ETAA1ΔAAD gene and protein. **(B)** HCT116 and HCT116 ETAA1ΔAAD cells were lysed and immunoblotted with ETAA1 antibodies. Upper band is full length ETAA1 and lower band is mutated ETAA1. ETAA1 electrophoretic mobility is altered following CPT treatment independent of its interaction with ATR. **(C)** Schematic of the TOPBP1-AID gene and protein. **(D)** HCT116 WT and TOPBP1-AID cells were treated with 500 μM IAA for the indicated times. Cells were lysed and immunoblotted with the indicated antibodies. Upper band is full length TOPBP1-AID and lower band is TOPBP1. **(E)** Schematic of TOPBP1 degradation by the auxin inducible degron system.

which can bind RPA and localize to sites of DNA damage but is incapable of binding and activating ATR (Bass et al., 2016).

Unlike ETAA1, TOPBP1 is required for cell viability and has essential functions during the initiation of DNA replication (Garcia et al., 2005). We attempted to mutate the TOPBP1-AAD in HCT116 cells using CRISPR-Cas9 but were unsuccessful, consistent with the observation that inactivation of the TOPBP1-AAD results in cell death in mice (Zhou et al., 2013). To circumvent these obstacles, we tagged endogenous *TOPBP1* with an auxin inducible degron (AID) (Fig. 4.1C-E). The tag itself reduced TOPBP1 expression significantly but yielded viable cell lines that retained proliferative capacity (Fig. 4.1D, Fig. 4.2A and C). Addition of the auxin indole-3-acetic acid (IAA) resulted in specific and rapid degradation of TOPBP1, cell death, and block to proliferation (Fig. 4.1D, Fig. 4.2B,D). Thus, this approach provides a rapid method of inactivating TOPBP1.

In addition to producing cell lines defective for ETAA1 or TOPBP1, we generated ETAA1ΔAAD/TOPBP1-AID cells that are conditionally deficient for both ATR activating proteins. Prolonged IAA treatment in wild type (WT) or ETAA1ΔAAD cells did not increase γH2AX levels, a biomarker for DNA damage (Fig. 4.2E). However, cells containing the TOPBP1-degron stopped growing and began to accumulate DNA damage as indicated by induction of γH2AX and phosphorylated RPA (Fig. 4.1D, Fig. 4.2B, E). Cells deficient for both ETAA1 and TOPBP1-AID exhibited much more severe genomic instability evident by fragmented nuclei and high levels of γH2AX consistent with the conclusion that these ATR activators function in separate pathways (Fig. 4.2E).

To examine replication stress signaling in cells defective for ETAA1 or TOPBP1, cells were treated with 100 nM camptothecin (CPT) for four hours following a two-hour pretreatment with IAA. As previously observed in other cell types (Bass et al., 2016), loss of ETAA1-dependent ATR activation resulted in a reduction in RPA phosphorylation but did not strongly affect CHK1 phosphorylation (Fig. 4.2F). While addition of the AID tag lowered endogenous

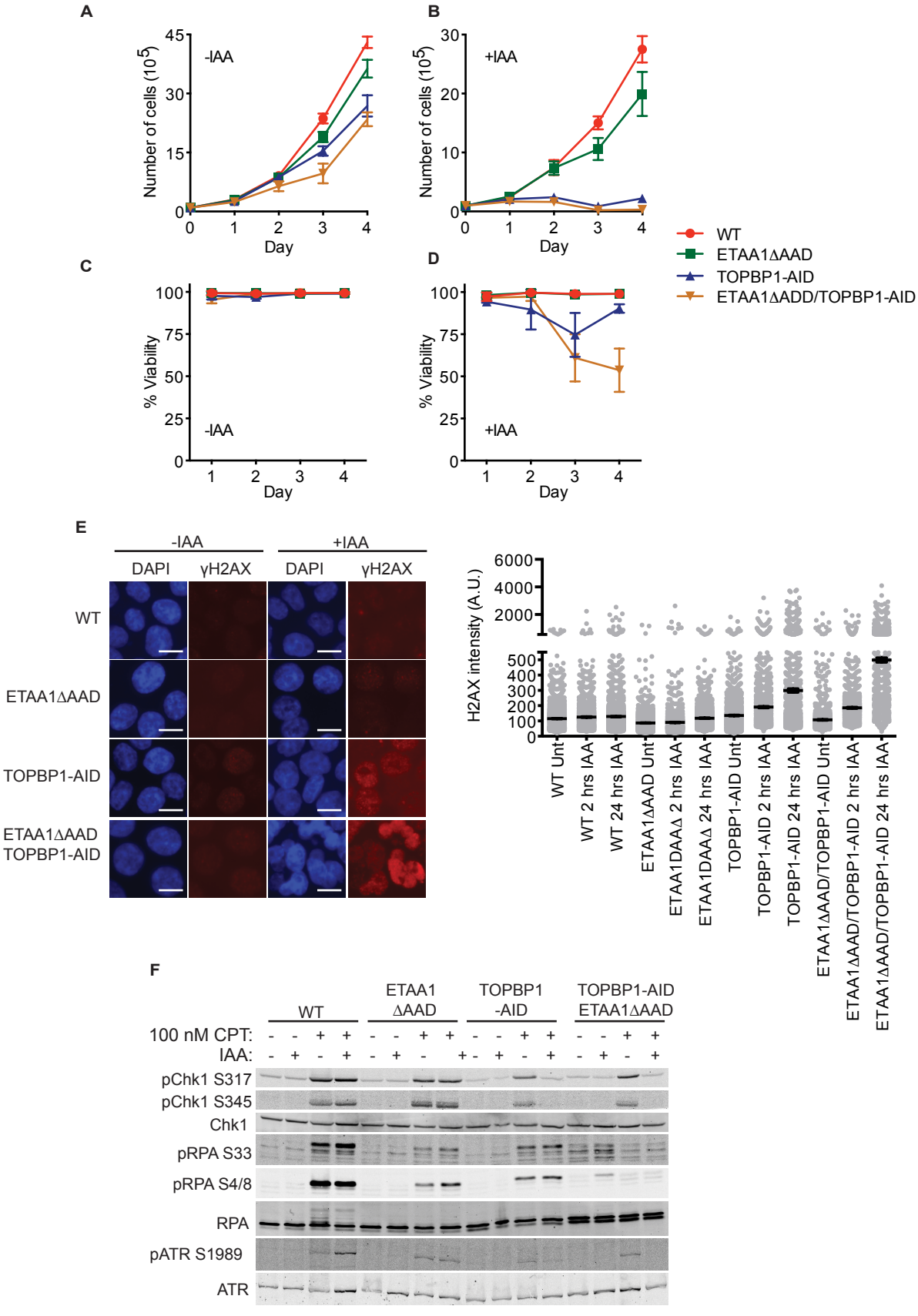

Figure 4.2 Characterization of ETAA1 and TOPBP1-deficient cell lines.

Figure 4.2 Characterization of ETAA1 and TOPBP1-deficient cell lines (continued). (A, B) HCT116 WT, ETAA1Δ AAD, TOPBP1-AID, and ETAA1ΔAAD/TOPBP1-AID cells were left untreated **(A)** or treated **(B)** with 500 μM IAA. Cells numbers were counted every 24 hours. **(C and D)** Same as in **A** and **B** but viability was measured by trypan blue. **(E)** HCT116 (WT), ETAA1ΔAAD, TOPBP1-AID, and ETAA1ΔAAD/TOPBP1-AID cells were treated with DMSO or IAA for 2 or 24 hours and γH2AX induction measured by immunofluorescence imaging. Representative images and quantification are shown. Scale bar is 10 μM. **(F)** Cells were treated with 100 nM CPT for four hours following a two-hour pretreatment with IAA or DMSO as indicated, then lysed and immunoblotted with the indicated antibodies.

TOPBP1 levels, these cells remained capable of activating ATR and only showed reduced ATR signaling after treatment with IAA to degrade TOPBP1 (Fig. 4.2F). Cells deficient for both ETAA1 and TOPBP1 exhibited more severe defects in RPA and ATR phosphorylation than the single mutants further demonstrating that ETAA1 and TOPBP1 function in separate pathways to activate ATR (Fig. 4.2F).

Quantitative phosphoproteomics identifies ETAA1 and TOPBP1-dependent phosphosites

To examine how each ATR activator differentially regulates ATR signaling responses, we compared the nuclear phosphoproteomes of wild type cells to cells deficient for each ATR activator using SILAC-mass spectrometry (Fig 4.3A). WT, ETAA1ΔADD and TOPBP1-AID cells labeled with heavy (^{13}C) or light (^{12}C) arginine and lysine were treated for four hours with 100 nM CPT following a two-hour pretreatment with IAA. Cells were harvested, combined in a 1:1 ratio, nuclei isolated, lysed, and fractionated into soluble nuclear extract and insoluble/chromatin-bound proteins. The nuclear soluble proteins were proteolyzed by treatment with trypsin while chromatin bound proteins were denatured in 8 M urea and subsequently proteolyzed by LysC and trypsin. Phosphopeptides from each fraction were enriched using TiO_2 beads and identified and quantified by liquid chromatography-tandem mass spectrometry (LC-MS/MS). The abundance of each phosphopeptide in wild type compared to the ATR-activator deficient cell line was measured. Three replicates of TOPBP1-AID cells and four replicates of ETAA1ΔAAD cells were analyzed.

Using this approach, we identified a total of 20,674 unique phosphosites on 4,045 proteins. Phosphosites that were observed at least twice with a median decrease in abundance in activator-deficient cells of at least 1.5 fold in either the nuclear soluble or chromatin fractions were considered as dependent on that activator (Fig. 4.3B). Using these criteria, 285 phosphosites were ETAA1-dependent, 724 phosphosites TOPBP1-dependent, and 118 phosphosites were dependent on both ATR activators (Fig. 4.3C). These phosphorylation sites

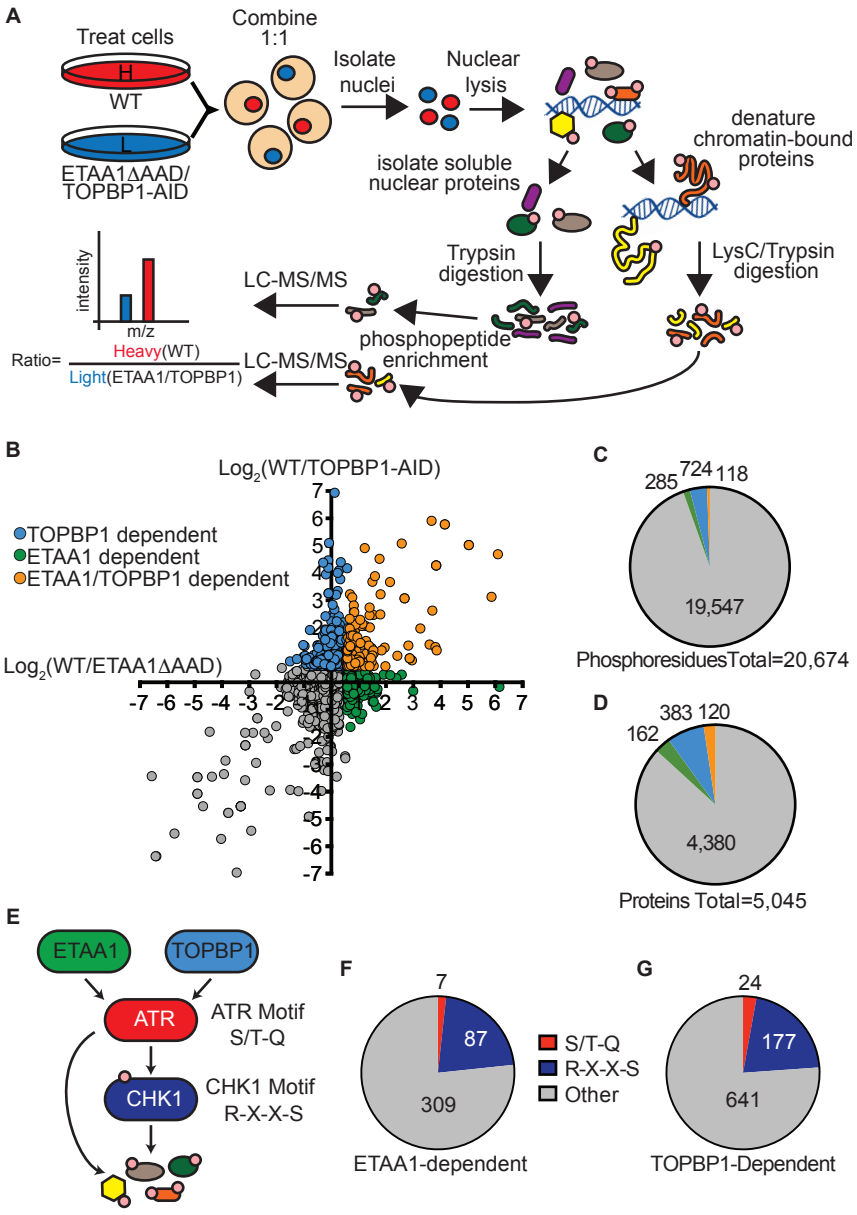

Figure 4.3 Quantitative phosphoproteomics identifies ETAA1 and TOPBP1-dependent phosphorylation sites. **(A)** Schematic of SILAC-phosphoproteomics approach. **(B)** Scatter plot of phosphoproteomic data. Each point represents a phosphosite and the X and Y value corresponds to the log2 transformed ratios of ETAA1 and TOPBP1 dependent phosphorylation events. Higher ratio values correspond to more phosphorylation in wild type (WT) cells than in ETAA1ΔAAD or TOPBP1-AID cells. **(C)** Number of phosphosites and **(D)** phosphoproteins dependent on ETAA1, TOPBP1, or both ATR activators. **(E)** Diagram of ATR signaling pathway with preferred phosphorylation motifs of ATR and CHK1. **(F,G)** Abundance of ATR and CHK1 motifs in ETAA1 and TOPBP1-dependent phosphorylation sites.

were located on 162 proteins unique to ETAA1, 383 proteins unique to TOPBP1, and 120 proteins regulated by both ETAA1 and TOPBP1 (Fig. 4.3D). Tables 4.1, 4.2 and 4.3 contain a complete list of all ETAA1, TOPBP1, and dual-dependent phosphosites and are provided at the end of this chapter.

While ATR has been found to phosphorylate a variety of sequences, it preferentially phosphorylates serine or threonines followed by a glutamine (S/T-Q) (Kim et al., 1999). CHK1 preferentially phosphorylates serine with an arginine in the -3 position (R-X-X-S) (O'Neill et al., 2002) (Fig. 4.3E). Of the 403 ETAA1-dependent phosphorylation sites only 7 corresponded to the preferred ATR motif, while 87 had a CHK1 phosphorylation motif. Of the 842 TOPBP1-dependent phosphorylation sites 24 contained an ATR motif, while 177 had a CHK1 phosphorylation motif (Fig. 4.3F, G). Thus, most of these phosphorylation events are likely to be indirectly targeted downstream of ATR by CHK1 or other ATR-regulated kinases.

Gene ontology analysis of ETAA1 and TOPBP1-dependent phosphorylation

To determine if ETAA1 or TOPBP1 regulate specific biological processes we performed a gene ontology (GO) enrichment analysis on the phosphoproteins regulated by each ATR-activator. To consolidate similar GO terms and easily visualize the relationship between terms, ClueGO was utilized to generate a functionally organized GO term network (Bindea et al., 2009). Phosphoproteins and their corresponding GO terms were assigned functional groups based on a kappa score that compares the observed events with those expected by random chance and iterative merging of groups containing 50% of the same proteins. The complete GO analysis is provided in Table 4.4 while Figures 4.4A and 4.5A display the resulting GO networks for TOPBP1 and ETAA1-dependent phosphoproteins, respectively.

Listed in Figures 4.4B and 4.5B are the ten most significantly enriched functional GO groups for TOPBP1 and ETAA1 along with the GO term with the highest percentage of associated genes from each group. The most highly enriched functional group for TOPBP1

A

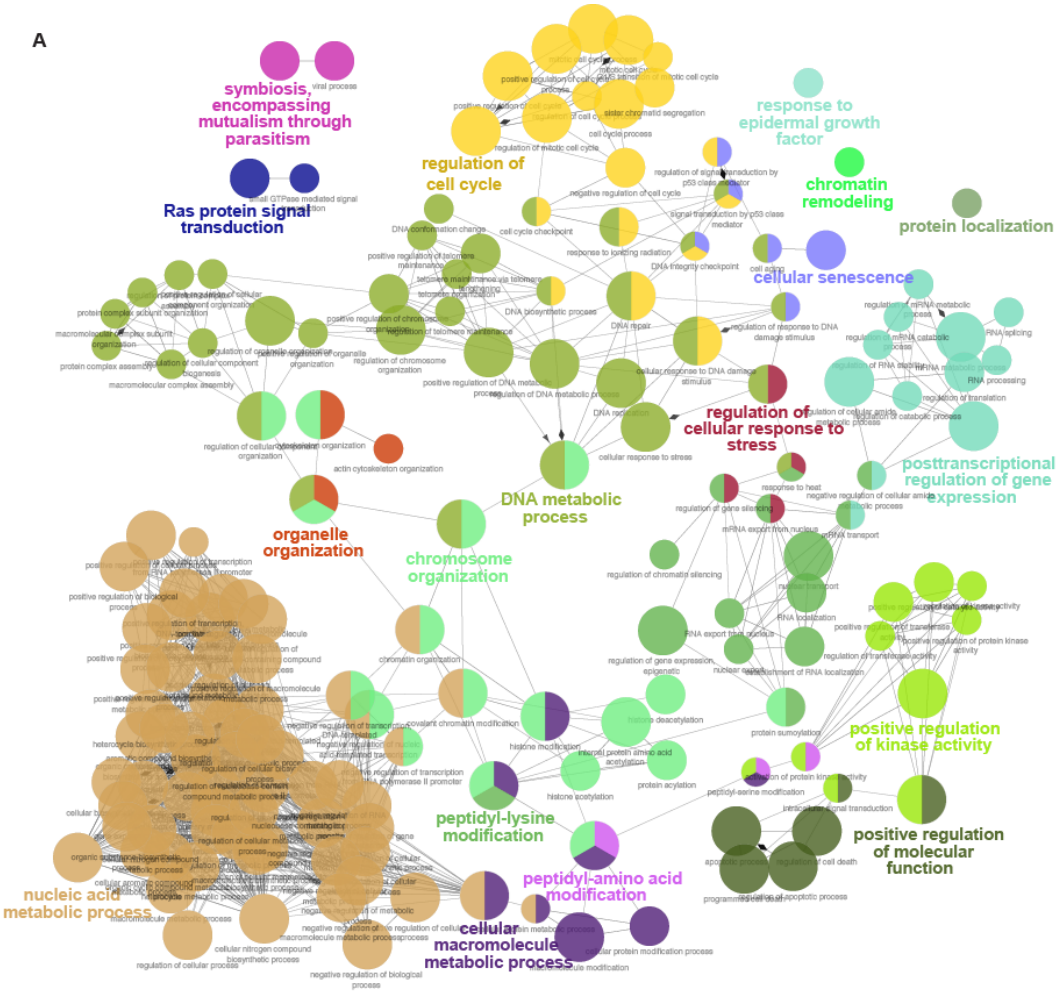

B

GO Term	Term P Value	Group P Value	Group	% Associated Proteins	# Proteins
regulation of cell cycle	2.45E-09	1.58E-20	Group01	6.3	78
response to ionizing radiation	3.52E-03	1.58E-20	Group01	10.1	17
chromosome organization	7.88E-21	2.13E-20	Group02	8.2	100
histone deacetylation	1.12E-03	2.13E-20	Group02	14.1	13
cellular macromolecule metabolic process	3.86E-16	2.67E-18	Group03	3.8	333
histone modification	3.76E-11	2.67E-18	Group03	9.9	46
peptidyl-lysine modification	1.84E-08	4.86E-18	Group04	9.6	38
regulation of chromatin silencing	2.33E-02	4.86E-18	Group04	26.1	6
organelle organization	2.82E-15	4.01E-17	Group05	4.9	187
actin cytoskeleton organization	1.09E-02	4.01E-17	Group05	6.0	37
DNA metabolic process	3.19E-09	2.13E-20	Group06	6.7	69
positive regulation of telomere maintenance	1.22E-02	1.87E-13	Group06	16.7	9
peptidyl-amino acid modification	1.94E-08	4.75E-11	Group07	6.0	79
activation of protein kinase activity	8.70E-03	4.75E-11	Group07	7.3	25
posttranscriptional regulation of gene expression	4.30E-05	3.21E-10	Group08	7.1	39
mRNA transport	7.81E-03	3.21E-10	Group08	9.9	16
cellular senescence	5.20E-04	6.07E-09	Group09	18.3	11
cell aging	5.01E-03	6.07E-09	Group09	12.4	13
nucleic acid metabolic process	3.70E-23	3.25E-08	Group10	4.8	255
covalent chromatin modification	7.41E-15	3.25E-08	Group10	10.0	58

Figure 4.4 TOPBP1-dependent phosphorylation gene ontology analysis.

Figure 4.4 TOPBP1-dependent phosphorylation gene ontology analysis (continued) (A) Functional GO network displaying grouping of GO terms enriched in TOPBP1-dependent phosphoproteins. Phosphoproteins and their corresponding GO terms were assigned functional groups after iterative merging of groups containing 50% of the same proteins. Each node in the network represents a GO term with a p value <0.05. A larger node size corresponds to more significant enrichment. Functional groups are indicated by color and represented in colored text by the most significant term in that group. Nodes with multiple colors belong to multiple groups. **(B)** Table displaying the ten most highly enriched GO groups. The first term for each group represents the GO term with the highest significant enrichment. The second term for each group had the highest percentage of associated proteins for that GO group.

A

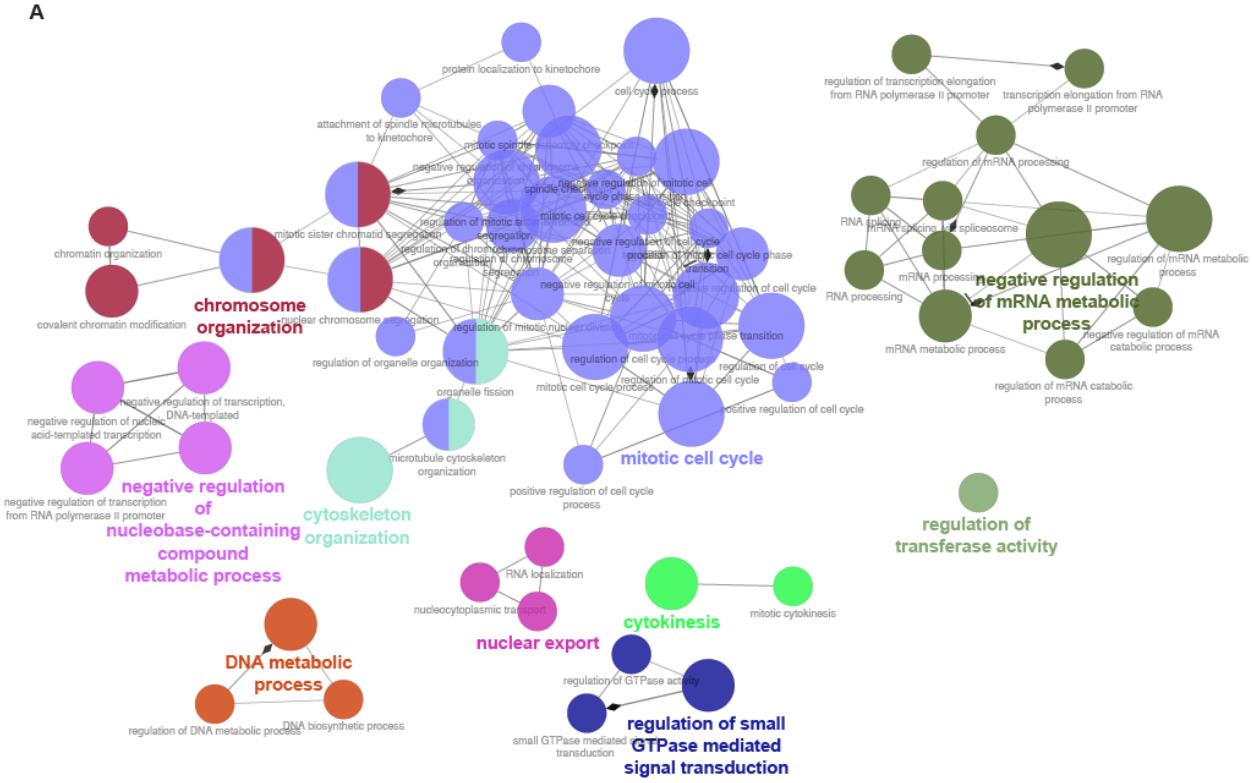

B

GO Term	Term P Value	Group P Value	Group	% Associated Proteins	# Proteins
mitotic cell cycle	6.70E-13	9.47E-17	Group01	5.2	54
spindle checkpoint	3.15E-05	9.47E-17	Group01	20.5	8
chromosome organization	1.76E-08	2.80E-10	Group02	4.2	51
mitotic sister chromatid segregation	4.44E-07	2.80E-10	Group02	10.6	16
negative regulation of mRNA metabolic process	1.10E-04	5.12E-08	Group03	12.5	10
regulation of transcription elongation from RNA polymerase II promoter	1.20E-02	5.12E-08	Group03	18.5	5
cytoskeleton organization	9.25E-05	1.38E-07	Group04	3.5	44
organelle fission	2.13E-04	1.38E-07	Group04	5.0	23
negative regulation of nucleobase-containing compound metabolic process	7.53E-04	1.83E-05	Group05	3.1	47
negative regulation of transcription from RNA polymerase II promoter	2.29E-03	1.83E-05	Group05	3.7	31
DNA metabolic process	1.22E-03	2.55E-05	Group06	3.5	36
DNA biosynthetic process	5.64E-03	2.55E-05	Group06	5.8	14
cytokinesis	4.13E-03	7.06E-05	Group07	7.5	11
mitotic cytokinesis	3.82E-02	7.06E-05	Group07	11.1	6
regulation of transferase activity	2.10E-02	9.60E-05	Group08	3.2	34
regulation of small GTPase mediated signal transduction	1.17E-03	1.39E-04	Group09	5.4	18
regulation of GTPase activity	7.62E-03	1.39E-04	Group09	4.2	21
nuclear export	2.13E-02	1.52E-04	Group10	5.8	12

Figure 4.5 ETAA1-dependent phosphorylation gene ontology analysis.(A) Functional GO network displaying grouping of GO terms enriched in ETAA1-dependent phosphoproteins. Network parameters are same as described in Fig. 4.4A. **(B)** Table displaying the ten most highly enriched GO groups. The first term for each group represents the GO term with the highest significant enrichment. The second term for each group had the highest percentage of associated genes for that GO group.

(colored yellow) contained the GO terms: regulation of cell cycle, mitotic cell cycle, and DNA integrity checkpoint.

The GO term from this group with the highest percentage of represented proteins is response to ionizing radiation. Other functional GO groups that TOPBP1 regulated include chromosome organization, cellular macromolecule metabolic process, and nucleic acid metabolic process. GO terms found in GO Group 1 (yellow), Group 6 (green), and Group 9 (blue) such as DNA integrity checkpoint, response to ionizing radiation, DNA repair, DNA replication, and cellular response to DNA damage stimulus are all consistent with the known functions for TOPBP1-dependent activation of ATR in response to DNA damage and replication stress. These terms were not highly enriched in ETAA1-dependent phosphorylation events suggesting TOPBP1 is the primary activator of ATR during DNA damage and replication stress signaling.

In contrast to TOPBP1, the most enriched functional GO group for ETAA1 contained the GO terms mitotic cell cycle, nuclear chromosome segregation, cell cycle process, and cell cycle checkpoint. The GO term with the highest percentage of represented genes from this group was spindle checkpoint. Other ETAA1-dependent GO groups were chromosome organization, negative regulation of mRNA metabolic process, cytoskeleton organization, and DNA metabolic process.

ETAA1 regulates and interacts with mitotic proteins

The significant enrichment of multiple mitotic GO terms in the phosphoproteome of ETAA1ΔAAD cells was striking since the experiment was not designed to identify mitotic ATR targets. Supporting a role in mitosis, our mass spectrometry analysis of ETAA1 protein complexes indicates that multiple mitotic proteins co-purify with ETAA1 including kinetochore and spindle-localized proteins such as BUB1, SGO2, KNL1 and NDC80 (Fig. 4.6A).

A

Protein	ETAA1 IP#1	ETAA1 IP#2	Control IP#1	Control IP#2
ETAA1	731	544	1	0
ATR	16	5	0	0
RPA70	51	69	7	9
BUB1	19	4	0	0
SGOL2	27	6	0	0
KNL1	34	14	0	0
NDC80	4	2	0	1
ZWINT	6	1	0	0
CLASP1	0	5	0	0

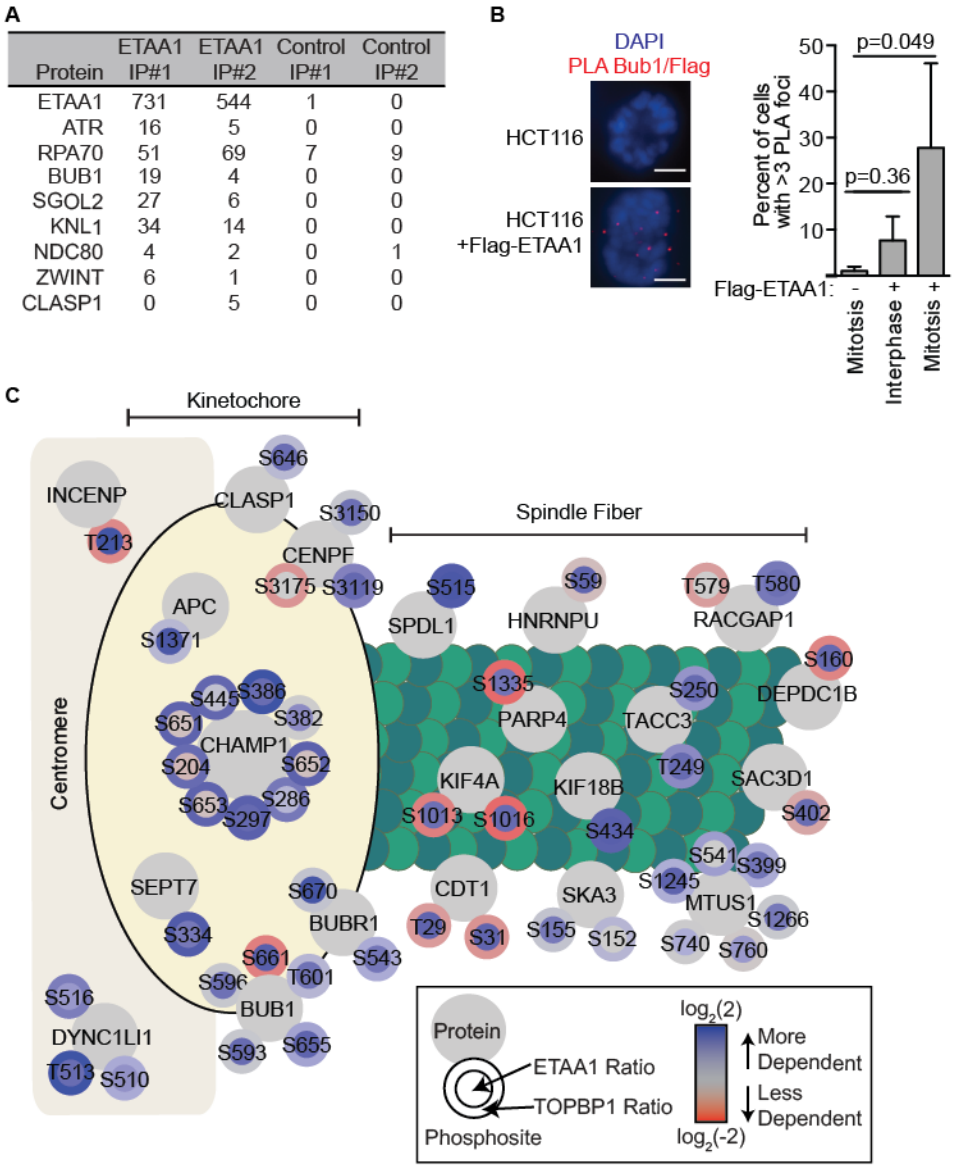

Figure 4.6 ETAA1 regulates phosphoproteins at kinetochores and spindles (A) Flag-ETAA1 was exogenously expressed in 293T cells, immunopurified, and co-purifying proteins were identified by mass spectrometry. Shown are the peptide counts for two experiments with two negative controls. Flag purifications from parental cells lacking Flag-ETAA1. **(B)** HCT116 cells with or without stable expression of Flag-ETAA1 were treated with 100 nM taxol for 2 hours, fixed, and Flag/BUB1 proximity ligation assay (PLA) signals measured in mitotic and interphase cells. Scale bar is 5 μM. Error bars are standard deviation. Significance was determined by ANOVA with a Dunnett multiple comparison post-test. **(C)** Diagram depicting the kinetochore and spindle associated phosphoproteins and sites detected in the ETAA1-dependent phosphoproteome. Each large grey circle contains the protein name with the smaller surrounding circles containing the observed phosphosites. The inner and outer phosphosite circle colors indicates the quantitative dependency on ETAA1 and TOPBP1 respectively.

Furthermore, we confirmed that ETAA1 co-localizes with Bub1 in cells trapped in mitosis with taxol using a proximity ligation assay (Fig. 4.6B).

Although both ETAA1 and TOPBP1 regulated phosphoproteins were enriched for the GO term mitotic cell cycle, only 21 (19.6%) of the 107 mitotic proteins identified were dependent on both activators suggesting they might regulate different subpathways during mitosis (Fig. 4.7A). Further analysis of these mitotic proteins revealed ETAA1-dependent phosphoproteins had a significant enrichment for proteins localizing to the kinetochore-centromere attachment site and mitotic spindle (Fig 4.7B-D), some of which are also ETAA1-interactors such as BUB1 and CLASP1. Notably, most of the kinetochore and spindle-localized proteins were phosphorylated in an ETAA1-dependent but not TOPBP1-dependent manner (Fig. 4.6C).

ETAA1 regulates Aurora B Kinase activity through an ATR pathway

ATR, via its downstream effector CHK1, regulates the mitotic kinase Aurora B to control cell division (Zachos et al., 2007; Peddibhotla et al., 2009; Petsalaki et al., 2011). To examine if ETAA1 or TOPBP1 regulates ATR activation of this pathway, Aurora B kinase activity was measured by Aurora B autophosphorylation on threonine 232 and by phosphorylation of its downstream substrate, histone 3 (H3) on serine 10 (Fig. 4.8A). Comparable to inhibition of ATR or CHK1, ETAA1ΔAAD cells had reduced autophosphorylation of Aurora B at T232 in mitotic cells whereas cells lacking TOPBP1 exhibited wild-type phosphorylation levels (Fig. 4.8B). Furthermore, complete knockout of ETAA1 resulted in decreased H3 S10 phosphorylation, which could be rescued by restoring expression of ETAA1 from a cDNA expression vector in ΔETAA1 cells indicating that the regulation of Aurora B is dependent on ETAA1 (Fig. 4.8C).

Loss of mitotic ETAA1-ATR signaling results in chromosome alignment defects

To examine the functional effects of mitotic ETAA1- and TOPBP1-dependent ATR signaling, we used live cell imaging to monitor progression of cells deficient for each ATR-

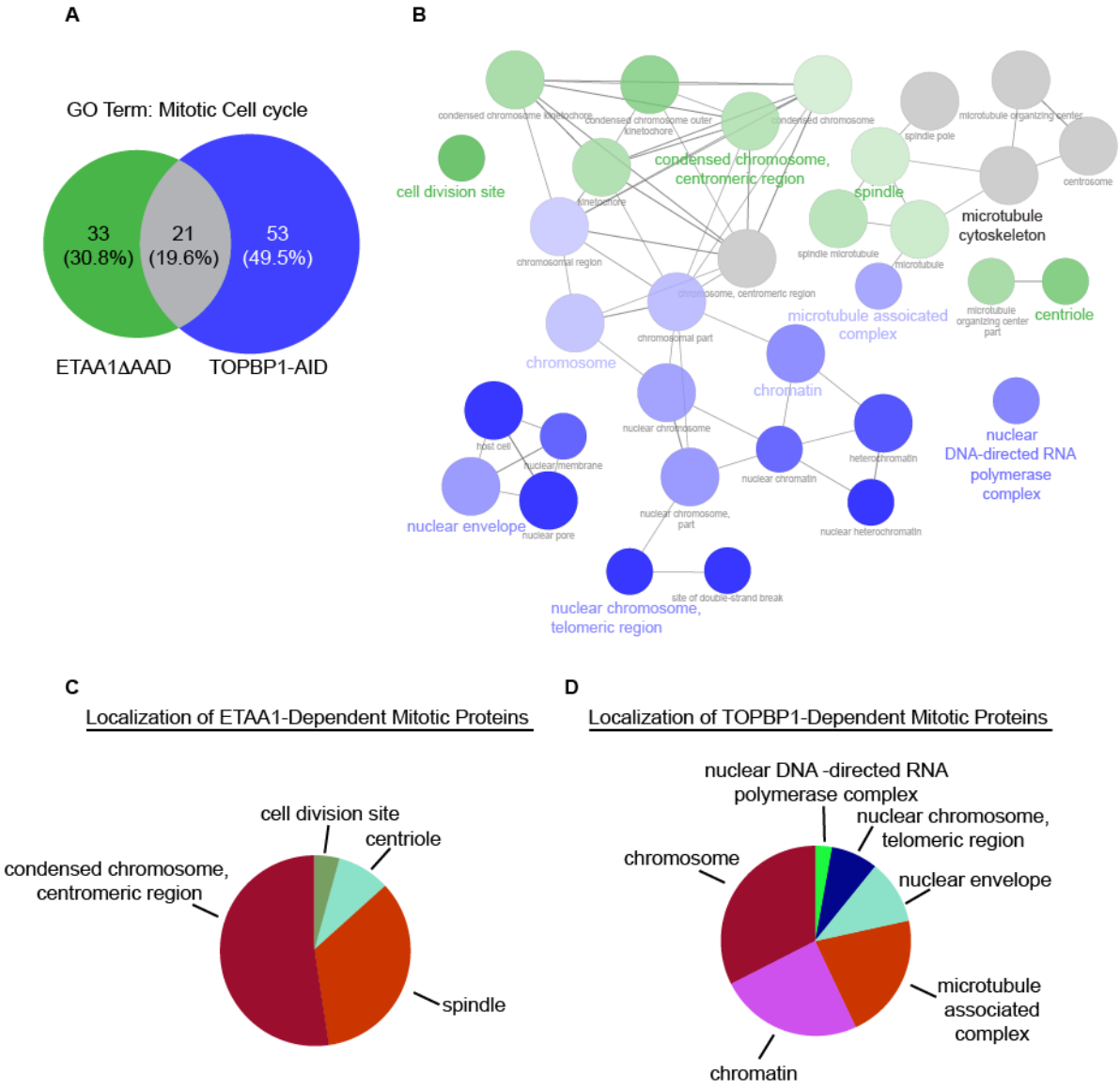

Figure 4.7 Analysis of ETAA1 and TOPBP1-dependent phosphoproteins. (A) Comparison of mitotic cell cycle phosphoproteins regulated by ETAA1 or TOPBP1. **(B)** GO network comparing localization of mitotic cell cycle proteins regulated by ETAA1 or TOPBP1. Each node in the network represents a localization term. Larger node size corresponds with a more significant enrichment. Node color denotes enrichment in ETAA1 or TOPBP1 clusters; darker green corresponds with more enriched in ETAA1 cluster while darker blue corresponds to more enrichment in TOPBP1 cluster. Grey nodes are not specific to either ETAA1 or TOPBP1. Similar localization GO terms were placed into functional groups with most significantly enriched term indicated by large colored text. **(C)** Overview chart displaying localization of ETAA1-dependent mitotic proteins. **(D)** Overview chart displaying localization of TOPBP1-dependent mitotic proteins.

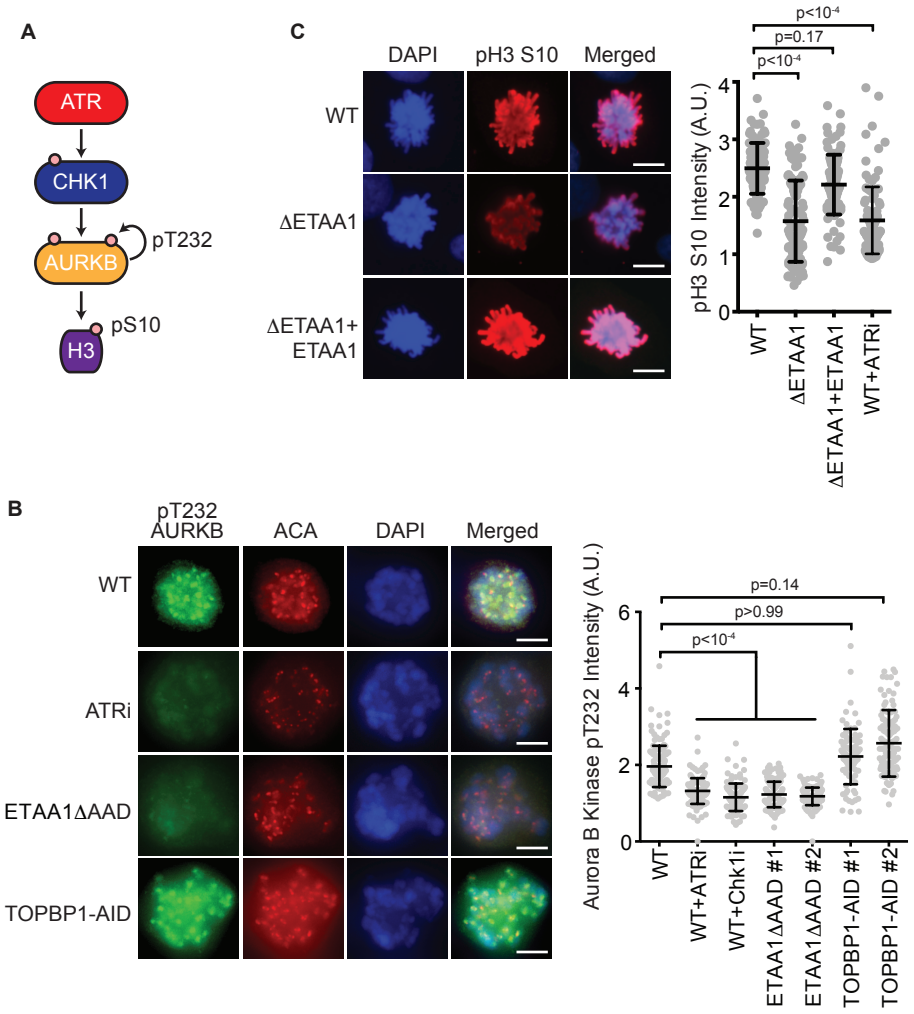

Figure 4.8 ETAA1-dependent ATR activation regulates Aurora B kinase activity. (A) Diagram of mitotic ATR signaling to Aurora B (AURKB). **(B).** Aurora B kinase activity measured by autophosphorylation on T232. HCT116 (WT), and two clones of ETAA1ΔAAD and TOPBP1-AID cells were arrested in G2 by addition of a CDK2 inhibitor, (RO-3306, 10 μM) for 16 hours to avoid replication stress induced by ATRi or TOPBP1 degradation. Cells were treated with IAA or ATRi for two hours then released into fresh media containing taxol, IAA or ATRi. Cells were fixed one hour after release. Shown are representative immunofluorescent images and quantification of Aurora B kinase pT232. Anti-centromere antibodies (ACA) were used to confirm kinetochore localization of Aurora B. Error bars represent standard deviation. **(C)** U2OS WT, ETAA1 null (ΔETAA1), and ΔETAA1 cells stably complemented with an ETAA1 expression vector were treated with 10 μM CDK2i for 16 hours, released for 1 hour into media with or without 1 μM ATRi and then fixed. Shown are representative immunofluorescent images and quantification of pH3 S10 in prometaphase cells. Scale bar is 5 μM. Significance for B and C was determined by ANOVA with a Dunnett multiple comparison post-test.

activator through mitosis. Cells expressing GFP-tagged Histone 2B for chromatin visualization were synchronized using double thymidine block and released into fresh media. After seven hours, cells had completed DNA replication and IAA was added at that point to degrade TOPBP1. Alternatively, we utilize a selective ATR inhibitor (ATRi), VE822, to inactivate ATR in G_2 phase cells. As cells progressed through mitosis each cell was scored for mitotic defects such as misaligned chromosomes during metaphase and the formation of lagging chromosomes or chromatin bridges during anaphase (Fig. 4.9A, B). There was no significant difference between cell lines in the time from nuclear envelope breakdown (NEB) to the onset of anaphase (Fig. 4.10A). Loss of ETAA1, TOPBP1, or inhibition of ATR kinase activity all resulted in an approximately two-fold increase in the frequency of anaphase bridges, which can form due to incomplete DNA replication or failure to decatenate separating chromosomes. Interestingly, the number of metaphases with misaligned chromosomes more than doubled in ETAA1ΔAAD and ATR inhibited cells and the number of lagging chromosomes was more than ten-fold higher than in WT cells (Fig. 4.9A, B). Many of the misaligned chromosomes in these cells became lagging chromosomes during anaphase and later formed micronuclei. TOPBP1-AID cells showed only a small increase in lagging chromosomes and did not display an increase in the number of metaphases with misaligned chromosomes (Fig. 4.9A, B).

To examine the severity of chromosome misalignment during metaphase, ETAA1ΔAAD, TOPBP1-AID and ATRi treated cells were stained with anti-centromere-antibodies (ACA) and scored for the number of chromosomes that were not aligned at the metaphase plate. There was a significant increase in both the frequency and severity of misalignment in ETAA1ΔAAD and ATRi treated cells but not in TOPBP1-AID cells (Fig. 4.9C, D). U2OS ETAA1 knockout cells also displayed an increase in the number of misaligned chromosomes and addition of an ETAA1 cDNA to the ΔETAA1 cells rescued the misalignment defect (Fig. 4.9E). These results suggest that ETAA1-ATR signaling is needed for proper attachment of the chromosomes to the spindle in unstressed cells.

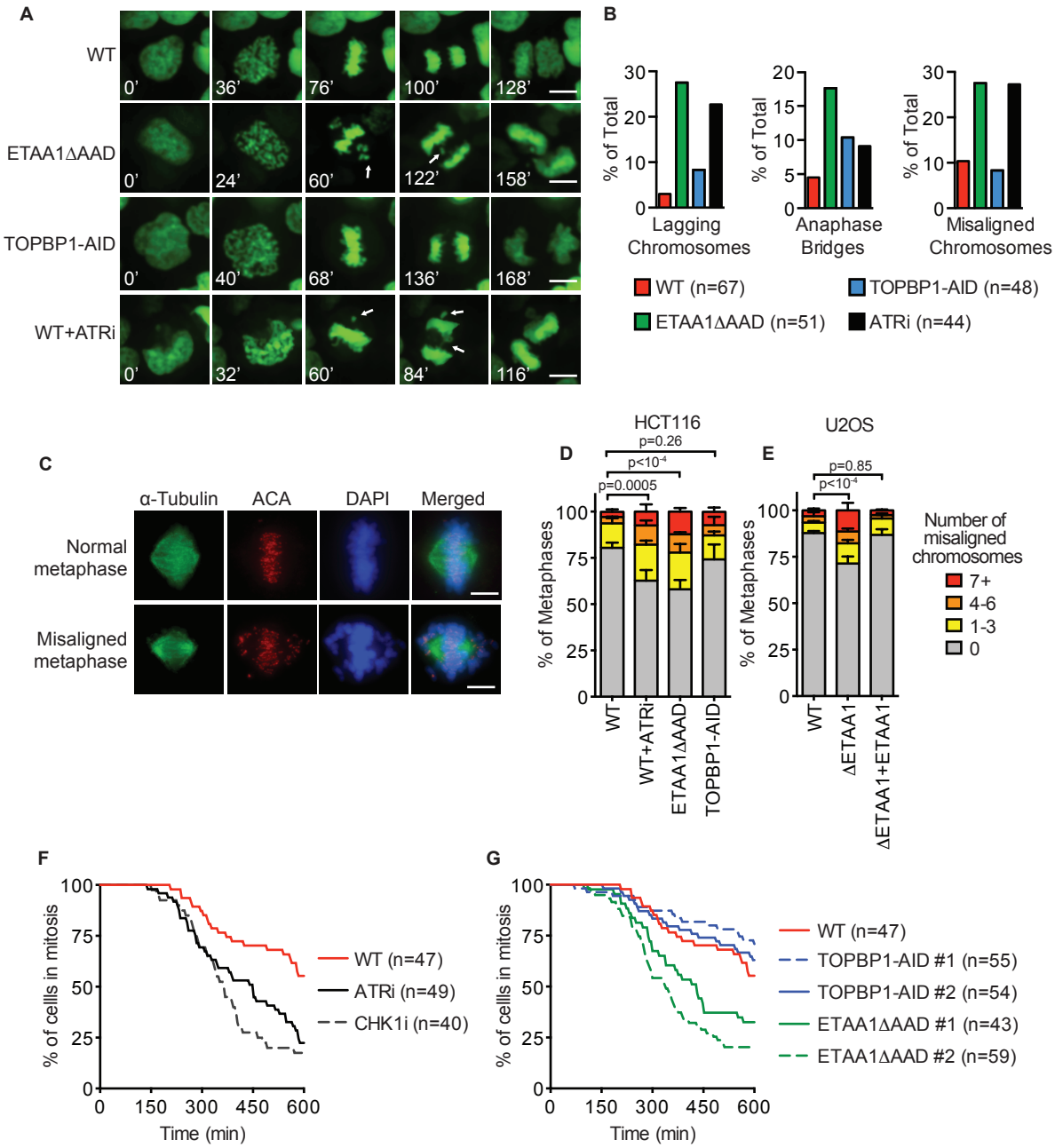

Figure 4.9 ETAA1 activation of ATR is required for proper chromosome alignment and a fully functional SAC. (A, B) HCT116 WT, ETAA1ΔAAD, and TOPBP1-AID cells expressing GFP-H2B for chromatin visualization were examined by live cell imaging and scored for defects during mitosis. ATRi or IAA was added 1.5 hours before beginning imaging. Representative time-lapse images are shown in **(A). W**hite arrows indicate anaphase bridges and misaligned or lagging chromosomes. Scale bar is 5 μM. **(B) Q**uantification of mitotic defects from live-cell imaging experiments. Listed is the total number of cells examined for each cell type. **(C)** Representative immunofluorescence images of normal and misaligned chromosomes during metaphase. Scale bar is 5 μM. **(D)** HCT116 WT, ETAA1ΔAAD, and TOPBP1-AID cells were arrested for 16 hours with CDK2i, treated with IAA or ATRi for 2 hours, released from CDK2i and fixed. Metaphase cells were scored for the number of misaligned chromosomes. **(E)** U2OS WT, ΔETAA1, and ΔETAA1 cells stably expressing ETAA1 were examined for chromosome misalignment as in **(D). (F)** Synchronized HCT116 cells expressing H2B-GFP were released from a double thymidine block and taxol, ATRi, or CHK1i were added 1.5 hours before starting imaging. **(G)** Same as in **(F)** but HCT116 WT, and two clones of ETAA1ΔAAD and TOPBP1-AID cells were examined for ability to sustain mitotic arrest during taxol treatment.

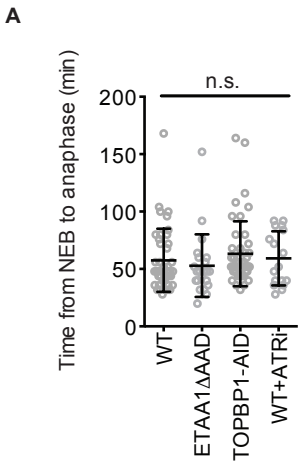

Figure 4.10 Length of mitosis is unchanged by loss of ETAA1, TOPBP1, or ATR activity. (A) HCT116 WT, ETAA1ΔAAD, and TOPBP1-AID cells expressing GFP-H2B for chromatin visualization were examined by live cell imaging and time between nuclear envelope breakdown (NEB) and onset of anaphase was measured. Significance was determined by ANOVA with a Dunnett multiple comparison post-test. n.s.= not significant, p>0.05.

Having observed that loss of ETAA1-dependent ATR signaling causes lower Aurora B kinase activity, decreased phosphorylation of kinetochore/spindle associated proteins, and defects in chromosome attachment we examined if ETAA1 and ATR are required for a fully functioning spindle assembly checkpoint (SAC). The SAC ensures genome stability by preventing the onset of anaphase until all chromosomes are properly attached via kinetochores to the spindle (Lara-Gonzalez et al., 2012). Cells expressing H2B-GFP were treated with ATRi and CHK1i and examined for ability to sustain mitotic arrest during treatment with taxol by live cell imaging. Entry into mitosis was determined by nuclear envelope breakdown (NEB) and plotted as time zero. Exit from mitosis was determined by chromosome decondensation. Ten hours after NEB only 22% of ATRi treated and 18% of CHK1i treated cells maintained mitotic arrest compared to 55% of untreated cells (Fig. 4.9F). To examine if ETAA1 or TOPBP1 primarily contributes to ATR regulation of the SAC, two ETAA1ΔAAD and TOPBP1-AID cell lines were examined for ability to maintain taxol-induced mitotic arrest. Both ETAA1ΔAAD clones showed an inability to sustain mitotic arrest with only 33% and 20% of cells remaining in mitosis ten hours after NEB (Fig. 4.9G). In contrast, mitotic arrest of TOPBP1-AID cells was comparable to those of control cells. Therefore, we conclude that ETAA1 is the primary regulator of ATR activation in mitosis to promote SAC activity.

Discussion

We utilized quantitative phosphoproteomics to define ETAA1 and TOPBP1-dependent signaling. These data identified ETAA1 as the primary regulator of ATR during mitosis at centromeric regions. ETAA1-dependent ATR signaling during mitosis promotes robust Aurora B kinase activity, proper separation of chromosomes, and a fully functioning SAC.

These data also indicate that TOPBP1 regulates more of the ATR response to replication stress than ETAA1 since more than twice as many phosphosites depend on

TOPBP1 than ETAA1 and replication-related proteins were much more highly enriched in the TOPBP1-dependent versus the ETAA1 phosphoproteomes. Together these results suggest that TOPBP1 is a principle ATR-activator during replication stress, while ETAA1 has important functions during the unstressed cell division cycle (Fig. 4.11A).

While we quantitated over 20,000 phosphosites, the phosphoproteomes lacked a large number of known direct ATR phosphorylation targets. Thus, further phosphorylation studies using additional strategies to enrich for direct targets are needed. Nonetheless, analysis of ETAA1-dependent phosphorylation events and interaction partners revealed ETAA1 functions at centromeric regions as a regulator of mitotic ATR activity (Fig. 4.11B). Loss of ETAA1 but not TOPBP1-dependent ATR activation phenocopies the mitotic defects caused by inhibiting ATR or CHK1 using small molecules. CHK1 inactivation impairs the spindle assembly checkpoint through deregulation of Aurora B and Bub proteins (Zachos et al., 2007; Peddibhotla et al., 2009; Petsalaki et al., 2011), both of which exhibit reduced phosphorylation in ETAA1ΔAAD cells. Additionally, ATR can localize to RPA-coated centromeric R-loops where it prevents the formation of lagging chromosomes (Kabeche et al., 2017), an anaphase defect observed in ETAA1ΔAAD cells.

Previous studies indicate that TOPBP1 does function during mitosis at sites of under-replication but that it is independent of ATR signaling (Pedersen et al., 2015). Additionally, TOPBP1 localizes to ultra-fine anaphase bridges and promotes their resolution through direct recruitment of topoisomerase IIα. (Germann et al., 2014; Broderick et al., 2015). Therefore, while TOPBP1 is active during mitosis, its functions do not appear tied to ATR activation.

Utilizing cells deficient for each ATR activator we were able to separate the functions of ATR during replication stress and a normal cell cycle. These findings expand the requirement for ETAA1 to enforce normal cell cycle progression as ETAA1 was recently found to activate ATR during an unperturbed S-phase to control the S/G_2 transition (Saldivar et al., 2018). This separation of function parallels how different $Mec1^{ATR}$ activators work in yeast where the

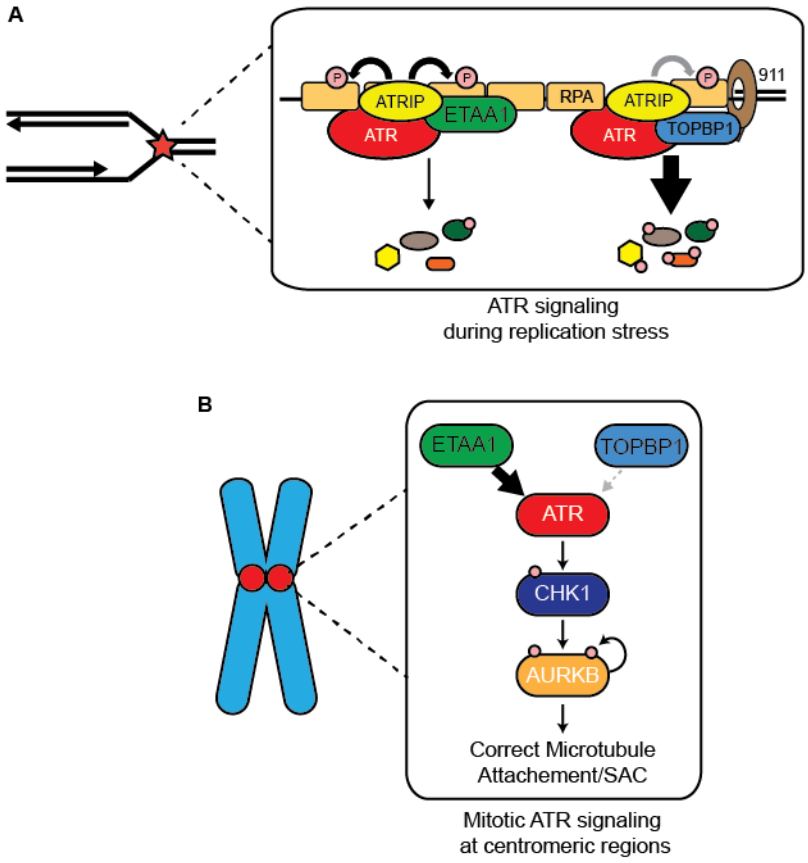

Figure 4.11 Models for ATR activation (A) ATR is primarily activated by TOPBP1 in response to replication stress leading to phosphorylation of hundreds of proteins. ETAA1 contributes to ATR activation in response to replication stress but regulates a smaller fraction of ATR substrates. **(B)** ETAA1 activates ATR localized to centromeric regions promoting full Aurora B activity, correct microtubule attachment, and a fully functional SAC.

TOPBP1 orthologue Dpb11 activates Mec1-Rad53 signaling during replication stress while the other Mec1 activators, Dna2 and Ddc1, activate Mec1 during an unperturbed cell cycle (Bastos de Oliveira et al., 2015). In conclusion, ETAA1 and TOPBP1 promote genome stability through regulation of different ATR signaling pathways with ETAA1 having a dominant function in controlling chromosome segregation during mitosis.

Conclusion

We utilized quantitative phosphoproteomics to compare the phosphoproteomes of cells deficient for ETAA1 and TOPBP1. We found that while TOPBP1 is primarily utilized to activate ATR in response to replication stress, ETAA1 promotes mitotic ATR signaling at centromeric regions. ETAA1-activation of ATR is required for proper mitotic progression, ensuring accurate kinetochore-microtubule attachment and full activation of the spindle assembly checkpoint. These findings expand our models for how ATR activators regulate ATR signaling and direct ATR to specific substrates.

Table 4.1 ETAA1-dependent phosphosites. ETAA1-dependent phosphosites are given below along with the Uniprot ID, modified residue, presence of ATR or CHK1 motif, and the number of experiments in which that peptide was observed. The ratio value is the $\log_2$ transformed ratio of WT /ETAA1 or TOPBP1 cells. Therefore, a higher value (darker green) is more dependent on ETAA1 or TOPBP1.

Table 4.1 ETAA1-dependent phosphosites.								
Phosphosite	**Uniprot**	**ATR Motif (SQ/TQ) CHK1 Motif (R-X-X-S)**	**Protein Name**	**Amino acid**	**ETAA1 Ratio**	**TOPBP1 Ratio**	**Count ETAA1ΔAAD**	**Count TOPBP1-AID**
ACSA S30	Q9NR19	R-X-X-S	ACSA	S	0.767824	-0.05229	3	4
ADAM9 T761	Q13443		ADAM9	T	0.803227	0.4368	6	6
ADDG S677	Q9UEY8		ADDG	S	1.59431	-0.16019	3	1
ADDG S681	Q9UEY8		ADDG	S	0.596173	-0.1644	4	3
AFAD S1779	P55196		AFAD	S	0.608904	-0.47574	4	2
AHNK S210	Q09666	R-X-X-S	AHNK	S	0.794339	0.43499	7	6
AHNK S332	Q09666		AHNK	S	0.741872	0.58294	3	5
AKA12 S1390	Q02952		AKA12	S	0.719315	0.24948	2	3
AKA12 S286	Q02952		AKA12	S	0.645333	0.55139	5	6
AKP13 S1565	Q12802	R-X-X-S	AKP13	S	0.691911	-0.14167	2	1
ALS2 S353	Q96Q42	R-X-X-S	ALS2	S	0.866037	0.06185	2	1
ALS2 S483	Q96Q42	R-X-X-S	ALS2	S	1.38173	0.10178	7	5
ALS2 S489	Q96Q42	SQ	ALS2	S	1.22625	0.08849	4	3
ALS2 S492	Q96Q42		ALS2	S	1.35095	0.20364	7	6
ANLN S323	Q9NQW6		ANLN	S	0.642964	-0.28007	6	5
APC S1371	P25054		APC	S	2.38789	0.1513	5	5
ARHG7 S694	Q14155	R-X-X-S	ARHG7	S	0.724999	0.04963	3	2
ARI1A S696	O14497	R-X-X-S	ARI1A	S	1.23695	0.24586	4	4
BCL9L S750	Q86UU0		BCL9L	S	0.607831	-0.04406	5	3
BCL9L S984	Q86UU0		BCL9L	S	0.888149	-0.38204	2	2
BCL9L S991	Q86UU0		BCL9L	S	0.898634	-0.38907	5	6
BCL9L T989	Q86UU0	R-X-X-S	BCL9L	T	0.888149	-0.42146	2	3
BPTF S1300	Q12830		BPTF	S	1.22669	-0.13423	2	2
BRAT1 S582	Q6PJG6		BRAT1	S	2.57957	0.28053	2	2
BRAT1 T581	Q6PJG6		BRAT1	T	2.57957	0.5839	2	1
BRD7 S279	Q9NPI1	R-X-X-S	BRD7	S	1.22138	0.45386	2	1
BUB1 S593	O43683		BUB1	S	0.708009	0.03689	7	6
BUB1 S596	O43683		BUB1	S	0.653774	0.03689	7	6
BUB1 S655	O43683		BUB1	S	0.795172	0.30314	3	3
BUB1 S661	O43683		BUB1	S	0.868553	-0.56957	2	1
BUB1 T601	O43683		BUB1	T	0.650029	0.16877	6	5
BUB1B S543	O60566		BUB1B	S	0.624896	0.24086	5	6
BUB1B S670	O60566		BUB1B	S	1.13635	0.06502	2	1
C2D1A S455	Q6P1N0		C2D1A	S	1.24957	-0.02912	4	4
CALD1 S789	Q05682		CALD1	S	0.970921	-0.36025	2	2
CBX8 S191	Q9HC52		CBX8	S	0.760519	-0.25828	3	4
CBY1 S9	Q9Y3M2		CBY1	S	0.920223	-0.25044	4	1
CCD14 S798	Q49A88		CCD14	S	0.799668	0.14718	3	5
CDT1 S31	Q9H211	R-X-X-S	CDT1	S	0.785843	-0.41665	3	5
CDT1 T29	Q9H211		CDT1	T	0.785843	-0.36882	3	5
CENPF S3119	P49454		CENPF	S	0.736125	0.53476	4	1
CENPF S3150	P49454		CENPF	S	0.668113	0.04236	7	6
CEP55 S428	Q53EZ4		CEP55	S	0.615725	-0.23091	4	5
CHMP7 S417	Q8WUX9		CHMP7	S	0.667937	0.32496	2	2
CLAP1 S1196	Q7Z460	SQ	CLAP1	S	1.5365	-0.05412	2	2
CLAP1 S646	Q7Z460	R-X-X-S	CLAP1	S	0.683202	0.13764	4	6
CLD12 S228	P56749		CLD12	S	0.626112	-0.3626	2	1
CLK1 S140	P49759	R-X-X-S	CLK1	S	0.707463	0.25854	2	2
CLK1 T138	P49759	R-X-X-S	CLK1	T	0.786049	-0.26286	2	2
CLMN S635	Q96JQ2		CLMN	S	2.00328	-0.72588	3	2
CN093 T283	Q9H972		CN093	T	0.797345	-0.30731	2	1
CP135 T1121	Q66GS9		CP135	T	0.943348	0.23687	5	5
CPSF2 S423	Q9P2I0		CPSF2	S	1.01861	0.17004	6	5
CROCC S488	Q5TZA2	R-X-X-S	CROCC	S	1.23702	0.01949	3	2
CROCC S494	Q5TZA2	R-X-X-S	CROCC	S	1.23702	-0.18174	3	4

Table 4.1 ETAA1-dependent phosphosites.								
Phosphosite	**Uniprot**	**ATR Motif (SQ/TQ) CHK1 Motif (R-X-X-S)**	**Protein Name**	**Amino acid**	**ETAA1 Ratio**	**TOPBP1 Ratio**	**Count ETAA1ΔAAD**	**Count TOPBP1-AID**
CROCC S512	Q5TZA2	R-X-X-S	CROCC	S	0.757378	-0.29808	2	2
CROCC T492	Q5TZA2		CROCC	T	1.23702	-0.03781	3	4
CS021 T377	Q8IVT2	R-X-X-S	CS021	T	0.600186	-0.59476	2	2
CT2NL S557	Q9P2B4		CT2NL	S	0.79693	-0.24398	5	3
CTF18 S225	Q8WVB6		CTF18	S	1.13849	-1.14976	3	1
CTR9 S1097	Q6PD62	R-X-X-S	CTR9	S	0.608325	0.12062	2	3
CTR9 S1099	Q6PD62		CTR9	S	0.686318	-0.09174	2	3
DAB2P S702	Q5VWQ8	R-X-X-S	DAB2P	S	1.51687	-0.71078	2	1
DBF4A S103	Q9UBU7		DBF4A	S	0.877823	0.04578	3	4
DDX54 S782	Q8TDD1		DDX54	S	0.946955	0.01164	4	4
DEN4C S1042	Q5VZ89	R-X-X-S	DEN4C	S	0.659285	-0.29488	3	2
DEP1B S160	Q8WUY9		DEP1B	S	0.726195	-0.52776	2	1
DHX16 S107	O60231		DHX16	S	1.26694	-0.28932	5	2
DMWD S495	Q09019	R-X-X-S	DMWD	S	0.595217	0.47537	2	2
DNJA1 S335	P31689		DNJA1	S	0.660777	0.07423	5	3
DPOA2 S141	Q14181		DPOA2	S	0.828144	-0.41758	5	6
DPOA2 S147	Q14181		DPOA2	S	0.654252	-0.46222	2	6
DPOA2 S152	Q14181		DPOA2	S	0.912037	-1.08281	5	5
DTL S512	Q9NZJ0		DTL	S	0.706995	-0.32366	3	1
DTL T516	Q9NZJ0		DTL	T	0.706995	-0.52458	4	1
DUS7 S369	Q16829		DUS7	S	0.671656	0.13973	2	2
DYRK2 S48	Q92630		DYRK2	S	1.16124	-0.35039	2	5
DYST S7510	Q03001	R-X-X-S	DYST	S	0.614945	0.15937	2	1
E41L2 S715	O43491		E41L2	S	0.636636	0.29678	2	1
EDC4 S879	Q6P2E9		EDC4	S	0.797731	-0.06287	3	3
ELAV1 S202	Q15717		ELAV1	S	0.602362	-0.17894	3	2
EMAL4 S94	Q9HC35	R-X-X-S	EMAL4	S	1.55297	-0.7047	2	1
ENL S411	Q03111		ENL	S	0.747946	0.22639	2	2
ENL S414	Q03111		ENL	S	0.747946	0.22639	2	2
ENL S419	Q03111		ENL	S	0.747946	0.22639	2	2
ENL S420	Q03111		ENL	S	0.747946	0.22639	2	2
ENL S421	Q03111		ENL	S	0.747946	0.22639	2	2
ERC6L S14	Q2NKX8		ERC6L	S	0.643764	0.30661	7	5
ERCC5 S341	P28715		ERCC5	S	0.595313	-0.32834	5	5
ERCC5 S384	P28715		ERCC5	S	0.719048	-0.25357	3	4
ERF S548	P50548		ERF	S	0.785152	0.1744	2	2
ES8L1 S182	Q8TE68	R-X-X-S	ES8L1	S	0.662205	0.06667	2	1
ESYT1 S820	Q9BSJ8		ESYT1	S	0.801841	-0.21734	2	3
F134C S435	Q86VR2	R-X-X-S	F134C	S	1.0536	0.28712	2	3
F134C S436	Q86VR2		F134C	S	1.0536	0.28712	2	3
F208B S1172	Q5VWN6		F208B	S	0.659454	0.48192	2	1
FA53C S232	Q9NYF3	R-X-X-S	FA53C	S	0.711367	0.40479	6	6
FA53C S234	Q9NYF3		FA53C	S	0.857511	0.40479	6	6
FA64A S131	Q9BSJ6		FA64A	S	0.619178	-0.46883	4	5
FIP1 S259	Q6UN15		FIP1	S	0.59388	-0.90457	3	2
FLII S436	Q13045		FLII	S	0.749835	-0.09866	2	2
FLII S856	Q13045		FLII	S	0.606916	0.363	3	1
FOXK1 T436	P85037		FOXK1	T	0.704939	-0.10315	2	3
GPBP1 S49	Q86WP2	R-X-X-S	GPBP1	S	0.717561	0.47186	3	2
GTSE1 S575	Q9NYZ3		GTSE1	S	0.796266	-0.34386	6	5
GTSE1 S580	Q9NYZ3		GTSE1	S	0.705498	-0.2206	5	5
H14 S2	P10412		H14	S	0.736821	0.22713	5	3
H14 T4	P10412		H14	T	0.736821	0.16792	5	2
HDGR2 S633	Q7Z4V5	R-X-X-S	HDGR2	S	6.1533	-0.16539	2	2
HIRP3 S227	Q9BW71		HIRP3	S	1.09101	0.31398	6	5
HMGA2 S44	P52926		HMGA2	S	0.720541	0.20639	7	6
HNRPU S59	Q00839		HNRPU	S	0.782744	-0.12069	4	3
IF2P S135	O60841		IF2P	S	1.11801	0.29631	6	6
IF4B S93	P23588		IF4B	S	0.925848	0.31115	5	4
INCE T213	Q9NQS7		INCE	T	1.18931	-0.48989	2	1
ISL2 S154	Q96A47		ISL2	S	0.81961	-0.51072	4	6
ISL2 S157	Q96A47		ISL2	S	0.689412	-0.51072	4	6
JCAD S755	Q9P266		JCAD	S	0.616973	0.57522	2	4

Table 4.1 ETAA1-dependent phosphosites.								
Phosphosite	**Uniprot**	**ATR Motif (SQ/TQ) CHK1 Motif (R-X-X-S)**	**Protein Name**	**Amino acid**	**ETAA1 Ratio**	**TOPBP1 Ratio**	**Count ETAA1ΔAAD**	**Count TOPBP1-AID**
JCAD S757	Q9P266	R-X-X-S	JCAD	S	0.616973	0.57522	2	4
K1671 S1757	Q9BY89		K1671	S	0.804632	-0.09517	2	5
K1671 S1760	Q9BY89		K1671	S	0.804632	-0.52195	2	1
KCTD3 S612	Q9Y597		KCTD3	S	0.603379	-0.04941	3	3
KCTD3 S711	Q9Y597		KCTD3	S	0.628447	-0.40124	2	1
KCTD3 T608	Q9Y597	R-X-X-S	KCTD3	T	0.614757	-0.03336	3	2
KI21A S1212	Q7Z4S6		KI21A	S	1.42444	0.09464	5	1
KI21A S1271	Q7Z4S6		KI21A	S	1.38758	0.24727	2	2
KIF4A S1016	O95239		KIF4A	S	0.709291	-1.62847	2	3
KLF4 S254	O43474		KLF4	S	0.819522	0.29151	3	2
LAD1 S121	O00515		LAD1	S	0.914856	-0.1707	4	1
LARP7 S300	Q4G0J3	R-X-X-S	LARP7	S	3.00193	-0.31219	5	4
LEO1 S300	Q8WVC0		LEO1	S	0.861876	-0.08461	3	1
LIN54 S310	Q6MZP7		LIN54	S	0.778377	-0.63682	4	6
LIN54 S314	Q6MZP7		LIN54	S	0.778377	0.14952	7	6
LMBL3 S608	Q96JM7		LMBL3	S	0.587461	0.14966	7	5
LSR S464	Q86X29		LSR	S	0.640417	-0.01364	2	3
LYN S13	P07948		LYN	S	1.41133	0.15676	4	2
M3K2 S153	Q9Y2U5		M3K2	S	0.595408	0.10423	3	2
M3K2 S331	Q9Y2U5	R-X-X-S	M3K2	S	0.613826	-0.05969	4	2
MAGG1 S303	Q96MG7		MAGG1	S	0.612683	0.03309	2	6
MAP1A S526	P78559		MAP1A	S	0.981341	0.19954	2	2
MAP1A S527	P78559		MAP1A	S	0.981341	0.19954	2	2
MARK2 S486	Q7KZI7		MARK2	S	0.602418	0.27953	3	2
MAST2 S209	Q6P0Q8	R-X-X-S	MAST2	S	0.601697	0.54634	3	4
MCAF1 S477	Q6VMQ6		MCAF1	S	0.882535	-0.26207	3	1
MCAF1 S559	Q6VMQ6	R-X-X-S	MCAF1	S	1.22472	0.23045	3	5
MCRS1 S282	Q96EZ8		MCRS1	S	0.610511	0.17758	3	2
MDC1 S1820	Q14676		MDC1	S	0.633013	-0.28083	5	6
MEX3C S537	Q5U5Q3	R-X-X-S/SQ	MEX3C	S	0.750864	0.13159	5	6
MEX3D T510	Q86XN8		MEX3D	T	0.780142	0.46957	2	3
MIB2 S309	Q96AX9	R-X-X-S	MIB2	S	0.615796	-0.41431	4	5
MIIP S303	Q5JXC2	R-X-X-S	MIIP	S	0.613437	0.27882	3	4
MLL1 S161	Q03164	R-X-X-S	MLL1	S	0.617918	-0.43673	3	3
MLL1 T163	Q03164	R-X-X-S	MLL1	T	1.05977	-0.34622	2	3
MLXPL S614	Q9NP71	R-X-X-S	MLXPL	S	0.909888	0.22543	3	4
MTUS1 S1245	Q9ULD2		MTUS1	S	0.799916	0.21711	4	6
MTUS1 S1266	Q9ULD2		MTUS1	S	0.603027	0.028	2	1
MTUS1 S399	Q9ULD2		MTUS1	S	0.629363	0.24452	2	3
MUS81 S95	Q96NY9		MUS81	S	0.764856	0.33583	2	1
MY15B S1025	Q96JP2		MY15B	S	1.64653	-0.89148	3	6
NDRG1 S2	Q92597		NDRG1	S	0.700568	0.21624	4	3
NDRG1 T366	Q92597	R-X-X-S	NDRG1	T	0.683562	0.28284	3	2
NELFE S51	P18615	R-X-X-S	NELFE	S	0.782269	-0.06209	2	2
NHS S530	Q6T4R5		NHS	S	0.620458	0.01678	3	4
NOL8 S890	Q76FK4		NOL8	S	0.829812	-0.30879	5	3
NOL8 T888	Q76FK4		NOL8	T	0.829812	-0.30879	5	3
NOP56 S314	O00567		NOP56	S	0.607358	0.32331	3	4
OFD1 S663	O75665		OFD1	S	0.585443	-1.02248	3	6
OFD1 S669	O75665		OFD1	S	0.625282	-0.63028	5	6
OFD1 S789	O75665		OFD1	S	0.772477	-1.15037	3	1
PA2G4 T11	Q9UQ80		PA2G4	T	0.975703	0.34596	2	2
PAIRB S328	Q8NC51		PAIRB	S	0.718397	0.4631	2	1
PAIRB S330	Q8NC51		PAIRB	S	1.16434	0.02304	8	5
PALLD Y731	Q8WX93		PALLD	Y	1.00236	0.17847	2	2
PAPOG S525	Q9BWT3		PAPOG	S	0.815739	0.01121	3	1
PARP4 S1335	Q9UKK3	R-X-X-S	PARP4	S	0.642748	-0.71734	4	3
PCY1A T342	P49585		PCY1A	T	0.657823	0.43392	2	2
PHF3 S1133	Q92576		PHF3	S	0.885262	-0.1418	4	6
PHRF1 S5	Q9P1Y6		PHRF1	S	1.05839	-1.34839	3	4
PI4KB S428	Q9UBF8		PI4KB	S	1.19178	0.3611	6	4
PKHA6 S777	Q9Y2H5	R-X-X-S	PKHA6	S	0.874723	-0.25309	2	4
PKN2 T958	Q16513		PKN2	T	0.606916	-0.15991	5	5

Table 4.1 ETAA1-dependent phosphosites.								
Phosphosite	**Uniprot**	**ATR Motif (SQ/TQ) CHK1 Motif (R-X-X-S)**	**Protein Name**	**Amino acid**	**ETAA1 Ratio**	**TOPBP1 Ratio**	**Count ETAA1ΔAAD**	**Count TOPBP1-AID**
PP16A S418	Q96I34		PP16A	S	2.16302	0.26988	2	2
PP2BB S471	P16298	R-X-X-S	PP2BB	S	0.911863	0.10621	3	1
PRR12 S1104	Q9ULL5		PRR12	S	0.649753	-0.27026	2	6
PTN2 S304	P17706		PTN2	S	0.586272	-0.24951	4	3
PTN21 S637	Q16825		PTN21	S	0.604316	0.24895	2	2
PTN3 S372	P26045		PTN3	S	0.824106	-0.16655	2	3
PTTG1 S165	O95997		PTTG1	S	0.662661	-0.52511	6	5
PUR6 S27	P22234		PUR6	S	0.873863	0.09802	3	1
PURB S6	Q96QR8		PURB	S	1.11986	-0.08317	2	3
R3GEF S168	Q8TBN0		R3GEF	S	1.39495	-0.26747	2	5
R3GEF S179	Q8TBN0		R3GEF	S	1.39495	0.11488	2	4
R51A1 S120	Q96B01	SQ	R51A1	S	1.30141	-0.0994	2	1
RAB8A S185	P61006		RAB8A	S	0.701344	0.50614	2	2
RAF1 S244	P04049		RAF1	S	0.58665	0.58458	2	1
RANB3 S100	Q9H6Z4		RANB3	S	1.25048	0.36598	3	5
RANB3 S101	Q9H6Z4		RANB3	S	1.33069	0.14287	3	6
RANB9 S485	Q96S59		RANB9	S	0.592445	0.10814	5	3
RAVR1 S17	Q8IY67		RAVR1	S	0.832525	-0.21826	3	4
RBL1 S749	P28749		RBL1	S	1.66317	-0.37692	5	6
RBL1 S762	P28749		RBL1	S	1.65908	-0.33303	5	6
RBMX S88	P38159		RBMX	S	0.777451	0.25108	4	6
RBP1 S29	Q15311	R-X-X-S	RBP1	S	0.682034	0.28387	4	5
REPS1 S562	Q96D71	R-X-X-S	REPS1	S	1.91516	0.28143	2	3
RERE S1106	Q9P2R6		RERE	S	0.790689	0.48553	2	1
RERE S1113	Q9P2R6		RERE	S	0.790689	0.48553	2	1
RERE S1115	Q9P2R6	R-X-X-S	RERE	S	0.790689	0.48553	2	1
RERE S142	Q9P2R6		RERE	S	0.635025	0.41868	3	1
RERE S642	Q9P2R6		RERE	S	0.943434	0.51712	3	4
RERE T599	Q9P2R6		RERE	T	0.648097	0.17517	3	3
RFC1 S283	P35251		RFC1	S	0.819567	-0.18082	2	1
RGL3 S569	Q3MIN7		RGL3	S	0.970854	0.15043	4	4
RGPS2 S329	Q86X27		RGPS2	S	0.608738	-0.01332	3	1
RGPS2 T326	Q86X27		RGPS2	T	0.928351	-0.01332	2	1
RHG17 S575	Q68EM7		RHG17	S	0.801912	0.22318	2	6
RHG17 S674	Q68EM7		RHG17	S	0.598825	0.51995	3	3
RHG17 S676	Q68EM7	R-X-X-S	RHG17	S	0.598825	0.51995	3	3
RHPN2 S654	Q8IUC4		RHPN2	S	0.708765	-0.63332	2	1
RIN1 S210	Q13671		RIN1	S	0.74149	0.28286	3	6
RIOK1 S22	Q9BRS2		RIOK1	S	0.747883	0.54815	5	3
RIOK2 S380	Q9BVS4		RIOK2	S	1.49567	0.04768	2	1
RIOK2 S382	Q9BVS4		RIOK2	S	1.49567	0.04768	2	1
RLF S632	Q13129		RLF	S	1.00382	0.40545	3	4
RN219 S210	Q5W0B1		RN219	S	0.666393	0.45954	2	4
ROA2 S85	P22626	R-X-X-S	ROA2	S	0.697685	-0.56175	3	3
RPIA T107	P49247		RPIA	T	0.987088	0.07382	2	1
RS2 S264	P15880		RS2	S	0.593367	-0.08135	2	1
RTKN S106	Q9BST9	R-X-X-S	RTKN	S	0.869003	0.0404	2	5
RUNX2 S28	Q13950	R-X-X-S	RUNX2	S	1.27417	-0.46023	3	6
SAC31 S402	A6NKF1	R-X-X-S	SAC31	S	0.694122	-0.28847	2	1
SAMH1 T592	Q9Y3Z3		SAMH1	T	0.694476	-0.29963	5	5
SARG T456	Q9BW04		SARG	T	1.23351	0.39164	4	5
SC16A S1178	O15027		SC16A	S	0.738033	-0.50173	3	1
SCRIB S1486	Q14160	R-X-X-S	SCRIB	S	0.597221	0.11849	2	1
SDS3 S32	Q9H7L9		SDS3	S	0.674551	-0.25402	3	4
SETD2 S754	Q9BYW2		SETD2	S	0.686523	0.15924	2	1
SH319 S150	Q5HYK7		SH319	S	1.27047	0.30252	2	2
SH3R1 S735	Q7Z6J0		SH3R1	S	1.04921	-0.13903	2	2
SIN1 S510	Q9BPZ7	R-X-X-S	SIN1	S	0.657731	0.14496	3	2
SKA3 S155	Q8IX90		SKA3	S	0.60046	0.06757	4	4
SNPC4 S599	Q5SXM2		SNPC4	S	0.647987	-0.09808	2	2
SOX4 S354	Q06945		SOX4	S	0.971295	-0.65203	2	2
SQSTM S332	Q13501		SQSTM	S	0.746657	-0.0037	5	4
SRCAP S568	Q6ZRS2		SRCAP	S	0.615322	0.47051	2	2

Table 4.1 ETAA1-dependent phosphosites.								
Phosphosite	**Uniprot**	**ATR Motif (SQ/TQ) CHK1 Motif (R-X-X-S)**	**Protein Name**	**Amino acid**	**ETAA1 Ratio**	**TOPBP1 Ratio**	**Count ETAA1ΔAAD**	**Count TOPBP1-AID**
SRGP1 S1005	Q7Z6B7		SRGP1	S	0.71642	-0.62211	2	3
SRRM1 S310	Q8IYB3		SRRM1	S	0.775093	0.16993	2	5
SRRM1 S657	Q8IYB3		SRRM1	S	0.726134	0.08298	3	4
SSFA2 S352	P28290		SSFA2	S	0.916629	0.51299	3	1
SSFA2 S746	P28290		SSFA2	S	0.660992	0.58306	6	5
STMN1 S38	P16949		STMN1	S	0.718029	-0.10961	7	6
STRN3 S229	Q13033		STRN3	S	0.747578	0.09221	4	3
TACC2 S2072	O95359	R-X-X-S	TACC2	S	1.02899	0.33743	2	6
TACC2 S2226	O95359		TACC2	S	1.24329	0.29619	3	6
TACC2 S2317	O95359		TACC2	S	0.898406	0.39408	4	6
TACC2 S2321	O95359		TACC2	S	0.898406	0.39408	4	6
TACC3 S250	Q9Y6A5		TACC3	S	0.722379	0.40991	3	6
TACC3 T249	Q9Y6A5		TACC3	T	0.703758	0.47931	4	5
TB10B S707	Q4KMP7		TB10B	S	1.64966	0.1296	2	5
TFE2 S379	P15923		TFE2	S	0.64612	0.47384	6	6
TNC18 S1038	O15417		TNC18	S	0.993928	-0.27075	3	4
TPIS S58	P60174	R-X-X-S	TPIS	S	0.683066	-0.8347	8	6
TPRN S241	Q4KMQ1		TPRN	S	0.727528	-0.4088	2	2
TR150 S55	Q9Y2W1	R-X-X-S	TR150	S	0.677441	-0.0212	5	6
TR150 S575	Q9Y2W1	R-X-X-S	TR150	S	0.86769	0.22462	5	5
UB2J1 S266	Q9Y385	R-X-X-S	UB2J1	S	1.02655	0.49088	5	6
UBP36 S667	Q9P275		UBP36	S	0.603027	-0.41588	3	5
US6NL S680	Q92738		US6NL	S	1.05949	0.20727	3	5
VCIP1 S998	Q96JH7	R-X-X-S	VCIP1	S	1.61655	0.17486	3	4
VGLL4 S101	Q14135	R-X-X-S	VGLL4	S	1.43328	-0.35874	3	3
VGLL4 S103	Q14135	R-X-X-S	VGLL4	S	1.43328	-0.07599	3	3
WNK1 S2011	Q9H4A3		WNK1	S	0.708659	-0.00929	4	3
WNK1 S2012	Q9H4A3		WNK1	S	0.667211	-0.12496	5	4
WNK1 S2027	Q9H4A3		WNK1	S	1.02084	0.17172	3	3
WNK1 S2029	Q9H4A3		WNK1	S	1.15653	0.5175	4	4
WNK1 S2032	Q9H4A3		WNK1	S	1.15653	0.5175	4	4
Y103	(blank)		(blank)	Y	0.722029	0.41175	2	1
YTDC1 T148	Q96MU7		YTDC1	T	1.21851	0.21325	3	6
Z3H7B T240	Q9UGR2		Z3H7B	T	0.67229	-0.13324	2	2
ZBED4 S609	O75132	R-X-X-S	ZBED4	S	0.685097	-0.6405	2	1
ZC3HD S64	Q5T200		ZC3HD	S	1.33297	-0.12265	4	5
ZFAN5 S48	O76080		ZFAN5	S	0.709291	0.35539	3	4
ZN318 S1856	Q5VUA4		ZN318	S	0.672561	-0.11486	5	5
ZN318 S40	Q5VUA4	R-X-X-S	ZN318	S	1.69681	-0.24734	4	1
ZO1 S1617	Q07157		ZO1	S	0.61995	0.18663	6	5
ZO1 S912	Q07157	R-X-X-S	ZO1	S	0.961884	-0.85664	3	3

Table 4.2 TOPBP1-dependent phosphosites. TOPBP1-dependent phosphosites are given below along with the Uniprot ID, modified residue, presence of ATR or CHK1 motif, and the number of experiments in which that peptide was observed. The ratio value is the $\log_2$ transformed ratio of WT /ETAA1 or TOPBP1 cells. Therefore, a higher value (darker green) is more dependent on ETAA1 or TOPBP1.

Table 4.2 TOPBP1-dependent phosphosites

Phosphosite	Uniprot	ATR Motif (SQ/TQ) CHK1 Motif (R-X-X-S)	Protein Name	Amino acid	ETAA1 Ratio	TOPBP1 Ratio	Count ETAA1ΔAAD	Count TOPBP1-AID
4EBP1 S65	Q13541		4EBP1	S	0.018774	1.42573	6	6
4EBP1 T46	Q13541		4EBP1	T	-0.07551	0.702899	3	3
4EBP1 T68	Q13541		4EBP1	T	0.08134	0.961179	4	2
4EBP1 T70	Q13541		4EBP1	T	0.094308	1.01085	7	6
AAPK1 S356	Q13131		AAPK1	S	0.17479	0.635801	6	6
ABI1 S222	Q8IZP0	R-X-X-S/SQ	ABI1	S	0.445409	2.19374	1	3
ABI2 Y213	Q9NYB9		ABI2	Y	0.24306	0.902503	5	4
ACOD S198	O00767		ACOD	S	0.579663	0.668426	1	2
ADAM9 S752	Q13443		ADAM9	S	0.052972	0.674896	1	2
ADDA S355	P35611		ADDA	S	0.212881	0.81052	2	3
ADNP S709	Q9H2P0		ADNP	S	-0.06309	1.26879	2	4
AEBP2 S24	Q6ZN18		AEBP2	S	0.342678	1.26022	7	5
AF9 S483	P42568		AF9	S	0.474254	0.836828	1	2
AFAD S1172	P55196		AFAD	S	0.128058	0.838508	4	6
AFAD S1182	P55196		AFAD	S	0.10528	0.838508	7	6
AHNK S2397	Q09666		AHNK	S	0.156745	1.199	3	2
AHNK S5077	Q09666		AHNK	S	0.303568	0.930245	4	6
AHNK S93	Q09666		AHNK	S	0.430927	0.621524	7	6
AKA11 S433	Q9UKA4		AKA11	S	-0.15701	1.53725	1	3
AKA11 T1100	Q9UKA4		AKA11	T	0.186078	1.00806	4	2
AKA12 S1328	Q02952		AKA12	S	0.425411	1.27638	4	4
AKA12 S1331	Q02952		AKA12	S	0.297337	0.626112	7	6
AKA12 S371	Q02952		AKA12	S	0.313151	0.652601	6	3
AKA12 S483	Q02952		AKA12	S	0.506399	0.685716	5	3
AKA12 S598	Q02952		AKA12	S	0.31734	0.724738	8	6
AKA12 S644	Q02952		AKA12	S	0.511639	0.60046	7	6
AKA12 S645	Q02952		AKA12	S	0.511639	0.60046	7	6
AKA12 T642	Q02952		AKA12	T	0.133492	0.799087	4	4
AKA12 T646	Q02952		AKA12	T	0.251204	0.992177	5	4
AKTS1 S183	Q96B36		AKTS1	S	0.413756	1.12428	2	2
AKTS1 S203	Q96B36		AKTS1	S	0.017067	0.733084	5	4
ALG3 S13	Q92685	R-X-X-S	ALG3	S	-0.23601	1.02883	2	2
AMD S918	P19021		AMD	S	0.480369	1.37095	4	5
AN32A S17	P39687	R-X-X-S	AN32A	S	0.4755	1.17376	1	3
ANK3 S1459	Q12955	R-X-X-S	ANK3	S	-0.2947	0.742955	3	3
ANR11 S1878	Q6UB99		ANR11	S	-0.05872	0.779218	6	4
ANR17 S2045	O75179		ANR17	S	0.369006	1.09228	4	6
ANR17 S2047	O75179		ANR17	S	0.131589	0.957543	6	5
ANR17 S2067	O75179		ANR17	S	0.438399	1.73202	1	2
ANR32 S159	Q9BQI6		ANR32	S	-0.52701	0.654619	1	2
ANS1A Y834	Q92625		ANS1A	Y	0.153902	1.06516	2	2
APC1 S377	Q9H1A4		APC1	S	0.050606	2.83946	4	4
ARHGG S174	Q5VV41		ARHGG	S	0.195222	0.654985	6	5
ARHGI S1101	Q6ZSZ5		ARHGI	S	0.280979	1.10969	4	5
ARHGI S1103	Q6ZSZ5	R-X-X-S	ARHGI	S	-0.03159	0.702746	7	5
ARI1A S715	O14497		ARI1A	S	0.53047	0.762142	1	3
ARI1A S769	O14497		ARI1A	S	0.005525	0.769179	3	3
ARI4B S666	Q4LE39	R-X-X-S	ARI4B	S	-0.45003	0.862511	3	2
ARI4B S675	Q4LE39		ARI4B	S	-0.03614	0.938399	6	6

Table 4.2 TOPBP1-dependent phosphosites								
Phosphosite	Uniprot	ATR Motif (SQ/TQ) CHK1 Motif (R-X-X-S)	Protein Name	Amino acid	ETAA1 Ratio	TOPBP1 Ratio	Count ETAA1ΔAAD	Count TOPBP1-AID
ARL3 S5	P36405		ARL3	S	0.312954	0.631337	4	4
ARRB1 S412	P49407		ARRB1	S	0.039279	0.732194	3	2
ASAP2 S822	O43150	R-X-X-S	ASAP2	S	0.241474	0.955462	2	2
ATAD2 S342	Q6PL18		ATAD2	S	0.348799	0.673737	4	3
ATG9A S656	Q7Z3C6	R-X-X-S	ATG9A	S	0.231678	1.29154	2	3
ATG9A S828	Q7Z3C6		ATG9A	S	0.443552	1.43018	5	4
ATR S436	Q13535	R-X-X-S	ATR	S	-0.16411	1.00076	4	2
ATRX S1352	P46100		ATRX	S	-0.08358	1.60189	4	3
ATRX S634	P46100		ATRX	S	0.068723	0.765704	4	2
BAG3 S194	O95817		BAG3	S	0.185993	2.20571	2	4
BAG3 S195	O95817		BAG3	S	0.212693	1.39678	4	5
BAP18 S96	Q8IXM2		BAP18	S	0.239727	1.03168	5	5
BAZ1A S1417	Q9NRL2		BAZ1A	S	0.297837	0.731369	3	3
BAZ1B S1342	Q9UIG0	R-X-X-S	BAZ1B	S	0.367483	0.644779	6	5
BAZ1B S160	Q9UIG0		BAZ1B	S	0.01455	0.652326	4	4
BBX S478	Q8WY36		BBX	S	-0.54294	0.783262	7	4
BBX S479	Q8WY36	R-X-X-S	BBX	S	-0.5161	0.783262	7	4
BBX S481	Q8WY36		BBX	S	-0.55618	0.783262	7	3
BBX S844	Q8WY36		BBX	S	0.182057	0.618333	7	4
BCAS3 S480	Q9H6U6		BCAS3	S	0.578697	1.97311	5	4
BCAS3 S488	Q9H6U6		BCAS3	S	0.578118	0.893893	1	2
BCL7C S126	Q8WUZ0	R-X-X-S	BCL7C	S	0.042784	0.690998	7	6
BCLF1 S183	Q9NYF8	SQ	BCLF1	S	0.037031	0.665666	5	3
BIG2 S218	Q9Y6D5		BIG2	S	0.157303	0.940881	6	6
BORG4 S174	Q9H3Q1		BORG4	S	-0.04796	0.885106	4	2
BRM1L S197	Q5PSV4		BRM1L	S	0.011353	0.942909	1	4
BRMS1 S237	Q9HCU9		BRMS1	S	-0.08896	0.69073	2	3
BRWD1 S2018	Q9NSI6		BRWD1	S	-0.25096	0.665817	1	2
BRWD1 S2020	Q9NSI6		BRWD1	S	-0.25096	0.665817	1	2
BRWD1 S696	Q9NSI6	R-X-X-S	BRWD1	S	-0.22482	0.894294	3	4
BUD13 S239	Q9BRD0		BUD13	S	0.108491	0.675013	1	4
BUD13 S240	Q9BRD0		BUD13	S	0.243547	0.675013	2	4
BUD13 T123	Q9BRD0	R-X-X-S	BUD13	T	0.039974	0.587941	3	4
CA144 S107	Q7Z422		CA144	S	0.001298	1.47303	6	2
CA144 S37	Q7Z422		CA144	S	0.312009	0.642378	7	6
CA226 S222	A1L170	R-X-X-S	CA226	S	-0.30185	1.71664	2	2
CA226 S223	A1L170	R-X-X-S	CA226	S	-0.30185	1.71664	2	2
CAF1A S203	Q13111		CAF1A	S	0.143524	0.822263	4	5
CAF1B S429	Q13112		CAF1B	S	0.003537	0.831521	5	5
CAMP2 S1019	Q08AD1	R-X-X-S	CAMP2	S	0.09842	0.706287	2	4
CAP1 S308	Q01518		CAP1	S	0.068126	1.19333	6	4
CAP1 S310	Q01518		CAP1	S	0.09692	1.19333	6	4
CAPON S266	O75052		CAPON	S	0.204767	1.25743	3	3
CB044 S468	Q9H6R7		CB044	S	0.356031	0.681404	4	3
CBX5 S11	P45973		CBX5	S	0.245374	0.810222	4	3
CBX5 S12	P45973		CBX5	S	0.245374	0.810222	4	3
CBX5 S13	P45973		CBX5	S	0.245374	0.810222	4	3
CBX5 S14	P45973		CBX5	S	0.245374	0.810222	4	3
CBX8 S311	Q9HC52	R-X-X-S	CBX8	S	0.107822	0.838451	4	5
CC165 S1812	Q9Y4B5	R-X-X-S	CC165	S	0.109026	1.86492	1	2
CC165 S1814	Q9Y4B5	R-X-X-S	CC165	S	0.109026	1.86492	1	2
CC85C S246	A6NKD9		CC85C	S	0.030265	0.606158	7	6
CCDC6 S52	Q16204		CCDC6	S	0.361655	0.74028	3	2
CCDC9 S202	Q9Y3X0	R-X-X-S	CCDC9	S	-0.1555	0.627887	1	3
CCNL1 S342	Q9UK58		CCNL1	S	0.011066	0.800165	6	6
CDA7L S108	Q96GN5		CDA7L	S	0.294077	0.939753	2	2
CDC23 T562	Q9UJX2		CDC23	T	0.019346	0.698396	1	5
CDK17 S9	Q00537	R-X-X-S	CDK17	S	0.144958	0.79703	2	4
CDYL1 S201	Q9Y232		CDYL1	S	-0.05567	0.603787	6	6
CE170 S1521	Q5SW79		CE170	S	-0.0573	0.849185	5	4
CE170 S1522	Q5SW79		CE170	S	-0.0573	0.781752	5	5
CE170 S838	Q5SW79	R-X-X-S	CE170	S	0.013049	0.61899	3	4
CG043 S495	Q8WVR3	R-X-X-S	CG043	S	0.484491	1.36474	4	3

Table 4.2 TOPBP1-dependent phosphosites								
Phosphosite	Uniprot	ATR Motif (SQ/TQ) CHK1 Motif (R-X-X-S)	Protein Name	Amino acid	ETAA1 Ratio	TOPBP1 Ratio	Count ETAA1ΔAAD	Count TOPBP1-AID
CHAP1 S204	Q96JM3		CHAP1	S	-0.15999	0.705934	7	6
CHAP1 S286	Q96JM3		CHAP1	S	0.16337	0.610428	7	5
CHAP1 S445	Q96JM3		CHAP1	S	0.087887	0.753605	5	3
CHAP1 S651	Q96JM3		CHAP1	S	-0.09463	0.808615	5	3
CHAP1 S652	Q96JM3		CHAP1	S	-0.09463	0.834567	5	3
CHAP1 S653	Q96JM3		CHAP1	S	-0.09463	0.808615	5	3
CI078 Y147	Q9NZ63		CI078	Y	0.250719	0.605335	4	2
CIZ1 S838	Q9ULV3		CIZ1	S	0.20964	0.653519	6	5
CLK3 S280	P49761		CLK3	S	0.273237	1.33777	2	3
CLK3 S281	P49761		CLK3	S	0.273237	1.33777	3	3
CLK3 S283	P49761		CLK3	S	0.257888	0.63006	3	5
COPA S173	P53621		COPA	S	0.117296	0.638793	4	3
CPSF1 S765	Q10570		CPSF1	S	0.079429	1.54775	5	2
CPSF1 S766	Q10570	R-X-X-S/SQ	CPSF1	S	0.108313	1.38156	6	5
CQ096 S173	A6NHQ4		CQ096	S	0.000636	0.645794	4	2
CQ096 S184	A6NHQ4	R-X-X-S	CQ096	S	0.002936	0.608809	4	2
CR025 S67	Q96B23	R-X-X-S	CR025	S	0.287354	0.6277	3	2
CRKL S184	P46109		CRKL	S	-0.08183	0.601411	1	2
CRKL S185	P46109		CRKL	S	-0.08183	0.601411	1	3
CTU2 S435	Q2VPK5		CTU2	S	0.253958	0.782583	2	2
CUED2 Y275	Q9H467		CUED2	Y	-0.20015	0.703559	1	2
DAB2P S978	Q5VWQ8		DAB2P	S	0.313478	2.02801	2	3
DAP1 S3	P51397		DAP1	S	0.162597	0.984271	3	2
DBNL S283	Q9UJU6		DBNL	S	0.228247	0.710261	2	5
DCP1A S62	Q9NPI6	R-X-X-S	DCP1A	S	0.293875	1.5996	3	2
DDX24 S82	Q9GZR7		DDX24	S	0.061882	0.591679	8	6
DHX16 S160	O60231		DHX16	S	0.00173	1.49214	2	4
DHX29 S200	Q7Z478		DHX29	S	0.327457	0.841732	7	6
DKC1 S21	O60832		DKC1	S	-0.10895	1.03017	7	5
DMAP1 T445	Q9NPF5		DMAP1	T	0.0397	0.592035	5	2
DNJC5 T11	Q9H3Z4		DNJC5	T	0.125244	0.637253	2	2
DNM3A S105	Q9Y6K1		DNM3A	S	0.077516	1.52421	3	3
DOCK7 S1383	Q96N67	R-X-X-S	DOCK7	S	0.239398	0.940174	3	4
DOCK7 S2129	Q96N67		DOCK7	S	0.048097	0.678523	3	3
DOCK7 S452	Q96N67	R-X-X-S	DOCK7	S	0.176706	1.02233	5	5
DOCK7 S888	Q96N67	R-X-X-S	DOCK7	S	0.136454	1.90115	1	2
DOCK7 S900	Q96N67		DOCK7	S	0.224739	0.722204	4	4
DOT1L S447	Q8TEK3		DOT1L	S	0.191548	0.601316	4	2
DOT1L S902	Q8TEK3		DOT1L	S	0.116764	0.982967	5	3
DPYL3 S522	Q14195		DPYL3	S	-0.10815	4.46284	6	4
DSG2 Y1013	Q14126		DSG2	Y	0.331934	0.665257	1	2
DYHC1 S4368	Q14204	R-X-X-S	DYHC1	S	0.259544	0.752749	3	2
EHBP1 S428	Q8NDI1		EHBP1	S	0.046701	0.711407	6	5
EIF3B S81	P55884		EIF3B	S	-0.07885	0.66339	1	3
EIF3B S85	P55884		EIF3B	S	0.090989	0.71721	2	4
EIF3G T41	O75821		EIF3G	T	0.069702	0.601031	7	4
ELL S319	P55199	R-X-X-S	ELL	S	-0.08841	1.23691	1	2
ELOA1 S251	Q14241	SQ	ELOA1	S	-0.04493	1.38072	1	2
EMAL4 S144	Q9HC35		EMAL4	S	0.172876	0.968718	5	5
ENAH T489	Q8N8S7		ENAH	T	-0.11134	0.85814	1	2
EP15R S108	Q9UBC2		EP15R	S	0.123549	0.662015	3	2
EPHA2 T898	P29317		EPHA2	T	-0.94878	0.822894	1	2
EPN1 S454	Q9Y6I3		EPN1	S	-0.38517	0.880646	4	3
EPN1 T470	Q9Y6I3		EPN1	T	-0.34452	0.773743	7	3
ERBB3 S982	P21860		ERBB3	S	-0.42239	0.665211	1	3
ERCC5 T338	P28715		ERCC5	T	0.370611	1.10213	1	2
ERRFI S249	Q9UJM3		ERRFI	S	0.114135	2.42089	2	4
ERRFI S251	Q9UJM3	R-X-X-S	ERRFI	S	0.277271	2.42089	5	4
ERRFI S273	Q9UJM3		ERRFI	S	0.09031	1.32949	4	2
ERRFI S334	Q9UJM3	R-X-X-S	ERRFI	S	0.582845	1.52751	3	2
ERRFI S461	Q9UJM3		ERRFI	S	0.570269	1.50927	1	2
F122B S115	Q7Z309		F122B	S	0.454808	1.46869	7	6
F122B S119	Q7Z309		F122B	S	0.356369	1.45854	7	6

Table 4.2 TOPBP1-dependent phosphosites								
Phosphosite	Uniprot	ATR Motif (SQ/TQ) CHK1 Motif (R-X-X-S)	Protein Name	Amino acid	ETAA1 Ratio	TOPBP1 Ratio	Count ETAA1ΔAAD	Count TOPBP1-AID
F122B S137	Q7Z309		F122B	S	0.023242	1.32608	4	2
F122B S24	Q7Z309	R-X-X-S	F122B	S	0.01985	1.6673	3	4
F122B S25	Q7Z309	R-X-X-S	F122B	S	0.2949	1.88491	7	4
F122B S50	Q7Z309	R-X-X-S	F122B	S	0.361053	1.42542	5	4
F169A S635	Q9Y6X4		F169A	S	-0.09766	3.26616	4	3
F169A S636	Q9Y6X4		F169A	S	-0.09766	3.26616	4	3
F208A S927	Q9UK61		F208A	S	-0.00225	1.92227	3	5
F208B S2037	Q5VWN6	R-X-X-S	F208B	S	0.101582	0.589668	6	6
FA53B S178	Q14153		FA53B	S	0.241352	1.28607	2	2
FA53B S179	Q14153		FA53B	S	0.242389	1.69171	4	4
FA53C S273	Q9NYF3	R-X-X-S/SQ	FA53C	S	0.236952	0.801821	1	2
FAF1 S582	Q9UNN5	R-X-X-S	FAF1	S	0.481712	0.769913	2	4
FAK1 S910	Q05397		FAK1	S	-0.10558	0.755229	6	4
FARP1 S427	Q9Y4F1		FARP1	S	-0.28611	0.668755	1	5
FAS S2236	P49327	R-X-X-S	FAS	S	0.406646	1.10064	1	4
FAT1 S4272	Q14517		FAT1	S	-0.49498	0.731936	6	5
FAT1 S4276	Q14517		FAT1	S	-0.41876	0.909658	3	3
FBX42 S488	Q6P3S6	R-X-X-S	FBX42	S	0.184979	3.21053	1	3
FBX42 S552	Q6P3S6		FBX42	S	0.390448	0.775926	1	2
FCHO1 S583	O14526		FCHO1	S	-0.15224	0.602485	1	2
FCHO1 S585	O14526	R-X-X-S	FCHO1	S	-0.15224	0.69682	1	2
FCHO2 S403	Q0JRZ9	R-X-X-S	FCHO2	S	0.291721	1.14809	1	2
FCHO2 S488	Q0JRZ9	R-X-X-S	FCHO2	S	0.504757	1.338	5	6
FCHO2 S496	Q0JRZ9		FCHO2	S	0.503383	1.32642	5	6
FCHO2 T495	Q0JRZ9		FCHO2	T	0.418892	1.50357	3	3
FGD1 S48	P98174	R-X-X-S	FGD1	S	-0.2238	1.93428	4	3
FGD1 S50	P98174		FGD1	S	-0.24623	1.67645	4	4
FKBP3 S36	Q00688		FKBP3	S	-0.08628	1.70189	1	2
FND3A S213	Q9Y2H6		FND3A	S	0.01591	0.647821	2	3
FOSL1 S101	P15407		FOSL1	S	0.357721	1.99816	3	2
FOXK2 S398	Q01167	R-X-X-S	FOXK2	S	0.003746	0.629846	7	6
FUBP2 S125	Q92945	SQ	FUBP2	S	-0.09718	0.994798	1	2
FUBP2 S129	Q92945		FUBP2	S	-0.09718	0.994798	1	2
FXR2 S601	P51116		FXR2	S	0.304978	0.811774	6	5
FXR2 S603	P51116		FXR2	S	0.038155	0.811774	6	5
FYV1 S23	Q9Y2I7		FYV1	S	-0.00855	0.857742	1	2
GCP60 S43	Q9H3P7		GCP60	S	0.307545	0.919988	1	2
GEPH S188	Q9NQX3		GEPH	S	-0.00432	0.601316	5	6
GEPH S194	Q9NQX3		GEPH	S	-0.00347	0.601316	5	6
GIPC1 S232	O14908	R-X-X-S	GIPC1	S	0.507508	0.767824	4	6
GLYR1 S130	Q49A26	R-X-X-S	GLYR1	S	-0.10388	4.19912	5	5
GLYR1 S158	Q49A26		GLYR1	S	0.35242	4.40061	3	5
GON4L S206	Q3T8J9		GON4L	S	0.116365	2.6762	3	3
GRIN1 S73	Q7Z2K8	R-X-X-S	GRIN1	S	-0.10914	1.03682	1	3
GRIN1 S850	Q7Z2K8	R-X-X-S	GRIN1	S	-0.37771	0.602362	2	3
GSK3A S278	P49840		GSK3A	S	0.104104	1.74084	2	3
GULP1 S211	Q9UBP9		GULP1	S	0.285256	1.0267	4	3
H12 S2	P16403		H12	S	0.041673	0.853517	2	4
HCFC1 S2019	P51610	R-X-X-S	HCFC1	S	0.12366	6.93605	3	2
HDAC4 S467	P56524	R-X-X-S	HDAC4	S	0.296545	1.1944	3	4
HDAC4 S632	P56524	R-X-X-S	HDAC4	S	0.207034	2.03091	6	5
HDC S264	Q9UBI9		HDC	S	0.269742	0.660262	3	4
HDC S268	Q9UBI9		HDC	S	0.269742	0.660262	3	4
HDC S272	Q9UBI9		HDC	S	0.220454	0.74676	2	2
HEAT6 S395	Q6AI08		HEAT6	S	0.322446	1.02531	2	2
HEAT6 S396	Q6AI08	R-X-X-S	HEAT6	S	0.322446	1.02531	2	2
HECD1 S1772	Q9ULT8	R-X-X-S	HECD1	S	0.309448	1.53824	4	3
HECD1 S357	Q9ULT8	R-X-X-S	HECD1	S	0.235482	0.968883	1	2
HLTF S397	Q14527		HLTF	S	0.144177	1.02704	3	5
HLTF S398	Q14527		HLTF	S	0.144177	1.02704	3	5
HLTF S400	Q14527		HLTF	S	0.144177	1.02704	3	5
HMGA1 S9	P17096	SQ	HMGA1	S	-0.50092	1.35561	2	2
HMGA1 T53	P17096		HMGA1	T	0.152768	1.02843	1	4

Table 4.2 TOPBP1-dependent phosphosites								
Phosphosite	Uniprot	ATR Motif (SQ/TQ) CHK1 Motif (R-X-X-S)	Protein Name	Amino acid	ETAA1 Ratio	TOPBP1 Ratio	Count ETAA1ΔAAD	Count TOPBP1-AID
HMGA2 S2	P52926		HMGA2	S	0.479541	1.04782	1	5
HMGX4 S497	Q9UGU5		HMGX4	S	0.37829	0.622462	4	5
HMGX4 S502	Q9UGU5		HMGX4	S	0.407625	0.776357	3	2
HMGX4 S512	Q9UGU5		HMGX4	S	-0.02191	0.704252	4	2
HNF1B S279	P35680	R-X-X-S	HNF1B	S	-0.08337	5.09733	3	2
HNRPM Y64	P52272		HNRPM	Y	-0.41629	0.693324	1	5
HOMEZ T451	Q8IX15	R-X-X-S	HOMEZ	T	0.153546	0.704075	4	3
HTSF1 S702	O43719		HTSF1	S	-0.0286	0.864209	2	2
I2BP1 S436	Q8IU81		I2BP1	S	0.127765	0.707914	4	3
ID2 S14	Q02363	R-X-X-S	ID2	S	0.378051	0.794686	5	6
IF2B2 S162	Q9Y6M1		IF2B2	S	0.034259	1.22113	4	3
IF4G2 S395	P78344		IF4G2	S	0.349026	0.678072	4	4
IF4G2 T385	P78344		IF4G2	T	0.058663	0.87887	1	3
IF4G2 T508	P78344	R-X-X-S	IF4G2	T	0.174406	0.927669	5	6
ILF3 T592	Q12906		ILF3	T	0.191942	0.641911	1	2
IRS1 S527	P35568	R-X-X-S	IRS1	S	0.213254	0.685378	4	3
IRS2 S388	Q9Y4H2		IRS2	S	-0.0978	0.8383	1	2
IRS2 S391	Q9Y4H2		IRS2	S	-0.32408	0.88144	1	2
ITPR3 S1832	Q14573	R-X-X-S	ITPR3	S	0.144219	1.35377	2	3
ITPR3 S916	Q14573		ITPR3	S	-0.35916	1.01028	2	3
ITSN1 S904	Q15811		ITSN1	S	-0.29163	0.605589	4	2
JHD2C T505	Q15652	R-X-X-S	JHD2C	T	0.256045	0.598937	1	3
JIP4 S183	O60271		JIP4	S	0.301002	0.910963	3	3
JMY S888	Q8N9B5	R-X-X-S	JMY	S	-0.13248	1.23915	4	4
JMY S889	Q8N9B5	R-X-X-S	JMY	S	-0.10919	1.43087	5	3
JUNB T255	P17275		JUNB	T	0.353662	0.844627	4	3
JUND S255	P17535		JUND	S	-0.09439	0.650489	7	5
K0284 S829	Q9Y4F5		K0284	S	0.249705	0.596554	5	6
K0284 S972	Q9Y4F5		K0284	S	0.318651	0.718565	3	4
K0913 S567	A7E2V4	R-X-X-S	K0913	S	-0.62728	1.00166	2	4
K0930 S304	Q6ICG6		K0930	S	-0.01232	1.04872	5	4
K0930 S351	Q6ICG6	R-X-X-S	K0930	S	-0.00835	0.608921	1	2
K0930 S353	Q6ICG6	R-X-X-S	K0930	S	-0.00835	0.608921	1	2
K0930 T293	Q6ICG6		K0930	T	-0.04862	0.700091	1	2
K1211 S873	Q6ZU35		K1211	S	-0.03139	0.58807	1	3
K1211 S874	Q6ZU35	R-X-X-S	K1211	S	0.525468	0.58807	3	3
K1211 T875	Q6ZU35		K1211	T	-0.03139	0.58807	1	3
K6PF S667	P08237		K6PF	S	0.22404	0.89933	5	4
KANL1 S268	Q7Z3B3		KANL1	S	0.035591	1.08488	3	2
KANL3 S515	Q9P2N6	R-X-X-S	KANL3	S	-0.05754	1.19812	1	4
KAT5 S86	Q92993		KAT5	S	-0.03514	0.647453	2	2
KAT6A S1113	Q92794		KAT6A	S	-0.75638	0.681494	3	4
KHDR1 Y440	Q07666		KHDR1	Y	-0.27114	0.826104	2	2
KI67 S3042	P46013		KI67	S	-0.48459	0.738552	1	3
KI67 S584	P46013		KI67	S	0.028286	0.766807	4	4
KI67 Y340	P46013		KI67	Y	-0.33841	1.21033	2	2
KIF15 S1141	Q9NS87		KIF15	S	0.441739	0.913939	3	4
KIF15 T1144	Q9NS87		KIF15	T	0.441739	0.913939	3	4
KIF23 S18	Q02241	SQ	KIF23	S	0.467737	1.46077	3	3
KITH S231	P04183		KITH	S	-0.95691	0.974815	1	2
KLDC4 S407	Q8TBB5		KLDC4	S	0.03196	0.728312	3	3
KLDC4 S413	Q8TBB5		KLDC4	S	-0.05901	0.905351	6	6
KLDC4 T403	Q8TBB5		KLDC4	T	0.082975	0.728312	1	3
KLF3 S250	P57682		KLF3	S	0.095047	1.24888	5	4
KLF3 S71	P57682		KLF3	S	0.341303	0.832363	2	5
KPCD S299	Q05655		KPCD	S	0.044553	1.09535	2	4
KPCD S645	Q05655		KPCD	S	-0.03657	0.675635	4	3
KPCD T295	Q05655	TQ	KPCD	T	-0.0106	0.884168	2	3
KPYM S37	P14618		KPYM	S	0.203106	0.696928	3	4
KS6A1 S363	Q15418		KS6A1	S	-0.14877	1.11522	5	5
KS6A1 T359	Q15418		KS6A1	T	-0.14877	1.29977	5	4
KS6A3 S369	P51812		KS6A3	S	0.070735	0.853117	4	4
KS6B1 S441	P23443		KS6B1	S	-0.0523	1.27131	1	2

Table 4.2 TOPBP1-dependent phosphosites								
Phosphosite	Uniprot	ATR Motif (SQ/TQ) CHK1 Motif (R-X-X-S)	Protein Name	Amino acid	ETAA1 Ratio	TOPBP1 Ratio	Count ETAA1ΔAAD	Count TOPBP1-AID
KS6B1 T444	P23443		KS6B1	T	0.020564	1.27131	2	3
KTNB1 Y337	Q9BVA0	R-X-X-S	KTNB1	Y	-0.19362	0.60005	2	2
LAP2A S424	P42166		LAP2A	S	0.012211	0.664091	1	4
LAP2A S433	P42166		LAP2A	S	0.328837	0.719697	1	2
LAP2A T74	P42166	R-X-X-S	LAP2A	T	0.350837	0.644502	3	2
LAR1B S340	Q659C4	R-X-X-S	LAR1B	S	0.396598	0.611267	5	6
LARP1 T782	Q6PKG0		LARP1	T	0.163987	1.80117	2	2
LARP1 T785	Q6PKG0		LARP1	T	0.077808	1.82204	2	3
LARP1 T788	Q6PKG0		LARP1	T	0.083384	1.30184	3	3
LIMA1 S132	Q9UHB6	R-X-X-S	LIMA1	S	-0.03937	0.660016	7	6
LIMA1 S374	Q9UHB6		LIMA1	S	-0.12047	1.13402	2	5
LIMA1 S490	Q9UHB6		LIMA1	S	0.037874	0.738811	7	6
LIMA1 S609	Q9UHB6		LIMA1	S	-0.00399	0.75232	7	6
LIMA1 S686	Q9UHB6		LIMA1	S	-0.09923	0.589571	6	5
LIMA1 S698	Q9UHB6		LIMA1	S	-0.40471	0.630512	1	2
LIPA1 S239	Q13136		LIPA1	S	0.17463	0.966395	6	5
LMNB1 S393	P20700		LMNB1	S	0.055612	0.894061	4	4
LRC8B S184	Q6P9F7		LRC8B	S	0.214318	0.629639	2	2
LSR T501	Q86X29		LSR	T	0.151209	0.59182	1	2
MAP2 S1795	P11137	R-X-X-S	MAP2	S	0.528552	0.702479	2	4
MAP2 S1798	P11137		MAP2	S	0.315798	0.665936	1	4
MAP2 S1799	P11137		MAP2	S	0.315798	0.702479	1	4
MAPK5 T368	Q8IW41		MAPK5	T	-0.3673	0.67912	1	2
MARCS S167	P29966		MARCS	S	0.136848	1.56896	1	2
MARK2 S40	Q7KZI7		MARK2	S	0.524164	1.04984	3	3
MBB1A S1243	Q9BQG0	R-X-X-S	MBB1A	S	-0.79912	0.849199	1	2
MBB1A T1244	Q9BQG0		MBB1A	T	-0.32649	0.849199	2	2
MCAF1 S557	Q6VMQ6	R-X-X-S	MCAF1	S	-0.37409	1.3027	1	2
MCM3 T722	P25205		MCM3	T	0.148642	0.65378	4	2
MD13L S2083	Q71F56	R-X-X-S	MD13L	S	-0.2062	0.802317	2	3
MDC1 S1399	Q14676		MDC1	S	-0.3384	0.658518	3	2
MDC1 S1400	Q14676		MDC1	S	-0.40517	0.714228	2	2
MDC1 S168	Q14676		MDC1	S	-0.22183	0.686523	7	3
MDC1 S1775	Q14676		MDC1	S	-0.67394	0.592062	6	3
MDC1 S990	Q14676		MDC1	S	-0.05499	1.16999	2	3
MDC1 S995	Q14676		MDC1	S	-0.1617	1.28744	3	4
MDC1 T1608	Q14676		MDC1	T	0.256048	0.829038	6	6
MDC1 T378	Q14676		MDC1	T	-0.32287	0.710614	3	4
MDHC S241	P40925	R-X-X-S	MDHC	S	0.118493	1.02829	1	3
MED14 S1136	O60244		MED14	S	-0.11202	0.617424	4	3
MED14 S1142	O60244		MED14	S	-0.01995	0.668185	3	4
MED14 S617	O60244	R-X-X-S	MED14	S	0.099109	0.626673	5	5
MED24 S862	O75448	R-X-X-S	MED24	S	0.012354	1.7746	3	2
MGAP S534	Q8IWI9	R-X-X-S	MGAP	S	0.02148	0.66239	4	5
MICA3 S1221	Q7RTP6		MICA3	S	0.579373	4.17249	2	2
MILK2 S247	Q8IY33		MILK2	S	0.421587	0.751207	1	3
MILK2 S649	Q8IY33	R-X-X-S	MILK2	S	0.27739	0.948526	4	6
MILK2 S658	Q8IY33		MILK2	S	0.299077	0.587077	3	6
MK01 T185	P28482		MK01	T	0.104529	1.72459	2	2
MK01 Y187	P28482		MK01	Y	0.314759	2.11589	6	4
MK03 T202	P27361		MK03	T	-0.19174	0.798337	2	2
MK03 Y204	P27361		MK03	Y	-0.19174	0.857901	4	3
MK14 S2	Q16539	SQ	MK14	S	0.379177	1.21785	5	4
MKL2 S66	Q9ULH7		MKL2	S	0.209391	1.66407	1	2
MLL1 S2201	Q03164		MLL1	S	-0.21364	1.4727	1	2
MLL1 T1845	Q03164		MLL1	T	0.093121	0.728051	5	4
MOT1 S467	P53985		MOT1	S	0.064469	0.78626	1	2
MPP8 S392	Q99549	R-X-X-S	MPP8	S	-0.01957	0.874948	2	5
MPP8 S85	Q99549		MPP8	S	0.331591	0.591581	3	2
MRCKA S1719	Q5VT25		MRCKA	S	0.555914	1.14444	1	2
MRCKG S1482	Q6DT37	R-X-X-S	MRCKG	S	0.027432	0.596554	2	5
MRE11 S688	P49959		MRE11	S	0.100465	0.621149	6	4
MRE11 S689	P49959		MRE11	S	0.100465	0.621149	6	4

Table 4.2 TOPBP1-dependent phosphosites								
Phosphosite	Uniprot	ATR Motif (SQ/TQ) CHK1 Motif (R-X-X-S)	Protein Name	Amino acid	ETAA1 Ratio	TOPBP1 Ratio	Count ETAA1ΔAAD	Count TOPBP1-AID
MTA1 S449	Q13330		MTA1	S	-0.11594	1.21176	7	6
MVD1 S96	P53602	R-X-X-S	MVD1	S	0.027951	1.00741	4	5
MYCB2 S2751	O75592	R-X-X-S	MYCB2	S	0.023468	0.83293	7	6
MYCB2 S3467	O75592	R-X-X-S	MYCB2	S	-0.07491	0.794187	2	2
MYO9B S1935	Q13459		MYO9B	S	0.104049	0.686419	3	3
NAA10 S186	P41227		NAA10	S	0.558855	1.30624	2	4
NAB1 S183	Q13506		NAB1	S	0.345623	0.928973	4	2
NAB1 S395	Q13506	R-X-X-S	NAB1	S	0.294706	0.812868	3	5
NAB2 S159	Q15742	R-X-X-S	NAB2	S	0.374956	1.56584	3	3
NAB2 S162	Q15742		NAB2	S	0.374956	1.56584	3	3
NAB2 S171	Q15742		NAB2	S	0.55768	1.56584	2	2
NBN S432	O60934		NBN	S	0.32262	0.688675	2	2
NCOAT S364	O60502		NCOAT	S	0.17594	0.899635	4	2
NEK1 S1008	Q96PY6		NEK1	S	0.381283	0.619674	2	2
NEK4 S563	P51957		NEK4	S	-0.30351	0.78031	1	4
NEK9 S868	Q8TD19		NEK9	S	0.172487	1.51783	7	6
NEK9 S869	Q8TD19		NEK9	S	0.166683	1.48037	7	6
NEUL4 S502	Q96JN8	R-X-X-S	NEUL4	S	-0.05589	0.920674	1	3
NEUL4 S902	Q96JN8		NEUL4	S	0.120352	0.615322	3	3
NEUL4 S907	Q96JN8		NEUL4	S	0.120352	0.615322	3	3
NFAT5 S145	O94916		NFAT5	S	-0.4454	1.09565	3	3
NIPA S359	Q86WB0		NIPA	S	-0.09564	0.626039	1	4
NIPBL S274	Q6KC79		NIPBL	S	-0.03226	0.609824	3	4
NIPBL S280	Q6KC79		NIPBL	S	-0.56923	0.721946	2	2
NKTR S463	P30414		NKTR	S	-0.32976	0.690551	1	3
NOLC1 S508	Q14978		NOLC1	S	0.073957	1.43621	2	4
NOLC1 S622	Q14978		NOLC1	S	0.04675	1.71145	3	4
NOLC1 S698	Q14978		NOLC1	S	-0.12207	0.60521	8	6
NOLC1 T607	Q14978		NOLC1	T	0.376718	1.37443	5	5
NOLC1 T610	Q14978		NOLC1	T	0.376718	1.00562	4	3
NOP56 S591	O00567	SQ	NOP56	S	0.062536	0.964635	1	2
NPAT S1151	Q14207		NPAT	S	-0.53138	0.597984	5	4
NPM S139	P06748		NPM	S	-0.1489	0.640158	3	3
NPM S227	P06748		NPM	S	-0.78496	0.896233	1	3
NPM S254	P06748		NPM	S	0.162057	0.670931	2	3
NRIP1 S564	P48552		NRIP1	S	0.035979	2.47171	4	2
NSN5C T141	Q63ZY6		NSN5C	T	0.333996	0.662205	1	3
NTR1 S401	P30989		NTR1	S	-0.0345	1.10131	6	5
NTR1 S403	P30989		NTR1	S	0.347439	1.10143	1	3
NTR1 S404	P30989		NTR1	S	-0.17428	1.04838	3	3
NU133 S45	Q8WUM0		NU133	S	-0.18203	0.934277	2	4
NU133 S50	Q8WUM0		NU133	S	-0.05347	0.945863	2	4
NU188 S1709	Q5SRE5		NU188	S	0.103934	0.790601	5	5
NUCL T121	P19338		NUCL	T	-1.01911	1.36793	1	2
NUMA1 S1862	Q14980	R-X-X-S	NUMA1	S	-0.36186	0.784202	5	5
NUP53 S73	Q8NFH5		NUP53	S	-0.24219	0.87688	2	2
ORC6 T195	Q9Y5N6		ORC6	T	0.422188	0.611833	2	3
OSB10 S188	Q9BXB5	R-X-X-S	OSB10	S	-0.01537	0.674044	2	3
OSB10 T190	Q9BXB5	R-X-X-S	OSB10	T	-0.13946	1.02531	2	2
P121C S165	A8CG34		P121C	S	-0.29226	4.38488	3	2
P5CR1 S301	P32322		P5CR1	S	0.031532	0.59388	2	3
P66B S129	Q8WXI9		P66B	S	0.2529	0.761966	7	3
PA1B2 S2	P68402	SQ	PA1B2	S	-0.05715	1.06523	7	3
PAF S72	Q15004		PAF	S	0.345208	0.80091	7	6
PAIRB S234	Q8NC51		PAIRB	S	0.163112	0.625501	5	5
PAIRB T232	Q8NC51		PAIRB	T	0.287354	0.637935	3	4
PAK4 S181	O96013	R-X-X-S	PAK4	S	0.220949	0.688315	6	6
PARP1 T368	P09874		PARP1	T	0.073683	0.902421	4	3
PATL1 S184	Q86TB9		PATL1	S	0.274888	1.10766	4	4
PAXI Y88	P49023		PAXI	Y	0.056136	0.597019	5	4
PB1 S10	Q86U86	R-X-X-S	PB1	S	-0.22383	0.607579	6	6
PB1 S39	Q86U86	R-X-X-S	PB1	S	-0.13373	0.847756	7	6
PB1 T9	Q86U86	R-X-X-S	PB1	T	0.023043	0.654985	3	3

Table 4.2 TOPBP1-dependent phosphosites								
Phosphosite	Uniprot	ATR Motif (SQ/TQ) CHK1 Motif (R-X-X-S)	Protein Name	Amino acid	ETAA1 Ratio	TOPBP1 Ratio	Count ETAA1ΔAAD	Count TOPBP1-AID
PCDH1 S962	Q08174		PCDH1	S	0.316531	0.892988	2	5
PCM1 S1494	Q15154		PCM1	S	-0.02584	0.79362	1	2
PDD2L S20	Q9BRP1		PDD2L	S	0.482332	2.03859	1	2
PDZD8 S530	Q8NEN9		PDZD8	S	0.375362	1.28179	2	2
PDZD8 S538	Q8NEN9		PDZD8	S	-0.25046	1.1273	4	3
PDZD8 T527	Q8NEN9		PDZD8	T	0.375362	1.28179	2	2
PDZD8 T528	Q8NEN9		PDZD8	T	0.375362	1.28179	2	2
PERQ2 S593	Q6Y7W6		PERQ2	S	-0.00878	0.597499	2	2
PF21A T350	Q96BD5	R-X-X-S	PF21A	T	0.199625	0.716899	2	2
PHC1 S862	P78364	R-X-X-S	PHC1	S	-0.14076	0.626673	2	2
PHC1 T922	P78364		PHC1	T	0.156341	0.867979	4	2
PHF12 S662	Q96QT6		PHF12	S	-0.03156	1.00973	3	3
PHF2 S539	O75151		PHF2	S	0.125998	0.941343	4	2
PHF2 S899	O75151	R-X-X-S	PHF2	S	-0.2612	0.772815	4	6
PHF3 S1925	Q92576	R-X-X-S	PHF3	S	-0.08139	0.777283	2	3
PHLA2 S141	Q53GA4		PHLA2	S	0.092653	0.922462	4	5
PHLA2 S144	Q53GA4		PHLA2	S	0.248221	0.630405	4	2
PHLA2 S42	Q53GA4		PHLA2	S	0.375401	0.603611	4	2
PIAS1 S485	O75925		PIAS1	S	0.035342	0.748093	1	5
PIEZ1 S1646	Q92508	R-X-X-S	PIEZ1	S	-0.33119	0.613207	1	2
PININ S100	Q9H307	R-X-X-S	PININ	S	0.088305	0.876095	7	4
PKCB1 S406	Q9ULU4		PKCB1	S	0.128598	0.842399	3	2
PKCB1 S444	Q9ULU4		PKCB1	S	-0.28557	0.894837	1	2
PKCB1 S488	Q9ULU4		PKCB1	S	-0.37462	0.839797	5	4
PKCB1 S490	Q9ULU4		PKCB1	S	-0.27097	0.858061	7	6
PKCB1 S737	Q9ULU4		PKCB1	S	-0.55457	0.775935	3	2
PKCB1 S754	Q9ULU4		PKCB1	S	-0.17762	1.06874	2	2
PKCB1 S756	Q9ULU4		PKCB1	S	-0.34874	0.65104	7	6
PKHG5 S907	O94827	R-X-X-S	PKHG5	S	0.077927	0.946881	2	2
PKP4 S273	Q99569	R-X-X-S	PKP4	S	0.258388	1.08415	2	2
PLEC S4396	Q15149		PLEC	S	0.107152	1.29213	1	2
PLPL6 S353	Q8IY17		PLPL6	S	0.089634	0.702978	1	2
PO210 S1848	Q8TEM1		PO210	S	-0.04423	0.833752	1	2
PO210 S1852	Q8TEM1		PO210	S	-0.04423	0.833752	1	2
PO210 S1874	Q8TEM1	R-X-X-S	PO210	S	-0.19553	0.625364	3	3
PP4R2 S226	Q9NY27		PP4R2	S	0.406537	0.610314	4	2
PP6R1 S759	Q9UPN7		PP6R1	S	0.031113	0.950767	2	3
PPIG S696	Q13427	SQ	PPIG	S	-0.01156	0.726831	3	3
PR40A S34	O75400	R-X-X-S	PR40A	S	0.124857	0.668143	5	4
PRC2A S1690	P48634		PRC2A	S	0.260628	0.675329	2	3
PRC2C S1246	Q9Y520		PRC2C	S	0.249385	0.93757	1	2
PRDM2 S739	Q13029	R-X-X-S	PRDM2	S	0.530806	1.4418	2	3
PRDM2 S742	Q13029		PRDM2	S	0.25214	1.55179	2	3
PRKDC S893	P78527		PRKDC	S	0.325847	0.617393	2	3
PRP4B S23	Q13523		PRP4B	S	-0.04043	0.88534	4	3
PRP4B S568	Q13523		PRP4B	S	-0.19883	1.9062	2	2
PRP4B S569	Q13523		PRP4B	S	-0.19883	0.600705	1	3
PSD3 T1019	Q9NYI0		PSD3	T	0.122607	0.833173	3	2
PTRF S300	Q6NZI2		PTRF	S	0.168849	0.656277	2	2
PUR6 S107	P22234		PUR6	S	0.298658	0.633385	1	3
PYGO2 T302	Q9BRQ0		PYGO2	T	0.498864	0.694894	4	2
PYR1 S1859	P27708		PYR1	S	0.292233	0.787934	7	6
QCR1 S23	P31930		QCR1	S	-0.1761	0.606754	2	5
RAD50 T690	Q92878		RAD50	T	-0.20512	1.25898	4	2
RAF1 S621	P04049		RAF1	S	0.048366	1.156	6	3
RAI1 S1374	Q7Z5J4		RAI1	S	-0.10434	0.716877	3	4
RALY S135	Q9UKM9		RALY	S	-0.13951	0.765195	5	6
RANB9 S482	Q96S59	R-X-X-S	RANB9	S	0.521955	0.613154	1	2
RB12B S250	Q8IXT5		RB12B	S	0.524665	0.941407	7	4
RB12B S375	Q8IXT5		RB12B	S	-0.02984	1.55208	2	3
RBBP6 S516	Q7Z6E9		RBBP6	S	0.274379	0.700529	3	3
RBM10 S733	P98175		RBM10	S	0.003026	0.821439	3	4
RBM15 Y546	Q96T37		RBM15	Y	-0.00703	0.774619	2	2

Table 4.2 TOPBP1-dependent phosphosites								
Phosphosite	Uniprot	ATR Motif (SQ/TQ) CHK1 Motif (R-X-X-S)	Protein Name	Amino acid	ETAA1 Ratio	TOPBP1 Ratio	Count ETAA1ΔAAD	Count TOPBP1-AID
RBM25 S703	P49756		RBM25	S	0.157936	0.785843	5	3
RBNS5 S215	Q9H1K0		RBNS5	S	0.045443	1.46085	1	3
RBNS5 S219	Q9H1K0		RBNS5	S	0.285605	0.602086	2	2
RBP1 S34	Q15311		RBP1	S	-0.21841	1.56565	1	3
RBP2 S1400	P49792		RBP2	S	-0.08319	1.02008	1	4
RBP2 S786	P49792		RBP2	S	-0.61633	0.660506	1	3
RECQ5 S727	O94762		RECQ5	S	0.141534	1.46944	6	5
REQU T248	Q92785		REQU	T	0.017352	0.722553	3	3
RFC1 T161	P35251		RFC1	T	0.253747	1.29531	7	6
RHG21 S856	Q5T5U3	R-X-X-S	RHG21	S	0.328262	0.647913	2	5
RHG29 S1029	Q52LW3		RHG29	S	-0.18784	3.95233	5	2
RHG29 S949	Q52LW3	R-X-X-S	RHG29	S	-0.33169	0.839557	5	4
RING1 T238	Q06587	R-X-X-S	RING1	T	0.163756	0.729096	1	2
RING1 T243	Q06587		RING1	T	-0.33712	0.838901	1	3
RL14 S139	P50914		RL14	S	-0.53264	1.03621	6	5
RPA43 S316	Q3B726	R-X-X-S	RPA43	S	-0.06136	0.587941	8	6
RPC5 S161	Q9NVU0		RPC5	S	-0.15654	0.664665	2	3
RPC5 S162	Q9NVU0	SQ	RPC5	S	-0.3715	0.664665	2	3
RPC5 S522	Q9NVU0		RPC5	S	0.05339	0.593828	2	2
RPRD2 S1099	Q5VT52	R-X-X-S	RPRD2	S	-0.0478	1.21207	7	5
RPTOR S863	Q8N122		RPTOR	S	0.047107	0.621993	5	4
RS6 S236	P62753	R-X-X-S	RS6	S	0.135535	0.852398	6	6
RS6 S240	P62753		RS6	S	0.393313	1.69681	5	3
RS6 S244	P62753		RS6	S	-0.77482	1.9201	1	2
RTN3 S30	O95197		RTN3	S	0.302332	1.1688	2	2
RTN4 S15	Q9NQC3		RTN4	S	0.489603	0.669571	8	6
RTN4 S7	Q9NQC3		RTN4	S	0.237808	0.74122	5	4
S26A6 S752	Q9BXS9		S26A6	S	-0.31262	1.18516	1	2
S4A7 S556	Q9Y6M7		S4A7	S	0.040192	0.692338	2	3
S4A7 T557	Q9Y6M7		S4A7	T	0.013749	0.692338	2	3
SAC2 S1103	Q9Y2H2		SAC2	S	-0.0949	0.820889	3	3
SAC2 S935	Q9Y2H2		SAC2	S	0.101064	0.763242	5	4
SAC2 S940	Q9Y2H2		SAC2	S	0.2221	0.899485	5	3
SAP30 S131	O75446	R-X-X-S	SAP30	S	-0.02477	1.13069	8	4
SAP30 S138	O75446		SAP30	S	0.219779	1.17233	8	4
SCAPE S85	Q9BY12		SCAPE	S	0.521352	1.04875	2	4
SCML2 S499	Q9UQR0		SCML2	S	-0.27	0.723877	6	3
SDS3 S234	Q9H7L9	R-X-X-S	SDS3	S	-0.09696	0.924328	7	6
SENP3 S169	Q9H4L4		SENP3	S	-0.16093	0.640898	7	6
SENP3 S181	Q9H4L4		SENP3	S	-0.26856	1.0355	6	5
SET1A S1169	O15047		SET1A	S	-0.42167	1.3452	3	2
SET1A T1167	O15047	R-X-X-S	SET1A	T	-0.49745	1.35249	3	2
SF3B1 T434	O75533		SF3B1	T	0.094371	0.748805	5	4
SFR19 S239	Q9H7N4		SFR19	S	0.011554	1.22367	4	2
SFR19 S500	Q9H7N4	R-X-X-S	SFR19	S	-0.06708	1.02411	6	6
SFR19 S612	Q9H7N4	R-X-X-S	SFR19	S	0.238665	3.34554	3	3
SFR19 S614	Q9H7N4	R-X-X-S	SFR19	S	0.238665	4.00978	3	2
SFR19 S724	Q9H7N4		SFR19	S	-0.27299	0.931105	4	4
SFR19 S725	Q9H7N4		SFR19	S	-0.06965	0.931105	6	4
SFR19 T976	Q9H7N4		SFR19	T	0.079975	1.02817	3	4
SH24A S315	Q9H788	R-X-X-S	SH24A	S	0.190736	0.762987	4	3
SHAN2 S1330	Q9UPX8	R-X-X-S	SHAN2	S	-0.06401	0.647078	1	2
SHAN2 S67	Q9UPX8	R-X-X-S	SHAN2	S	0.12032	1.6999	2	3
SHC1 S426	P29353		SHC1	S	0.012211	0.960512	1	2
SHRM2 S1036	Q13796	R-X-X-S	SHRM2	S	0.019061	0.63911	7	5
SHRM2 S456	Q13796		SHRM2	S	-0.21073	0.977744	3	3
SI1L1 S1433	O43166		SI1L1	S	-0.15613	0.744075	1	2
SIN3A S1108	Q96ST3		SIN3A	S	-0.13976	0.862432	3	5
SIN3A S1112	Q96ST3		SIN3A	S	-0.21481	0.915253	3	6
SIN3A S277	Q96ST3		SIN3A	S	-0.46977	1.2649	4	2
SIN3A S832	Q96ST3		SIN3A	S	0.215865	0.842778	7	6
SIN3A S940	Q96ST3		SIN3A	S	-0.07666	0.587845	4	4
SIN3A T1111	Q96ST3		SIN3A	T	0.15549	0.651758	1	2

Table 4.2 TOPBP1-dependent phosphosites								
Phosphosite	Uniprot	ATR Motif (SQ/TQ) CHK1 Motif (R-X-X-S)	Protein Name	Amino acid	ETAA1 Ratio	TOPBP1 Ratio	Count ETAA1ΔAAD	Count TOPBP1-AID
SIR1 S14	Q96EB6		SIR1	S	0.405217	0.737254	6	6
SIR1 S47	Q96EB6		SIR1	S	0.307846	0.70186	7	4
SLBP S7	Q14493	R-X-X-S	SLBP	S	-0.01486	0.750676	2	2
SMBT1 S765	Q9UHJ3	R-X-X-S	SMBT1	S	0.399538	0.739589	5	2
SMRC2 S347	Q8TAQ2		SMRC2	S	0.074518	1.05596	6	3
SMRCD S132	Q9H4L7	SQ	SMRCD	S	0.10916	0.844546	1	2
SP130 S442	Q9H0E3		SP130	S	0.32458	0.902549	3	5
SP130 S855	Q9H0E3		SP130	S	-0.01197	0.716433	3	4
SP130 T856	Q9H0E3		SP130	T	-0.01197	0.716433	3	4
SP6 S20	Q3SY56		SP6	S	0.104888	1.98645	3	2
SPAG1 S418	Q07617		SPAG1	S	0.54336	0.72657	3	4
SPE39 S121	Q9H9C1	R-X-X-S	SPE39	S	0.446044	0.930018	1	2
SPHK2 S484	Q9NRA0		SPHK2	S	0.327228	3.77442	1	2
SPN90 S122	Q9NZQ3		SPN90	S	0.158854	0.856081	1	2
SPY4 S125	Q9C004		SPY4	S	0.118963	0.891541	3	2
SRCAP S1940	Q6ZRS2		SRCAP	S	-0.06956	0.736215	3	4
SRP72 S621	O76094		SRP72	S	-0.11546	0.609188	8	6
SRP72 T624	O76094		SRP72	T	-0.10084	0.616734	8	6
SRRM1 S393	Q8IYB3		SRRM1	S	-0.0874	1.56267	8	6
SRRM1 S756	Q8IYB3		SRRM1	S	0.189831	0.922655	5	6
SRRM2 S1008	Q9UQ35		SRRM2	S	0.008774	0.762902	1	2
SRRM2 S1012	Q9UQ35		SRRM2	S	0.059217	0.71308	4	5
SRRM2 S1014	Q9UQ35		SRRM2	S	-0.04091	0.663846	7	6
SRRM2 S1233	Q9UQ35	SQ	SRRM2	S	0.111842	0.714487	4	3
SRRM2 S1421	Q9UQ35	R-X-X-S	SRRM2	S	-0.03548	0.701682	2	3
SRRM2 S1441	Q9UQ35	R-X-X-S	SRRM2	S	0.160676	0.647821	5	6
SRRM2 S1458	Q9UQ35		SRRM2	S	0.087882	0.760956	4	4
SRRM2 S1497	Q9UQ35	R-X-X-S	SRRM2	S	0.524118	1.11783	5	5
SRRM2 S1502	Q9UQ35		SRRM2	S	-0.26096	0.618896	3	2
SRRM2 S1517	Q9UQ35	R-X-X-S	SRRM2	S	-0.04167	1.02	1	4
SRRM2 S1542	Q9UQ35	SQ	SRRM2	S	0.067363	0.606904	3	3
SRRM2 S783	Q9UQ35		SRRM2	S	0.296193	1.94223	3	5
SRRM2 S950	Q9UQ35		SRRM2	S	0.100709	0.649294	7	6
SRRM2 S968	Q9UQ35		SRRM2	S	0.266397	0.776305	2	3
SRRM2 S972	Q9UQ35		SRRM2	S	0.256528	0.689389	2	2
SRRM2 S973	Q9UQ35		SRRM2	S	0.256528	0.689389	2	2
SRRM2 S974	Q9UQ35		SRRM2	S	0.256528	0.689389	2	2
SRRM2 T829	Q9UQ35		SRRM2	T	-0.05481	0.882925	1	2
SSFA2 S591	P28290		SSFA2	S	0.248656	0.676635	1	2
SSFA2 S668	P28290		SSFA2	S	0.082566	0.612022	1	2
STK39 S385	Q9UEW8		STK39	S	0.016068	0.683921	5	4
STK39 T354	Q9UEW8		STK39	T	-0.25106	0.794437	2	3
SVIL S245	O95425		SVIL	S	0.287584	0.615895	4	3
SYMPK S1173	Q92797		SYMPK	S	-0.0687	0.614757	2	2
SYNE2 S6389	Q8WXH0		SYNE2	S	-0.78519	0.90273	2	3
SYNRG S1075	Q9UMZ2	R-X-X-S	SYNRG	S	-0.20655	2.41973	3	2
SYTC S8	P26639		SYTC	S	0.285295	0.664392	2	2
TAF9B S147	Q9HBM6		TAF9B	S	-0.00036	0.934108	1	2
TAF9B S153	Q9HBM6		TAF9B	S	-0.05846	0.910039	2	2
TAOK1 S965	Q7L7X3		TAOK1	S	0.134615	0.845232	1	3
TAU S411	P10636		TAU	S	0.154842	0.683023	1	4
TAU S519	P10636		TAU	S	0.132884	0.795684	2	4
TB10B S687	Q4KMP7	R-X-X-S	TB10B	S	-0.92276	0.679694	2	5
TB182 S1029	Q9C0C2		TB182	S	0.174998	1.02304	4	2
TB182 S1385	Q9C0C2		TB182	S	0.373899	0.683641	4	3
TB182 S836	Q9C0C2	SQ	TB182	S	0.086506	0.874915	3	2
TCF20 Y1632	Q9UGU0		TCF20	Y	0.209066	0.684741	2	2
TDIF2 S381	Q5QJE6		TDIF2	S	0.081985	0.726395	2	4
TENC1 S1003	Q63HR2		TENC1	S	-0.0719	1.47611	2	2
TF3C4 S611	Q9UKN8		TF3C4	S	-0.22805	0.718707	3	3
THOC1 S2	Q96FV9		THOC1	S	0.128029	0.968008	3	3
TIF1A S1042	O15164	R-X-X-S	TIF1A	S	-0.16766	0.891108	2	2
TIF1A S667	O15164		TIF1A	S	-0.15161	0.771209	2	3

Table 4.2 TOPBP1-dependent phosphosites								
Phosphosite	Uniprot	ATR Motif (SQ/TQ) CHK1 Motif (R-X-X-S)	Protein Name	Amino acid	ETAA1 Ratio	TOPBP1 Ratio	Count ETAA1ΔAAD	Count TOPBP1-AID
TIF1B S19	Q13263		TIF1B	S	-0.06486	1.08644	8	6
TIF1B S473	Q13263	R-X-X-S	TIF1B	S	-0.0009	1.08706	8	6
TIF1B Y458	Q13263		TIF1B	Y	-0.27593	0.628767	2	2
TISD S125	P47974	R-X-X-S	TISD	S	0.058524	0.660837	3	3
TISD S490	P47974		TISD	S	0.233888	0.878498	1	2
TNC18 S995	O15417		TNC18	S	0.521855	0.633013	4	3
TOB1 S205	P50616		TOB1	S	0.253505	0.851682	3	4
TOB1 T204	P50616		TOB1	T	0.253505	0.851682	3	4
TOP2B S1424	Q02880		TOP2B	S	-0.11167	0.621431	4	3
TOP2B S1522	Q02880		TOP2B	S	-0.00428	0.592828	7	6
TOP2B S1524	Q02880		TOP2B	S	-0.03667	0.594644	7	6
TOP2B S1550	Q02880	R-X-X-S	TOP2B	S	-0.4645	0.624215	2	3
TOP2B S1552	Q02880		TOP2B	S	-0.4645	0.624215	2	3
TOPB1 S860	Q92547	R-X-X-S	TOPB1	S	0.287354	4.09071	2	3
TP53B S1068	Q12888	SQ	TP53B	S	-0.1639	0.820622	3	3
TP53B S1317	Q12888	R-X-X-S	TP53B	S	-0.28309	1.12188	2	3
TP53B S1320	Q12888		TP53B	S	-0.09979	1.30561	1	2
TP53B T919	Q12888		TP53B	T	0.0297	0.913186	4	3
TP53B T922	Q12888		TP53B	T	-0.03184	1.08706	5	4
TRAF2 S11	Q12933		TRAF2	S	0.004897	2.23285	5	4
TRAF2 T7	Q12933		TRAF2	T	0.196229	2.23285	7	4
TREF1 S715	Q96PN7		TREF1	S	-0.48825	1.07211	3	3
TRIO S2455	O75962		TRIO	S	-0.21177	0.655077	2	3
TRMB S27	Q9UBP6	R-X-X-S	TRMB	S	0.559149	0.736935	3	3
TRPM4 S1103	Q8TD43		TRPM4	S	-1.01034	0.941282	1	2
TSSC4 S143	Q9Y5U2		TSSC4	S	0.04698	0.744333	1	3
TSYL2 S17	Q9H2G4	R-X-X-S	TSYL2	S	-0.89648	0.857172	3	5
TSYL2 S18	Q9H2G4		TSYL2	S	-1.25389	0.857172	3	5
TSYL2 S20	Q9H2G4		TSYL2	S	-0.97761	1.32941	2	2
TTYH2 S504	Q9BSA4		TTYH2	S	-0.24257	1.83491	1	2
U5S1 S19	Q15029		U5S1	S	0.561898	0.845912	6	6
UBA1 S21	P22314		UBA1	S	-0.01165	0.861003	5	2
UBE2O S87	Q9C0C9		UBE2O	S	0.239642	0.719052	5	4
UBE2O S89	Q9C0C9		UBE2O	S	0.239642	0.719052	5	4
UBN2 S11	Q6ZU65		UBN2	S	-0.48655	0.760945	2	2
UBP10 S576	Q14694		UBP10	S	0.110388	0.681317	7	4
UBP20 S132	Q9Y2K6		UBP20	S	0.195675	1.6568	2	2
UBP20 S134	Q9Y2K6		UBP20	S	0.195675	1.6568	2	2
UCK1 S253	Q9HA47	R-X-X-S	UCK1	S	0.342782	1.52677	3	3
ULK1 S477	O75385		ULK1	S	0.475707	1.16053	4	3
ULK1 S479	O75385		ULK1	S	0.475707	1.16053	4	3
ULK1 S758	O75385		ULK1	S	0.199751	1.11463	1	2
ULK1 T625	O75385		ULK1	T	0.407826	0.96303	6	3
UNG S23	P13051		UNG	S	-0.25343	0.733962	7	6
UNG S63	P13051		UNG	S	-0.00139	0.741057	5	2
UNG T60	P13051		UNG	T	-0.10933	0.829301	5	3
UT14A S29	Q9BVJ6		UT14A	S	-0.22336	0.642008	3	3
UT14A S445	Q9BVJ6	SQ	UT14A	S	0.28629	1.855	3	2
VEZF1 S197	Q14119		VEZF1	S	0.320311	1.1648	1	2
VIP2 S1108	O43314		VIP2	S	0.274769	0.658006	1	3
VP26B S304	Q4G0F5		VP26B	S	0.207143	0.815389	1	2
VRK3 S59	Q8IV63		VRK3	S	0.475085	0.591584	5	6
WAP53 S491	Q9BUR4		WAP53	S	0.272579	2.13806	2	5
WDR11 S626	Q9BZH6		WDR11	S	-0.09086	1.0277	1	2
WDR7 S1456	Q9Y4E6		WDR7	S	0.182184	0.681881	1	3
WIZ S983	O95785		WIZ	S	0.141825	0.598175	1	3
XPO4 S521	Q9C0E2		XPO4	S	0.364372	0.721504	4	3
XRN1 S1656	Q8IZH2		XRN1	S	0.016639	0.665379	1	2
XRN1 S1657	Q8IZH2		XRN1	S	0.016639	0.665379	1	2
XRN2 S487	Q9H0D6		XRN2	S	-0.15748	0.728628	1	2
Y272	(blank)		(blank)	Y	0.301471	0.789187	1	4
YBOX1 S165	P67809		YBOX1	S	0.265832	0.592541	2	2
YBOX1 S174	P67809		YBOX1	S	0.262433	0.592541	1	2

Table 4.2 TOPBP1-dependent phosphosites								
Phosphosite	Uniprot	ATR Motif (SQ/TQ) CHK1 Motif (R-X-X-S)	Protein Name	Amino acid	ETAA1 Ratio	TOPBP1 Ratio	Count ETAA1ΔAAD	Count TOPBP1-AID
YBOX1 S2	P67809		YBOX1	S	0.030265	0.595122	2	2
YETS2 S575	Q9ULM3		YETS2	S	-0.11691	0.648356	4	5
YRDC S60	Q86U90		YRDC	S	0.339935	1.03837	3	3
YTDC2 S1279	Q9H6S0		YTDC2	S	0.315163	1.24803	4	5
Z280C S80	Q8ND82		Z280C	S	-0.09516	0.990249	3	5
Z280C T540	Q8ND82		Z280C	T	0.229219	1.38637	2	2
Z280D S545	Q6N043		Z280D	S	0.25084	1.39709	5	4
ZBT7A S511	O95365		ZBT7A	S	-0.00045	0.779872	4	5
ZBTB3 S549	Q9H5J0		ZBTB3	S	-0.07282	0.652693	3	2
ZC3H4 S1104	Q9UPT8		ZC3H4	S	0.238	1.00712	5	5
ZC3HD S1010	Q5T200	R-X-X-S	ZC3HD	S	-1.50703	0.772795	2	2
ZC3HD S1210	Q5T200	R-X-X-S	ZC3HD	S	0.042504	0.98675	5	5
ZC3HD S198	Q5T200		ZC3HD	S	-0.00404	0.588325	5	6
ZC3HD S316	Q5T200		ZC3HD	S	0.321618	0.667756	4	6
ZC3HD S318	Q5T200	R-X-X-S	ZC3HD	S	-0.06596	0.657091	6	6
ZC3HD S325	Q5T200		ZC3HD	S	0.007913	0.616358	6	6
ZC3HD S333	Q5T200	R-X-X-S	ZC3HD	S	0.11405	0.718088	3	4
ZC3HD S387	Q5T200	R-X-X-S	ZC3HD	S	0.182819	0.749062	2	3
ZC3HD S833	Q5T200		ZC3HD	S	0.123401	0.995521	1	5
ZC3HD S837	Q5T200		ZC3HD	S	0.496207	0.676492	3	5
ZC3HD S845	Q5T200	R-X-X-S	ZC3HD	S	0.021906	0.797612	1	3
ZC3HD S848	Q5T200		ZC3HD	S	0.021906	0.797612	1	2
ZC3HD S853	Q5T200		ZC3HD	S	0.021906	0.797612	1	3
ZC3HD T1033	Q5T200		ZC3HD	T	-0.00845	0.700351	4	5
ZC3HD T317	Q5T200		ZC3HD	T	0.208392	0.694657	6	6
ZC3HE S515	Q6PJT7		ZC3HE	S	0.039138	0.793688	6	6
ZCH18 S67	Q86VM9		ZCH18	S	0.497068	0.701211	4	4
ZDHC5 S529	Q9C0B5	R-X-X-S	ZDHC5	S	0.514905	0.876273	1	3
ZDHC5 Y533	Q9C0B5		ZDHC5	Y	0.514905	0.904917	1	3
ZMYM4 S1181	Q5VZL5	R-X-X-S	ZMYM4	S	0.118493	0.708231	3	6
ZMYM4 S122	Q5VZL5		ZMYM4	S	0.145774	1.1306	2	4
ZN316 S10	A6NFI3		ZN316	S	-0.18355	0.741578	7	4
ZN318 S501	Q5VUA4	SQ	ZN318	S	0.040542	1.99105	1	2
ZN444 S235	Q8N0Y2		ZN444	S	0.202136	0.887805	1	2
ZN507 S195	Q8TCN5		ZN507	S	0.53067	1.4031	1	2
ZN592 S334	Q92610		ZN592	S	-0.47593	0.679784	3	3
ZN592 S573	Q92610		ZN592	S	0.124228	0.600175	5	6
ZN592 S74	Q92610		ZN592	S	-0.03716	0.650941	1	2
ZN592 S78	Q92610	R-X-X-S	ZN592	S	0.050049	0.764346	5	3
ZN687 S1057	Q8N1G0		ZN687	S	-0.44099	1.03471	7	6
ZN687 S1106	Q8N1G0		ZN687	S	-0.0216	1.43629	2	5
ZN687 S251	Q8N1G0		ZN687	S	-0.06367	0.657457	3	2
ZN768 S97	Q9H5H4		ZN768	S	0.152146	0.828225	4	2
ZNRF2 S82	Q8NHG8	R-X-X-S	ZNRF2	S	0.217851	0.737841	1	4
ZYX S281	Q15942		ZYX	S	0.404819	0.931154	2	3

Table 4.3 ETAA1 and TOPBP1-dependent phosphosites. ETAA1 and TOPBP1-dependent phosphosites are given below along with the Uniprot ID, modified residue, presence of ATR or CHK1 motif, and the number of experiments in which that peptide was observed. The ratio value is the $\log_2$ transformed ratio of WT /ETAA1 or TOPBP1 cells. Therefore, a higher value (darker green) is more dependent on ETAA1 or TOPBP1.

Table 4.3 ETAA1 and TOPBP1-dependent phosphosites								
Phosphosite	Uniprot	ATR Motif (SQ/TQ) CHK1 Motif (R-X-X-S)	Protein Name	Amino acid	ETAA1 Ratio	TOPBP1 Ratio	Count ETAA1ΔAAD	Count TOPBP1-AID
ADA19 S802	Q9H013	R-X-X-S	ADA19	S	1.55292	0.600437	1	2
AHNK T490	Q09666		AHNK	T	0.741316	0.662844	4	6
AKA12 S283	Q02952		AKA12	S	0.716684	1.29731	5	5
AKA12 S648	Q02952		AKA12	S	0.645898	0.615785	2	2
AKA12 S697	Q02952	R-X-X-S	AKA12	S	0.719052	0.699907	1	3
AKA12 S698	Q02952		AKA12	S	0.719052	0.699907	1	3
AKA12 T597	Q02952		AKA12	T	0.591967	0.687777	4	4
AKTS1 S202	Q96B36		AKTS1	S	0.623118	0.733084	5	3
ANXA1 S37	P04083		ANXA1	S	0.589284	0.857583	1	2
AT2C2 S7	O75185		AT2C2	S	2.5815	5.08286	1	2
ATRIP S239	Q8WXE1		ATRIP	S	0.641638	0.636915	4	3
BAIP2 S325	Q9UQB8		BAIP2	S	1.10554	0.7582	4	5
BCL9L S25	Q86UU0		BCL9L	S	0.714224	0.618509	1	4
BCR S459	P11274		BCR	S	0.892449	0.847359	4	4
BRD1 S128	O95696		BRD1	S	1.44679	0.89476	3	6
BRD9 S566	Q9H8M2		BRD9	S	0.681	1.96614	5	3
CAMP1 S575	Q5T5Y3		CAMP1	S	0.71352	1.10735	2	2
CCNT2 S480	O60583		CCNT2	S	0.930397	1.13297	3	3
CHAP1 S297	Q96JM3		CHAP1	S	0.714487	0.853203	5	4
CHAP1 S386	Q96JM3		CHAP1	S	0.692606	1.55699	1	2
CHD8 S2046	Q9HCK8		CHD8	S	0.7019	0.618161	6	5
CLASR S335	Q8N2M8		CLASR	S	2.41943	0.971737	1	4
CND1 S1333	Q15021		CND1	S	0.591201	0.688225	1	2
DC1L1 T513	Q9Y6G9		DC1L1	T	0.692017	1.33405	2	2
DCP1A S525	Q9NPI6		DCP1A	S	0.772646	1.03069	3	5
EHBP1 S436	Q8NDI1		EHBP1	S	0.662661	0.58938	6	6
ELYS S1160	Q8WYP5		ELYS	S	0.721063	0.632827	5	6
ERCC5 S563	P28715		ERCC5	S	2.87389	0.883621	4	2
F101B S26	Q8N5W9		F101B	S	0.594071	0.763836	3	3
F10A1 S75	P50502		F10A1	S	0.855432	1.71233	4	4
F10A1 S76	P50502		F10A1	S	0.724476	1.71233	4	4
F10A1 S79	P50502		F10A1	S	0.789938	1.71233	4	4
F18B2 S6	Q96ET8		F18B2	S	1.37268	1.35075	2	2
FAS Y45	P49327		FAS	Y	0.678162	0.678029	1	2
GCFC2 S19	P16383		GCFC2	S	1.04013	0.938329	2	2
GORS1 S220	Q9BQQ3		GORS1	S	1.11297	1.37751	5	4
GORS1 T237	Q9BQQ3		GORS1	T	0.603027	1.13534	5	4
HMGA2 S101	P52926		HMGA2	S	0.601031	0.626392	7	3
HMGA2 S102	P52926	SQ	HMGA2	S	0.587269	1.15023	3	2
HMGA2 S105	P52926		HMGA2	S	0.737193	0.906572	7	4
HMGA2 T100	P52926		HMGA2	T	0.587269	0.60421	1	2
HMGX4 S197	Q9UGU5		HMGX4	S	0.601401	1.17709	2	3
HUWE1 S3373	Q7Z6Z7		HUWE1	S	1.41967	0.673513	3	3
IMA2 S62	P52292		IMA2	S	0.700795	0.636355	5	2
IMA2 T61	P52292		IMA2	T	0.860367	0.719402	1	2
K0284 S969	Q9Y4F5		K0284	S	0.902267	0.718565	2	2
KHDR1 S18	Q07666		KHDR1	S	1.28321	0.707878	2	3
KI18B S434	Q86Y91	SQ	KI18B	S	0.880646	0.831796	1	3
KI21A S1239	Q7Z4S6		KI21A	S	1.33629	0.669662	5	6
KLH36 S17	Q8N4N3		KLH36	S	0.856086	1.50141	2	2
KPCD Y313	Q05655		KPCD	Y	0.882213	0.702622	3	2
LIPS S950	Q05469		LIPS	S	0.739848	1.85667	2	2
LRCH3 S415	Q96II8	R-X-X-S	LRCH3	S	0.674641	0.656542	3	3
M3K1 S250	Q13233		M3K1	S	1.27472	0.653707	2	2
M3K1 S252	Q13233	R-X-X-S	M3K1	S	1.27472	0.653707	2	2

Table 4.3 ETAA1 and TOPBP1-dependent phosphosites								
Phosphosite	Uniprot	ATR Motif (SQ/TQ) CHK1 Motif (R-X-X-S)	Protein Name	Amino acid	ETAA1 Ratio	TOPBP1 Ratio	Count ETAA1ΔAAD	Count TOPBP1-AID
MAP1A S1069	P78559		MAP1A	S	0.645077	0.741111	2	2
MAP2 S1782	P11137		MAP2	S	1.16941	0.735435	1	2
MRCKA S1721	Q5VT25		MRCKA	S	0.663481	1.14444	1	2
MX2 S385	P20592		MX2	S	6.095	4.69346	1	2
MYD88 S244	Q99836		MYD88	S	0.760264	1.79628	2	2
NHRF1 S290	O14745	R-X-X-S	NHRF1	S	0.719227	0.750991	3	2
NO40 S114	Q9NP64	R-X-X-S	NO40	S	1.47975	0.749384	3	5
OAS3 T365	Q9Y6K5		OAS3	T	0.725436	1.5864	1	2
PALLD S1104	Q8WX93		PALLD	S	0.825224	2.59477	4	5
PALLD S1116	Q8WX93	R-X-X-S	PALLD	S	1.5479	2.46968	5	5
PALLD S1118	Q8WX93	R-X-X-S	PALLD	S	1.41548	2.01314	5	5
PALLD S1121	Q8WX93		PALLD	S	1.40757	2.46121	4	6
PALLD S641	Q8WX93		PALLD	S	1.22621	4.91476	4	3
PALLD S688	Q8WX93		PALLD	S	1.51035	3.68549	3	6
PALLD S766	Q8WX93		PALLD	S	1.79327	2.48962	2	3
PALLD S893	Q8WX93	R-X-X-S	PALLD	S	1.40387	2.73645	5	5
PALLD T704	Q8WX93		PALLD	T	1.25222	2.07165	2	3
PATL1 S177	Q86TB9		PATL1	S	0.632933	1.36783	3	4
PATL1 T178	Q86TB9	R-X-X-S	PATL1	T	0.643487	1.3881	5	5
PDE7A S84	Q13946	R-X-X-S	PDE7A	S	0.865048	0.873999	3	2
PHF12 S131	Q96QT6	R-X-X-S	PHF12	S	1.54898	1.17082	4	2
PHIP S1315	Q8WWQ0	R-X-X-S	PHIP	S	3.81517	1.2926	1	2
PIAS1 S483	O75925		PIAS1	S	0.633571	0.748093	1	2
PKP3 S314	Q9Y446	R-X-X-S	PKP3	S	0.678613	2.33322	3	2
PRC2C T2673	Q9Y520		PRC2C	T	0.847917	0.594644	4	6
PRDX3 S237	P30048		PRDX3	S	3.26158	1.97263	1	2
PTRF T302	Q6NZI2		PTRF	T	0.933827	0.656277	2	2
PTSS1 S439	P48651		PTSS1	S	0.889242	2.11866	2	3
PURB S8	Q96QR8		PURB	S	1.11986	2.06856	2	2
PYRG1 S571	P17812		PYRG1	S	0.609254	0.70779	5	3
RANG S14	P43487		RANG	S	0.586531	1.08678	2	4
RANG T13	P43487		RANG	T	0.641912	0.770618	3	2
RANG T15	P43487		RANG	T	0.598556	0.995797	1	2
RGAP1 T580	Q9H0H5		RGAP1	T	0.663026	0.60046	6	3
RIN1 S258	Q13671		RIN1	S	0.762902	1.01778	1	2
RIR2 S20	P31350		RIR2	S	1.48192	1.25574	5	4
RNF8 S157	O76064	R-X-X-S	RNF8	S	0.829021	2.81486	5	5
SCRIB S1140	Q14160		SCRIB	S	3.70117	2.62919	3	5
SEPT7 S334	Q16181		SEPT7	S	0.607701	0.965987	5	3
SKP2 S64	Q13309		SKP2	S	0.844948	0.919988	2	3
SLMAP S148	Q14BN4		SLMAP	S	1.1163	0.732052	1	3
SOS1 S1275	Q07889		SOS1	S	0.615981	1.27965	1	4
SPDLY S515	Q96EA4		SPDLY	S	1.05693	2.28735	2	2
SRRM2 S1539	Q9UQ35	R-X-X-S	SRRM2	S	1.40218	0.591967	2	2
STIM2 S609	Q9P246	R-X-X-S	STIM2	S	0.691579	0.773701	3	2
STIM2 S613	Q9P246		STIM2	S	0.742997	0.680909	2	2
STMN1 S16	P16949		STMN1	S	0.588905	0.603027	7	6
TBC30 S713	Q9Y2I9		TBC30	S	3.85659	1.16742	2	2
TJAP1 T422	Q5JTD0		TJAP1	T	0.808856	0.872001	6	4
TOB2 S222	Q14106		TOB2	S	0.711054	0.701999	1	5
TOM34 S186	Q15785	R-X-X-S	TOM34	S	0.962162	0.833416	5	4
UBP10 S547	Q14694		UBP10	S	0.59684	0.880646	2	4
ULK1 S544	O75385		ULK1	S	1.13895	2.13767	1	2
ULK1 S623	O75385		ULK1	S	0.647268	0.96303	5	5
YBOX1 S167	P67809		YBOX1	S	0.599935	0.592541	2	2
ZC3H1 S28	O60293		ZC3H1	S	0.898789	1.25564	2	3
ZCCHV S378	Q7Z2W4		ZCCHV	S	1.01557	0.587799	2	2
ZN576 S23	Q9H609		ZN576	S	0.960254	1.65019	4	5
ZN608 S627	Q9ULD9		ZN608	S	0.767655	3.11686	1	3
ZN609 S413	O15014	R-X-X-S/SQ	ZN609	S	0.64589	1.25978	4	4
ZN609 S491	O15014		ZN609	S	0.726243	1.02857	6	6
ZN609 S576	O15014		ZN609	S	0.887915	0.892663	7	6
ZN609 S578	O15014		ZN609	S	0.947105	0.612777	7	6

Table 4.4 ETAA1-dependent GO terms. Gene ontology analysis of ETAA1-dependent phosphoproteins was completed using ClueGO. Similar GO terms were grouped into functional GO Groups. The GO term, p-value for each term, GO Group, and p-value for each GO group are provided. The number of genes and % of genes associated with each GO term are also provided.

Table 4.4 ETAA1-dependent GO terms					
GO Term	**Term p-value**	**Group p-value**	**GO Groups**	**% Associated Genes**	**# Genes**
mitotic cell cycle	6.70E-13	9.47E-17	Group01	5.19	54.00
mitotic cell cycle process	3.09E-09	9.47E-17	Group01	4.97	43.00
chromosome organization	1.76E-08	9.47E-17	Group01	4.17	51.00
regulation of cell cycle	8.08E-08	9.47E-17	Group01	4.05	50.00
cell cycle process	1.84E-07	9.47E-17	Group01	3.84	53.00
mitotic sister chromatid segregation	4.44E-07	9.47E-17	Group01	10.60	16.00
mitotic cell cycle phase transition	1.64E-06	9.47E-17	Group01	5.23	30.00
regulation of mitotic cell cycle	1.88E-06	9.47E-17	Group01	4.83	33.00
nuclear chromosome segregation	4.47E-06	9.47E-17	Group01	6.77	21.00
spindle checkpoint	3.15E-05	9.47E-17	Group01	20.51	8.00
chromosome separation	1.10E-04	9.47E-17	Group01	12.50	10.00
regulation of mitotic sister chromatid segregation	1.50E-04	9.47E-17	Group01	14.06	9.00
regulation of cell cycle process	1.67E-04	9.47E-17	Group01	4.14	31.00
organelle fission	2.13E-04	9.47E-17	Group01	5.01	23.00
cell cycle checkpoint	4.33E-04	9.47E-17	Group01	6.45	16.00
regulation of mitotic nuclear division	5.25E-04	9.47E-17	Group01	7.78	13.00
regulation of chromosome segregation	8.56E-04	9.47E-17	Group01	10.00	10.00
negative regulation of cell cycle	9.73E-04	9.47E-17	Group01	4.12	27.00
microtubule cytoskeleton organization	1.32E-03	9.47E-17	Group01	4.48	23.00
negative regulation of mitotic cell cycle	1.92E-03	9.47E-17	Group01	5.45	17.00
mitotic spindle assembly checkpoint	2.91E-03	9.47E-17	Group01	17.65	6.00
regulation of organelle organization	6.45E-03	9.47E-17	Group01	3.12	40.00
regulation of mitotic cell cycle phase transition	8.20E-03	9.47E-17	Group01	4.49	19.00
mitotic cell cycle checkpoint	1.87E-02	9.47E-17	Group01	6.36	11.00
negative regulation of cell cycle process	2.00E-02	9.47E-17	Group01	4.69	16.00
positive regulation of cell cycle	3.21E-02	9.47E-17	Group01	4.31	17.00
positive regulation of cell cycle process	3.38E-02	9.47E-17	Group01	4.90	14.00
attachment of spindle microtubules to kinetochore	3.52E-02	9.47E-17	Group01	14.71	5.00
regulation of chromosome organization	3.62E-02	9.47E-17	Group01	4.63	15.00
protein localization to kinetochore	3.81E-02	9.47E-17	Group01	21.05	4.00
negative regulation of chromosome organization	3.83E-02	9.47E-17	Group01	6.98	9.00
negative regulation of mitotic cell cycle phase transition	4.57E-02	9.47E-17	Group01	5.31	12.00
chromosome organization	1.76E-08	2.80E-10	Group02	4.17	51.00
mitotic sister chromatid segregation	4.44E-07	2.80E-10	Group02	10.60	16.00
nuclear chromosome segregation	4.47E-06	2.80E-10	Group02	6.77	21.00
covalent chromatin modification	1.01E-03	2.80E-10	Group02	4.32	25.00
chromatin organization	6.77E-03	2.80E-10	Group02	3.65	28.00
negative regulation of mRNA metabolic process	1.10E-04	5.12E-08	Group03	12.50	10.00
regulation of mRNA metabolic process	1.27E-04	5.12E-08	Group03	6.34	18.00
mRNA metabolic process	1.01E-03	5.12E-08	Group03	3.79	32.00
RNA processing	6.08E-03	5.12E-08	Group03	3.36	33.00
mRNA processing	1.07E-02	5.12E-08	Group03	4.13	21.00
regulation of transcription elongation from RNA polymerase II promoter	1.20E-02	5.12E-08	Group03	18.52	5.00
transcription elongation from RNA polymerase II promoter	1.22E-02	5.12E-08	Group03	8.18	9.00
regulation of mRNA processing	1.84E-02	5.12E-08	Group03	7.76	9.00
negative regulation of mRNA catabolic process	2.06E-02	5.12E-08	Group03	12.50	6.00
regulation of mRNA catabolic process	2.24E-02	5.12E-08	Group03	6.21	11.00

Table 4.4 ETAA1-dependent GO terms					
GO Term	**Term p-value**	**Group p-value**	**GO Groups**	**% Associated Genes**	**# Genes**
RNA splicing	4.42E-02	5.12E-08	Group03	4.04	18.00
mRNA splicing, via spliceosome	4.58E-02	5.12E-08	Group03	4.52	15.00
cytoskeleton organization	9.25E-05	1.38E-07	Group04	3.48	44.00
organelle fission	2.13E-04	1.38E-07	Group04	5.01	23.00
microtubule cytoskeleton organization	1.32E-03	1.38E-07	Group04	4.48	23.00
negative regulation of nucleobase-containing compound metabolic process	7.53E-04	1.83E-05	Group05	3.13	47.00
negative regulation of nucleic acid-templated transcription	1.01E-03	1.83E-05	Group05	3.29	41.00
negative regulation of transcription from RNA polymerase II promoter	2.29E-03	1.83E-05	Group05	3.66	31.00
negative regulation of transcription, DNA-templated	3.45E-03	1.83E-05	Group05	3.25	39.00
DNA metabolic process	1.22E-03	2.55E-05	Group06	3.51	36.00
DNA biosynthetic process	5.64E-03	2.55E-05	Group06	5.83	14.00
regulation of DNA metabolic process	1.99E-02	2.55E-05	Group06	4.34	18.00
cytokinesis	4.13E-03	7.06E-05	Group07	7.53	11.00
mitotic cytokinesis	3.82E-02	7.06E-05	Group07	11.11	6.00
regulation of transferase activity	2.10E-02	9.60E-05	Group08	3.16	34.00
regulation of small GTPase mediated signal transduction	1.17E-03	1.39E-04	Group09	5.41	18.00
regulation of GTPase activity	7.62E-03	1.39E-04	Group09	4.23	21.00
small GTPase mediated signal transduction	2.73E-02	1.39E-04	Group09	3.85	21.00
nuclear export	2.13E-02	1.52E-04	Group10	5.80	12.00
nucleocytoplasmic transport	2.29E-02	1.52E-04	Group10	4.02	20.00
RNA localization	2.87E-02	1.52E-04	Group10	5.26	13.00

Table 4.5 TOPBP1-dependent GO terms. Gene ontology analysis of ETAA1-dependent phosphoproteins was completed using ClueGO. Similar GO terms were grouped into functional GO Groups. The GO term, p-value for each term, GO Group, and p-value for each GO Group are provided. The number of genes and % of genes associated with each GO term are also provided.

Table 4.5 TOPBP1-dependent GO terms					
GO Term	**Term p-value**	**Group p-value**	**GO Groups**	**% Associated Genes**	**# Genes**
regulation of cell cycle	2.45E-09	1.58E-20	Group01	6.32	78.00
mitotic cell cycle	2.51E-09	1.58E-20	Group01	7.12	74.00
cell cycle process	3.64E-08	1.58E-20	Group01	5.87	81.00
mitotic cell cycle process	6.37E-07	1.58E-20	Group01	6.58	57.00
cellular response to DNA damage stimulus	1.08E-05	1.58E-20	Group01	6.33	53.00
positive regulation of cell cycle	3.94E-05	1.58E-20	Group01	8.12	32.00
DNA repair	2.25E-04	1.58E-20	Group01	6.90	37.00
positive regulation of cell cycle process	3.05E-04	1.58E-20	Group01	8.74	25.00
regulation of mitotic cell cycle	3.76E-04	1.58E-20	Group01	6.30	43.00
negative regulation of cell cycle	1.81E-03	1.58E-20	Group01	6.11	40.00
sister chromatid segregation	3.12E-03	1.58E-20	Group01	8.64	21.00
response to ionizing radiation	3.52E-03	1.58E-20	Group01	10.06	17.00
regulation of cell cycle process	8.59E-03	1.58E-20	Group01	5.61	42.00
DNA integrity checkpoint	8.75E-03	1.58E-20	Group01	9.39	17.00
DNA biosynthetic process	9.00E-03	1.58E-20	Group01	8.33	20.00
regulation of signal transduction by p53 class mediator	1.07E-02	1.58E-20	Group01	8.87	18.00
cell cycle checkpoint	1.44E-02	1.58E-20	Group01	8.06	20.00
signal transduction by p53 class mediator	2.40E-02	1.58E-20	Group01	7.33	22.00
G1/S transition of mitotic cell cycle	3.28E-02	1.58E-20	Group01	7.60	20.00
chromosome organization	7.88E-21	2.13E-20	Group02	8.18	100.00
chromatin organization	1.40E-15	2.13E-20	Group02	9.00	69.00
organelle organization	2.82E-15	2.13E-20	Group02	4.92	187.00
covalent chromatin modification	7.41E-15	2.13E-20	Group02	10.02	58.00
histone modification	3.76E-11	2.13E-20	Group02	9.89	46.00
DNA metabolic process	3.19E-09	2.13E-20	Group02	6.72	69.00
peptidyl-lysine modification	1.84E-08	2.13E-20	Group02	9.57	38.00
peptidyl-amino acid modification	1.94E-08	2.13E-20	Group02	6.04	79.00
cytoskeleton organization	1.28E-07	2.13E-20	Group02	5.94	75.00
negative regulation of nucleic acid-templated transcription	1.77E-07	2.13E-20	Group02	5.94	74.00
negative regulation of transcription, DNA-templated	3.27E-06	2.13E-20	Group02	5.75	69.00
regulation of cellular component organization	4.11E-05	2.13E-20	Group02	4.53	111.00
internal protein amino acid acetylation	4.78E-04	2.13E-20	Group02	11.04	18.00
histone acetylation	8.20E-04	2.13E-20	Group02	11.18	17.00
histone deacetylation	1.12E-03	2.13E-20	Group02	14.13	13.00
negative regulation of transcription from RNA polymerase II promoter	1.84E-03	2.13E-20	Group02	5.67	48.00
protein sumoylation	2.31E-03	2.13E-20	Group02	13.27	13.00
protein acylation	4.22E-03	2.13E-20	Group02	8.77	20.00
cellular macromolecule metabolic process	3.86E-16	2.67E-18	Group03	3.82	333.00
histone modification	3.76E-11	2.67E-18	Group03	9.89	46.00
peptidyl-lysine modification	1.84E-08	2.67E-18	Group03	9.57	38.00
peptidyl-amino acid modification	1.94E-08	2.67E-18	Group03	6.04	79.00
macromolecule modification	5.12E-06	2.67E-18	Group03	4.00	180.00
cellular protein modification process	6.42E-04	2.67E-18	Group03	3.85	163.00
cellular protein metabolic process	2.02E-02	2.67E-18	Group03	3.55	186.00
peptidyl-serine modification	4.77E-02	2.67E-18	Group03	6.82	23.00
peptidyl-lysine modification	1.84E-08	4.86E-18	Group04	9.57	38.00
regulation of gene expression, epigenetic	5.73E-05	4.86E-18	Group04	9.00	27.00
nuclear transport	1.44E-04	4.86E-18	Group04	7.14	36.00

Table 4.5 TOPBP1-dependent GO terms					
GO Term	**Term p-value**	**Group p-value**	**GO Groups**	**% Associated Genes**	**# Genes**
RNA localization	1.12E-03	4.86E-18	Group04	8.91	22.00
establishment of RNA localization	1.50E-03	4.86E-18	Group04	9.39	20.00
protein sumoylation	2.31E-03	4.86E-18	Group04	13.27	13.00
mRNA transport	7.81E-03	4.86E-18	Group04	9.94	16.00
RNA export from nucleus	9.09E-03	4.86E-18	Group04	10.34	15.00
nuclear export	1.38E-02	4.86E-18	Group04	8.70	18.00
negative regulation of cellular amide metabolic process	1.87E-02	4.86E-18	Group04	8.19	19.00
response to heat	2.02E-02	4.86E-18	Group04	9.20	16.00
regulation of chromatin silencing	2.33E-02	4.86E-18	Group04	26.09	6.00
regulation of gene silencing	3.95E-02	4.86E-18	Group04	10.91	12.00
mRNA export from nucleus	4.69E-02	4.86E-18	Group04	10.71	12.00
organelle organization	2.82E-15	4.01E-17	Group05	4.92	187.00
cytoskeleton organization	1.28E-07	4.01E-17	Group05	5.94	75.00
actin cytoskeleton organization	1.09E-02	4.01E-17	Group05	5.95	37.00
chromosome organization	7.88E-21	1.87E-13	Group06	8.18	100.00
organelle organization	2.82E-15	1.87E-13	Group06	4.92	187.00
DNA metabolic process	3.19E-09	1.87E-13	Group06	6.72	69.00
regulation of DNA metabolic process	3.44E-06	1.87E-13	Group06	8.43	35.00
cellular response to DNA damage stimulus	1.08E-05	1.87E-13	Group06	6.33	53.00
cellular response to stress	1.55E-05	1.87E-13	Group06	4.86	96.00
regulation of chromosome organization	2.10E-05	1.87E-13	Group06	8.95	29.00
regulation of cellular component organization	4.11E-05	1.87E-13	Group06	4.53	111.00
DNA replication	5.19E-05	1.87E-13	Group06	8.81	28.00
DNA repair	2.25E-04	1.87E-13	Group06	6.90	37.00
regulation of organelle organization	2.47E-04	1.87E-13	Group06	5.22	67.00
positive regulation of DNA metabolic process	4.20E-04	1.87E-13	Group06	9.44	22.00
positive regulation of chromosome organization	9.63E-04	1.87E-13	Group06	10.53	18.00
telomere maintenance via telomere lengthening	3.26E-03	1.87E-13	Group06	13.95	12.00
response to ionizing radiation	3.52E-03	1.87E-13	Group06	10.06	17.00
regulation of cellular response to stress	3.81E-03	1.87E-13	Group06	5.99	40.00
cell aging	5.01E-03	1.87E-13	Group06	12.38	13.00
protein complex assembly	5.26E-03	1.87E-13	Group06	4.71	70.00
regulation of response to DNA damage stimulus	5.35E-03	1.87E-13	Group06	9.33	18.00
DNA conformation change	6.00E-03	1.87E-13	Group06	8.03	22.00
telomere organization	7.81E-03	1.87E-13	Group06	9.94	16.00
DNA integrity checkpoint	8.75E-03	1.87E-13	Group06	9.39	17.00
DNA biosynthetic process	9.00E-03	1.87E-13	Group06	8.33	20.00
positive regulation of telomere maintenance	1.22E-02	1.87E-13	Group06	16.67	9.00
macromolecular complex subunit organization	1.42E-02	1.87E-13	Group06	4.22	92.00
macromolecular complex assembly	1.43E-02	1.87E-13	Group06	4.37	82.00
cell cycle checkpoint	1.44E-02	1.87E-13	Group06	8.06	20.00
protein complex subunit organization	1.51E-02	1.87E-13	Group06	4.43	77.00
regulation of telomere maintenance	1.87E-02	1.87E-13	Group06	12.79	11.00
regulation of protein complex assembly	1.96E-02	1.87E-13	Group06	6.62	28.00
response to heat	2.02E-02	1.87E-13	Group06	9.20	16.00
signal transduction by p53 class mediator	2.40E-02	1.87E-13	Group06	7.33	22.00
positive regulation of cellular component organization	2.59E-02	1.87E-13	Group06	4.75	60.00
positive regulation of organelle organization	4.21E-02	1.87E-13	Group06	5.52	37.00
regulation of cellular component biogenesis	4.35E-02	1.87E-13	Group06	5.11	46.00
peptidyl-amino acid modification	1.94E-08	4.75E-11	Group07	6.04	79.00
activation of protein kinase activity	8.70E-03	4.75E-11	Group07	7.25	25.00

Table 4.5 TOPBP1-dependent GO terms					
GO Term	**Term p-value**	**Group p-value**	**GO Groups**	**% Associated Genes**	**# Genes**
peptidyl-serine modification	4.77E-02	4.75E-11	Group07	6.82	23.00
posttranscriptional regulation of gene expression	4.30E-05	3.21E-10	Group08	7.14	39.00
mRNA metabolic process	3.04E-04	3.21E-10	Group08	5.92	50.00
regulation of cellular amide metabolic process	3.05E-04	3.21E-10	Group08	7.28	33.00
regulation of translation	9.02E-04	3.21E-10	Group08	7.33	30.00
regulation of mRNA catabolic process	6.52E-03	3.21E-10	Group08	9.60	17.00
mRNA transport	7.81E-03	3.21E-10	Group08	9.94	16.00
regulation of catabolic process	1.22E-02	3.21E-10	Group08	5.20	50.00
RNA splicing	1.62E-02	3.21E-10	Group08	6.52	29.00
negative regulation of cellular amide metabolic process	1.87E-02	3.21E-10	Group08	8.19	19.00
regulation of mRNA metabolic process	3.19E-02	3.21E-10	Group08	7.39	21.00
RNA processing	3.76E-02	3.21E-10	Group08	4.99	49.00
regulation of RNA stability	4.36E-02	3.21E-10	Group08	9.04	15.00
cellular senescence	5.20E-04	6.07E-09	Group09	18.33	11.00
cell aging	5.01E-03	6.07E-09	Group09	12.38	13.00
regulation of response to DNA damage stimulus	5.35E-03	6.07E-09	Group09	9.33	18.00
DNA integrity checkpoint	8.75E-03	6.07E-09	Group09	9.39	17.00
regulation of signal transduction by p53 class mediator	1.07E-02	6.07E-09	Group09	8.87	18.00
signal transduction by p53 class mediator	2.40E-02	6.07E-09	Group09	7.33	22.00
nucleic acid metabolic process	3.70E-23	3.25E-08	Group10	4.79	255.00
heterocycle metabolic process	3.88E-20	3.25E-08	Group10	4.42	274.00
cellular aromatic compound metabolic process	3.36E-19	3.25E-08	Group10	4.38	273.00
organic cyclic compound metabolic process	4.39E-19	3.25E-08	Group10	4.32	279.00
RNA metabolic process	7.71E-19	3.25E-08	Group10	4.76	229.00
cellular nitrogen compound metabolic process	6.35E-18	3.25E-08	Group10	4.22	283.00
regulation of nucleobase-containing compound metabolic process	2.99E-17	3.25E-08	Group10	4.81	211.00
gene expression	1.15E-16	3.25E-08	Group10	4.43	247.00
regulation of cellular metabolic process	2.40E-16	3.25E-08	Group10	4.24	268.00
cellular macromolecule metabolic process	3.86E-16	3.25E-08	Group10	3.82	333.00
regulation of cellular macromolecule biosynthetic process	8.92E-16	3.25E-08	Group10	4.79	201.00
chromatin organization	1.40E-15	3.25E-08	Group10	9.00	69.00
regulation of macromolecule biosynthetic process	1.69E-15	3.25E-08	Group10	4.74	204.00
regulation of biosynthetic process	5.69E-15	3.25E-08	Group10	4.61	212.00
regulation of RNA metabolic process	6.69E-15	3.25E-08	Group10	4.82	192.00
covalent chromatin modification	7.41E-15	3.25E-08	Group10	10.02	58.00
regulation of cellular biosynthetic process	1.02E-14	3.25E-08	Group10	4.62	209.00
regulation of metabolic process	2.69E-14	3.25E-08	Group10	4.05	277.00
regulation of gene expression	3.00E-14	3.25E-08	Group10	4.53	214.00
regulation of primary metabolic process	4.04E-14	3.25E-08	Group10	4.16	260.00
cellular nitrogen compound biosynthetic process	5.27E-14	3.25E-08	Group10	4.40	226.00
regulation of macromolecule metabolic process	6.74E-14	3.25E-08	Group10	4.14	260.00
heterocycle biosynthetic process	1.12E-13	3.25E-08	Group10	4.55	206.00
cellular macromolecule biosynthetic process	1.19E-13	3.25E-08	Group10	4.35	228.00
regulation of nitrogen compound metabolic process	1.50E-13	3.25E-08	Group10	4.16	253.00
organic cyclic compound biosynthetic process	2.63E-13	3.25E-08	Group10	4.48	210.00
macromolecule biosynthetic process	3.31E-13	3.25E-08	Group10	4.29	231.00

Table 4.5 TOPBP1-dependent GO terms					
GO Term	**Term p-value**	**Group p-value**	**GO Groups**	**% Associated Genes**	**# Genes**
aromatic compound biosynthetic process	7.42E-13	3.25E-08	Group10	4.50	204.00
nucleic acid-templated transcription	1.73E-12	3.25E-08	Group10	4.67	184.00
regulation of nucleic acid-templated transcription	1.17E-11	3.25E-08	Group10	4.65	176.00
macromolecule metabolic process	4.99E-11	3.25E-08	Group10	3.57	338.00
negative regulation of cellular macromolecule biosynthetic process	6.91E-11	3.25E-08	Group10	6.20	91.00
negative regulation of cellular biosynthetic process	1.71E-10	3.25E-08	Group10	5.93	97.00
negative regulation of cellular process	2.76E-10	3.25E-08	Group10	4.28	202.00
cellular biosynthetic process	8.00E-10	3.25E-08	Group10	3.91	251.00
negative regulation of nucleobase-containing compound metabolic process	1.80E-09	3.25E-08	Group10	5.93	89.00
organic substance biosynthetic process	1.86E-09	3.25E-08	Group10	3.88	253.00
negative regulation of gene expression	2.50E-09	3.25E-08	Group10	5.52	102.00
negative regulation of macromolecule metabolic process	2.99E-09	3.25E-08	Group10	4.92	133.00
negative regulation of biological process	4.30E-09	3.25E-08	Group10	4.08	213.00
positive regulation of nucleobase-containing compound metabolic process	4.70E-09	3.25E-08	Group10	5.48	102.00
negative regulation of cellular metabolic process	6.85E-09	3.25E-08	Group10	4.88	131.00
negative regulation of RNA metabolic process	8.04E-09	3.25E-08	Group10	6.07	81.00
regulation of cellular process	9.01E-09	3.25E-08	Group10	3.36	365.00
negative regulation of nitrogen compound metabolic process	9.41E-09	3.25E-08	Group10	4.97	124.00
negative regulation of metabolic process	2.18E-08	3.25E-08	Group10	4.69	140.00
positive regulation of macromolecule metabolic process	4.34E-08	3.25E-08	Group10	4.57	145.00
positive regulation of metabolic process	7.30E-08	3.25E-08	Group10	4.46	153.00
positive regulation of cellular metabolic process	8.06E-08	3.25E-08	Group10	4.53	145.00
negative regulation of nucleic acid-templated transcription	1.77E-07	3.25E-08	Group10	5.94	74.00
transcription from RNA polymerase II promoter	2.76E-07	3.25E-08	Group10	4.93	112.00
positive regulation of biosynthetic process	5.19E-07	3.25E-08	Group10	5.10	100.00
positive regulation of cellular biosynthetic process	1.05E-06	3.25E-08	Group10	5.08	98.00
positive regulation of RNA metabolic process	1.11E-06	3.25E-08	Group10	5.36	85.00
positive regulation of macromolecule biosynthetic process	1.16E-06	3.25E-08	Group10	5.18	92.00
regulation of transcription from RNA polymerase II promoter	2.25E-06	3.25E-08	Group10	4.92	102.00
positive regulation of gene expression	2.37E-06	3.25E-08	Group10	5.03	96.00
positive regulation of cellular process	2.49E-06	3.25E-08	Group10	3.90	202.00
negative regulation of transcription, DNA-templated	3.27E-06	3.25E-08	Group10	5.75	69.00
positive regulation of nitrogen compound metabolic process	4.83E-06	3.25E-08	Group10	4.38	135.00
positive regulation of transcription, DNA-templated	7.43E-06	3.25E-08	Group10	5.28	80.00
positive regulation of biological process	2.48E-05	3.25E-08	Group10	3.73	217.00
negative regulation of transcription from RNA polymerase II promoter	1.84E-03	3.25E-08	Group10	5.67	48.00
positive regulation of transcription from RNA polymerase II promoter	1.46E-02	3.25E-08	Group10	4.90	58.00
cellular protein metabolic process	2.02E-02	3.25E-08	Group10	3.55	186.00
positive regulation of molecular function	1.85E-05	6.66E-08	Group11	4.90	92.00
regulation of apoptotic process	2.13E-04	6.66E-08	Group11	4.95	78.00
regulation of cell death	2.71E-04	6.66E-08	Group11	4.82	83.00

Table 4.5 TOPBP1-dependent GO terms					
GO Term	**Term p-value**	**Group p-value**	**GO Groups**	**% Associated Genes**	**# Genes**
apoptotic process	3.05E-04	6.66E-08	Group11	4.64	92.00
programmed cell death	4.49E-04	6.66E-08	Group11	4.53	96.00
intracellular signal transduction	4.41E-02	6.66E-08	Group11	3.91	111.00
positive regulation of molecular function	1.85E-05	1.62E-06	Group12	4.90	92.00
positive regulation of kinase activity	4.12E-04	1.62E-06	Group12	6.58	39.00
positive regulation of catalytic activity	5.18E-04	1.62E-06	Group12	4.92	75.00
positive regulation of transferase activity	5.56E-04	1.62E-06	Group12	6.11	45.00
activation of protein kinase activity	8.70E-03	1.62E-06	Group12	7.25	25.00
positive regulation of protein kinase activity	2.43E-02	1.62E-06	Group12	5.95	33.00
regulation of transferase activity	2.43E-02	1.62E-06	Group12	4.92	53.00
regulation of kinase activity	2.85E-02	1.62E-06	Group12	5.15	46.00
intracellular signal transduction	4.41E-02	1.62E-06	Group12	3.91	111.00
peptidyl-serine modification	4.77E-02	1.62E-06	Group12	6.82	23.00
regulation of cellular response to stress	3.81E-03	6.56E-06	Group13	5.99	40.00
response to heat	2.02E-02	6.56E-06	Group13	9.20	16.00
regulation of gene silencing	3.95E-02	6.56E-06	Group13	10.91	12.00
mRNA export from nucleus	4.69E-02	6.56E-06	Group13	10.71	12.00
symbiosis, encompassing mutualism through parasitism	1.17E-03	6.56E-06	Group14	5.62	50.00
viral process	1.37E-03	6.56E-06	Group14	5.73	47.00
chromatin remodeling	1.06E-02	4.89E-05	Group15	9.70	16.00
protein localization	4.79E-02	5.76E-05	Group16	3.93	109.00
Ras protein signal transduction	3.59E-03	6.49E-05	Group17	7.28	27.00
small GTPase mediated signal transduction	1.85E-02	6.49E-05	Group17	6.06	33.00
response to epidermal growth factor	3.05E-02	7.24E-05	Group17	17.02	8.00

CHAPTER V

DISCUSSION AND FUTURE DIRECTIONS

Summary

ATR is an apical DNA damage response (DDR) kinase that promotes genome stability by regulating the cell division cycle and cellular stress responses (Saldivar et al., 2017). ATR signaling coordinates the DNA replication stress response, controls the S/G_2 and G_2/M transitions to ensure completion of DNA replication before mitosis, and ensures proper chromosome separation during mitosis (Cimprich and Cortez, 2008; Saldivar et al., 2018; Kabeche et al., 2017; Zachos et al., 2007). ATR can phosphorylate hundreds of proteins in response to replication stress regulating a wide range of biological processes including DNA metabolism, cell cycle regulation, protein metabolism, and gene expression (Matsuoka et al., 2007). Emphasizing the critical functions of ATR as a master regulator of genome maintenance, loss of ATR is incompatible with life, and mutations in ATR result in the disease Seckel syndrome (O'Driscoll et al., 2003).

The essential function of ATR is to coordinate cellular responses to RS (Nam et al., 2011a). ATR and its obligate binding partner ATRIP, localize to sites of RS through an interaction with RPA on ssDNA (Zou and Elledge, 2003). However, ATR localization to sites of RS is not sufficient for its activation, ATR requires an activating protein to stimulate its kinase activity. Vertebrate cells utilize two ATR-activating proteins to regulate ATR activity, TOPBP1 and ETAA1 (Bass et al., 2016; Haahr et al., 2016; Feng et al., 2016; Kumagai et al., 2006). Once activated, ATR initiates a signaling cascade that results in decreased origin firing, stabilization of stalled replication forks, and halts cell cycle progression.

During my graduate studies I have identified a new ATR activator, ETAA1, and examined how both ETAA1 and TOPBP1 direct ATR signaling. Chapter III describes the identification of ETAA1 as a novel ATR activator and its functions to promote genome stability during RS. Chapter IV describes how I utilize quantitative phosphoproteomics to identify ETAA1 and TOPBP1 substrates and the discovery of a unique function of ETAA1 to regulate mitotic ATR signaling at centromeric regions.

Discussion

Defining ATR/Mec1 activators

In my thesis work I identified ETAA1 as a second ATR activating protein in vertebrate cells, ten years after the identification of the first ATR activating protein, TOPBP1. Although studies during the past decade have expanded our knowledge of how ATR and Mec1 are regulated by activating proteins, some questions remain outstanding. First, are there additional ATR/Mec1 activators? Second, how do these activators stimulate ATR/Mec1 kinase activity? Lastly, how do these different activators direct ATR/Mec1 toward specific substrates?

In yeast, three proteins can activate $Mec1^{ATR}$: $Dpb11^{TOPBP1}$, $Ddc1^{Rad9}$, and Dna2 (Mordes et al., 2008b; Navadgi-Patil and Burgers, 2009, 2008a; Kumar and Burgers, 2013). However, only the TOPBP1/DPB11 activation pathway of ATR/Mec1 appears to be conserved throughout eukaryotes. While Rad9 and $Ddc1^{Rad9}$ are both part of checkpoint clamps required to recruit TOPBP1/Dpb11, Rad9 cannot activate ATR on its own, unlike its yeast counterpart DDC1. Similarly, human DNA2 cannot stimulate ATR kinase activity. Conversely, yeast do not contain an obvious ETAA1 homolog. Although the human orthologues of $Ddc1^{Rad9}$, DNA2, do not activate ATR, these Mec1 activators and ETAA1 may be functional orthologues based on how they direct ATR/Mec1 signaling, a process described later.

At least two papers suggest that there may be additionally Mec1 activators in yeast, and the recent discovery of proteins that regulate ATR signaling may hint at the presence of additional ATR activators (Bandhu et al., 2014; Bastos de Oliveira et al., 2015; Reynolds et al., 2017). Although direct evolutionary conservation does not seem a promising method of identifying new ATR/Mec1 activators, defining the characteristics of an ATR/Mec1 activation domain may assist with identification of novel activators. Extensive work from the Peter Burgers lab has identified common features in Mec1 activators and ongoing work by Vaughn Thada in our laboratory is expanding the definition of an ATR activating domain. The only common structural or sequence feature of ATR and Mec1 activators is the presence of two aromatic residues contained within an intrinsically disordered region. Although this is a loose biochemical definition of an AAD/MAD, potential ATR activating proteins that have lacked obvious aromatic residues have failed to stimulate ATR in our kinase assays. Therefore, a biochemical definition of what defines an AAD/MAD combined with genetic and/or proteomic screening for ATR signaling pathway defects may reveal additional activators.

Characterizing how ATR/Mec1 activators work

Exactly how ATR and Mec1 are stimulated by activating-proteins has not been described but likely involves conformation changes of the kinase upon binding by the activating protein (Mordes and Cortez, 2008). ATR-activating proteins utilize the same surface of ATR for activation, as a point mutant that disrupted the ability of TOPBP1 to activate ATR also prevented activation by ETAA1 (Bass et al., 2016). Additionally, interchanging of the of Dpb11 and Dna2 MADs still promotes Mec1 activation, suggesting a common mechanism of Mec1 activation (Kumar and Burgers, 2013).

Structures of the $Mec1^{ATR}$-$Ddc2^{ATRIP}$ complex reveal that they form a dimer of heterodimers with butterfly-like architecture, similar to the dimeric architecture of Tel1, the ATM orthologue (Wang et al., 2017; Deshpande et al., 2017; Rao et al., 2018). Heterodimerization is

mediated using interactions between the PRD and FAT domains of Mec1^{ATR} and the coiled-coil of Ddc2^{ATRIP} (Ball and Cortez, 2005; Itakura et al., 2005; Wang et al., 2017). The PRD keeps the Mec1 activation pocket in a closed conformation, which is likely opened after binding of a Mec1/ATR activator. Although ATR/Mec1 forms a dimeric complex, it is not known if two activating proteins are required for activation of both ATR molecules. The activation domain lies at the dimerization interface and therefore a single ATR/Mec1 activating protein may be able to activate both molecules. Future structural studies incorporating AAD/MADs into the ATR/Mec1 complex are required to obtain a detailed understanding of ATR/Mec1 activation.

Benefits of having multiple ATR/Mec1 activators

Another remaining question is if ATR/Mec1 activators stimulate ATR/Mec1 kinase activity though the same mechanism, why do cells require multiple activators? Having multiple activators appears to account for more than just a contingency plan in case one activation pathway fails, as ATR and Mec1 activators have some non-redundant functions in cells. Below, I will detail the possible benefits of utilizing multiple ATR activators, including temporal regulation of ATR, separation of ATR signaling pathways, and promoting response to more diverse DNA lesions (Fig 5.1)

Temporal regulation of ATR signaling

The utilization of multiple ATR activators may be a conserved regulatory mechanism for checkpoint activation throughout eukaryotes. Although the unique functions of each Mec1^{ATR} activator have not been fully defined, there are several common themes between Mec1^{ATR} and ATR activation that may explain why multiple activators are used for checkpoint signaling. First, the cell-cycle-specific utilization of each Mec1^{ATR} activator allows for temporal regulation of Mec1^{ATR} throughout the process of cell division (Navadgi-Patil and Burgers, 2011). Ddc1^{Rad9} activates Mec1^{ATR} during G1, while both Ddc1^{Rad9} and Dpb11^{TOPBP1} activate Mec1^{ATR} during G_2

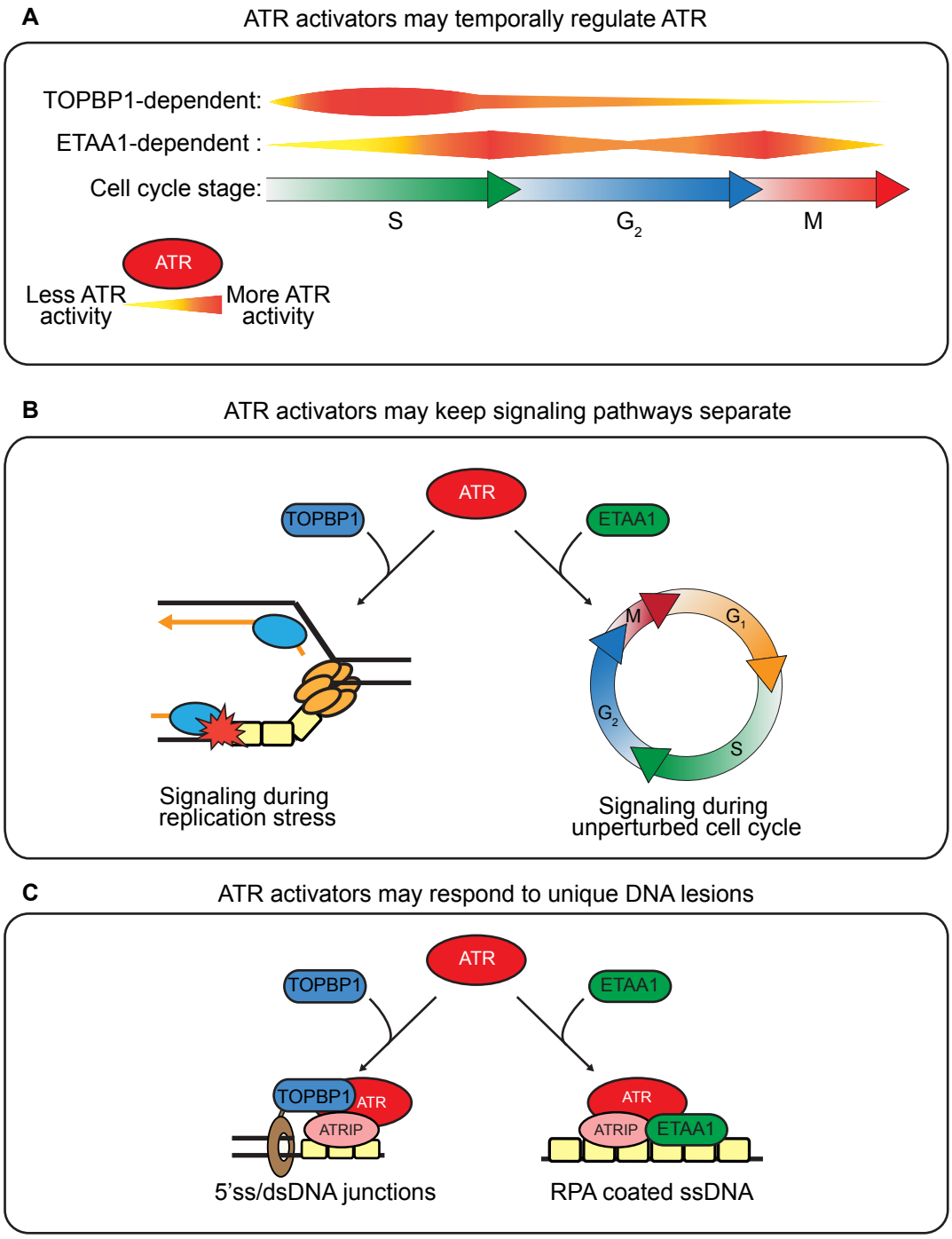

Figure 5.1 Potential benefits of utilizing multiple ATR activators. (A) Utilizing multiple ATR activators may provide temporal regulation of ATR signaling throughout the cell cycle. TOPBP1 is highly utilized during S-phase while ETAA1 is used at G_2/S and mitotic cell cycle transitions. (**B**) Use of different activators may keep ATR signaling pathways distinct. TOPBP1 is primarily utilized during replication stress while ETAA1 promotes ATR regulation of cell cycle transition. **(C)** Utilizing multiple activators that are recruited by different substrates may allow ATR to respond to a wider range of genomic threats.

(Navadgi-Patil et al., 2011; Navadgi-Patil and Burgers, 2009). During S-phase, all three Mec1^{ATR} activators contribute to Mec1^{ATR} activation with partial redundancy.

I have observed a similar cell-cycle specific usage of ETAA1 and TOPBP1 (Fig. 5.1A). Both activators are utilized during S-phase when ATR signaling is highest. However, during mitosis only ETAA1 is required to promote ATR signaling at centromeric regions. Previous studies indicate that TOPBP1 does function during mitosis at sites of under-replication but that it is independent of ATR signaling (Pedersen et al., 2015). Additionally, TOPBP1 localizes to ultra-fine anaphase bridges and promotes their resolution through direct recruitment of topoisomerase IIα. (Germann et al., 2014; Broderick et al., 2015). Therefore, while TOPBP1 is active during mitosis, its functions do not appear tied to ATR activation. Utilizing certain activators at specific times during cell cycle progression may direct ATR signaling to substrates required for that specific stage of the cell cycle.

Separation of ATR signaling pathways

Another potential benefit of having multiple ATR/Mec1 activators is that they may keep different signaling pathways distinct (Fig 5.1B). ATR functions throughout the cell cycle to coordinate responses to genotoxic stress and regulate cell cycle transitions. Using cells deficient for ETAA1 or TOPBP1, we were able to separate the functions of ATR during replication stress and a normal cell cycle. We found that ETAA1-dependent ATR activity controlled the anaphase to metaphase transition through regulation of the SAC. These findings expand the requirement for ETAA1 to enforce normal cell cycle progression as ETAA1 activates ATR during an unperturbed S-phase to control the S/G_2 transition (Saldivar et al., 2018). Conversely, we identified TOPBP1 as the primary activator of ATR in response to replication stress. These findings suggest each activator may regulate a separate ATR pathway, ETAA1 regulating ATR signaling to promote optimal cell cycle progression and TOPBP1 promoting cellular responses to replication stress. This separation of function parallels how different

Mec1^{ATR} activators work in yeast where Dpb11^{TOPBP1} activates Mec1^{ATR}-Rad53^{CHK1} signaling during replication stress while the other Mec1^{ATR} activators, Dna2 and Ddc1^{Rad9}, activate Mec1 during an unperturbed cell cycle (Bastos de Oliveira et al., 2015). Therefore, although there is no apparent yeast homolog of ETAA1, Dna2 and Ddc1 may be functional orthologs. Utilizing different activators may ensure separation of ATR/Mec1 signaling pathways, keeping responses to RS distinct from signaling during a normal, unperturbed cell cycle.

ATR activators may respond to unique DNA lesions

In all of these models of ATR/Mec1 activation, the advantage of having multiple activating proteins is to direct ATR to specific and potentially distinct substrates. But how do these ATR/Mec1 activators direct ATR activity toward specific substrates? In yeast, Mec1^{ATR} activators direct Mec1^{ATR} to phosphorylate substrates proximal to the activator, promoting localization-dependent Mec1 signaling (Lanz et al., 2018). Localization of ETAA1 or TOPBP1 may similarly regulate ATR. Indeed, one of the distinguishing differences between ETAA1 and TOPBP1 is their mode of recruitment to sites of RS. ETAA1 is localized through two RPA-interaction motifs that are both sufficient for its binding to RPA (Haahr et al., 2016; Lee et al., 2016; Bass et al., 2016; Feng et al., 2016). TOPBP1 recruitment to 5' ss/dsDNA junctions is dependent on MRN, RHINO, and a direct interaction with the phosphorylated C-terminal tail of RAD9 of the 9-1-1 (Cotta-Ramusino et al., 2011; Lee et al., 2007a; Duursma et al., 2013). These different modes of recruitment may ensure ATR can be activated at a wide range of DNA lesions and influence which ATR substrates get phosphorylated (Fig 5.1C).

Although 5' junctions limit TOPBP1 localization, it is the primary activator of ATR during RS. Therefore, most stalled forks must naturally generate a 5' junction or be processed by fork remodeling proteins to contain a junction. Following uncoupling of the helicase and polymerase activities, DNA polymerase α (Pol α) forms 5' junctions as it continues to synthesize primers ahead of the stalled polymerase, promoting checkpoint activation (Fig. 5.2 A).

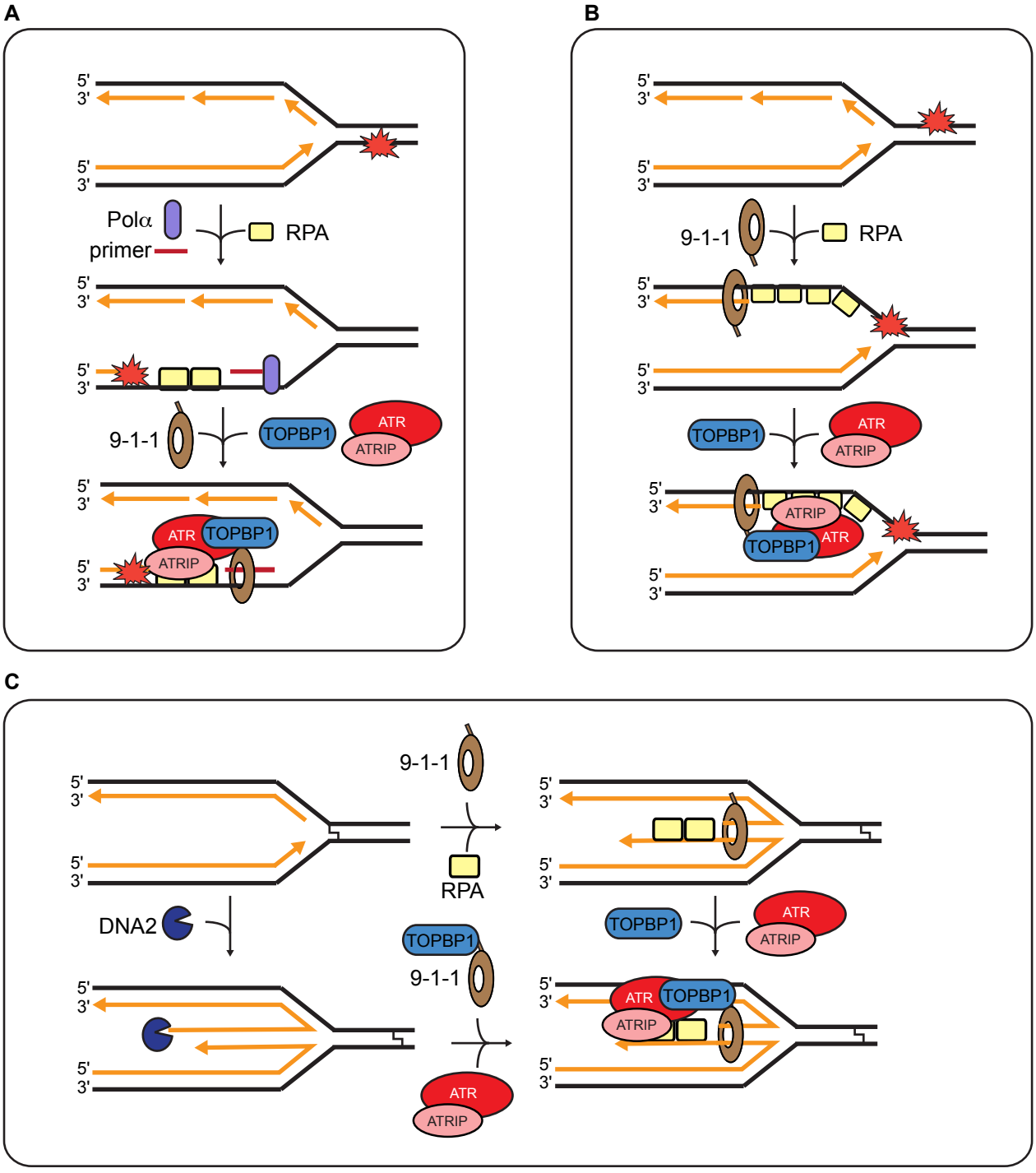

Figure 5.2 Generation of 5' ss/dsDNA junctions for TOPBP1 activation. (A) Lesions on the lagging strand can causes helicase and polymerase uncoupling generating ssDNA, but may not have a 5' junction. DNA polymerase α forms 5' junctions as it continues to synthesize primers ahead of the stalled polymerase, promoting TOPBP1 recruitment. **(B)** A stalled lagging strand naturally forms 5' junctions due to discontinuous synthesis of Okazaki fragments from RNA-DNA primers. **(C)** For DNA lesions that do not generate ssDNA, the stalled fork can be reversed to generate a 5' junction to promote TOPBP1 recruitment. If the leading strand is longer than the lagging strand, the regressed arm would have to be resected by an exonuclease such as DNA2 to generate a 5' junction.

(Van et al., 2010; Michael et al., 2000). A stalled lagging strand also naturally forms 5' junctions due to the discontinuous synthesis of Okazaki fragments from RNA-DNA primers (Fig. 5.2 B). Therefore, continued DNA primer synthesis is one mechanism ensuring TOPBP1 recruitment to stalled forks.

For DNA lesions that do not generate ssDNA a potential mechanism to protect forks and recruit ATR and TOPBP1 is fork reversal (Fig. 5.2 C). When forks stall, fork remodeling enzymes can regress the replication fork protruding the regressed arm consisting of annealed nascent DNA. If the nascent lagging strand is shorter than the nascent leading strand, then fork reversal would have sufficiently generated a 5' junction. However, if the leading strand was longer than the lagging strand, the regressed arm must be resected by 5'-to-3' exonucleases such as DNA2 to generate a 5' ss/dsDNA junction. Similarly, lesions such as DSBs can activate ATR but require processing by exonucleases such as Exo1 to generate ssDNA to localize ATR/ATRIP and a 5' junction to recruit TOPBP1 (Fig. 5.3 A).

While TOPBP1 is the primary activator of ATR during S-phase, ETAA1 does contribute to ATR signaling to a lesser extent. While most DNA lesions can generate a 5' junction to localize TOPBP1, ETAA1 may be required for DNA lesions that lack a 5' ss/dsDNA junction but contain RPA-coated ssDNA. One such common DNA structure is a R-loop, a three stranded nucleic acid structure composed of a DNA:RNA hybrid and the displaced ssDNA loop (Skourti-Stathaki and Proudfoot, 2014). R-loops impede DNA replication causing genome instability (Gan et al., 2011). R-loops form naturally when a nascent RNA transcript behind an elongating Polymerase II (Pol II) duplexes with the DNA template strand, displacing the non-template strand (Fig. 5.3B). RPA can bind the displaced ssDNA strand and can elicit checkpoint response through recruitment of ATR/ATRIP.

Activation of ATR at R-loops may require ETAA1 which can be recruited by RPA on the displaced strand, while lack of a 5' junction should preclude TOPBP1 localization to R-loops

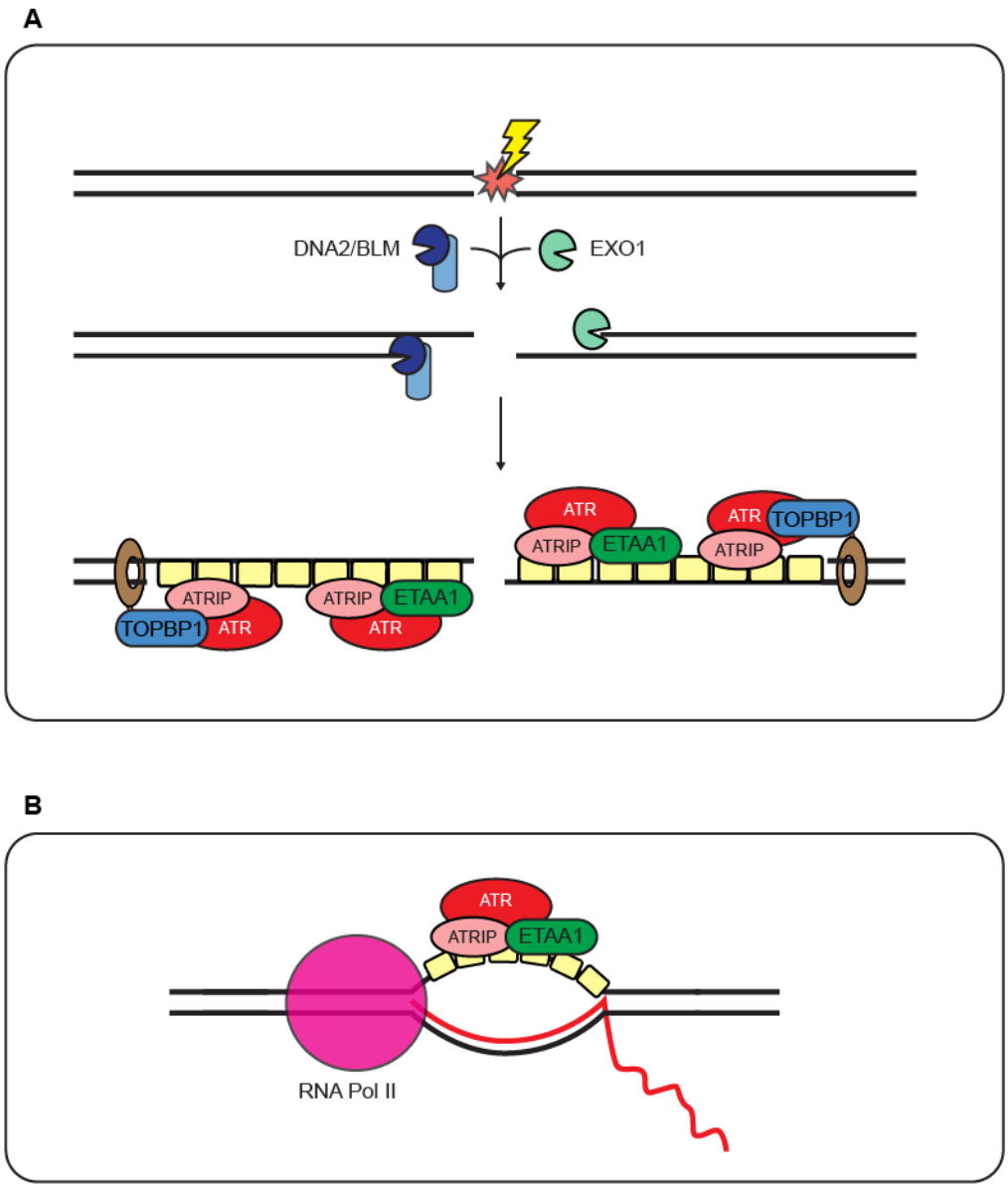

Figure 5.3 DNA structures that may require ETAA1 activation of ATR. **(A)** Double strand breaks can be extensively resected by two pathways dependent on EXO1 and DNA2/BLM. Long-range resection may require ETAA1 to activate ATR molecules localized too far away from the 5' junction. **(B)** R-loops are three stranded nucleic acid structure composed of a DNA:RNA hybrid and the displaced ssDNA loop. R-loops do not contain 5' junctions and therefore may require ETAA1 to activate ATR.

(Fig. 5.3 B). Although this hypothesis has not yet been directly tested, my studies outlined in this dissertation in combination with findings from the Zou lab suggest ATR signaling at R-loops is dependent on ETAA1. The Zou lab discovered that ATR recruitment to centromeres during mitosis is dependent on centromeric R-loop formation (Kabeche et al., 2017). Additionally, work described in Chapter IV demonstrated that ETAA1 but not TOPBP1 is required for mitotic ATR signaling at centromeric regions. Therefore, the dependence on ETAA1 but not TOPBP1 for ATR signaling at centromeric regions may reflect an inability of TOPBP1 to localize to R-loops, requiring ETAA1 activation of ATR.

Studies have shown that increasing the amount of ssDNA increases ATR signaling, even if the number of 5' ss/dsDNA junctions are kept constant (MacDougall et al., 2007; Shiotani et al., 2013). Therefore, cells may utilize ETAA1 following extensive DNA resection to bolster ATR signaling by activation of ATR molecules localized too far away from a junction to interact with TOPBP1 (Fig. 5.4 A). Following formation of a DSB, MRN and CtIP initiate resection, processing the ends of the DNA breaks by short range resection. MRN then recruits and stimulates EXO1 and/or DNA2/BLM to promote long-range resection (Nimonkar et al., 2011; Zhu et al., 2008). As resection becomes more extensive, localized ATR signaling away from the junction may become more ETAA1-dependent.

Topoisomerase poisons such as CPT and ETOP can induce double strand breaks that are extensively resected promoting ATR activation (Gobbini et al., 2013). Hyperphosphorylation of RPA is used as a common readout for long-range resection (Cruz-García et al., 2014). Interestingly, loss of ETAA1 reduces RPA phosphorylation after treatment with CPT, despite an increase in ssDNA and RPA accumulation at sites of replication (Bass et al., 2016). These results show that even though resection is still occurring, RPA is not getting phosphorylated supporting a model for ETAA1 activation of ATR on long stretches of ssDNA.

While loss of ETAA1 decreased RPA phosphorylation during RS, other ATR substrates such as CHK1 and MCM2 are more dependent on TOPBP1. CHK1 phosphorylation requires the replisome component CLASPIN (Kumagai and Dunphy, 2000), and MCM2 is part of the replicative helicase. Thus, it is possible that the proximity to the replisome where it may be more likely to have a 5' DNA junction to load 9-1-1/TOPBP1 could determine ETAA1 versus TOPBP1 dependency.

Regulation of ETAA1

Checkpoint initiation requires concentrating ATR and its activators at sites of RS to promote an interaction. By requiring independent recruitment of two protein complexes to sites of RS, cells prevent spurious activation of ATR. TOPBP1 localization to sites of RS is very distinct from ATR, relying on a different DNA substrate, a 5' ss/dsDNA junction, and different recruiting proteins: 9-1-1, MRN, and RHINO. In contrast, ETAA1 and ATR recruitment is mediated by the same substrate, RPA-coated ssDNA. Surprisingly, although ETAA1 appears to have fewer requirements to colocalize with ATR, it is not the primary activator during RS. Therefore, I hypothesize that cells employ additional mechanisms that regulate ETAA1 ability to activate ATR during RS.

ETAA1 is phosphorylated during replication stress

In support of this hypothesis, I have observed that after addition of RS-inducing agents ETAA1 becomes more difficult to detect by western blotting in many different cell types suggesting either a decrease in ETAA1 levels or a change in its electrophoretic mobility due to post-translational modifications (PTMs) (Fig. 3.11E; Fig. 5.4 A). Alteration of protein levels or modification of ETAA1 by PTMs may serve as mechanisms to regulate ETAA1 activity during

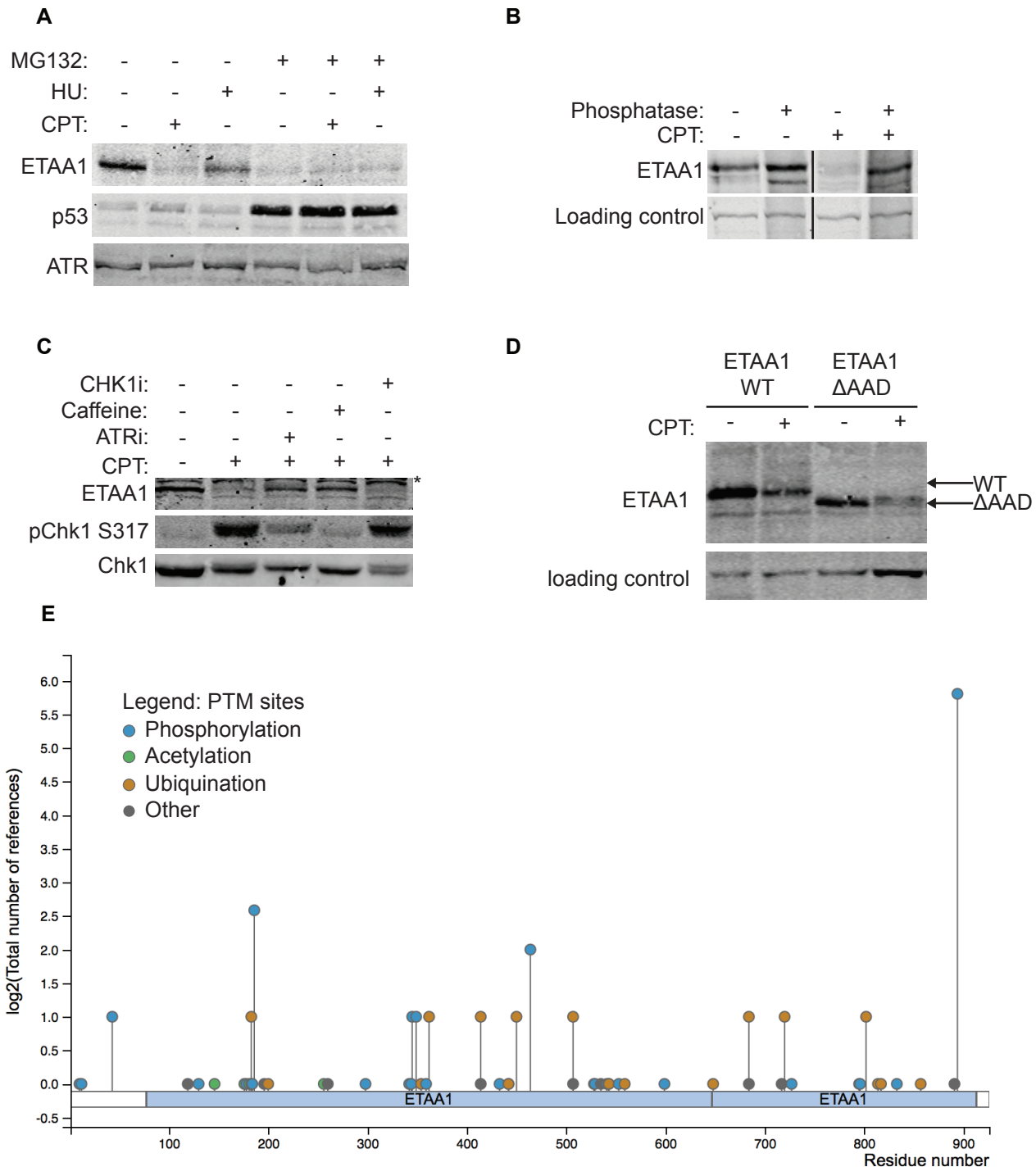

Figure 5.4 ETAA1 is phosphorylated during replication stress. (A) HeLA cells were treated with 100 nM CPT or 2 mM HU for four hours following a 1.5 hour pretreatment with DMSO or MG132. Cell were harvested, lysed proteins examined by western blotting following separation by SDS-PAGE. **(B)** Hela cells were left untreated or treated for four hours with 100 nM CPT. Cells were collected, lysed, and treated with lambda phosphatase for 20 min. **(C)** HeLa cells were pretreated with the indicated kinase inhibitors prior to a four hour treatment with 100 nM CPT. Asterisk denotes a non-specific band. **(D)** HCT116 Wild type and ΔAAD cells were treated with 100 nM CPT for 4 hrs before separation separation by SDS-PAGE and detection of proteins by western blotting. **(E)** ETAA1 PTM sites and frequency they are referenced. Diagram was exported from Phosphosite Plus.

RS. To test if RS induces ETAA1 degradation, cells were pretreated with the proteasome inhibitor MG132 before addition of CPT. Although MG132 treatment prevented proteasomal degradation of p53, it did not stabilize ETAA1 levels suggesting the inability to detect ETAA1 is not due to degradation by the proteasome (Fig. 5.4 A).

ETAA1 has been identified as an ATR substrate in two phosphoproteomic screens and is phosphorylated by ATR in our kinase assays (Matsuoka et al., 2007; Haahr et al., 2016). To examine if the difficulties in detecting ETAA1 during RS is due to phosphorylation, cell lysates were treated with lambda phosphatase before separation by SDS-PAGE. Treatment with phosphatase restored the appearance of ETAA1 to that of an untreated control, demonstrating that ETAA1 is phosphorylated during RS (Fig. 5.4B). Since ETAA1 has been identified as an ATR substrate and its phosphorylation is induced by RS, I examined if ETAA1 phosphorylation could be prevented by treatment with ATR or CHK1 inhibitors. Inhibition of ATR by VE-821 and caffeine prevented ETAA1 phosphorylation while inhibition of CHK1 did not affect ETAA1 modification demonstrating that ETAA1 is phosphorylated by ATR (Fig. 5.4C). ETAA1 phosphorylation does not appear dependent on its ability to interact and activate ATR as ETAA1 is still modified in ETAA1ΔAAD cells (Fig. 5.4 D). Many sites on ETAA1 are phosphorylated (Fig. 5.4E), some of which are S/TQ sites and therefore likely candidates as sites of phosphorylation by ATR.

To examine if ETAA1 phosphorylation serves any regulatory functions, I examined kinetics of ATR signaling and modification of ETAA1 at different times post treatment with CPT (Fig. 5.5 A). An hour post CPT addition, nearly 50% of ETAA1 was modified, measured by reduced ETAA1 detection (Fig. 5.5 B). Modification of ETAA1 continued to increase during 24 hours of CPT treatment. In comparison, I observed no detectable difference in TOPBP1 throughout the duration of the time course (Fig 5.5 A).

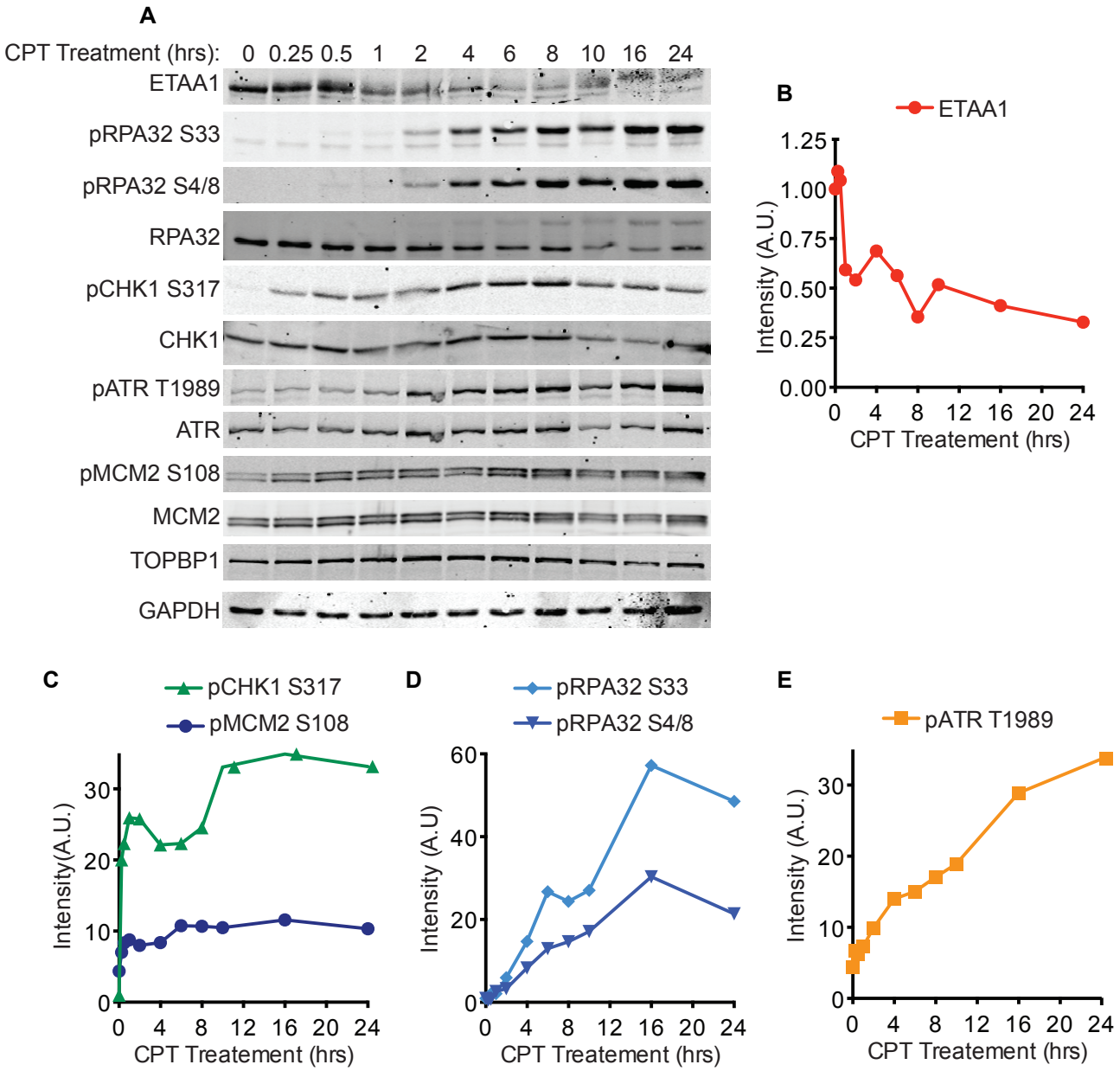

Figure 5.5 Kinetics of ETAA1 modification and ATR signaling. (A) HeLa cells were treated with 100 nM CPT for the indicated times before cells were harvested, lysed, and proteins separated by SDS-PAGE and detected by western blotting. **(B)** Intensity of ETAA1 over time. Detectable ETAA1 levels decrease due to phosphorylation that alters the electrophoretic mobility of ETAA1. **(C)** Relative intensity of pCHK1 S317 and pMCM2 S108, substrates dependent on TOPBP1 activation of ATR. **(D)** Relative intensity of RPA phosphorylation on S33 and S4/8, substrates that are dependent on ETAA1 activation of ATR. **(E)** Relative intentisy of pATR 1989, a marker of ATR activation.

In addition to monitoring modifications of ATR activators I also examined phosphorylation of ATR substrates previously shown to be dependent on ETAA1 or TOPBP1. Just 15 minutes after CPT addition, CHK1 and MCM2 phosphorylation rose to over half their maximum detected levels and plateaued around 2 hours (Fig. 5.5 C). In contrast, RPA phosphorylation was not detected until two hours after CPT treatment and continued to increase over the course of 16 hours (Fig. 5.5 D). Similarly, throughout the 24 hours of CPT treatment I observed a steady increase in autophosphorylation of ATR on S1989, a readout of ATR activation (Fig. 5.5 E) (Nam et al., 2011b; Liu et al., 2011). Strikingly, proteins dependent on TOPBP1 activation of ATR such as MCM2 and CHK1 are phosphorylated early, well before ETAA1 is modified. Meanwhile, RPA phosphorylation is only detectable at later timepoints, after large amounts of ETAA1 is modified. Therefore, phosphorylation of ETAA1 may be a prerequisite for its ability to stimulate ATR.

ETAA1 demonstrates delayed localization to sites of replication stress

To examine if ETAA1 modification might correspond with ETAA1 localization to sites of RS, I examined localization of RPA, TOPBP1, and ETAA1 at differing times post treatment with CPT (Fig. 5.6 A-D). Just 30 minutes after addition of CPT, around 20% of cells in an asynchronous population begin to form RPA or TOPBP1 foci. Throughout a 16-hour time course the percentage of cells with TOPBP1 and RPA foci continued to increase, reaching 40% two hours after addition of CPT and ending around 90% after 16 hours. In comparison, only 10% of cells contain ETAA1 foci after 4 hours of CPT treatment and only 20-25% of cells are ETAA1-foci positive after 16 hours. Although the amount of RPA-coated ssDNA was sufficient to form foci at 30 min, ETAA1 recruitment is delayed until four hours (Fig. 5.6 A). Therefore, while an interaction with RPA is required for its localization to sites of RS, it may not be solely sufficient. The similar kinetics of ETAA1 modification and its localization to foci present a potential model for ETAA1 phosphorylation to promote its recruitment to sites of RS.

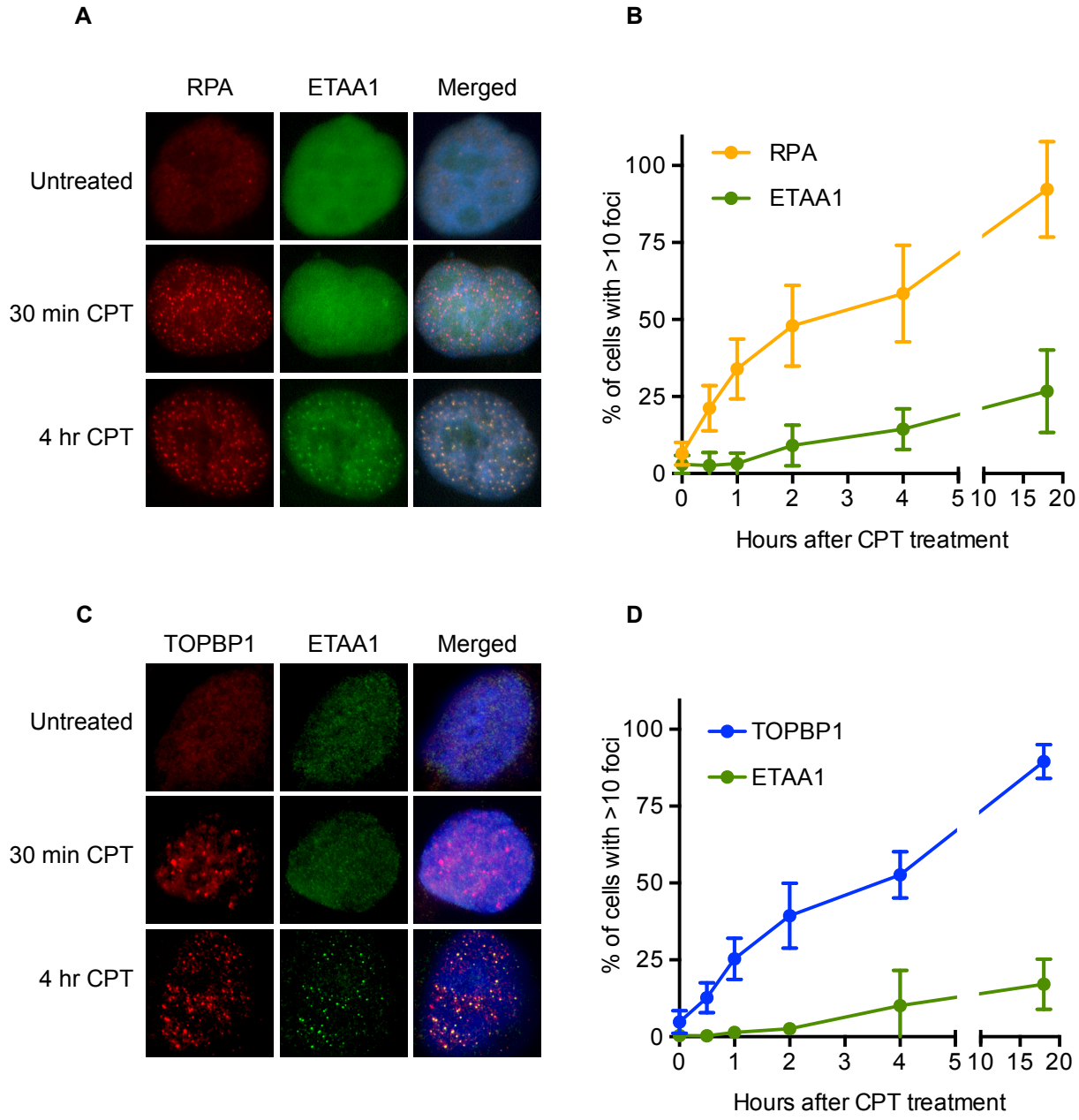

Figure 5.6 Kinetics of recruitment of ETAA1, TOPBP1, and RPA. **(A)** U2OS cells stably expressing GFP-Flag ETAA1 were treated with 100 nM CPT for the indicated times and examined for localization of ETAA1 and RPA**. (B)** Quantification of percentage of cells with 10 or more ETAA1 or RPA foci. **(C)** Same as in A but cells were examined for TOPBP1 and ETAA1. **(D)** Quantification of percentage of cells with 10 or more ETAA1 or RPA foci.

Future directions

Defining mechanism of ETAA1 regulation

Findings from these initial experiments could direct future studies of ETAA1 and further define how ETAA1 and TOPBP1 function through different pathways to regulate ATR signaling. One future direction of study could identify important ETAA1 modification sites and identify the modifying enzymes. ETAA1 appears to be heavily phosphorylated during RS and is likely an ATR substrate, although its ability to activate ATR is not required for its modification. Activation of ATR by TOPBP1 may promote an initial, early signaling cascade that results in phosphorylation of CHK1 and MCM2 and substrates proximal to the 5' junction (Fig 5.7A). ETAA1 may activate ATR at later time points, following its phosphorylation and subsequent recruitment to sites of RS, sustaining the checkpoint signal (Fig 5.7B). This would allow ATR to phosphorylate substrates away from the initial site of damage, as extensive resection and DNA processing may require ATR localization away from a 5' ss/dsDNA junction. Of interest would be to identify how phosphorylation of ETAA1 regulates its activity and test if ETAA1 phosphorylation is required for its recruitment to sites of RS.

TOPBP1 is regulated at the level of recruitment, requiring formation of additional DNA substrates and protein complexes to colocalize with ATR. Since ETAA1 recruitment utilizes the same substrate as ATR, PTMs may serve as an additional level of regulation to limit ETAA1 localization and prevent spurious ATR activation. The use of phosphomimetic and phosphodead mutants of ETAA1 may reveal the significance of these PTMs and establish if these phosphorylation sites are required for proper ETAA1 recruitment. Furthermore, if localization is the main determinant of which activator is utilized and which substrates are phosphorylated, it would be interesting to observe how swapping the RAD9-interaction domain of TOPBP1 with

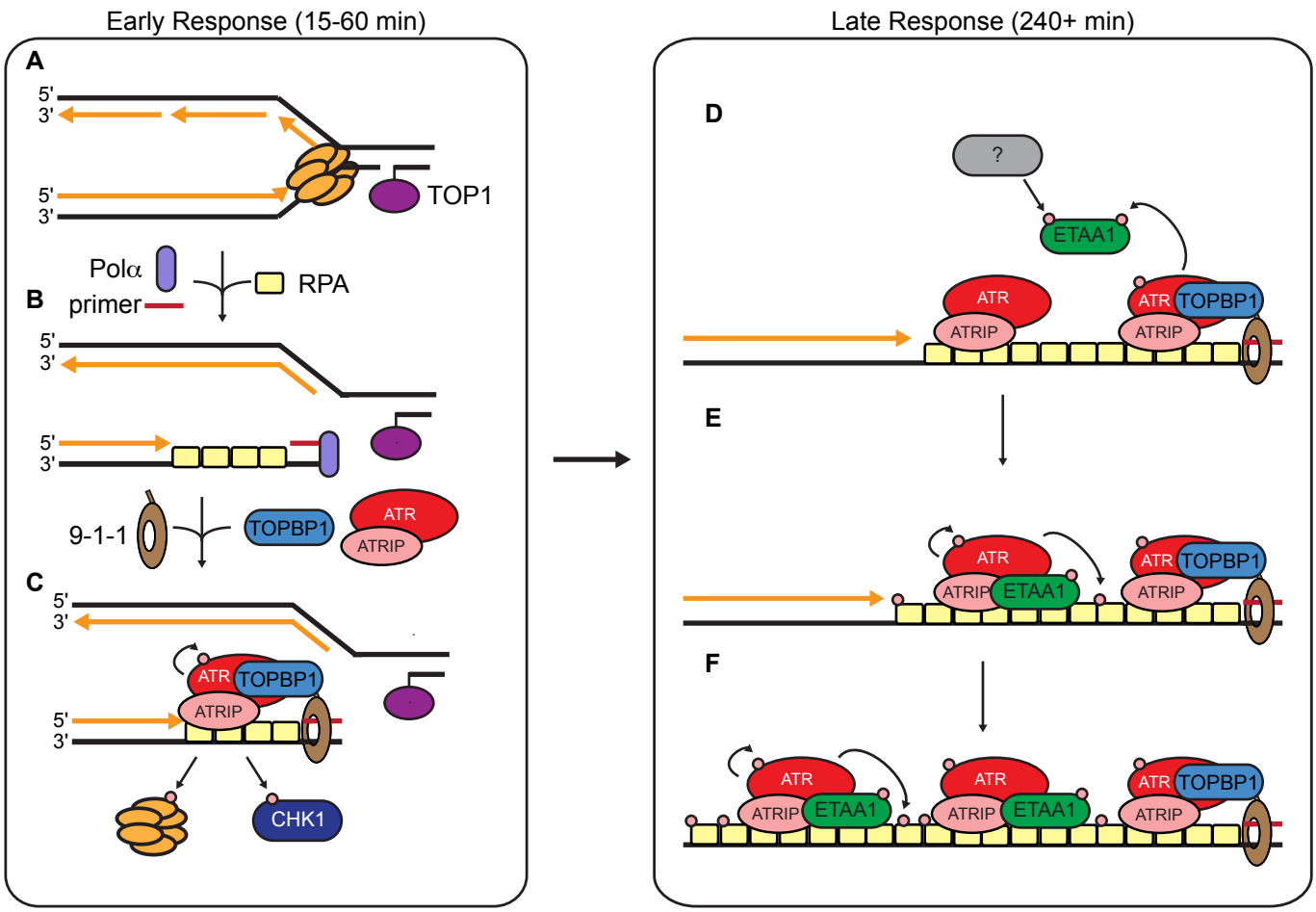

Figure 5.7 Model of ETAA1 regulation and ATR signaling after treatment with camptothecin. **(A)** Treatment with CPT traps topoisomerase 1 on DNA. **(B)** Double strand breaks form when the replication fork collides with the trapped topoisomerase. **(C)** Shortly after addition of CPT, RPA and TOPBP1 are recruited to sites of replication stress and CHK1 and MCM2 are phosphorylated by ATR. ATR also autophosphorylates S1981. **(D)** During the course of the next few hours, the broken fork is resected and processed for repair by HR generating more ssDNA. ETAA1 is phosphorylated by ATR promoting its recruitment. Additional kinases or modifying enzymes may also be utilized. **(E)** ETAA1 activates ATR away from the 5' junction promoting phosphorylation of proximal substrates such as RPA. **(F)** As ssDNA continues to accumulate ETAA1 continues to activate ATR resulting in increased RPA phosphorylation and ATR autophosphorylation.

the RPA-interaction motifs of ETAA1 would affect ATR signaling. Would this ETAA1-RAD9 fusion protein be able to promote phosphorylation of substrates that were normally dependent on TOPBP1. Would the ETAA1 fusion protein localize to sites of RS earlier like TOPBP1 or later like ETAA1? Such experiments would provide needed details about how each ATR activator is regulated and the determinants of which activator is utilized.

Comparing ETAA1 and TOPBP1 substrate specificity

An additional route of study would be to examine if ETAA1 is indeed required for DNA lesions that lack 5' junctions. To examine ETAA1 dependency, one could monitor dependence on ETAA1 at resected double strand breaks and R-loops. Double strand breaks could be induced by CPT treatment or irradiating cells synchronized in S-phase. The extent of resection could be modulated by siRNAs to genes that positively or negatively regulate resection such as BRCA1 (breast cancer type 1 susceptibility protein) and 53BP1 (p53 binding protein 1) (Cruz-García et al., 2014; Bunting et al., 2010; Daley and Sung, 2014), and examine ATR signaling in cells deficient for ETAA1 or TOPBP1. Overexpression of nucleases may also increase the amount of resection, leading to increased ETAA1 dependency for ATR signaling.

To investigate the requirement for ETAA1 at R-loops, I would examine ETAA1 and TOPBP1 localization to R-loops using immunofluorescence, proximity ligation assays, and immunoprecipitations. R-loops can be detected by an antibody, S9.6, that specifically recognizes DNA:RNA hybrids to facilitate these experiments (Boguslawski et al., 1986). As previously mentioned, ATR recruitment to centromeric regions is dependent on R-loop formation and this may explain the dependency for ETAA1 activation during mitosis. I would examine if ETAA1 localization to centromeres is also dependent on R-loops, or alternatively, if ETAA1 utilizes an interaction with one of its mitotic interaction partners for its localization.

To determine the DNA substrate specificity of ETAA1, one could also examine ATR activation in *Xenopus* egg extracts after addition of predefined DNA substrates. Different ATR activating structures can be produced by annealing oligos to ssDNA plasmids such as M13 (MacDougall et al., 2007; Duursma et al., 2013). Biotinylation of oligos can block 5' or 3' ends and oligos can be spaced to alter the amount of ssDNA on the plasmids. Similar approaches in *Xenopus* extracts have shown that although a 5' end is required for checkpoint activation, the amount of ssDNA adjacent to the junction results in increased CHK1 phosphorylation (MacDougall et al., 2007). I believe this may reflect an initial requirement for TOPBP1-dependent ATR activation but propagation of signaling as ETAA1 continues to activate ATR accumulated along the ssDNA. Immunodepletion of ETAA1 may prevent a further increase in CHK1 phosphorylation as the amount of ssDNA next to a primer is extended. Furthermore, if ETAA1 regulation by phosphorylation is a conserved mechanism, it would be interesting to examine if addition of phosphomimetic ETAA1 would activate structures without a 5' junction.

Conclusions

The findings in this dissertation have contributed to the field of replication stress signaling and expanded our models for ATR activation. In Chapter III, I identified the previously uncharacterized protein, ETAA1 as a novel ATR activator and demonstrated that it functioned in a pathway independent from TOPBP1. In Chapter IV, I used quantitative phosphoproteomics to examine how ETAA1 and TOPBP1 direct ATR signaling and revealed a unique function of ETAA1 to promote mitotic ATR signaling at centromeric regions.

Future studies may investigate some of the proposed models for how ETAA1 and TOPBP1 differentially regulate ATR signaling. Although these pathways function independently,

there may be some crosstalk between pathways regulating ETAA1 function. Additionally, a combination of *in vivo* and *in vitro* systems may be able to determine if ATR preferentially utilizes each activator at different DNA substrates.

REFERENCES

Ammazzalorso, F., L.M. Pirzio, M. Bignami, A. Franchitto, and P. Pichierri. 2010. ATR and ATM differently regulate WRN to prevent DSBs at stalled replication forks and promote replication fork recovery. *EMBO J.* 29:3156–69. doi:10.1038/emboj.2010.205.

Anantha, R.W., V.M. Vassin, and J.A. Borowiec. 2007. Sequential and synergistic modification of human RPA stimulates chromosomal DNA repair. *J. Biol. Chem.* 282:35910–23. doi:10.1074/jbc.M704645200.

Araki, H., S.H. Leem, A. Phongdara, and A. Sugino. 1995. Dpb11, which interacts with DNA polymerase II(epsilon) in Saccharomyces cerevisiae, has a dual role in S-phase progression and at a cell cycle checkpoint. *Proc. Natl. Acad. Sci. U. S. A.* 92:11791–5. doi:10.1073/PNAS.92.25.11791.

Bakkenist, C.J., and M.B. Kastan. 2003. DNA damage activates ATM through intermolecular autophosphorylation and dimer dissociation. *Nature*. 421:499–506. doi:10.1038/nature01368.

Ball, H.L., and D. Cortez. 2005. ATRIP Oligomerization Is Required for ATR-dependent Checkpoint Signaling. *J. Biol. Chem.* 280:31390–31396. doi:10.1074/jbc.M504961200.

Ball, H.L., M.R. Ehrhardt, D.A. Mordes, G.G. Glick, W.J. Chazin, and D. Cortez. 2007. Function of a conserved checkpoint recruitment domain in ATRIP proteins. *Mol. Cell. Biol.* 27:3367–77. doi:10.1128/MCB.02238-06.

Ball, H.L., J.S. Myers, and D. Cortez. 2005. ATRIP Binding to Replication Protein A-Single-stranded DNA Promotes ATR – ATRIP Localization but Is Dispensable for Chk1 Phosphorylation. 16:2372–2381. doi:10.1091/mbc.E04.

Bandhu, A., J. Kang, K. Fukunaga, G. Goto, and K. Sugimoto. 2014. Ddc2 mediates Mec1 activation through a Ddc1- or Dpb11-independent mechanism. *PLoS Genet.* 10:e1004136. doi:10.1371/journal.pgen.1004136.

Banin, S., L. Moyal, S. Shieh, Y. Taya, C.W. Anderson, L. Chessa, N.I. Smorodinsky, C. Prives, Y. Reiss, Y. Shiloh, and Y. Ziv. 1998. Enhanced phosphorylation of p53 by ATM in response to DNA damage. *Science*. 281:1674–7.

Bansbach, C.E., R. Bétous, C.A. Lovejoy, G.G. Glick, and D. Cortez. 2009. The annealing helicase SMARCAL1 maintains genome integrity at stalled replication forks. *Genes Dev.* 23:2405–2414.

Baretić, D., and R.L. Williams. 2014. PIKKs--the solenoid nest where partners and kinases meet. *Curr. Opin. Struct. Biol.* 29:134–42. doi:10.1016/j.sbi.2014.11.003.

Bass, T.E., J.W. Luzwick, G. Kavanaugh, C. Carroll, H. Dungrawala, G.G. Glick, M.D. Feldkamp, R. Putney, W.J. Chazin, and D. Cortez. 2016. ETAA1 acts at stalled replication forks to maintain genome integrity. *Nat. Cell Biol.* 18:1185–1195. doi:10.1038/ncb3415.

Bastos de Oliveira, F.M., D. Kim, J.R. Cussiol, J. Das, M.C. Jeong, L. Doerfler, K.H. Schmidt, H. Yu, and M.B. Smolka. 2015. Phosphoproteomics Reveals Distinct Modes of Mec1/ATR Signaling during DNA Replication. 57. 1124-1132 pp.

Bennetzen, M. V, D.H. Larsen, J. Bunkenborg, J. Bartek, J. Lukas, and J.S. Andersen. 2010.

Site-specific phosphorylation dynamics of the nuclear proteome during the DNA damage response. *Mol. Cell. Proteomics*. 9:1314–23. doi:10.1074/mcp.M900616-MCP200.

Bindea, G., B. Mlecnik, H. Hackl, P. Charoentong, M. Tosolini, A. Kirilovsky, W.-H. Fridman, F. Pagès, Z. Trajanoski, and J. Galon. 2009. ClueGO: a Cytoscape plug-in to decipher functionally grouped gene ontology and pathway annotation networks. *Bioinformatics*. 25:1091–3. doi:10.1093/bioinformatics/btp101.

Blackford, A.N., and S.P. Jackson. 2017. ATM, ATR, and DNA-PK: The Trinity at the Heart of the DNA Damage Response. *Mol. Cell*. 66:801–817. doi:10.1016/J.MOLCEL.2017.05.015.

Blackford, A.N., J. Nieminuszczy, R.A. Schwab, Y. Galanty, S.P. Jackson, and W. Niedzwiedz. 2015. TopBP1 interacts with BLM to maintain genome stability but is dispensable for preventing BLM degradation. *Mol. Cell*. 57:1133–41. doi:10.1016/j.molcel.2015.02.012.

Boerkoel, C.F., H. Takashima, J. John, J. Yan, P. Stankiewicz, L. Rosenbarker, J.-L. André, R. Bogdanovic, A. Burguet, S. Cockfield, I. Cordeiro, S. Fründ, F. Illies, M. Joseph, I. Kaitila, G. Lama, C. Loirat, D.R. McLeod, D. V. Milford, E.M. Petty, F. Rodrigo, J.M. Saraiva, B. Schmidt, G.C. Smith, J. Spranger, A. Stein, H. Thiele, J. Tizard, R. Weksberg, J.R. Lupski, and D.W. Stockton. 2002. Mutant chromatin remodeling protein SMARCAL1 causes Schimke immuno-osseous dysplasia. *Nat. Genet.* 30:215–220. doi:10.1038/ng821.

Boguslawski, S.J., D.E. Smith, M.A. Michalak, K.E. Mickelson, C.O. Yehle, W.L. Patterson, and R.J. Carrico. 1986. Characterization of monoclonal antibody to DNA · RNA and its application to immunodetection of hybrids. *J. Immunol. Methods*. 89:123–130. doi:10.1016/0022-1759(86)90040-2.

Bolderson, E., N. Tomimatsu, D.J. Richard, D. Boucher, R. Kumar, T.K. Pandita, S. Burma, and K.K. Khanna. 2010. Phosphorylation of Exo1 modulates homologous recombination repair of DNA double-strand breaks. *Nucleic Acids Res.* 38:1821. doi:10.1093/NAR/GKP1164.

Borowski, A., U. Dirksen, L. Lixin, R.L. Shi, U. Göbel, and E.M. Schneider. 2006. Structure and function of ETAA16: a novel cell surface antigen in Ewing's tumours. *Cancer Immunol. Immunother.* 55:363–74. doi:10.1007/s00262-005-0017-6.

Bray, F., J. Ferlay, I. Soerjomataram, R.L. Siegel, L.A. Torre, and A. Jemal. 2018. Global cancer statistics 2018: GLOBOCAN estimates of incidence and mortality worldwide for 36 cancers in 185 countries. *CA. Cancer J. Clin.* doi:10.3322/caac.21492.

Broderick, R., J. Nieminuszczy, A.N. Blackford, A. Winczura, and W. Niedzwiedz. 2015. TOPBP1 recruits TOP2A to ultra-fine anaphase bridges to aid in their resolution. *Nat. Commun.* 6:6572. doi:10.1038/ncomms7572.

Brosh, R.M., J.L. Li, M.K. Kenny, J.K. Karow, M.P. Cooper, R.P. Kureekattil, I.D. Hickson, and V. a Bohr. 2000. Replication protein A physically interacts with the Bloom's syndrome protein and stimulates its helicase activity. *J. Biol. Chem.* 275:23500–8. doi:10.1074/jbc.M001557200.

Bunting, S.F., E. Callén, N. Wong, H.-T. Chen, F. Polato, A. Gunn, A. Bothmer, N. Feldhahn, O. Fernandez-Capetillo, L. Cao, X. Xu, C.-X. Deng, T. Finkel, M. Nussenzweig, J.M. Stark, and A. Nussenzweig. 2010. 53BP1 Inhibits Homologous Recombination in Brca1-Deficient Cells by Blocking Resection of DNA Breaks. *Cell*. 141:243–254. doi:10.1016/j.cell.2010.03.012.

Bussen, W., S. Raynard, V. Busygina, A.K. Singh, and P. Sung. 2007. Holliday junction

processing activity of the BLM-Topo IIIalpha-BLAP75 complex. *J. Biol. Chem.* 282:31484–92. doi:10.1074/jbc.M706116200.

Carr, A.M., A.L. Paek, and T. Weinert. 2011. DNA replication: Failures and inverted fusions. *Semin. Cell Dev. Biol.* 22:866–874. doi:10.1016/J.SEMCDB.2011.10.008.

Carroll, C., A. Badu-Nkansah, T. Hunley, A. Baradaran-Heravi, D. Cortez, and H. Frangoul. 2013. Schimke Immunoosseous Dysplasia associated with undifferentiated carcinoma and a novel SMARCAL1 mutation in a child. *Pediatr. Blood Cancer*. 60:E88-90. doi:10.1002/pbc.24542.

Chaganti, R.S., S. Schonberg, and J. German. 1974. A manyfold increase in sister chromatid exchanges in Bloom's syndrome lymphocytes. *Proc. Natl. Acad. Sci. U. S. A.* 71:4508–12.

Chan, D.W., B.P.-C. Chen, S. Prithivirajsingh, A. Kurimasa, M.D. Story, J. Qin, and D.J. Chen. 2002. Autophosphorylation of the DNA-dependent protein kinase catalytic subunit is required for rejoining of DNA double-strand breaks. *Genes Dev.* 16:2333–8. doi:10.1101/gad.1015202.

Chaturvedi, R., M. Asim, M.B. Piazuelo, F. Yan, D.P. Barry, J.C. Sierra, A.G. Delgado, S. Hill, R.A. Casero, L.E. Bravo, R.L. Dominguez, P. Correa, D.B. Polk, M.K. Washington, K.L. Rose, K.L. Schey, D.R. Morgan, R.M. Peek, and K.T. Wilson. 2014. Activation of EGFR and ERBB2 by Helicobacter pylori Results in Survival of Gastric Epithelial Cells With DNA Damage. *Gastroenterology*. 146:1739–1751.e14. doi:10.1053/j.gastro.2014.02.005.

Childs, E.J., E. Mocci, D. Campa, P.M. Bracci, S. Gallinger, M. Goggins, D. Li, R.E. Neale, S.H. Olson, G. Scelo, L.T. Amundadottir, W.R. Bamlet, M.F. Bijlsma, A. Blackford, M. Borges, P. Brennan, H. Brenner, H.B. Bueno-de-Mesquita, F. Canzian, G. Capurso, G.M. Cavestro, K.G. Chaffee, S.J. Chanock, S.P. Cleary, M. Cotterchio, L. Foretova, C. Fuchs, N. Funel, M. Gazouli, M. Hassan, J.M. Herman, I. Holcatova, E.A. Holly, R.N. Hoover, R.J. Hung, V. Janout, T.J. Key, J. Kupcinskas, R.C. Kurtz, S. Landi, L. Lu, E. Malecka-Panas, A. Mambrini, B. Mohelnikova-Duchonova, J.P. Neoptolemos, A.L. Oberg, I. Orlow, C. Pasquali, R. Pezzilli, C. Rizzato, A. Saldia, A. Scarpa, R.Z. Stolzenberg-Solomon, O. Strobel, F. Tavano, Y.K. Vashist, P. Vodicka, B.M. Wolpin, H. Yu, G.M. Petersen, H.A. Risch, and A.P. Klein. 2015a. Common variation at 2p13.3, 3q29, 7p13 and 17q25.1 associated with susceptibility to pancreatic cancer. *Nat. Genet.* 47:911–916. doi:10.1038/ng.3341.

Childs, E.J., E. Mocci, D. Campa, P.M. Bracci, S. Gallinger, M. Goggins, D. Li, R.E. Neale, S.H. Olson, G. Scelo, L.T. Amundadottir, W.R. Bamlet, M.F. Bijlsma, A. Blackford, M. Borges, P. Brennan, H. Brenner, H.B. Bueno-de-Mesquita, F. Canzian, G. Capurso, G.M. Cavestro, K.G. Chaffee, S.J. Chanock, S.P. Cleary, M. Cotterchio, L. Foretova, C. Fuchs, N. Funel, M. Gazouli, M. Hassan, J.M. Herman, I. Holcatova, E.A. Holly, R.N. Hoover, R.J. Hung, V. Janout, T.J. Key, J. Kupcinskas, R.C. Kurtz, S. Landi, L. Lu, E. Malecka-Panas, A. Mambrini, B. Mohelnikova-Duchonova, J.P. Neoptolemos, A.L. Oberg, I. Orlow, C. Pasquali, R. Pezzilli, C. Rizzato, A. Saldia, A. Scarpa, R.Z. Stolzenberg-Solomon, O. Strobel, F. Tavano, Y.K. Vashist, P. Vodicka, B.M. Wolpin, H. Yu, G.M. Petersen, H.A. Risch, and A.P. Klein. 2015b. Common variation at 2p13.3, 3q29, 7p13 and 17q25.1 associated with susceptibility to pancreatic cancer. *Nat. Genet.* 47:911–6. doi:10.1038/ng.3341.

Chiruvella, K.K., Z. Liang, and T.E. Wilson. 2013. Repair of Double-Strand Breaks by End Joining. *Cold Spring Harb. Perspect. Biol.* 5. doi:10.1101/CSHPERSPECT.A012757.

Ciccia, A., A.L. Bredemeyer, M.E. Sowa, M.-E. Terret, P. V Jallepalli, J.W. Harper, and S.J. Elledge. 2009. The SIOD disorder protein SMARCAL1 is an RPA-interacting protein involved in replication fork restart. *Genes Dev.* 23:2415–25. doi:10.1101/gad.1832309.

Ciccia, A., and S.J. Elledge. 2010. The DNA damage response: making it safe to play with knives. *Mol. Cell*. 40:179–204. doi:10.1016/j.molcel.2010.09.019.

Ciccia, A., A. V Nimonkar, Y. Hu, I. Hajdu, Y.J. Achar, L. Izhar, S. a Petit, B. Adamson, J.C. Yoon, S.C. Kowalczykowski, D.M. Livingston, L. Haracska, and S.J. Elledge. 2012. Polyubiquitinated PCNA recruits the ZRANB3 translocase to maintain genomic integrity after replication stress. *Mol. Cell*. 47:396–409. doi:10.1016/j.molcel.2012.05.024.

Cimprich, K. a, and D. Cortez. 2008. ATR: an essential regulator of genome integrity. *Nat. Rev. Mol. Cell Biol.* 9:616–27. doi:10.1038/nrm2450.

Colaert, N., K. Helsens, L. Martens, J. Vandekerckhove, and K. Gevaert. 2009. Improved visualization of protein consensus sequences by iceLogo. *Nat. Methods*. 6:786–787. doi:10.1038/nmeth1109-786.

Collura, A., J. Blaisonneau, G. Baldacci, and S. Francesconi. 2005. The fission yeast Crb2/Chk1 pathway coordinates the DNA damage and spindle checkpoint in response to replication stress induced by topoisomerase I inhibitor. *Mol. Cell. Biol.* 25:7889–99. doi:10.1128/MCB.25.17.7889-7899.2005.

Cook, J.G. 2009. Replication licensing and the DNA damage checkpoint. *Front. Biosci. (Landmark Ed.* 14:5013–30.

Cortez, D., S. Guntuku, J. Qin, S.J. Elledge, D. Durocher, S.P. Jackson, Y. Shiloh, K.A. Cimprich, T.B. Shin, C.T. Keith, S.L. Schreiber, E.J. Brown, D. Baltimore, R.J. Edwards, N.J. Bentley, A.M. Carr, V. Paciotti, M. Clerici, G. Lucchini, M.P. Longhese, J. Rouse, S.P. Jackson, T. Wakayama, T. Kondo, S. Ando, K. Matsumoto, K. Sugimoto, M.H. Brodsky, J.J. Sekelsky, G. Tsang, R.S. Hawley, G.M. Rubin, B.A. Desany, A.A. Alcasabas, J.B. Bachant, S.J. Elledge, X. Zhao, E.G. Muller, R. Rothstein, B. Xu, S. Kim, and M.B. Kastan. 2001. ATR and ATRIP: partners in checkpoint signaling. *Science*. 294:1713–6. doi:10.1126/science.1065521.

Costanzo, V., D. Shechter, P.J. Lupardus, K.A. Cimprich, M. Gottesman, and J. Gautier. 2003. An ATR- and Cdc7-Dependent DNA Damage Checkpoint that Inhibits Initiation of DNA Replication. *Mol. Cell*. 11:203–213. doi:10.1016/S1097-2765(02)00799-2.

Cotta-Ramusino, C., E.R.M. 3, 3rd, K. Hurov, M.E. Sowa, J.W. Harper, and S.J. Elledge. 2011. A DNA Damage Response Screen Identifies RHINO: a 9-1-1 and TopBP1 interacting protein required for ATR signaling. *Science*. 332:1313. doi:10.1126/SCIENCE.1203430.

Couch, F., and C. Bansbach. 2013. ATR phosphorylates SMARCAL1 to prevent replication fork collapse. *Genes …*. 1610–1623. doi:10.1101/gad.214080.113.to.

Cox, J., and M. Mann. 2008. MaxQuant enables high peptide identification rates, individualized p.p.b.-range mass accuracies and proteome-wide protein quantification. *Nat. Biotechnol.* 26:1367–1372. doi:10.1038/nbt.1511.

Cox, J., N. Neuhauser, A. Michalski, R.A. Scheltema, J. V. Olsen, and M. Mann. 2011. Andromeda: A Peptide Search Engine Integrated into the MaxQuant Environment. *J. Proteome Res.* 10:1794–1805. doi:10.1021/pr101065j.

Croteau, D.L., V. Popuri, P.L. Opresko, and V.A. Bohr. 2014. Human RecQ helicases in DNA

repair, recombination, and replication. *Annu. Rev. Biochem.* 83:519–52. doi:10.1146/annurev-biochem-060713-035428.

Cruz-García, A., A. López-Saavedra, and P. Huertas. 2014. BRCA1 Accelerates CtIP-Mediated DNA-End Resection. *Cell Rep.* 9:451–459. doi:10.1016/J.CELREP.2014.08.076.

Daley, J.M., and P. Sung. 2014. 53BP1, BRCA1, and the choice between recombination and end joining at DNA double-strand breaks. *Mol. Cell. Biol.* 34:1380–8. doi:10.1128/MCB.01639-13.

Deckbar, D., P.A. Jeggo, and M. Löbrich. 2011. Understanding the limitations of radiation-induced cell cycle checkpoints. *Crit. Rev. Biochem. Mol. Biol.* 46:271–83. doi:10.3109/10409238.2011.575764.

Delacroix, S., J.M. Wagner, M. Kobayashi, K. -i. Yamamoto, and L.M. Karnitz. 2007a. The Rad9-Hus1-Rad1 (9-1-1) clamp activates checkpoint signaling via TopBP1. *Genes Dev.* 21:1472–1477. doi:10.1101/gad.1547007.

Delacroix, S., J.M. Wagner, M. Kobayashi, K. Yamamoto, and L.M. Karnitz. 2007b. The Rad9-Hus1-Rad1 (9-1-1) clamp activates checkpoint signaling via TopBP1. *Genes Dev.* 21:1472–7. doi:10.1101/gad.1547007.

Deshpande, I., A. Seeber, K. Shimada, J.J. Keusch, H. Gut, and S.M. Gasser. 2017. Structural Basis of Mec1-Ddc2-RPA Assembly and Activation on Single-Stranded DNA at Sites of Damage. *Mol. Cell*. 68:431–445.e5. doi:10.1016/j.molcel.2017.09.019.

Dungrawala, H., K.P. Bhat, R. Le Meur, W.J. Chazin, X. Ding, S.K. Sharan, S.R. Wessel, A.A. Sathe, R. Zhao, and D. Cortez. 2017. RADX Promotes Genome Stability and Modulates Chemosensitivity by Regulating RAD51 at Replication Forks. *Mol. Cell*. 67:374–386.e5. doi:10.1016/J.MOLCEL.2017.06.023.

Dungrawala, H., and D. Cortez. 2015. Purification of proteins on newly synthesized DNA using iPOND. *Methods Mol. Biol.* 1228:123–31. doi:10.1007/978-1-4939-1680-1_10.

Dungrawala, H., K.L. Rose, K.P. Bhat, K.N. Mohni, G.G. Glick, F.B. Couch, and D. Cortez. 2015. The Replication Checkpoint Prevents Two Types of Fork Collapse without Regulating Replisome Stability. *Mol. Cell*. 59:998–1010. doi:10.1016/j.molcel.2015.07.030.

Duursma, A.M., R. Driscoll, J.E. Elias, and K.A. Cimprich. 2013. A role for the MRN complex in ATR activation via TOPBP1 recruitment. *Mol. Cell*. 50:116–22. doi:10.1016/j.molcel.2013.03.006.

Ellis, N.A., J. Groden, T.-Z. Ye, J. Straughen, D.J. Lennon, S. Ciocci, M. Proytcheva, and J. German. 1995. The Bloom's syndrome gene product is homologous to RecQ helicases. *Cell*. 83:655–666. doi:10.1016/0092-8674(95)90105-1.

Ellison, V., and B. Stillman. 2003. Biochemical characterization of DNA damage checkpoint complexes: clamp loader and clamp complexes with specificity for 5' recessed DNA. *PLoS Biol.* 1:E33. doi:10.1371/journal.pbio.0000033.

Fanning, E., V. Klimovich, and A.R. Nager. 2006. A dynamic model for replication protein A (RPA) function in DNA processing pathways. *Nucleic Acids Res.* 34:4126–37. doi:10.1093/nar/gkl550.

Feldkamp, M.D., A.C. Mason, B.F. Eichman, and W.J. Chazin. 2014. Structural analysis of replication protein A recruitment of the DNA damage response protein SMARCAL1.

Biochemistry. 53:3052–61. doi:10.1021/bi500252w.

Feng, S., Y. Zhao, Y. Xu, S. Ning, W. Huo, M. Hou, G. Gao, J. Ji, R. Guo, and D. Xu. 2016. Ewing Tumor-associated Antigen 1 Interacts with Replication Protein A to Promote Restart of Stalled Replication Forks. *J. Biol. Chem.* 291:21956–21962. doi:10.1074/jbc.C116.747758.

Gan, W., Z. Guan, J. Liu, T. Gui, K. Shen, J.L. Manley, and X. Li. 2011. R-loop-mediated genomic instability is caused by impairment of replication fork progression. *Genes Dev.* 25:2041–56. doi:10.1101/gad.17010011.

Garcia, V., K. Furuya, and A.M. Carr. 2005. Identification and functional analysis of TopBP1 and its homologs. *DNA Repair (Amst).* 4:1227–1239. doi:10.1016/J.DNAREP.2005.04.001.

Ge, X.Q., and J.J. Blow. 2010. Chk1 inhibits replication factory activation but allows dormant origin firing in existing factories. *J. Cell Biol.* 191:1285–97. doi:10.1083/jcb.201007074.

German, J., and B. Alhadeff. 2001. Analysis of sister-chromatid exchanges. *Curr. Protoc. Hum. Genet.* Chapter 8:Unit 8.6. doi:10.1002/0471142905.hg0806s02.

Germann, S.M., V. Schramke, R.T. Pedersen, I. Gallina, N. Eckert-Boulet, V.H. Oestergaard, and M. Lisby. 2014. TopBP1/Dpb11 binds DNA anaphase bridges to prevent genome instability. *J. Cell Biol.* 204:45–59. doi:10.1083/jcb.201305157.

Gobbini, E., D. Cesena, A. Galbiati, A. Lockhart, and M.P. Longhese. 2013. Interplays between ATM/Tel1 and ATR/Mec1 in sensing and signaling DNA double-strand breaks. *DNA Repair (Amst).* 12:791–799. doi:10.1016/J.DNAREP.2013.07.009.

Goodwin, J.F., V. Kothari, J.M. Drake, S. Zhao, E. Dylgjeri, J.L. Dean, M.J. Schiewer, C. McNair, J.K. Jones, A. Aytes, M.S. Magee, A.E. Snook, Z. Zhu, R.B. Den, R.C. Birbe, L.G. Gomella, N.A. Graham, A.A. Vashisht, J.A. Wohlschlegel, T.G. Graeber, R.J. Karnes, M. Takhar, E. Davicioni, S.A. Tomlins, C. Abate-Shen, N. Sharifi, O.N. Witte, F.Y. Feng, and K.E. Knudsen. 2015. DNA-PKcs-Mediated Transcriptional Regulation Drives Prostate Cancer Progression and Metastasis. *Cancer Cell*. 28:97–113. doi:10.1016/J.CCELL.2015.06.004.

Gottlieb, T.M., and S.P. Jackson. 1993. The DNA-dependent protein kinase: Requirement for DNA ends and association with Ku antigen. *Cell*. 72:131–142. doi:10.1016/0092-8674(93)90057-W.

Haahr, P., S. Hoffmann, M.A.X. Tollenaere, T. Ho, L.I. Toledo, M. Mann, S. Bekker-Jensen, M. Räschle, and N. Mailand. 2016. Activation of the ATR kinase by the RPA-binding protein ETAA1. *Nat. Cell Biol.* 18:1196–1207. doi:10.1038/ncb3422.

Hoeijmakers, J.H.J. 2009. DNA Damage, Aging, and Cancer. *N. Engl. J. Med.* 361:1475–1485. doi:10.1056/NEJMra0804615.

Imseng, S., and C.H. Aylett. 2018. Architecture and activation of phosphatidylinositol 3-kinase related kinases. *Curr. Opin. Struct. Biol.* 49:177–189. doi:10.1016/J.SBI.2018.03.010.

Itakura, E., I. Sawada, and A. Matsuura. 2005. Dimerization of the ATRIP protein through the coiled-coil motif and its implication to the maintenance of stalled replication forks. *Mol. Biol. Cell*. 16:5551–62. doi:10.1091/mbc.e05-05-0427.

Jackson, S.P., and J. Bartek. 2009. The DNA-damage response in human biology and disease. *Nature*. 461:1071–8. doi:10.1038/nature08467.

Kabeche, L., H.D. Nguyen, R. Buisson, and L. Zou. 2017. A mitosis-specific and R loop-driven ATR pathway promotes faithful chromosome segregation. *Science*. eaan6490. doi:10.1126/science.aan6490.

Kaelin, W.G. 2005. The Concept of Synthetic Lethality in the Context of Anticancer Therapy. *Nat. Rev. Cancer*. 5:689–698. doi:10.1038/nrc1691.

Karlsson-Rosenthal, C., and J.B.A. Millar. 2006. Cdc25: mechanisms of checkpoint inhibition and recovery. *Trends Cell Biol.* 16:285–92. doi:10.1016/j.tcb.2006.04.002.

Kile, A.C., D.A. Chavez, J. Bacal, S. Eldirany, D.M. Korzhnev, I. Bezsonova, B.F. Eichman, and K.A. Cimprich. 2015. HLTF's Ancient HIRAN Domain Binds 3' DNA Ends to Drive Replication Fork Reversal. *Mol. Cell*. 58:1090–100. doi:10.1016/j.molcel.2015.05.013.

Kim, S.T., D.S. Lim, C.E. Canman, and M.B. Kastan. 1999. Substrate specificities and identification of putative substrates of ATM kinase family members. *J. Biol. Chem.* 274:37538–43. doi:10.1074/JBC.274.53.37538.

Klein, A.P., B.M. Wolpin, H.A. Risch, R.Z. Stolzenberg-Solomon, E. Mocci, M. Zhang, F. Canzian, E.J. Childs, J.W. Hoskins, A. Jermusyk, J. Zhong, F. Chen, D. Albanes, G. Andreotti, A.A. Arslan, A. Babic, W.R. Bamlet, L. Beane-Freeman, S.I. Berndt, A. Blackford, M. Borges, A. Borgida, P.M. Bracci, L. Brais, P. Brennan, H. Brenner, B. Bueno-de-Mesquita, J. Buring, D. Campa, G. Capurso, G.M. Cavestro, K.G. Chaffee, C.C. Chung, S. Cleary, M. Cotterchio, F. Dijk, E.J. Duell, L. Foretova, C. Fuchs, N. Funel, S. Gallinger, J.M. M. Gaziano, M. Gazouli, G.G. Giles, E. Giovannucci, M. Goggins, G.E. Goodman, P.J. Goodman, T. Hackert, C. Haiman, P. Hartge, M. Hasan, P. Hegyi, K.J. Helzlsouer, J. Herman, I. Holcatova, E.A. Holly, R. Hoover, R.J. Hung, E.J. Jacobs, K. Jamroziak, V. Janout, R. Kaaks, K.-T. Khaw, E.A. Klein, M. Kogevinas, C. Kooperberg, M.H. Kulke, J. Kupcinskas, R.J. Kurtz, D. Laheru, S. Landi, R.T. Lawlor, I.-M. Lee, L. LeMarchand, L. Lu, N. Malats, A. Mambrini, S. Mannisto, R.L. Milne, B. Mohelníková-Duchoňová, R.E. Neale, J.P. Neoptolemos, A.L. Oberg, S.H. Olson, I. Orlow, C. Pasquali, A. V. Patel, U. Peters, R. Pezzilli, M. Porta, F.X. Real, N. Rothman, G. Scelo, H.D. Sesso, G. Severi, X.-O. Shu, D. Silverman, et al. 2018. Genome-wide meta-analysis identifies five new susceptibility loci for pancreatic cancer. *Nat. Commun.* 9:556. doi:10.1038/s41467-018-02942-5.

Krenn, V., and A. Musacchio. 2015. The Aurora B Kinase in Chromosome Bi-Orientation and Spindle Checkpoint Signaling. *Front. Oncol.* 5:225. doi:10.3389/fonc.2015.00225.

Kumagai, A., and W.G. Dunphy. 2000. Claspin, a Novel Protein Required for the Activation of Chk1 during a DNA Replication Checkpoint Response in Xenopus Egg Extracts. *Mol. Cell*. 6:839–849. doi:10.1016/S1097-2765(05)00092-4.

Kumagai, A., J. Lee, H.Y. Yoo, and W.G. Dunphy. 2006. TopBP1 activates the ATR-ATRIP complex. *Cell*. 124:943–55. doi:10.1016/j.cell.2005.12.041.

Kumar, S., and P.M. Burgers. 2013. Lagging strand maturation factor Dna2 is a component of the replication checkpoint initiation machinery. *Genes Dev.* 27:313–21. doi:10.1101/gad.204750.112.

Lanz, M.C., S. Oberly, E.J. Sanford, S. Sharma, A. Chabes, and M.B. Smolka. 2018. Separable roles for Mec1/ATR in genome maintenance, DNA replication, and checkpoint signaling. *Genes Dev.* 32:822–835. doi:10.1101/gad.308148.117.

Lara-Gonzalez, P., F.G. Westhorpe, and S.S. Taylor. 2012. The Spindle Assembly Checkpoint. *Curr. Biol.* 22:R966–R980. doi:10.1016/J.CUB.2012.10.006.

Lee, J.-H., and T.T. Paull. 2005. Direct Activation of the ATM Protein Kinase by the Mre11/Rad50/Nbs1 Complex. *Science (80-.).* 304:93–96. doi:10.1126/science.1091496.

Lee, J., A. Kumagai, and W.G. Dunphy. 2007a. The Rad9-Hus1-Rad1 Checkpoint Clamp Regulates Interaction of TopBP1 with ATR. *J. Biol. Chem.* 282:28036–28044. doi:10.1074/jbc.M704635200.

Lee, J., A. Kumagai, and W.G. Dunphy. 2007b. The Rad9-Hus1-Rad1 Checkpoint Clamp Regulates Interaction of TopBP1 with ATR. *J. Biol. Chem.* 282:28036–28044. doi:10.1074/JBC.M704635200.

Lee, Y.-C., Q. Zhou, J. Chen, and J. Yuan. 2016. RPA-Binding Protein ETAA1 Is an ATR Activator Involved in DNA Replication Stress Response. *Curr. Biol.* 26:3257–3268. doi:10.1016/j.cub.2016.10.030.

Lin, J.J., and A. Dutta. 2007. ATR pathway is the primary pathway for activating G2/M checkpoint induction after re-replication. *J. Biol. Chem.* 282:30357–62. doi:10.1074/jbc.M705178200.

Lindsey-Boltz, L.A., M.G. Kemp, C. Capp, and A. Sancar. 2015. RHINO forms a stoichiometric complex with the 9-1-1 checkpoint clamp and mediates ATR-Chk1 signaling. *Cell Cycle*. 14:99–108. doi:10.4161/15384101.2014.967076.

Liu, S., B. Shiotani, M. Lahiri, A. Maréchal, A. Tse, C.C.Y. Leung, J.N.M. Glover, X.H. Yang, and L. Zou. 2011. ATR autophosphorylation as a molecular switch for checkpoint activation. *Mol. Cell*. 43:192–202. doi:10.1016/j.molcel.2011.06.019.

Lovejoy, C.A., and D. Cortez. 2009. Common mechanisms of PIKK regulation. *DNA Repair (Amst).* 8:1004–8. doi:10.1016/j.dnarep.2009.04.006.

Lovejoy, C.A., X. Xu, C.E. Bansbach, G.G. Glick, R. Zhao, F. Ye, B.M. Sirbu, L.C. Titus, Y. Shyr, and D. Cortez. 2009. Functional genomic screens identify CINP as a genome maintenance protein. *Proc. Natl. Acad. Sci. U. S. A.* 106:19304–9. doi:10.1073/pnas.0909345106.

Lukas, J., C. Lukas, and J. Bartek. 2004. Mammalian cell cycle checkpoints: signalling pathways and their organization in space and time. *DNA Repair (Amst).* 3:997–1007. doi:10.1016/J.DNAREP.2004.03.006.

MacDougall, C.A., T.S. Byun, C. Van, M. Yee, and K.A. Cimprich. 2007. The structural determinants of checkpoint activation. *Genes Dev.* 21:898–903. doi:10.1101/gad.1522607.

Macheret, M., and T.D. Halazonetis. 2015. DNA Replication Stress as a Hallmark of Cancer. *Annu. Rev. Pathol. Mech. Dis.* 10:425–448. doi:10.1146/annurev-pathol-012414-040424.

Mahaney, B.L., K. Meek, and S.P. Lees-Miller. 2009. Repair of ionizing radiation-induced DNA double strand breaks by non-homologous end-joining. *Biochem. J.* 417:639. doi:10.1042/BJ20080413.

Mailand, N., J. Falck, C. Lukas, R.G. Syljuâsen, M. Welcker, J. Bartek, and J. Lukas. 2000. Rapid destruction of human Cdc25A in response to DNA damage. *Science*. 288:1425–9.

Majka, J., S.K. Binz, M.S. Wold, and P.M.J. Burgers. 2006. Replication protein A directs loading of the DNA damage checkpoint clamp to 5'-DNA junctions. *J. Biol. Chem.* 281:27855–61. doi:10.1074/jbc.M605176200.

Matsuoka, S., B.A. Ballif, A. Smogorzewska, E.R. McDonald, K.E. Hurov, J. Luo, C.E. Bakalarski, Z. Zhao, N. Solimini, Y. Lerenthal, Y. Shiloh, S.P. Gygi, and S.J. Elledge. 2007. ATM and ATR substrate analysis reveals extensive protein networks responsive to DNA damage. *Science*. 316:1160–6. doi:10.1126/science.1140321.

McIntosh, D., and J.J. Blow. 2012. Dormant origins, the licensing checkpoint, and the response to replicative stresses. *Cold Spring Harb. Perspect. Biol.* 4. doi:10.1101/cshperspect.a012955.

Mehta, A., and J.E. Haber. 2014. Sources of DNA Double-Strand Breaks and Models of Recombinational DNA Repair. *Cold Spring Harb. Perspect. Biol.* 6. doi:10.1101/CSHPERSPECT.A016428.

Mer, G., A. Bochkarev, R. Gupta, E. Bochkareva, L. Frappier, C.J. Ingles, A.M. Edwards, and W.J. Chazin. 2000. Structural Basis for the Recognition of DNA Repair Proteins UNG2, XPA, and RAD52 by Replication Factor RPA. *Cell*. 103:449–456. doi:10.1016/S0092-8674(00)00136-7.

Meraldi, P., and P.K. Sorger. 2005. A dual role for Bub1 in the spindle checkpoint and chromosome congression. *EMBO J.* 24:1621–33. doi:10.1038/sj.emboj.7600641.

Michael, W.M., R. Ott, E. Fanning, and J. Newport. 2000. Activation of the DNA replication checkpoint through RNA synthesis by primase. *Science*. 289:2133–7.

Miosge, L.A., Y. Sontani, A. Chuah, K. Horikawa, T.A. Russell, Y. Mei, M. V. Wagle, D.R. Howard, A. Enders, D.C. Tscharke, C.C. Goodnow, and I.A. Parish. 2017. Systems-guided forward genetic screen reveals a critical role of the replication stress response protein ETAA1 in T cell clonal expansion. *Proc. Natl. Acad. Sci.* 114:E5216–E5225. doi:10.1073/PNAS.1705795114.

Mohni, K.N., G.M. Kavanaugh, and D. Cortez. 2014. ATR pathway inhibition is synthetically lethal in cancer cells with ERCC1 deficiency. *Cancer Res.* 74:2835–45. doi:10.1158/0008-5472.CAN-13-3229.

Mordes, D.A., and D. Cortez. 2008. Activation of ATR and related PIKKs. *Cell Cycle*. 7:2809–12. doi:10.4161/cc.7.18.6689.

Mordes, D.A., G.G. Glick, R. Zhao, and D. Cortez. 2008a. TopBP1 activates ATR through ATRIP and a PIKK regulatory domain. *Genes Dev.* 22:1478–89. doi:10.1101/gad.1666208.

Mordes, D.A., E.A. Nam, and D. Cortez. 2008b. Dpb11 activates the Mec1-Ddc2 complex. *Proc. Natl. Acad. Sci. U. S. A.* 105:18730–4. doi:10.1073/pnas.0806621105.

Muñoz, I.M., K. Hain, A.-C. Déclais, M. Gardiner, G.W. Toh, L. Sanchez-Pulido, J.M. Heuckmann, R. Toth, T. Macartney, B. Eppink, R. Kanaar, C.P. Ponting, D.M.J. Lilley, and J. Rouse. 2009. Coordination of structure-specific nucleases by human SLX4/BTBD12 is required for DNA repair. *Mol. Cell*. 35:116–27. doi:10.1016/j.molcel.2009.06.020.

Mutreja, K., J. Krietsch, J. Hess, S. Ursich, M. Berti, F.K. Roessler, R. Zellweger, M. Patra, G. Gasser, and M. Lopes. 2018. ATR-Mediated Global Fork Slowing and Reversal Assist Fork Traverse and Prevent Chromosomal Breakage at DNA Interstrand Cross-Links. *Cell Rep.* 24:2629–2642.e5. doi:10.1016/j.celrep.2018.08.019.

Nam, E.A., R. Zhao, and D. Cortez. 2011a. Analysis of mutations that dissociate G(2) and essential S phase functions of human ataxia telangiectasia-mutated and Rad3-related (ATR) protein kinase. *J. Biol. Chem.* 286:37320–7. doi:10.1074/jbc.M111.276113.

Nam, E.A., R. Zhao, G.G. Glick, C.E. Bansbach, D.B. Friedman, and D. Cortez. 2011b. Thr-1989 phosphorylation is a marker of active ataxia telangiectasia-mutated and Rad3-related (ATR) kinase. *J. Biol. Chem.* 286:28707–14. doi:10.1074/jbc.M111.248914.

Natsume, T., T. Kiyomitsu, Y. Saga, and M.T. Kanemaki. 2016. Rapid Protein Depletion in Human Cells by Auxin-Inducible Degron Tagging with Short Homology Donors. *Cell Rep.* 15:210–218. doi:10.1016/j.celrep.2016.03.001.

Navadgi-Patil, V.M., and P.M. Burgers. 2008a. Yeast DNA replication protein Dpb11 activates the Mec1/ATR checkpoint kinase. *J. Biol. Chem.* 283:35853–9. doi:10.1074/jbc.M807435200.

Navadgi-Patil, V.M., and P.M. Burgers. 2008b. Yeast DNA replication protein Dpb11 activates the Mec1/ATR checkpoint kinase. *J. Biol. Chem.* 283:35853–9. doi:10.1074/jbc.M807435200.

Navadgi-Patil, V.M., and P.M. Burgers. 2009. The unstructured C-terminal tail of the 9-1-1 clamp subunit Ddc1 activates Mec1/ATR via two distinct mechanisms. *Mol. Cell*. 36:743–53. doi:10.1016/j.molcel.2009.10.014.

Navadgi-Patil, V.M., and P.M. Burgers. 2011. Cell-cycle-specific activators of the Mec1/ATR checkpoint kinase. *Biochem. Soc. Trans.* 39:600–5. doi:10.1042/BST0390600.

Navadgi-Patil, V.M., S. Kumar, and P.M. Burgers. 2011. The unstructured C-terminal tail of yeast Dpb11 (human TopBP1) protein is dispensable for DNA replication and the S phase checkpoint but required for the G2/M checkpoint. *J. Biol. Chem.* 286:40999–1007. doi:10.1074/jbc.M111.283994.

Neelsen, K.J., and M. Lopes. 2015. Replication fork reversal in eukaryotes: from dead end to dynamic response. *Nat. Rev. Mol. Cell Biol.* 16:207–220. doi:10.1038/nrm3935.

Nieto-Soler, M., I. Morgado-Palacin, V. Lafarga, E. Lecona, M. Murga, E. Callen, D. Azorin, J. Alonso, A.J. Lopez-Contreras, A. Nussenzweig, and O. Fernandez-Capetillo. 2016. Efficacy of ATR inhibitors as single agents in Ewing sarcoma. *Oncotarget*. 7:58759–58767. doi:10.18632/oncotarget.11643.

Nigg, E.A. 2001. Mitotic kinases as regulators of cell division and its checkpoints. *Nat. Rev. Mol. Cell Biol.* 2:21–32. doi:10.1038/35048096.

Nimonkar, A. V, J. Genschel, E. Kinoshita, P. Polaczek, J.L. Campbell, C. Wyman, P. Modrich, and S.C. Kowalczykowski. 2011. BLM-DNA2-RPA-MRN and EXO1-BLM-RPA-MRN constitute two DNA end resection machineries for human DNA break repair. *Genes Dev.* 25:350–62. doi:10.1101/gad.2003811.

O'Connor, M.J. 2015. Targeting the DNA Damage Response in Cancer. *Mol. Cell*. 60:547–560. doi:10.1016/J.MOLCEL.2015.10.040.

O'Driscoll, M., V.L. Ruiz-Perez, C.G. Woods, P.A. Jeggo, and J.A. Goodship. 2003. A splicing mutation affecting expression of ataxia–telangiectasia and Rad3–related protein (ATR) results in Seckel syndrome. *Nat. Genet.* 33:497–501. doi:10.1038/ng1129.

O'Neill, T., L. Giarratani, P. Chen, L. Iyer, C.-H. Lee, M. Bobiak, F. Kanai, B.-B. Zhou, J.H. Chung, and G.A. Rathbun. 2002. Determination of substrate motifs for human Chk1 and hCds1/Chk2 by the oriented peptide library approach. *J. Biol. Chem.* 277:16102–15. doi:10.1074/jbc.M111705200.

Peddibhotla, S., M.H. Lam, M. Gonzalez-Rimbau, and J.M. Rosen. 2009. The DNA-damage effector checkpoint kinase 1 is essential for chromosome segregation and cytokinesis. *Proc. Natl. Acad. Sci. U. S. A.* 106:5159–64. doi:10.1073/pnas.0806671106.

Pedersen, R.T., T. Kruse, J. Nilsson, V.H. Oestergaard, and M. Lisby. 2015. TopBP1 is required at mitosis to reduce transmission of DNA damage to G1 daughter cells. *J. Cell Biol.* 210:565–82. doi:10.1083/jcb.201502107.

Peng, C.Y., P.R. Graves, R.S. Thoma, Z. Wu, A.S. Shaw, and H. Piwnica-Worms. 1997. Mitotic and G2 checkpoint control: regulation of 14-3-3 protein binding by phosphorylation of Cdc25C on serine-216. *Science*. 277:1501–5.

Perry, J., and N. Kleckner. 2003. The ATRs, ATMs, and TORs are giant HEAT repeat proteins. *Cell*. 112:151–5. doi:10.1016/S0092-8674(03)00033-3.

Petsalaki, E., T. Akoumianaki, E.J. Black, D.A.F. Gillespie, and G. Zachos. 2011. Phosphorylation at serine 331 is required for Aurora B activation. *J. Cell Biol.* 195:449–66. doi:10.1083/jcb.201104023.

Pines, J. 2011. Cubism and the cell cycle: the many faces of the APC/C. *Nat. Rev. Mol. Cell Biol.* 12:427–438. doi:10.1038/nrm3132.

Plank, J.L., J. Wu, and T.-S. Hsieh. 2006. Topoisomerase IIIalpha and Bloom's helicase can resolve a mobile double Holliday junction substrate through convergent branch migration. *Proc. Natl. Acad. Sci. U. S. A.* 103:11118–23. doi:10.1073/pnas.0604873103.

Priestley, A., H.J. Beamish, D. Gell, A.G. Amatucci, M.C. Muhlmann-Diaz, B.K. Singleton, G.C. Smith, T. Blunt, L.C. Schalkwyk, J.S. Bedford, S.P. Jackson, P.A. Jeggo, and G.E. Taccioli. 1998. Molecular and biochemical characterisation of DNA-dependent protein kinase-defective rodent mutant irs-20. *Nucleic Acids Res.* 26:1965–73.

Putnam, C.D., T.K. Hayes, and R.D. Kolodner. 2010. Post-replication repair suppresses duplication-mediated genome instability. *PLoS Genet.* 6:e1000933. doi:10.1371/journal.pgen.1000933.

Raaijmakers, L.M., P. Giansanti, P.A. Possik, J. Mueller, D.S. Peeper, A.J.R. Heck, and A.F.M. Altelaar. 2015. PhosphoPath: Visualization of Phosphosite-centric Dynamics in Temporal Molecular Networks. *J. Proteome Res.* 14:4332–4341. doi:10.1021/acs.jproteome.5b00529.

Rao, Q., M. Liu, Y. Tian, Z. Wu, Y. Hao, L. Song, Z. Qin, C. Ding, H.-W. Wang, J. Wang, and Y. Xu. 2018. Cryo-EM structure of human ATR-ATRIP complex. *Cell Res.* 28:143–156. doi:10.1038/cr.2017.158.

Raynard, S., W. Bussen, and P. Sung. 2006. A double Holliday junction dissolvasome comprising BLM, topoisomerase IIIalpha, and BLAP75. *J. Biol. Chem.* 281:13861–4. doi:10.1074/jbc.C600051200.

Reynolds, J.J., L.S. Bicknell, P. Carroll, M.R. Higgs, R. Shaheen, J.E. Murray, D.K. Papadopoulos, A. Leitch, O. Murina, Ž. Tarnauskaitė, S.R. Wessel, A. Zlatanou, A. Vernet, A. von Kriegsheim, R.M.A. Mottram, C. V Logan, H. Bye, Y. Li, A. Brean, S. Maddirevula, R.C. Challis, K. Skouloudaki, A. Almoisheer, H.S. Alsaif, A. Amar, N.J. Prescott, M.B. Bober, A. Duker, E. Faqeih, M.Z. Seidahmed, S. Al Tala, A. Alswaid, S. Ahmed, J.Y. Al-Aama, J. Altmüller, M. Al Balwi, A.F. Brady, L. Chessa, H. Cox, R. Fischetto, R. Heller, B.D. Henderson, E. Hobson, P. Nürnberg, E.F. Percin, A. Peron, L. Spaccini, A.J. Quigley,

S. Thakur, C.A. Wise, G. Yoon, M. Alnemer, P. Tomancak, G. Yigit, A.M.R. Taylor, M.A.M. Reijns, M.A. Simpson, D. Cortez, F.S. Alkuraya, C.G. Mathew, A.P. Jackson, and G.S. Stewart. 2017. Mutations in DONSON disrupt replication fork stability and cause microcephalic dwarfism. *Nat. Genet.* 49:537–549. doi:10.1038/ng.3790.

Royou, A., H. Macias, and W. Sullivan. 2005. The Drosophila Grp/Chk1 DNA damage checkpoint controls entry into anaphase. *Curr. Biol.* 15:334–9. doi:10.1016/j.cub.2005.02.026.

Ruiz, S., C. Mayor-Ruiz, V. Lafarga, M. Murga, M. Vega-Sendino, S. Ortega, and O. Fernandez-Capetillo. 2016. A Genome-wide CRISPR Screen Identifies CDC25A as a Determinant of Sensitivity to ATR Inhibitors. *Mol. Cell*. 62:307–313. doi:10.1016/J.MOLCEL.2016.03.006.

Saka, Y., and M. Yanagida. 1993. Fission yeast cut5+, required for S phase onset and M phase restraint, is identical to the radiation-damage repair gene rad4+. *Cell*. 74:383–393. doi:10.1016/0092-8674(93)90428-S.

Saldivar, J.C., D. Cortez, and K.A. Cimprich. 2017. The essential kinase ATR: ensuring faithful duplication of a challenging genome. *Nat. Rev. Mol. Cell Biol.* 18:622–636. doi:10.1038/nrm.2017.67.

Saldivar, J.C., S. Hamperl, M.J. Bocek, M. Chung, T.E. Bass, F. Cisneros-Soberanis, K. Samejima, L. Xie, J.R. Paulson, W.C. Earnshaw, D. Cortez, T. Meyer, and K.A. Cimprich. 2018. An intrinsic S/G2 checkpoint enforced by ATR. *Science*. 361:806–810. doi:10.1126/science.aap9346.

Savitsky, K., A. Bar-Shira, S. Gilad, G. Rotman, Y. Ziv, L. Vanagaite, D.A. Tagle, S. Smith, T. Uziel, S. Sfez, M. Ashkenazi, I. Pecker, M. Frydman, R. Harnik, S.R. Patanjali, A. Simmons, G.A. Clines, A. Sartiel, R.A. Gatti, L. Chessa, O. Sanal, M.F. Lavin, N.G. Jaspers, A.M. Taylor, C.F. Arlett, T. Miki, S.M. Weissman, M. Lovett, F.S. Collins, and Y. Shiloh. 1995. A single ataxia telangiectasia gene with a product similar to PI-3 kinase. *Science*. 268:1749–53.

Sawicka, M., P.H. Wanrooij, V.C. Darbari, E. Tannous, S. Hailemariam, D. Bose, A. V Makarova, P.M. Burgers, and X. Zhang. 2016. The Dimeric Architecture of Checkpoint Kinases Mec1ATR and Tel1ATM Reveal a Common Structural Organization. *J. Biol. Chem.* 291:13436–47. doi:10.1074/jbc.M115.708263.

Shannon, P., A. Markiel, O. Ozier, N.S. Baliga, J.T. Wang, D. Ramage, N. Amin, B. Schwikowski, and T. Ideker. 2003. Cytoscape: a software environment for integrated models of biomolecular interaction networks. *Genome Res.* 13:2498–504. doi:10.1101/gr.1239303.

Shiotani, B., H.D. Nguyen, P. Håkansson, A. Maréchal, A. Tse, H. Tahara, and L. Zou. 2013. Two distinct modes of ATR activation orchestrated by Rad17 and Nbs1. *Cell Rep.* 3:1651–62. doi:10.1016/j.celrep.2013.04.018.

Sibanda, B.L., D.Y. Chirgadze, D.B. Ascher, and T.L. Blundell. 2017. DNA-PKcs structure suggests an allosteric mechanism modulating DNA double-strand break repair. *Science*. 355:520–524. doi:10.1126/science.aak9654.

Singh, T.R., A.M. Ali, V. Busygina, S. Raynard, Q. Fan, C. Du, P.R. Andreassen, P. Sung, and A.R. Meetei. 2008. BLAP18/RMI2, a novel OB-fold-containing protein, is an essential component of the Bloom helicase-double Holliday junction dissolvasome. *Genes Dev.* 22:2856–68. doi:10.1101/gad.1725108.

Sirbu, B.M., F.B. Couch, J.T. Feigerle, S. Bhaskara, S.W. Hiebert, and D. Cortez. 2011. Analysis of protein dynamics at active, stalled, and collapsed replication forks. *Genes Dev.* 25:1320–7. doi:10.1101/gad.2053211.

Sirbu, B.M., W.H. McDonald, H. Dungrawala, A. Badu-Nkansah, G.M. Kavanaugh, Y. Chen, D.L. Tabb, and D. Cortez. 2013. Identification of proteins at active, stalled, and collapsed replication forks using isolation of proteins on nascent DNA (iPOND) coupled with mass spectrometry. *J. Biol. Chem.* 288:31458–67. doi:10.1074/jbc.M113.511337.

Skourti-Stathaki, K., and N.J. Proudfoot. 2014. A double-edged sword: R loops as threats to genome integrity and powerful regulators of gene expression. *Genes Dev.* 28:1384–96. doi:10.1101/gad.242990.114.

Sultana, R., T. Abdel-Fatah, C. Perry, P. Moseley, N. Albarakti, V. Mohan, C. Seedhouse, S. Chan, and S. Madhusudan. 2013. Ataxia Telangiectasia Mutated and Rad3 Related (ATR) Protein Kinase Inhibition Is Synthetically Lethal in XRCC1 Deficient Ovarian Cancer Cells. *PLoS One*. 8:e57098. doi:10.1371/journal.pone.0057098.

Toledo, L.I., M. Altmeyer, M.-B. Rask, C. Lukas, D.H. Larsen, L.K. Povlsen, S. Bekker-Jensen, N. Mailand, J. Bartek, and J. Lukas. 2013. ATR prohibits replication catastrophe by preventing global exhaustion of RPA. *Cell*. 155:1088–103. doi:10.1016/j.cell.2013.10.043.

Toledo, L.I., M. Murga, P. Gutierrez-Martinez, R. Soria, and O. Fernandez-Capetillo. 2008. ATR signaling can drive cells into senescence in the absence of DNA breaks. *Genes Dev.* 22:297–302. doi:10.1101/gad.452308.

Van, C., S. Yan, W.M. Michael, S. Waga, and K.A. Cimprich. 2010. Continued primer synthesis at stalled replication forks contributes to checkpoint activation. *J. Cell Biol.* 189:233–46. doi:10.1083/jcb.200909105.

Vassin, V.M., R.W. Anantha, E. Sokolova, S. Kanner, and J.A. Borowiec. 2009. Human RPA phosphorylation by ATR stimulates DNA synthesis and prevents ssDNA accumulation during DNA-replication stress. *J. Cell Sci.* 122:4070–80. doi:10.1242/jcs.053702.

Wang, J., J. Chen, and Z. Gong. 2013. TopBP1 controls BLM protein level to maintain genome stability. *Mol. Cell*. 52:667–78. doi:10.1016/j.molcel.2013.10.012.

Wang, X., H. Chu, M. Lv, Z. Zhang, S. Qiu, H. Liu, X. Shen, W. Wang, and G. Cai. 2016. Structure of the intact ATM/Tel1 kinase. *Nat. Commun.* 7:11655. doi:10.1038/ncomms11655.

Wang, X., T. Ran, X. Zhang, J. Xin, Z. Zhang, T. Wu, W. Wang, and G. Cai. 2017. 3.9 Å structure of the yeast Mec1-Ddc2 complex, a homolog of human ATR-ATRIP. *Science*. 358:1206–1209. doi:10.1126/science.aan8414.

Wanrooij, P.H., E. Tannous, S. Kumar, V.M. Navadgi-Patil, and P.M. Burgers. 2015. Probing the Mec1/ATR Checkpoint Activation Mechanism with Small Peptides. *J. Biol. Chem.* M115.687145-. doi:10.1074/jbc.M115.687145.

Williams, R.S., J.S. Williams, and J. a Tainer. 2007. Mre11-Rad50-Nbs1 is a keystone complex connecting DNA repair machinery, double-strand break signaling, and the chromatin template. *Biochem. Cell Biol.* 85:509–20. doi:10.1139/O07-069.

Williamson, C.T., R. Miller, H.N. Pemberton, S.E. Jones, J. Campbell, A. Konde, N. Badham, R. Rafiq, R. Brough, A. Gulati, C.J. Ryan, J. Francis, P.B. Vermulen, A.R. Reynolds, P.M. Reaper, J.R. Pollard, A. Ashworth, and C.J. Lord. 2016. ATR inhibitors as a synthetic lethal

therapy for tumours deficient in ARID1A. *Nat. Commun.* 7:13837. doi:10.1038/ncomms13837.

Wu, C., X. Miao, L. Huang, X. Che, G. Jiang, D. Yu, X. Yang, G. Cao, Z. Hu, Y. Zhou, C. Zuo, C. Wang, X. Zhang, Y. Zhou, X. Yu, W. Dai, Z. Li, H. Shen, L. Liu, Y. Chen, S. Zhang, X. Wang, K. Zhai, J. Chang, Y. Liu, M. Sun, W. Cao, J. Gao, Y. Ma, X. Zheng, S.T. Cheung, Y. Jia, J. Xu, W. Tan, P. Zhao, T. Wu, C. Wang, and D. Lin. 2012. Genome-wide association study identifies five loci associated with susceptibility to pancreatic cancer in Chinese populations. *Nat. Genet.* 44:62–6. doi:10.1038/ng.1020.

Wu, L., C.Z. Bachrati, J. Ou, C. Xu, J. Yin, M. Chang, W. Wang, L. Li, G.W. Brown, and I.D. Hickson. 2006. BLAP75/RMI1 promotes the BLM-dependent dissolution of homologous recombination intermediates. *Proc. Natl. Acad. Sci. U. S. A.* 103:4068–73. doi:10.1073/pnas.0508295103.

Wu, L., and I.D. Hickson. 2003. The Bloom's syndrome helicase suppresses crossing over during homologous recombination. *Nature*. 426:870–4. doi:10.1038/nature02253.

Xu, D., R. Guo, and A. Sobeck. 2008a. RMI, a new OB-fold complex essential for Bloom syndrome protein to maintain genome stability. *Genes ….* 2843–2855. doi:10.1101/gad.1708608.7.

Xu, X., S. Vaithiyalingam, G.G. Glick, D.A. Mordes, W.J. Chazin, and D. Cortez. 2008b. The basic cleft of RPA70N binds multiple checkpoint proteins, including RAD9, to regulate ATR signaling. *Mol. Cell. Biol.* 28:7345–53. doi:10.1128/MCB.01079-08.

Yamane, K., M. Kawabata, and T. Tsuruo. 1997. A DNA-Topoisomerase-11-Binding Protein with Eight Repeating Regions Similar to DNA-repair Enzymes and to a Cell-Cycle Regulator. *Eur. J. Biochem.* 250:794–799. doi:10.1111/j.1432-1033.1997.00794.x.

You, Z., and J.M. Bailis. 2010. DNA damage and decisions: CtIP coordinates DNA repair and cell cycle checkpoints. *Trends Cell Biol.* 20:402–409. doi:10.1016/j.tcb.2010.04.002.

Yu, C.E., J. Oshima, Y.H. Fu, E.M. Wijsman, F. Hisama, R. Alisch, S. Matthews, J. Nakura, T. Miki, S. Ouais, G.M. Martin, J. Mulligan, and G.D. Schellenberg. 1996. Positional cloning of the Werner's syndrome gene. *Science*. 272:258–62.

Yusufzai, T., and J.T. Kadonaga. 2010. Annealing helicase 2 (AH2), a DNA-rewinding motor with an HNH motif. *Proc. Natl. Acad. Sci. U. S. A.* 107:20970–3. doi:10.1073/pnas.1011196107.

Zachos, G., E.J. Black, M. Walker, M.T. Scott, P. Vagnarelli, W.C. Earnshaw, and D.A.F. Gillespie. 2007. Chk1 Is Required for Spindle Checkpoint Function. *Dev. Cell*. 12:247–260. doi:10.1016/J.DEVCEL.2007.01.003.

Zeman, M.K., and K.A. Cimprich. 2014. Causes and consequences of replication stress. *Nat. Cell Biol.* 16:2–9. doi:10.1038/ncb2897.

Zhou, Z.-W., C. Liu, T.-L. Li, C. Bruhn, A. Krueger, W. Min, Z.-Q. Wang, and A.M. Carr. 2013. An essential function for the ATR-activation-domain (AAD) of TopBP1 in mouse development and cellular senescence. *PLoS Genet.* 9:e1003702. doi:10.1371/journal.pgen.1003702.

Zhu, Z., W.-H. Chung, E.Y. Shim, S.E. Lee, and G. Ira. 2008. Sgs1 Helicase and Two Nucleases Dna2 and Exo1 Resect DNA Double-Strand Break Ends. *Cell*. 134:981–994. doi:10.1016/J.CELL.2008.08.037.

Zou, L., and S.J. Elledge. 2003. Sensing DNA damage through ATRIP recognition of RPA-ssDNA complexes. *Science*. 300:1542–8. doi:10.1126/science.1083430.

Zou, Y., Y. Liu, X. Wu, and S.M. Shell. 2006. Functions of human replication protein A (RPA): from DNA replication to DNA damage and stress responses. *J. Cell. Physiol.* 208:267–73. doi:10.1002/jcp.20622.